T.C.
SAKARYA ÜNİVERSİTESİ
FEN BİLİMLERİ ENSTİTÜSÜ

PİRİDİN-2-KARBOKSİLİK ASİT TÜREVLERİNİ İÇEREN YENİ METAL KOMPLEKSLERİNİN SENTEZİ, YAPISAL SPEKTROSKOPİK VE DOĞRUSAL OLMAYAN OPTİK ÖZELLİKLERİNİN ARAŞTIRILMASI

DOKTORA TEZİ

Merve ŞİMŞEK

Fizik Anabilim Dalı

TEMMUZ 2025

T.C.
SAKARYA ÜNİVERSİTESİ
FEN BİLİMLERİ ENSTİTÜSÜ

PİRİDİN-2-KARBOKSİLİK ASİT TÜREVLERİNİ İÇEREN YENİ METAL KOMPLEKSLERİNİN SENTEZİ, YAPISAL SPEKTROSKOPİK VE DOĞRUSAL OLMAYAN OPTİK ÖZELLİKLERİNİN ARAŞTIRILMASI

DOKTORA TEZİ

Merve ŞİMŞEK

Fizik Anabilim Dalı

Tez Danışmanı: Prof. Dr. Ömer TAMER

TEMMUZ 2025

Merve ŞİMŞEK tarafından hazırlanan "Piridin-2-Karboksilik Asit Türevlerini İçeren Yeni Metal Komplekslerinin Sentezi, Yapısal Spektroskopik ve Doğrusal Olmayan Optik Özelliklerinin Araştırılması" adlı tez çalışması 07.07.2025 tarihinde aşağıdaki jüri tarafından oy birliği/oy çokluğu ile Sakarya Üniversitesi Fen Bilimleri Enstitüsü Fizik Anabilim Dalı 'nda Doktora tezi olarak kabul edilmiştir.

Jüri Başkanı :	**Prof.Dr.Erdoğan TARCAN** Kocaeli Üniversitesi
Jüri Üyesi :	**Prof. Dr. Ömer TAMER** (Danışman) Sakarya Üniversitesi
Jüri Üyesi :	**Prof. Dr. Adil BAŞOĞLU** Sakarya Üniversitesi
Jüri Üyesi :	**Doc. Dr. Murat TUNA** Sakarya Üniversitesi
Jüri Üyesi :	**Dr. Öğr. Üyesi Bahadır SALMANKURT** Sakarya Uygulamalı Bilimler Üniversitesi

ETİK İLKE VE KURALLARA UYGUNLUK BEYANNAMESİ

Sakarya Üniversitesi Fen Bilimleri Enstitüsü Lisansüstü Eğitim-Öğretim Yönetmeliğine ve Yükseköğretim Kurumları Bilimsel Araştırma ve Yayın Etiği Yönergesine uygun olarak hazırlamış olduğum "PİRİDİN-2-KARBOKSİLİK ASİT TÜREVELERİNİ İÇEREN YENİ METAL KOMPLKESLERİN SENTEZİ, YAPISAL SPEKTROSKOPİK VE DOĞRUSAL OLMAYAN OPTİK ÖZELLİKLERİNİN ARAŞTIRILMASI" başlıklı tezin bana ait, özgün bir çalışma olduğunu; çalışmamın tüm aşamalarında yukarıda belirtilen yönetmelik ve yönergeye uygun davrandığımı, tezin içerdiği yenilik ve sonuçları başka bir yerden almadığımı, tezde kullandığım eserleri usulüne göre kaynak olarak gösterdiğimi, bu tezi başka bir bilim kuruluna akademik amaç ve unvan almak amacıyla vermediğimi ve 20.04.2016 tarihli Resmi Gazete'de yayımlanan Lisansüstü Eğitim ve Öğretim Yönetmeliğinin 9/2 ve 22/2 maddeleri gereğince Sakarya Üniversitesi'nin abonesi olduğu intihal yazılım programı kullanılarak Enstitü tarafından belirlenmiş ölçütlere uygun rapor alındığını, çalışmamla ilgili yaptığım bu beyana aykırı bir durumun ortaya çıkması halinde doğabilecek her türlü hukuki sorumluluğu kabul ettiğimi beyan ederim.

(07/07/2025)

Merve ŞİMŞEK

Ablama….

TEŞEKKÜR

Doktora tez sürecim boyunca, çalışmamın planlanmasından yürütülmesine kadar geçen her aşamada bilgi ve deneyimleriyle yol gösterici olan, kıymetli danışmanım Prof. Dr. Ömer TAMER'e en derin teşekkürlerimi ve saygılarımı sunarım. Ayrıca, bu süreçte görüş ve önerileriyle bilimsel katkı sağlayan, desteklerini esirgemeyen Prof. Dr. Yusuf ATALAY, Prof. Dr. Davut AVCI, Prof. Dr. Adil BAŞOĞLU, Prof. Dr. Erdoğan TARCAN, Prof.Dr.Necmi DEGE ve Doç. Dr. Murat TUNA'ya teşekkürlerimi ifade etmek isterim. Çalışmalarım süresince her zaman yanımda olan, bilimsel katkılarının yanı sıra manevi desteğini de esirgemeyen değerli meslektaşım Dr. Tuğba UĞUR GENÇ'e , Dr.Bilgenur YAŞA'ya, Dr.Emine Berrin ÇINAR'a ve manevi desteğini de esirgemeyen değerli arkadaşlarım Özge GÖRMÜŞ ve Fatih-Esra AYMAN'a içtenlikle teşekkür ederim.

Bu tez, Sakarya Üniversitesi Bilimsel Araştırma Projeleri Koordinatörlüğü (BAPK) tarafından 2023-19-44-48 proje numarası ile desteklenmiştir.

Merve ŞİMŞEK

İÇİNDEKİLER

Sayfa

ETİK İLKE VE KURALLARA UYGUNLUK BEYANNAMESİ v
TEŞEKKÜR ix
İÇİNDEKİLER xi
KISALTMALAR xiii
SİMGELER xv
ŞEKİL LİSTESİ xvii
ÖZET xix
SUMMARY xxiii
1. GİRİŞ 1
1.1. Karboksilik Asitler 5
2. LİTERATÜR ARAŞTIRMASI 11
3. BULGULAR VE TARTIŞMA 37
3.1. 6-kloropiridin-2-karboksilik Asidin Zn (II) ve Cu (II) Kompleksleri İçin Yapısal, Spektroskopik (FT-IR ve UV-Vis), Doğrusal Olmayan Optik ve Moleküler Yerleştirme Analizlerine İlişkin Deneysel ve Teorik Yaklaşımlar 37
3.2. 3-hidroksi ve 4-kloro ikameli piridin-2-karboksilik asidin yeni bir karışık ligand çinko(II) kompleksi: Sentez, karakterizasyon, NLO özellikleri ve DFT hesaplaması 40
3.3. Kompleks Oluşumun Statik Ve Frekansa Bağlı Doğrusal Olmayan Optik Özellikler Üzerindeki Etkisi: Birleşik Deneysel Ve Teorik Araştırma 42
3.4. 4-kloro-Piridin-2-Karboksilik asit içeren Co(II) kompleksinin belirgin yüksek statik/dinamik birinci ve ikinci mertebe yüksek kutuplanabilirliği üzerinde kompleks oluşumunun etkisinin araştırılması 45
3.5. 6-floropiridin-2-karboksilik asidin yeni bir Cu(II) kompleksinin yapısal, titreşimsel, termal ve doğrusal olmayan optik özelliklerinin araştırılması 48
4. SONUÇLAR VE TARTIŞMA 51
5. ÖNERİLER 55
KAYNAKLAR 57
EKLER 63
ÖZGEÇMİŞ 125

KISALTMALAR

CCDC : Combridge kristolografik veri merkezi
D-A : Dönor-Akseptör
DFT : Yoğunluk Fonksiyonel Teorisi
DOS : Yoğunluk durumları
FT-IR : Fourier Dönüşümlü Kızılötesi Spektroskopi
HF : Hartre Fock yöntemi
HOMO : En yüksek dolu moleküler orbital
ILCT : Ligand içi yük transferi
LMCT : Ligandtan metale yük transferi
LUMO : En düşük boş moleküler orbital
MEP : Moleküler Elektrostatik Potansiyel
MLCT : Metalden liganda yük transferi
NBO : Doğal Bağ Orbitali
NLO : Doğrusal Olmayan Optik
NMR : Nükleer Manyetik Rezonans
PDB : Protein veri bankası
SGH : İkinci harmonik üretim
TD-DFT : Zaman Bağlı Yoğunluk Fonksiyonel Teorisi
UV-Vis : Ultraviyole-Görünür Bölge
XRD : X-Işını Kırınımı
Z-scan : Z-Tarama Tekniği

SİMGELER

$\mathbf{K_i}$	: İnhibasyon sabiti [μM]
S	: Kimyasal yumuşaklık [eV^{-1}]
α	: Kutuplanabilirlik [esu]
β	: Birinci mertebe yüksek kutuplanabilirlik [esu]
γ	: İkinci mertebe yüksek kutuplanabilirlik[esu]
ΔE	: Enerji aralığı [eV]
Δα	: Yönelime bağlı kutuplanabilirlik [esu]
η	: Kimyasal sertlik [eV]
λ_{max}	: Maksimum soğurma dalga boyu [nm]
μ	: Dipol moment [Debye]
χ	: Elektronegatiflik [eV]
χ^3	: Üçüncü mertebe doğrusal olmayan optik alınganlık katsayısı [esu]

ŞEKİL LİSTESİ

Sayfa

Şekil 1.1. Piridin-2-karboksilik asit (pca), 4-kloro-piridin-2-karboksilik asit (4Clpca) ve 4-metoksi-piridin-2-karboksilik asit (4MeOpca) 2
Şekil 1.2. N,N'-o-fenilenbis(4-hidroksisalisilidenimin) (L), Nikel (NiL) ve Kobalt (CoL) metal-organik komplekslerinin moleküler yapısı..... 3
Şekil 1.3. Nikel, kobalt, bakır ve çinko içeren mezo-tetrakis(2,3,5,6-tetrafluoro-N, N-dimetil-4-anilinil) porfirin kompleksleri 4
Şekil 1.4. Karboksilik asit fonksiyonel grubunun genel yapısı 6
Şekil 1.5. Piridin-2-karboksilik asit molekülünün yapısı ($C_6H_5NO_2$)..... 7
Şekil 1.6. Piridin-2-karboksilik asit ligandının metal iyonlarına bağlanma modları [24]. 8
Şekil 2.1. Piridin-2-karboksilik asit ligandını içeren Mn(II) metal kompleksi..... 11
Şekil 2.2. Piridin-2-karboksilik asit ligandını içeren Mn(II) kompleksi..... 12
Şekil 2.3. $[SmNi(pic)_3(H_2O)_5]_n(ClO_4)_{2n}.3nH_2O$ komleksi (pic: Piridin-2-karboksilik asit)..... 12
Şekil 2.4. $[FePc_2(Me_2Bipy)]$ (Pc: Piridin 2-karboksilik asit ve Me_2Bipy:4,4'-dimetil-2,2'-bipiridil) kompleksi. 13
Şekil 2.5. $Cu(PC)_2 \cdot H_2O$ kompleksi (PC: piridin-2-karboksilik asit). 14
Şekil 2.6. $[Mg(pyc)_2(H_2O)_2] \cdot H_2O$ (pyc: piridin-2-karbokilik asit) kompleksi deneysel gösterimi..... 14
Şekil 2.7. $Cu(PC)_2 \cdot H_2O$ metal kompleksi (PC: piridin-2-karbokilik asit)..... 15
Şekil 2.8. $[Cu(pic)_2].2H_2O$ (pic: piridin-2-karbokilik asit) metal kompleksi 16
Şekil 2.9. Piridin-2-karboksilik asit içeren Zn(II), Ni(II) ve Mn(II) kompleksleri.... 17
Şekil 2.10. $[Mn(pic)_2(phen)] \cdot H_2O$ (pic: piridin2-karboksilik asit) kompleksi görseli 17
Şekil 2.11. $[Cu(pic)_2(phen)] \cdot H_2O$ (pic: piridin-2-karboksilik asit) kompleksi görseli 18
Şekil 2.12. $[Co(6\text{-}Mepic)(pic) \cdot 2H_2O]$ (6-Mepic: 6-metoksi-2-piridin-karbokdilik asit, pic: 2-piridin karboksilik asit) kompleksleri görseli 19
Şekil 2.13. Piperazinyum bis(pikolinat) PPPA tek dişli yapısının tek kristal görseli.20
Şekil 2.14.PCOH (trans-diaqua-bis(piridin-2-karboksilato)-cobalt(II) dihidratin) kompleksinin görseli 20
Şekil 2.15. Piridin-2-karboksilik ast ligandı ile elde edilmiş Zn pikolinat dihidrat (ZPD) kristalinin şeması 21
Şekil 2.16. 4-metoksipiridin-2-karboksilik asit içeren Mn(II) ve Cd(II) kompleksleri. 22
Şekil 2.17. a) $[CuPic_2]$ ve b) $[ZnPic_2(H_2O)_2]$ kompleksleri (Pic: Piridin-2-karboksilik asit)..... 22
Şekil 2.18. 6-metilpiridin-2-karboksilik asit içeren kompleksler 23
Şekil 2.19. Piridin-2-karboksilik asit içeren Metal(II) perklorat komplekslerinin yapısı 24

Şekil 2.20. $[Ga(Pic)_3]\cdot H_2O$ (Pic: piridin-2-karboksilik asit) için moleküler yapı için çizilmiş %50 olasılık düzeyinde elipsoidler. 25
Şekil 2.21. DFT/CAM-B3LYP seviyesi kullanılarak $[Mn(L_1)_2(NCS)_2]$ komleksi ve $[Co(L_1)_2(NCS)_2]$ kompleklsinin 'nin tek kristal yapıları ve $[Ni(L_1)_2(NCS)_2]$ (L_1:piridin-2-karboksilik asit) kompleksinin teorik olarak optimize edilmiş yapısı. 26
Şekil 2.22. a) $[Zn(MeOPic)_2\cdot(H_2O)_2]$ kompleksi b) $[Ni(MeOPic)_2\cdot(H_2O)_2]$ kompleksi (MeOPic: 4-metoksipiridin-2-karboksilik asit) 27
Şekil 2.23. 3,5-difloropiridin- 2 -karboksilik asit ligandı ile elde edilen Re(I) komleksi 27
Şekil 2.24. $\{Zn(HL)(H_2O)_2\}_n$ (HL = 4-(2,4-dikarboksifenil-piridin-2-karboksilik asit) kompleksi 28
Şekil 2.25. $[L_n(NO_3)(4picH)_2(H_2O)_4](NO_3)_2$ (4picH: 4-pikolinik sit) kristal yapısı.. 29
Şekil 2.26. $[Cu(5\text{-}npic)_2]_n$ (5-npic: 5-nitropiridin-2-karboksilik asit) kompleksi 30
Şekil 2.27. BTPCA (Benzotrial piridin-2-karboksilik asit)'nın optimize edilmiş moleküler yapısı 31
Şekil 2.28. Randhawa ve arkadaşları tarafından sentezlenen yeni ligandların görselleri 31
Şekil 2.29. Jamgohari ve arkadaşları tarafından sentezlenen piridin-2-karboksilik asit içeren metal kompleksleri 33
Şekil 2.30. Me_2N-pbt (-(4-dimetilaminofenil-benzotiazolat) ana ligandı kullanılarak elde edilen Pt(II) kompleksi. 34
Şekil 2.31. Piridin-2-karboksilik asit ve peroksit liganları kullanılarak elde edilen Fe(III) kompleksi..... 35

PİRİDİN-2-KARBOKSİLİK ASİT TÜREVLERİNİ İÇEREN YENİ METAL KOMPLEKSLERİNİN SENTEZİ, YAPISAL SPEKTROSKOPİK VE DOĞRUSAL OLMAYAN OPTİK ÖZELLİKLERİNİN ARAŞTIRILMASI

ÖZET

Bu tez çalışması, piridin-2-karboksilik asit türevlerini içeren geçiş metal komplekslerinin sentezi, elde edilen komplekslerin yapısal, elektronik ve doğrusal olmayan optik (NLO) özelliklerinin ayrıntılı biçimde araştırılmasına odaklanmaktadır. Elde edilen tüm metal-organik koordinasyon bileşiklerinin ilk kez sentezlenmiş olması ve yukarıda sıralanan çalışmaların bu kompleksler için ilk kez yapılıyor olması bu tez çalışmasının özgünlüğünü yansıtmaktadır. Özellikle, hem piridin-2-karboksilik asit türevleri hemde ikincil nötral ligan içeren geçiş metal kompleksleri üzerine literatürde sınırlı sayıda çalışma olması, mevcut çalışmanın etkin NLO özelliklerine sahip yeni malzemlerin araştırılmasına katkı sunan önemli bir çalışma olduğunu göstermektedir. Ligand yapılarında bulunan elektron verici ve çekici grupların kombinasyonu sayesinde, moleküller arası etkileşimlerin kuvvetlendirilmesi ve optoelektronik özelliklerin iyileştirilmesi hedeflenmiştir. Bu bağlamda, Zn(II), Cu(II), Co(II) ve Mn(II) geçiş metalleri iyonlarıyla oluşturulan yeni komplekslerin yapısal, elektronik ve optik özellikleri deneysel ve kuramsal yöntemlerle detaylı şekilde incelenmiştir.

Kristal yapılar üzerindeki analizler, yalnızca atomik koordinasyonların belirlenmesiyle sınırlı kalmayıp, aynı zamanda bu koordinasyonların elektronik geçişlere olan etkilerini de göz önünde bulundurmuştur. X-ışını kırınım verilerinden elde edilen geometrik parametreler, yoğunluk fonksiyonel teori (DFT) metodu ile elde edilen teorik sonuçlar ile karşılaştırılarak DFT yönteminin bu kompleksler üzerindeki etkinliği test edilmiştir. Bu çalışmada hem deneysel hem de kuramsal metodolojilerin bütüncül kullanımı, benzer yapılara sahip olan yeni komplekslerin teorik olarak incelenmesi aşamasında araştırmacılara yoğunluk fonksiyoneli, temel set ve spin durumu gibi önemli noktolarda öngörü oluşturacaktır. Bu bağlamda, $[Cu(6Fpca)_2(H_2O)]$ ve $[Zn(6Clpca)_2(H_2O)_2$ komplekslerinin bozulmuş oktahedral; $[Mn(6Brpca)_2(Dmdpy)].CH_3OH$ ve$[Zn(4Clpca)(3OHpca)(H_2O)_2]$ komplekslerinin bozulmuş oktahedral; $[Co(4Clpca)_2(H_2O)_2$ve $[Cu(6Clpca)_2]$ kompleksinin ise tetragonal piramidal koordinasyon geometrisi sergilediği belirlenmiştir.

FT-IR verileri, özellikle karboksilat gruplarının koordinasyon biçimlerinin belirlenmesinde önemli rol oynamıştır. O-H gerilmetitreşimleri 3188–3449 cm^{-1} aralığında gözlenirken, COO^- gruplarına ait asimetrik ve simetrik titreşimler arasındaki $\Delta\nu$ değerleri 318-473 cm^{-1} arasında değişmiş ve piridin halkasındaki karboksilat atomu üzerinden tek dişli bağlanma biçimini desteklemiştir. Ayrıca, piridin halkası soluklanma titreşimlerinin 986-1036 cm^{-1} aralığında kayma göstermesi, ligandların metal merkezleriyle etkili bir elektronik etkileşim içinde olduğunu ve piridin halkasında bulunan N atomu üzerinden metal kovalen bağ kurulduğunu teyit etmektedir.

UV-Vis çalışmaları göz önüne alındığında, özellikle Cu(II) ve Mn(II) komplekslerinde 300-400 nm aralığında gözlenen ligand-metal yük transfer (LMCT) bantları,

komplekslerin fotofiziksel ve doğrusal olmayan optik karakterlerini anlamada kritik rol oynamaktadır. Örneğin, $[Mn(6Brpca)_2(Dmdpy)].CH_3OH$ kompleksinde 206, 225, 263 ve 275.6 nm'de ligand içi $\pi\rightarrow\pi^*$ ve $n\rightarrow\pi^*$ geçişleri belirlenmiştir. Benzer şekilde, $[Cu(6Fpca)_2(H_2O)]$ kompleksinde 263 nm'de $\pi\rightarrow\pi^*$ ligand içi yük geçişi ve 369 nm'de LMCT geçişleri raporlanmıştır.

Çalışmada ayrıca, deneysel sonuçların doğrulanması amacıyla kuantum kimyasal hesaplamalara geniş yer verilmiş; TD-DFT, sınır moleküler orbital analizi ve doğal bağ orbital (NBO) hesaplamaları ile moleküllerin elektronik özellikleri ayrıntılı biçimde değerlendirilmiştir. Bu analizler sayesinde, kompleks içi yük dağılımı, komplekslerin elektronik yapı kararlılıkları ve kompleks içerisinde gerçekleşen yüksek enerjili konjugatif etkileşimler gibi özellikler detaylı araştırılmış ve NLO özellikleri ile arasındaki ilişki açıklanmıştır HOMO-LUMO enerji farkları arasında en düşük değerin $[Mn(6Brpca)_2(Dmdpy)]\cdot CH_3OH$ kompleksine ait olduğu belirlenmiş (2.425 eV), en yüksek farkın ise $[Zn(6Clpca)_2]$ kompleksinde olduğu hesaplanmıştır (4.640 eV). Bu enerji farkları ile NLO parametreleri arasında anlamlı korelasyonlar elde edilmiştir.

Tezin teorik kısmında, DFT ve TD-DFT yöntemleriyle yürütülen kuantum kimyasal hesaplamalar, komplekslerin elektronik yapıları ve NLO potansiyelleri üzerine önemli veriler sağlamıştır. Özellikle $[Mn(6Brpca)_2(Dmdpy)].CH_3OH$ (6Brpca: 6-bromopiridin-2-karboksilik asit, Dmdpy: 4,4-dimetil-2,2-bipiridil) kompleksinin statik $\langle\beta\rangle$ değeri $62.498x10^{-30}$ esu, frekansa-bağlı $\langle\beta\rangle$ değeri 11.448×10^{-30} esu, $\langle\gamma\rangle$ değeri ise statik olarak 387.88×10^{-36} esu ve frekansa-bağlı durumda 680.035×10^{-36} esu olarak hesaplanmıştır. Bu değerler, klasik NLO referans moleküllerini aşmakta olup, bu kompleksin ikinci ve üçüncü mertebe NLO uygulamalarda yüksek verimlilikle kullanılabileceğini göstermektedir.

Cu(II) kompleksleri ise hem $\langle\beta\rangle$ hem de $\langle\gamma\rangle$ parametreleri açısından kaydadeğer seviyede yanıtlar vererek, çeşitli NLO uygulamalarında kullanım potansiyelinin olduğu sonucuna varılmıştır. $[Cu(6Clpca)_2]$ (6Clpca:6-kloropiridin-2-karboksilik asit) kompleksinde $\langle\beta\rangle$ parametresi 10.40×10^{-30} esu, $\langle\gamma\rangle$ parametresi 4.0259×10^{-36} esu olarak belirlenmiştir. Zn(II) ve Co(II) komplekslerinin ise nispeten düşük NLO parametreleri sergilemesine rağmen, $[Co(4Clpca)_2(H_2O)_2]$ kompleksinde 532 nm de hesaplanmış gamma $\langle\gamma\rangle$ değerinin 433.93×10^{-36} esu gibi yüksek çıkması, kristal simetrisi ve orbital düzenlemelerin ikinci mertebe yüksek kutuplanabilirlik etkisini göstermektedir. $[Zn(4Clpca)(3OHpca)(H_2O)_2]$(4Clpca:4kloropiridin-2-karboksilik asit, 3OHpca: 3-hidroksipiridin-2-karboksilik asit) kompleksininn statik $\langle\beta\rangle$ değeri 4.5200×10^{-30} esu olarak hesaplanırken frekansa bağlı $\langle\beta\rangle$ değeri 4.720×10^{-30} olarak hesaplanmıştır. Aynı şekilde statik ve frekansa bağlı $\langle\gamma\rangle$ değerleri ise sırasıyla 39.106×10^{-36} esu ve 2258.9×10^{-36} olarak hesaplanmıştır. Tüm bu hesaplama sonucunda beta değeri frekansa bağlı değerinden yüksel çıkarken $\langle\gamma\rangle$ değeri frekasnı bağlı hesaplamalarda daha yüksek olarak elde edilmiştir. Bu da bize merkezi simetrik yapılarda beta değeri düşük çıkarken gamma değerinin merkezi simetrik yapıya bağlı olmadığını göstermektedir

Ayrıca, kararlı kristal sistemleri ile gözlemlenen yüksek NLO yanıtlar arasındaki ilişki, ligand-metal koordinasyonlarının düzenlemesiyle yakından ilişkilendirilmiştir. Özellikle, $[Mn(6Brpca)_2(Dmdpy)]\cdot CH_3OH$,$[Zn(3OHpca)(4Clpca)_2.H_2O]$ ve $[Cu(6Fpca)_2(H_2O)]$ komplekslerinde elde edilen yüksek $\langle\beta\rangle$ ve $\langle\gamma\rangle$ değerleri, bu tür yapıların NLO uygulamalarda aktif bileşen olarak kullanılabileceğine işaret etmektedir. Bu bulgu, gelecekteki çalışmalarda mantıklı ligand seçimi aşamasında,

geçiş metalinin spin durumu ve ligand geometrisinin eş zamanlı değerlendirilmesini öneren bir yaklaşımı desteklemektedir.

Sonuç olarak, bu tez çalışmasıyla, piridin-2-karboksilik asit türevleri ve Zn(II), Co(II), Mn(II) ve Cu(II) geçiş metallerini içeren metal-organik koordinasyon bileşiklerinin yalnızca kordinasyon kimyası açısından değil, aynı zamanda fonksiyonel malzeme geliştirme açısından da ele alındığı, disiplinler arası bir yaklaşımı benimseyerek ilerleyen bir çalışmadır. Bu sonuçlar ele alındığında komplekslerin, ligand seçimi, metal iyonu seçimi, koordinasyon geometrisi ve metal iyonun spin durumu gibi anahtar seçimlerin dikkatli yapılmasıyla, elde edilen kompleks bileşiklerin ileri düzeyde optik özelliklere sahip olabileceği kanıtlanmıştır. Bu kompleksler, özellikle ikinci ve üçüncü mertebe NLO uygulamaları için umut vaat etmektedir. Bu bulgular, gelecekte ileri moleküler tasarımların gerçekleştirilmesi ve yüksek performanslı özellikle elektronik, lazer teknolojileri, veri depolama sistemleri ve fotonik anahtarlama gibi alanlarda yeni nesil NLO materyallerin geliştirilmesine bilimsel katkı sağlayacağı düşünülmektedir.

SYNTHESIS, STRUCTURAL SPECTROSCOPIC AND NONLINEAR OPTICAL PROPERTIES OF NEW METALLIC COMPLEXES CONTAINING PYRIDINE-2-CARBOXYLIC ACID DERIVATIVES

SUMMARY

This thesis focuses on the synthesis of transition metal complexes containing pyridine-2-carboxylic acid derivatives and detailed investigation of the structural, electronic and nonlinear optical (NLO) properties of the obtained complexes. The fact that all the obtained metal-organic coordination compounds were synthesized for the first time and the above-mentioned studies were carried out for the first time for these complexes reflects the originality of this thesis work. In particular, the limited number of studies in the literature on transition metal complexes containing both pyridine-2-carboxylic acid derivatives and secondary neutral ligands indicates that the present study is an important study that contributes to the search for new materials with effective NLO properties. The combination of electron donating and withdrawing groups in the ligand structures is aimed to strengthen intermolecular interactions and improve optoelectronic properties. In this context, the structural, electronic and optical properties of new complexes formed with Zn(II), Cu(II), Co(II) and Mn(II) transition metal ions were investigated in detail by experimental and theoretical methods.

The analysis of the crystal structures was not limited to the determination of the atomic coordinations, but also considered the effects of these coordinations on the electronic transitions. The geometrical parameters obtained from X-ray diffraction data were compared with the theoretical results obtained by the density functional theory (DFT) method to test the efficiency of the DFT method on these complexes. The integrated use of both experimental and theoretical methodologies in this study will provide researchers with insights on important points such as density functional, basis set and spin state during the theoretical investigation of new complexes with similar structures. In this context, $[Cu(6Fpca)_2(H_2O)]$ and $[Zn(6Clpca)_2(H_2O)_2]$ complexes have distorted octahedral; [Mn(6Brpca)2 (Dmdpy)].CH3OH and $[Zn(4Clpca)(3OHpca)(H_2O)_2]$ complexes exhibit distorted octahedral; $[Co(4Clpca)_2(H_2O)_2]$ and $[Cu(6Clpca)_2(H_2O)_2]$ complexes exhibit tetragonal pyramidal coordination geometry.

FT-IR data played an important role in determining the coordination patterns of the carboxylate groups. O-H stretching vibrations were observed in the range of 3188-3449 cm^{-1}, while the Δν values between the asymmetric and symmetric vibrations of COO- groups ranged between 318-473 cm^{-1}, supporting the single-toothed bonding via the carboxylate atom in the pyridine ring. Moreover, the shift of the pyridine ring fading vibrations in the range of 986-1036 cm^{-1} confirms that the ligands have an effective electronic interaction with the metal centers and metal covalent bonding via the N atom in the pyridine ring.

Considering UV-Vis studies, the ligand-metal charge transfer (LMCT) bands observed in the 300-400 nm range, especially in Cu(II) and Mn(II) complexes, play a critical role in understanding the photophysical and nonlinear optical characters of the

complexes. For example, in the [Mn(6Brpca)$_2$(Dmdpy)].CH3OH complex, intra-ligand π→π* and n→π* transitions were detected at 206, 225, 263 and 275.6 nm. Similarly, π→π* intra-ligand charge transitions at 263 nm and LMCT transitions at 369 nm were reported in the [Cu(6Fpca)$_2$(H$_2$O)] complex.

In the study, quantum chemical calculations were also performed to confirm the experimental results and the electronic properties of the molecules were evaluated in detail by TD-DFT, boundary molecular orbital analysis and natural bond orbital (NBO) calculations. Through these analyses, properties such as charge distribution within the complex, electronic structure stability of the complexes and high-energy conjugative interactions within the complex were investigated in detail and the relationship between the NLO properties was explained. Among the HOMO-LUMO energy differences, the lowest value was determined to belong to the [Mn(6Brpca)$_2$ (Dmdpy)]-CH3OH complex (2.425 eV), while the highest difference was calculated for the [Zn(6Clpca) $_2$(H$_2$O)$_2$] complex (4.640 eV). Significant correlations were obtained between these energy differences and NLO parameters.

In the theoretical part of the thesis, quantum chemical calculations carried out by DFT and TD-DFT methods provided important data on the electronic structures and NLO potentials of the complexes. In particular, the static <β> value of the ncomplex [Mn(6Brpca)$_2$(Dmdpy)].CH3OH (6Brpca: 6-bromopyridine-2-carboxylic acid, Dmdpy: 4,4-dimethyl-2,2-bipyridyl carboxylic acid) is 62. 498×10^{-30} esu, the frequency-dependent <β> value was calculated as 11.448×10^{-30} esu, and the <γ> value was calculated as 387.88×10^{-36} esu statically and 680.035×10^{-36} esu in the frequency-dependent case. These values exceed the classical NLO reference molecules and indicate that this complex can be used with high efficiency in second and third order NLO applications.

The Cu(II) complexes gave remarkable responses in terms of both <β> and <γ> parameters, suggesting their potential for use in various NLO applications. In the [Cu(6Clpca)$_2$(H$_2$O)] (6Clpca: 6-chloropyridine-2-carboxylic acid) complex, the <β> parameter was determined as 10.40 ×10^{-30} esu and the <γ> parameter was determined as 4.0259×10^{-36} esu. Although Zn(II) and Co(II) complexes exhibit relatively low NLO parameters, the gamma <γ> value calculated at 532 nm in the [Co(4Clpca)$_2$(H$_2$O)$_2$] complex is as high as 433.93×10^{-36} esu, indicating the second-order high polarizability effect of crystal symmetry and orbital arrangements. The static <β> value of the [Zn(4Clpca)(3OHpca)(H$_2$O)$_2$] (4Clpca: 4-chloropyridine-2-carboxylic acid, 3OHpca: 3-hydroxypyridine-2-carboxylic acid) complex was calculated as 4.5200×10^{-30} esu while the frequency dependent <β> value was calculated as 4.720×10^{-30}. Similarly, static and frequency-dependent <γ> values were calculated as 39.106×10^{-36} esu and 2258.9×10^{-36}, respectively. As a result of all these calculations, the beta value is higher than its frequency dependent value, while the <γ> value is higher in frequency dependent calculations. This shows us that while the beta value is low in centrally symmetric structures, the gamma value does not depend on the centrally symmetric structure.

Moreover, the relationship between the stable crystal systems and the observed high NLO responses was closely related to the arrangement of ligand-metal coordinations. In particular, the high <β> and <γ> values obtained in [Mn(6Brpca)$_2$(Dmdpy)]-CH3OH, [Zn(3OHpca)(4Clpca)$_2$.H$_2$O] and [Cu(6Fpca)$_2$(H$_2$O)] complexes indicate that such structures can be used as active components in NLO applications. This finding supports an approach that suggests simultaneous evaluation of the spin state of

the transition metal and the ligand geometry in the logical ligand selection step in future studies.

In conclusion, this thesis is an interdisciplinary study in which metal-organic coordination compounds containing pyridine-2-carboxylic acid derivatives and the transition metals Zn(II), Co(II), Mn(II) and Cu(II) have been investigated not only in terms of coordination chemistry but also in terms of functional materials development. These results prove that the complexes obtained can have advanced optical properties if key choices such as ligand selection, metal ion selection, coordination geometry and spin state of the metal ion are made carefully. These complexes are particularly promising for second and third order NLO applications. These findings are expected to contribute scientifically to the realization of advanced molecular designs in the future and the development of next generation NLO materials with high performance, especially in areas such as electronics, laser technologies, data storage systems and photonic switching.

1. GİRİŞ

Günümüzde gelişen fotonik ve optoelektronik uygulamalarda, lazer tabanlı sistemler, elektro-optik modülatörler ve bütünleşmiş fotonik devreler gibi yüksek hassasiyet gerektiren alanlar için ileri düzey nonlineer optik (NLO) özellikler sergileyen yeni malzeme türlerine duyulan ihtiyaç giderek artmaktadır. NLO aktif materyaller, elektromanyetik radyasyona doğrusal olmayan yanıt oluşturarak; ikinci harmonik üretimi (SHG), frekans dönüştürme, optik karıştırma ve iki foton soğurma gibi birçok karmaşık optik olayın temel bileşeni haline gelmiştir[1, 2]. Bu doğrultuda hem moleküler yapı hem de elektronik özellik bakımından çeşitlilik gösteren organik, inorganik ve metal-organik türlerin NLO potansiyelleri son yıllarda yoğun biçimde incelenmekte ve yeni nesil fonksiyonel optik materyallerin tasarımı hedeflenmektedir.

Organik bileşikler, geniş π-konjuge sistemleri ve donör-akseptör (D-A) yapılarındaki elektron transfer kapasitesi sayesinde genellikle yüksek birinci mertebe yüksek kutuplanabilirlik (β) değerleri sergilemektedir. Bu moleküllerin yapısal olarak kolayca türevlendirilebilir olmaları, düşük üretim maliyetleri ve hızlı optik yanıt süreleri gibi önemli avantajları bulunurken; termal ve fotokimyasal kararlılıklarının düşüklüğü, çevresel koşullara duyarlılıkları ve kristal elde edilme zorlukları başlıca sınırlayıcı faktörler arasında yer almaktadır[3, 4].

Bunun tersine, inorganik kristaller (örneğin lityum niobat-$LiNbO_3$, potasyum dihidrojen fosfat-KDP, beta-baryum borat-BBO) yüksek optik şeffaflık, geniş optik band aralığı ve kristal kararlılığı gibi üstün fiziksel özellikleri sayesinde özellikle endüstriyel lazer uygulamalarında ön plana çıkmaktadır. Ancak, bu kristallerin yüksek sentez maliyetleri ve moleküler düzeyde ayarlanabilirliğe imkân vermemeleri gibi dezavantajları söz konusudur [5, 6].

Bu eksikliklerin giderilmesi amacıyla, organik ve inorganik bileşenlerin özelliklerini birleştiren hibrit yapılar olan metal-organik koordinasyon kompleksleri öne çıkmaktadır. Bu hibrit sistemler, organik ligandların konjuge elektron yapıları ile geçiş metallerinin redoks özelliklerini bir araya getirerek; geniş polarizabilite, yüksek hiperpolarizabilite ve etkin yük aktarımı gibi NLO özelliklerin ayarlanması açısından

kritik parametrelerin optimize edilmesini mümkün kılmaktadır. Ayrıca, bu yapılarda gözlemlenen ligand→metal (LMCT), metal→ligand (MLCT) ve metal→metal (MMCT) türü yük transferleri, ışıkla etkileşim süreçlerini güçlendirerek NLO yanıtlarını önemli ölçüde iyileştirmektedir. Söz konusu komplekslerin modüler yapısı sayesinde, farklı ligand-metal kombinasyonları kullanılarak elektronik özellikler moleküler düzeyde ayarlanabilir hale gelmiştir [7].

Tamer ve arkadaşlarının 2018 yılında yaptıkları çalışmada, piridin-2-karboksilik asit (pca) ve onun iki türevi olan 4-klorpiridin-2-karboksilik asit (4Clpca) ile 4-metoksipiridin-2-karboksilik asit (4MeOpca) moleküllerinin birinci mertebe doğrusal olmayan optik (NLO) tepkimeleri, yoğunluk fonksiyonel teorisi (DFT) yöntemiyle hesaplanarak karşılaştırmalı olarak analiz edilmiştir (Şekil 1.1). Elde edilen sonuçlara göre, NLO parametrelerinin büyüklük sıralaması şu şekilde belirlenmiştir: pca< 4MeOpca<4Clpca. Bu bulgular, molekül üzerine yerleştirilen elektron verici veya çekici grupların, elektronik yapıyı yeniden düzenleyerek molekülün doğrusal olmayan optik yanıtlarını artırabildiğini göstermektedir. Özellikle bu tür sübstitüentlerin, sistemin kutuplanabilirliğini ve yük dağılımını değiştirerek NLO özelliklerde anlamlı iyileştirmeler sağladığı ifade edilmiştir[8].

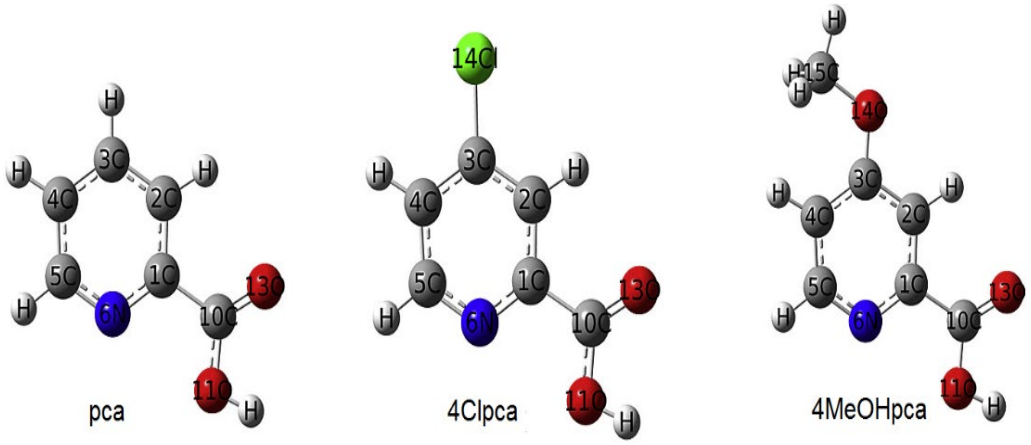

Şekil 1.1. Piridin-2-karboksilik asit (pca), 4-kloro-piridin-2-karboksilik asit (4Clpca) ve 4-metoksi-piridin-2-karboksilik asit (4MeOpca)

Manjunatha ve arkadaşları (2019) tarafından rapor edilen çalışmada, N,N'-o-fenilenbis(4-hidroksisalisilidenimin) (L) adlı Schiff bazı ligandı ve bu ligandın nikel ve kobalt içeren metal-organik kompleksleri doğrusal olmayan optik (NLO) özellikler bakımından detaylı bir şekilde araştırılmıştır. Çalışmada, Z-tarama yöntemi kullanılarak elde edilen sonuçlar, söz konusu komplekslerin 10^{-11} esu mertebesinde

önemli büyüklükte doğrusal olmayan kırılma indisine (n_2) sahip olduğunu ortaya koymuştur. Serbest ligand ile karşılaştırıldığında, kompleks yapılarının daha yüksek NLO yanıtı verdiği görülmüş; bu durum, ligand ile metal merkezi arasındaki etkin yük delokalizasyonuna bağlanmıştır. Ayrıca, nanosaniyelik lazer darbeleri altında gerçekleştirilen optik sınırlandırma testlerinde, komplekslerin dikkat çekici optik sınırlayıcı davranış sergilediği belirlenmiştir. Bu doğrusal olmama özelliklerinin temelinde, uygulanan elektrik alanın etkisiyle elektron bulutunda meydana gelen yer değiştirme ve buna bağlı yük transferi mekanizmalarının yattığı ifade edilmiştir. Artan NLO etkinliğinin potansiyel nedenleri arasında, özellikle merkezdeki metal atomunun delokalizasyon kapasitesini artırması ve -OH grubu içeren fenil halkasının metalle oluşturduğu donör-akseptör etkileşimlerinin katkısı ön plana çıkmaktadır (Şekil 1.2)[9].

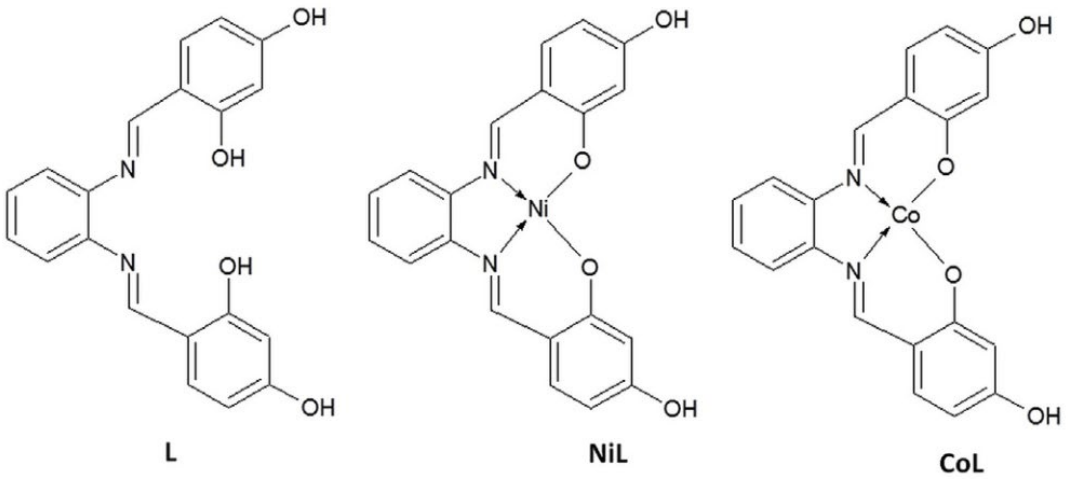

Şekil 1.2. N,N'-o-fenilenbis(4-hidroksisalisilidenimin) (L), Nikel (NiL) ve Kobalt (CoL) metal-organik komplekslerinin moleküler yapısı

Narendran ve çalışma arkadaşları 2015 yılında yaptıkları çalışmada, Şekil 2.7'de yapısı sunulan mezo-tetrakis(2,3,5,6-tetrafloro-N,N-dimetil-4-anilinil) porfirin ve bu bileşiğin nikel, kobalt, bakır ve çinko içeren metal komplekslerinin üçüncü dereceden doğrusal olmayan optik (NLO) parametrelerini Z-tarama tekniğiyle inceleyen deneysel bir araştırma gerçekleştirmiştir. Bu tür metaloporfirin bileşikleri, sahip oldukları üstün optik sınırlama davranışları sayesinde lazer güvenliği, optik sensör koruması ve fotonik cihazlar gibi teknolojik alanlarda dikkat çekici potansiyele sahiptir. Çalışmada elde edilen bulgular, porfirin halkasına metal iyonlarının koordinasyonu ile elektron çekici grupların molekül üzerinde bulunmasının, π-π

istiflenme eğilimini artırarak moleküller arası etkileşimleri güçlendirdiğini ve böylece doğrusal olmayan optik tepkileri anlamlı şekilde iyileştirdiğini ortaya koymaktadır. Bu bağlamda, hem elektron verici (N, N-dimetil amino) hem de elektron çekici sübstitüentler taşıyan metaloporfirin türevlerinin moleküler tasarımı, NLO performanslarını artırmak amacıyla rasyonel olarak değerlendirilmiştir. Deneysel olarak elde edilen NLO parametreleri, metalasyonun sistemin optoelektronik özellikleri üzerinde belirleyici rol oynadığını açıkça göstermiştir. Özellikle +2 oksidasyon durumuna sahip olan ve farklı d-kabuğu elektron yapılarına sahip geçiş metalleri seçilmiştir. Bu bağlamda, d-kabuğundaki elektron doluluğunun artmasıyla birlikte doğrusal olmayan optik yanıtların da paralel bir şekilde arttığı gözlemlenmiştir. Çalışmada, β ve üçüncü dereceden doğrusal olmayan optik geçirgenlik katsayısı olan $\chi^{(3)}$ parametrelerinin, merkezi metal iyonunun d-kabuğundaki elektron konfigürasyonuna bağlı olarak sistematik biçimde değiştiği rapor edilmiştir. Özellikle çinko içeren porfirin kompleksleri, kapalı kabuk yapıları, daha uzun uyarılmış durum ömürleri ve daha geniş π-elektron delokalizasyonu özellikleri sayesinde, açık kabuklu metal iyonlarıyla oluşturulan komplekslere kıyasla daha belirgin NLO davranışı sergilemiştir. Bu durum, çinko porfirinlerin doğrusal olmayan optik uygulamalar için özel bir öneme sahip olabileceğini ortaya koymaktadır (Şekil 1.3) [10].

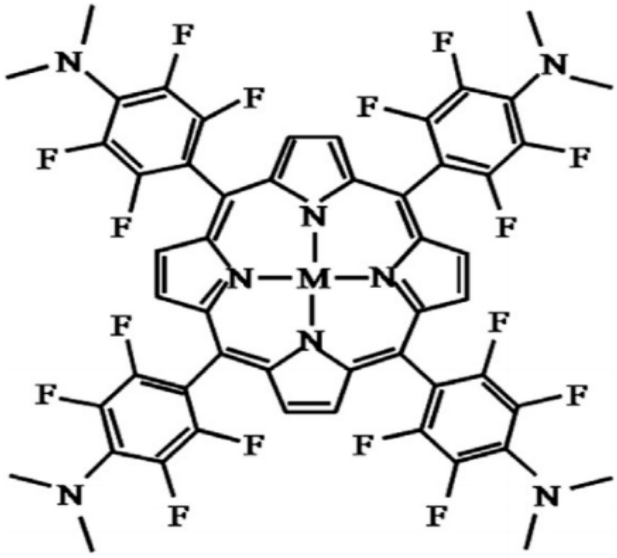

Şekil 1.3. Nikel, kobalt, bakır ve çinko içeren mezo-tetrakis(2,3,5,6-tetrafluoro-N, N-dimetil-4-anilinil) porfirin kompleksleri

Piridin türevi karboksilik asitler, yapılarında bulunan azot (N) ve oksijen (O) donor atomları sayesinde koordinatif olarak çift fonksiyonlu ligand davranışı sergileyerek, geçiş metalleriyle çeşitli koordinasyon modlarında kompleksleşme yeteneğine sahiptir. Bu tür ligandlar, oluşturdukları koordinasyon bileşikleriyle yalnızca geometrik çeşitlilik açısından zengin yapılar sunmakla kalmaz, aynı zamanda doğrusal olmayan optik (NLO) özellikler, lüminesans, paramanyetik davranış, iyon değişim kabiliyeti ve heterojen kataliz gibi çok sayıda ileri düzey teknolojik uygulama alanına katkı sağlayabilecek potansiyel fonksiyonel materyallerin geliştirilmesine de olanak tanır [11, 12]. Özellikle piridin halkasına bağlı karboksil gruplarının elektron yoğunluğu üzerindeki etkisi, ligandın metal iyonları ile gerçekleştirdiği koordinatif bağların seçiciliğini ve yönlendirilmişliğini önemli ölçüde belirler.

N ve O donor bölgelerinin varlığı sayesinde bu ligandlar, mono-, bi- ve polinükleer metal kompleksleri oluşturarak çok sayıda farklı bağlanma geometrisi sergileyebilir. Bu çeşitlilik, onların kristal mühendisliği, supramoleküler mimari ve fotonik malzeme sentezi gibi disiplinlerde temel yapı taşları olarak değerlendirilmesini mümkün kılar [13, 14]. Ayrıca, piridinkarboksilik asitlerin geçiş metalleriyle oluşturduğu kompleksler, ligand içi π–π^* geçişlere ek olarak, liganddan metale yük transferi (LMCT), metalden liganda yük transferi (MLCT) ve metalden metale yük transferi (MLCT) gibi elektronik süreçleri destekleyerek geniş bir optoelektronik spektruma sahiptir. Bu durum, söz konusu komplekslerin NLO materyalleri olarak kullanılabilirliğini önemli ölçüde artırmaktadır[7, 15].

Bununla birlikte, bu ligandların fizikokimyasal davranışları, bağlandıkları metal merkezinin koordinasyon çevresi, çözücü ortamın doğası, pH seviyesi, sıcaklık koşulları ve varsa ikincil ligandların varlığı gibi çevresel parametrelerden doğrudan etkilenmektedir. Bu faktörlerin elektronik yapı üzerinde oluşturduğu değişiklikler sayesinde, sistemin NLO cevabı moleküler düzeyde optimize edilebilmektedir[16]

1.1. Karboksilik Asitler

Karboksilik asitler, organik kimyada yaygın olarak karşılaşılan ve karakteristik olarak -COOH fonksiyonel grubunu taşıyan bileşiklerdir. Bu grup, bir karbonil (C=O) ve bir hidroksil (-OH) fonksiyonunun aynı karbon atomuna bağlanmasıyla oluşur. Moleküler düzeyde R-COOH genel formülüyle gösterilen bu bileşiklerde “R” grubu, genellikle alifatik zincirler, aromatik halkalar ya da heterosiklik yapılar şeklinde çeşitlenebilir.

Karboksilik asitler hem doğada bol miktarda bulunmakta hem de canlı organizmalarda metabolik süreçlerin düzenlenmesinde işlevsel roller üstlenmektedir[17].

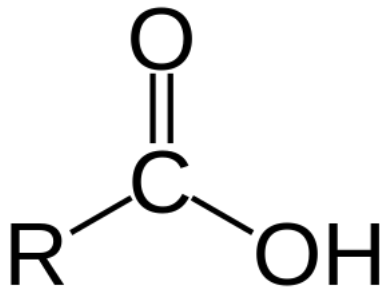

Şekil 1.4. Karboksilik asit fonksiyonel grubunun genel yapısı

Bu bileşik sınıfı, kimya endüstrisinde de önemli yer tutmakta olup; çeşitli sentez yollarında başlangıç maddesi, ara ürün ya da son ürün olarak geniş uygulama alanına sahiptir. Asidik özellikleri, karboksil grubunun su ortamında proton (H^+) verme eğilimine dayanmaktadır. Bu süreç sonucunda piridin-2-karboksilik asit anyonu ($R\text{-}COO^-$) oluşur ve bu anyonik form, metal iyonları ile güçlü koordinatif bağlar kurabilme kapasitesine sahiptir. Böylece, karboksilik asitler geçiş metalleriyle kompleks oluşturabilen değerli ligandlar haline gelir[18].

Karboksil grubunun hem proton transferine uygun yapısı hem de oksijen atomları üzerinde bulunan eşleşmemiş elektron çiftleri aracılığıyla koordinasyon yeteneği, bu bileşiklere çift işlevli kimyasal karakter kazandırmaktadır. Bu yönüyle karboksilik asitler yalnızca organik sentez tepkimelerinde değil, aynı zamanda koordinasyon kimyasında da temel bileşenler olarak öne çıkmaktadır. Özellikle geçiş metalleriyle oluşturdukları kompleksler, katalitik sistemlerde, ilaç kimyasında öncül yapı olarak, iyon değiştirici materyallerin üretiminde ve doğrusal olmayan optik (NLO) özellik gösteren yeni nesil malzemelerin araştırılması ve tasarımında yaygın olarak kullanılmaktadır[16, 19].

1.1.1. 2-piridinkarboksilik asit

Piridin-2-karboksilik asit (pikolinik asit) [20, 21], yapısal olarak piridin halkasına doğrudan bağlı bir karboksil grubu içeren heteroaromatik bir moleküldür. Bu bileşik hem aromatik azot atomunun hem de karboksil grubundaki oksijen atomlarının elektron donör özellikleri sayesinde, geçiş metalleri ile güçlü koordinatif bağlar kurabilen bifonksiyonel bir ligand görevi görür. Bu özellikleri dolayısıyla pikolinik

asit, özellikle biyoinorganik kimya ve koordinasyon kimyasında kompleks yapıların oluşturulmasında sıklıkla tercih edilmektedir[19]. Piridin halkasının planarlığı ve elektron dağılımındaki aromatik özellikler, karboksil grubunun asidik doğasıyla birlikte ligandın toplam elektronik karakterini ve metal iyonlarına olan afinite düzeyini etkilemektedir[13].

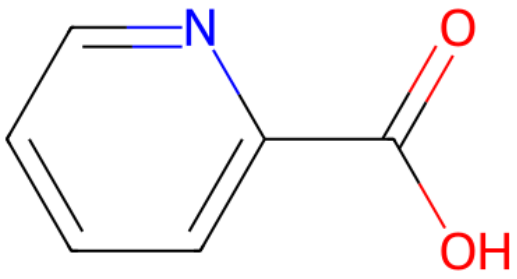

Şekil 1.5. Piridin-2-karboksilik asit molekülünün yapısı ($C_6H_5NO_2$)

Ayrıca piridin-2-karboksilik asit, biyolojik sistemlerde doğal olarak bulunmakta olup; metalloprotein yapılarında, enzimatik reaksiyonlarda ve metal iyonlarının biyolojik taşınımında rol alan yapılarla benzerlik gösteren moleküler modellerin geliştirilmesinde de kullanılmaktadır[7, 22, 23]. Bu yönüyle, piridin-2-karboksilik asit yalnızca teknolojik değil, aynı zamanda biyomedikal açıdan da işlevsel ve stratejik öneme sahip bir ligand türü olarak öne çıkmaktadır.

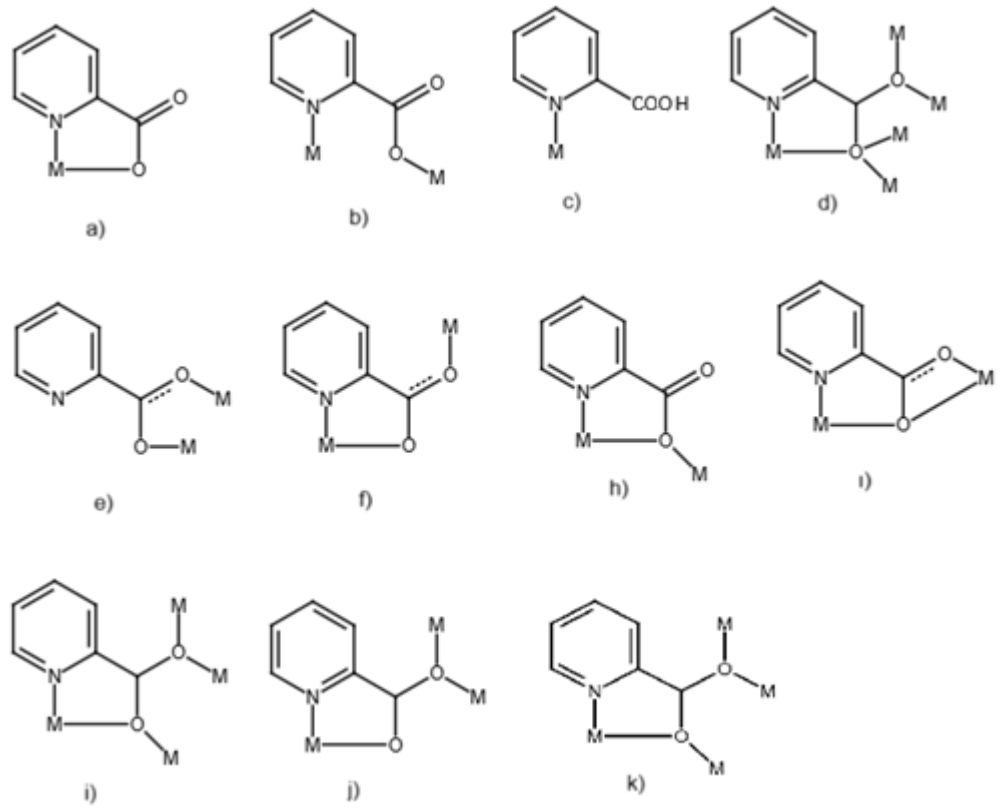

Şekil 1.6. Piridin-2-karboksilik asit ligandının metal iyonlarına bağlanma modları [24].

Piridin-2-karboksilik asit metal iyonlarına karşı sergilediği bağlanma davranışı, molekülün hem tek dişli- hem de iki dişli bir ligand olarak görev alabilmesini mümkün kılmakta, bu da oluşturulan koordinasyon komplekslerinin geometri ve simetrisinde önemli bir esneklik sağlamaktadır[14]. Karboksil grubunun proton verme kabiliyeti ve piridin azotunun eşlenmemiş elektronu, ligandın metal merkezlerine kararlı bağlar yapmasına olanak tanır[7]. Nitekim literatürde yer alan çalışmalarda, Cu (II), Mn (II) ve Co (II) iyonları ile oluşturulan piridin2-karboksilik asitkomplekslerinin birinci mertebe yüksek kutuplanabilirlik (β) değerlerine sahip olduğu ve HOMO-LUMO enerji boşluklarının dar olduğu belirlenmiştir[15, 16]. Bu elektronik özellikler, bu tür komplekslerin özellikle ikinci harmonik üretimi (SHG) gibi NLO (nonlineer optik) uygulamalarda değerlendirilebileceğini göstermektedir.

Ayrıca piridin-2-karboksilik asit, biyolojik sistemlerde doğal olarak bulunmakta olup; metalloprotein yapılarında, enzimatik reaksiyonlarda ve metal iyonlarının biyolojik taşınımında rol alan yapılarla benzerlik gösteren moleküler modellerin geliştirilmesinde de kullanılmaktadır [7, 19, 20]. Bu yönüyle, piridin-2-karboksilik asit

yalnızca teknolojik değil, aynı zamanda biyomedikal açıdan da işlevsel ve stratejik öneme sahip bir ligand türü olarak öne çıkmaktadır.

İncelenen literatür çalışmalarından yola çıkıldığında piridin karboksilik asit ve türevlerinin koordinasyon geometrisine daha yatkın olan yapısı sayesinde optik özelliklerinde iyi sonuçlar verileceği düşünülmüştür.

Karboksilik asit ligand türevlerinin metal komplkeslerine etkisini ve NLO etkisini detaylı olarak araştırmak için 6-bromopiridin-2-karboksilik asit (6Brpca), 6-floropiridin-2-karboksilik asit (6Fpca), 6-kloropiridin-2-karboksilik asit (6Clpca), 4-kloropiridin-2-karboksilik asit (4Clpca), 3,5-floropiridin-2-karboksilik asit (3,5Fpca) ve 4,4-dimetilpiridin-2-karboksilik asit (Dmdpy). Tüm bu detaylı bilgilendirmelerden yola çıkarak yapılan bu doktora tez çalışmasının amacı, piridin-2-karboksilik asit türevli ligandlar ile Zn(II), Cu(II), Co(II) ve Mn(II) geçiş metalleri arasında oluşan metal-organik komplekslerin sentezini gerçekleştirerek, bu yapıların kristalografik, spektroskopik ve teorik özelliklerini kapsamlı bir şekilde incelemek; özellikle doğrusal olmayan optik (NLO) performanslarını detaylı olarak değerlendirmektir. Çalışma kapsamında, ayrıca ligand yapısında yer alan halojen atomları (F, Cl, Br, I) ve elektronik etkili fonksiyonel grupların (-OCH_3, -OH vb.) komplekslerin yapısal ve elektronik özellikleri üzerindeki etkileri sistematik biçimde araştırılmıştır.

Bir diğer önemli boyut olarak, komplekslerin yapısal ve elektronik ortamını etkileyebilecek ikincil nötral ligandların katkısı da incelenmiştir. Bu tür ligandların koordinasyon geometrisi, elektron yoğunluğu dağılımı ve moleküler kutuplanabilirlik üzerindeki etkileri; tek kristal X-ışını kırınımı, FT-IR, UV-Vis spektroskopisi ve DFT-B3LYP/LanL2DZ düzeyindeki kuantum kimyasal hesaplamalarla değerlendirilmiştir. Hesaplamalar, HOMO–LUMO enerji seviyeleri, birinci mertebe yüksek kutuplanabilirlik (<β>) ve İkinci mertebe yüksek kutuplanabilirlik (<γ>) gibi temel NLO parametrelerinin belirlenmesine olanak sağlamıştır.

Bu çalışmayla hem ligand üzerindeki kimyasal modifikasyonların hem de ikincil nötral ligand varlığının komplekslerin NLO etkinliklerine katkısı açıkça ortaya konarak, NLO özelliklerin koordinasyon geometrisi, ligand alan etkisi ve elektron dağılımı ile nasıl ilişkili olduğu gösterilmiştir. Bu bağlamda tez, gelecekte optoelektronik, fotonik ve çok fotonlu uygulamalarda kullanılabilecek yeni nesil fonksiyonel materyallerin geliştirilmesine katkı sunmayı amaçlamaktadır.

2. LİTERATÜR ARAŞTIRMASI

Piridin-2-karboksilik asit ve türevlerine dayanan ligand sistemleri, koordinasyon kimyasında oldukça geniş bir uygulama yelpazesine sahiptir. Bu ligandların çeşitli metal iyonlarıyla oluşturduğu kompleksler genellikle $[M(C_5H_4COO)_2(H_2O)_n]$ genel formülüyle tanımlanmaktadır. Literatürde yer alan öncekiçalışmalar, piridin-2-karboksilik asit geçiş metalleriyle kompleksleşme eğilimini ortaya koymuştur. Bu kapsamda; mangan (Mn) [25], demir (Fe)[26], krom (Cr)[27], nikel (Ni)[28], bakır (Cu)[29], çinko (Zn)[30, 31], kadmiyum (Cd)[32], magnezyum (Mg)[33] ve cıva (Hg)[34] iyonlarıyla elde edilen pikolinat kompleksleri sentezlenmiş ve bu yapılar X-ışını kristalografi teknikleriyle detaylı olarak incelenmiştir. Bu çalışmalar, komplekslerin koordinasyon geometrilerini ve kristal örgü yapılarını aydınlatmak açısından önemli katkılar sağlamış; piridin-2-karboksilik asit çok yönlü bağlanma davranışının ortaya konmasına yardımcı olmuştur.

Huang ve arkadaşları tarafından 2004 yılında yürütülen bir diğer çalışmada, piridin-2-karboksilik asit ligandı içeren yeni bir manganez (Mn) kompleksi kristal ortamda başarıyla sentezlenmiştir (Şekil 2.1). Yapılan kristalografik analizler, kompleksin yapısal düzeni ve koordinasyon geometrisi hakkında ayrıntılı bilgiler sunmuş, bu tür bileşiklerin NLO ve koordinasyon kimyasası açısından önem taşıdığı vurgulanmıştır [35].

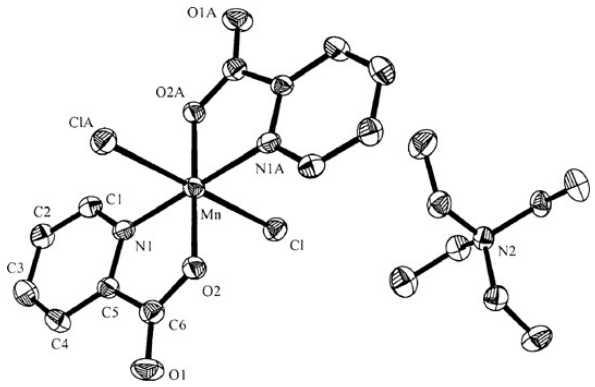

Şekil 2.1. Piridin-2-karboksilik asit ligandını içeren Mn(II) metal kompleksi

Heren ve arkadaşları 2006 yılında yaptıkları çalışmada, Mn(II) iyonu ile piridin-2-karboksilik asit arasında oluşan yeni bir polimerik koordinasyon düzenini tanımlamış

ve elde edilen yapının kristalografik özelliklerini detaylı bir şekilde rapor etmişlerdir. Çalışmada, kompleksin bağlanma modları ve termal kararlılığı da kapsamlı biçimde değerlendirilmiş, elde edilen üç boyutlu ağ yapısının yüksek yapısal stabilitesi sayesinde optoelektronik alanlarda potansiyel kullanım imkânı sunduğu ifade edilmiştir (Şekil 2.2) [36].

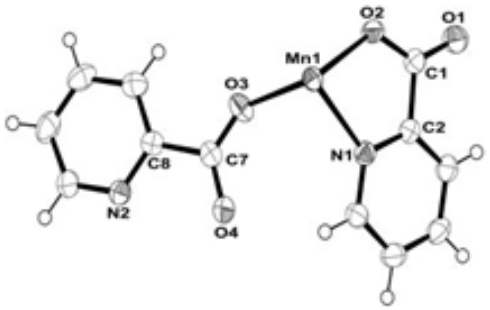

Şekil 2.2. Piridin-2-karboksilik asit ligandını içeren Mn(II) kompleksi

Öte yandan, Wu ve araştırma grubu (2005) tarafından gerçekleştirilen başka bir çalışmada, piridin-2-karboksilik asit ile Ni(II) iyonu arasında bir koordinasyon kompleksi sentezlenmiş ve bu kompleksin yapısal karakterizasyonu yapılmıştır. Analizler sonucunda, kompleksin merkezinde yer alan Ni(II) iyonunun bozulmuş oktahedral geometriye sahip bir koordinasyon küresi oluşturduğu belirlenmiştir (Şekil 2.3)[37].

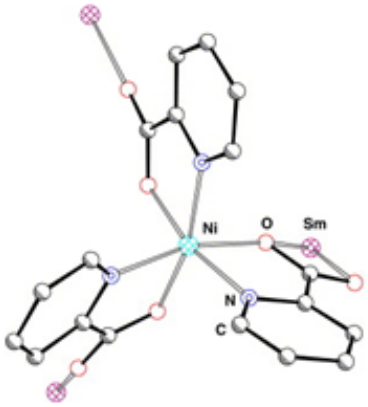

Şekil 2.3. $[SmNi(pic)_3(H_2O)_5]_n(ClO_4)_{2n}.3nH_2O$ komleksi (pic: Piridin-2-karboksilik asit)

Heren ve arkadaşları tarafından 2009 yılında gerçekleştirilen bir diğer çalışmada, piridin-2-karboksilik asit içeren ve iki farklı ligandı bünyesinde barındıran Cu(II) kristalleri başarıyla sentezlenmiştir. X-ışını kırınım yöntemi ile yapılan yapısal

analizler sonucunda, bu kristallerin de merkez metal çevresinde bozulmuş oktahedral geometrili bir yapı sergilediği ortaya konmuştur[36].

Novitskii ve çalışma arkadaşları tarafından 2009 yılında yürütülen araştırmada, demir (Fe) metal iyonu ile piridin karboksilik asit ve 4,4'-dimetil-2,2'-bipiridil olmak üzere iki farklı ligandın kullanıldığı yeni bir metal-organik kompleks sentezlenmiştir. Kristal yapısı detaylı olarak incelenen bu kompleksin, merkezdeki Fe(II) iyonunun bozulmuş oktahedral koordinasyon geometrisine sahip olduğu belirlenmiştir (Şekil 2.4)[38] .

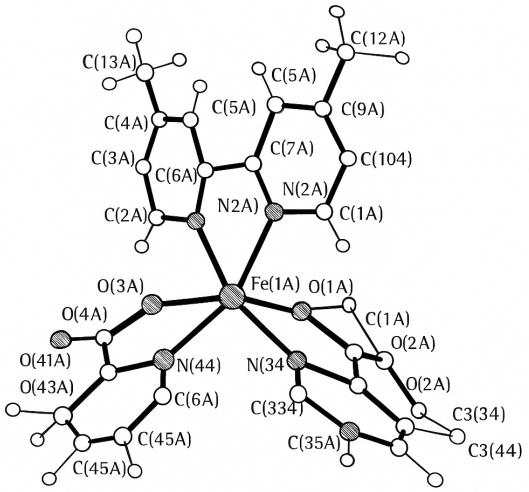

Şekil 2.4. [$FePc_2(Me_2Bipy)$] (Pc: Piridin 2-karboksilik asit ve Me_2Bipy:4,4'-dimetil-2,2'-bipiridil) kompleksi.

Wang ve arkadaşları de tarafından 2012 yılında yürütülen araştırmada, piridin-2-karboksilik asit ligandının bakır (Cu) metali ile kompleks oluşturma davranışı incelenmiştir. Bu çalışmada sentezlenen yeni metal-organik kompleksin kristal yapısı X-ışını kırınım yöntemiyle detaylı olarak karakterize edilmiştir. Araştırma sonuçlarına göre, ligand molekülü üzerindeki oksijen ve azot donor atomlarının Cu(II) metal iyonuna koordine olması sonucu, merkez atom çevresinde idealden sapmış bir oktahedral koordinasyon geometrisi oluştuğu belirlenmiştir (Şekil 2.5)[39].

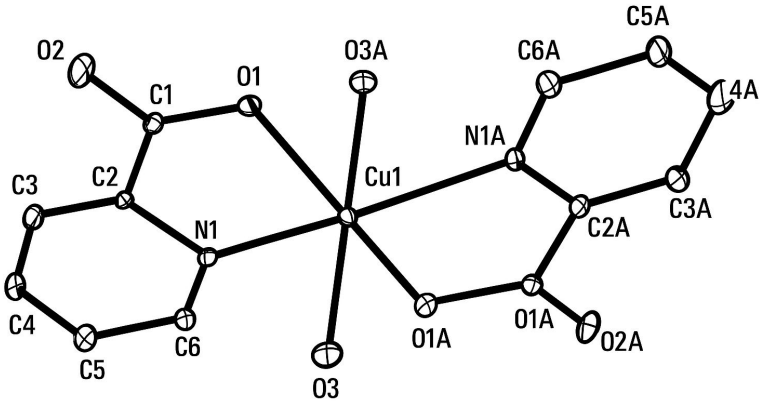

Şekil 2.5. $Cu(PC)_2 \cdot H_2O$ kompleksi (PC: piridin-2-karboksilik asit).

Ghadermazi ve çalışma arkadaşları 2012 yılında yürüttükleri araştırmada, piridin-2-karboksilik asit içeren yeni bir Mg(II) kompleksi sentezlenmiş ve bu kompleksin kristal yapısı X-ışını kırınım yöntemiyle detaylı olarak incelenmiştir. Yapısal analiz sonucunda, Mg(II) merkezli kompleksin bozulmuş bir oktahedral koordinasyon geometrisine sahip olduğu belirlenmiştir. Rapor edilen Mg kompleksinin kristal yapısı Şekil 2.6 de verilmiştir [40].

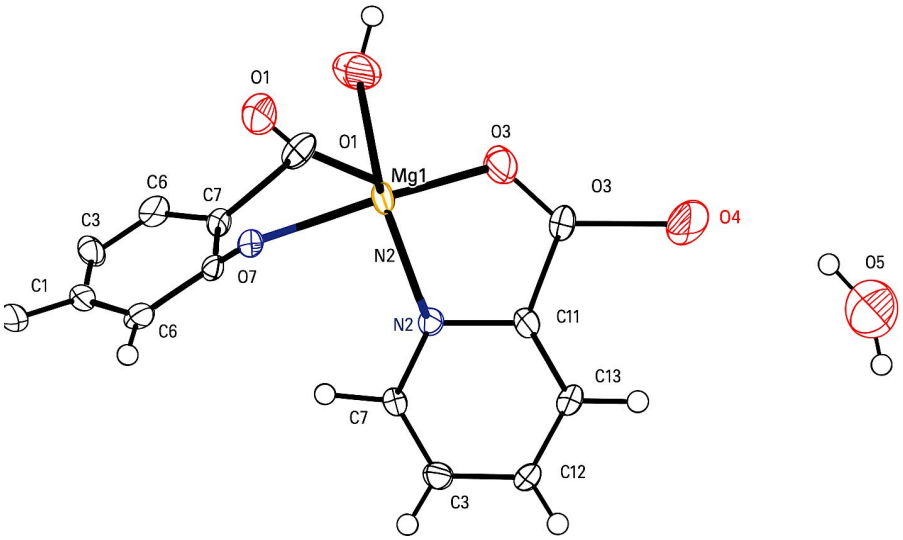

Şekil 2.6. $[Mg(pyc)_2(H_2O)_2] \cdot H_2O$ (pyc: piridin-2-karbokilik asit) kompleksi deneysel gösterimi

Wang ve çalışma arkadaşları 2012 yılında yaptıkları çalışmalarında ise, "Piridin-2-piridin-2-karboksilik asit içeren mononükleer bir bakır kompleksinin sentezi, kristal yapısı ve DNA'ya bağlanma özellikleri" başlıklı araştırmalarında, Cu (II) metal iyonu ile piridin-2-karboksilik asit ligandı arasında oluşan kompleksin sentezini

gerçekleştirmişlerdir (Şekil 2.7). Sentezlenen bu kompleksin kristalografik yapısı X-ışını kırınım (XRD) tekniği kullanılarak detaylı biçimde incelenmiş; ayrıca bileşiğin spektroskopik karakterizasyonu da yapılmıştır. Elde edilen sonuçlar, kompleksin UV bölgesindeki maksimum absorpsiyon zirvesinin artan miktarda DNA varlığında belirgin bir hipokromik ve batokromik etki gösterdiğini ortaya koydu ve düzlemsel $Cu(PC)_2 \cdot H_2O$ molekülünün DNA'nın baz çiftlerine yerleşebileceğini gösterdi [39].

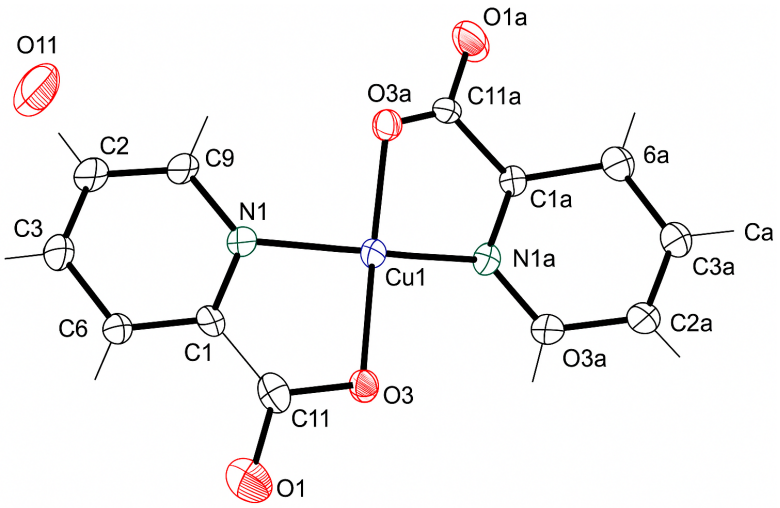

Şekil 2.7. $Cu(PC)_2 \cdot H_2O$ metal kompleksi (PC: piridin-2-karbokilik asit).

Li ve arkadaşları 2016 yılında yaptıkları çalışmalarında, oda sıcaklığında gerçekleştirdikleri katı-hâl sentezi yöntemiyle $[Cu(pic)_2].2H_2O$ formülüne sahip yeni bir bakır kompleksini elde etmişlerdir (Şekil 2.8). Araştırmada, kompleksin kristal yapısı X-ışını kırınım tekniği ile belirlenmiş; ayrıca FT-IR spektroskopisi ile fonksiyonel grupların karakterizasyonu ve termogravimetrik analiz ile termal bozunma davranışı detaylı biçimde incelenmiştir. Çalışma bulguları, kompleksin uzamış oktahedral koordinasyon geometrisine sahip olduğunu ve moleküller arası hidrojen bağları sayesinde iki boyutlu katmanlı bir yapı oluşturduğunu göstermiştir. Bu yapısal özelliklerin, metal-organik kompleks doğrusal olmayan optik (NLO) uygulamalarda değerlendirilebileceği önerilmiştir [41]

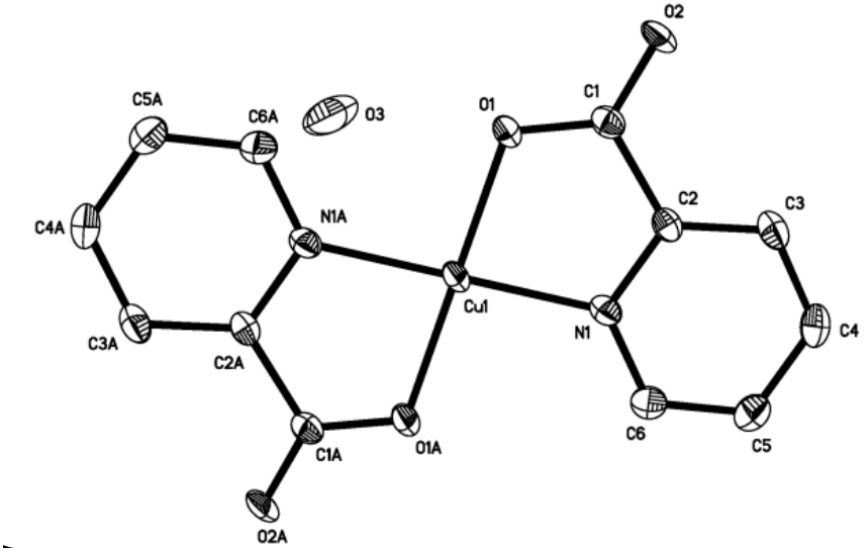

Şekil 2.8. $[Cu(pic)_2].2H_2O$ (pic: piridin-2-karbokilik asit) metal kompleksi

Celestine ve arkadaşları 2015 yılında yaptıkları çalışmalarında, piridin-2-karboksilik asit türevlerinin p-, d- ve f-blok metalleriyle oluşturduğu kompleksleri değerlendirmiş; bu yapıların yalnızca optik değil aynı zamanda biyolojik aktivitelere de sahip olduğunu ve inorganik farmasötik tasarımlar için önemli potansiyel taşıdığını göstermişlerdir [42].

Tamer ve arkadaşları 2015 yılında yaptıkları çalışmalarında, Ni(II)-pikolinat kompleksinin sentezini ve yapısal karakterizasyonunu gerçekleştirerek, düşük HOMO-LUMO enerji farkına sahip bu kompleksin kolayca kutuplanabilirlik olacağını ve birinci mertebe yüksek kutuplanabilirlik (<β>) değerini dinamik hesaplamalar sonucunda 1.012×10^{-30} değerinde olduğunu raporlayarak kompleksin önemli miktarda intramoleküler yük aktarımı sergilediğini bundan kaynaklı olarak ise NLO açısından etkin bir aday olduğunu ortaya koymuşlardır (Şekil 2.9)[43] .

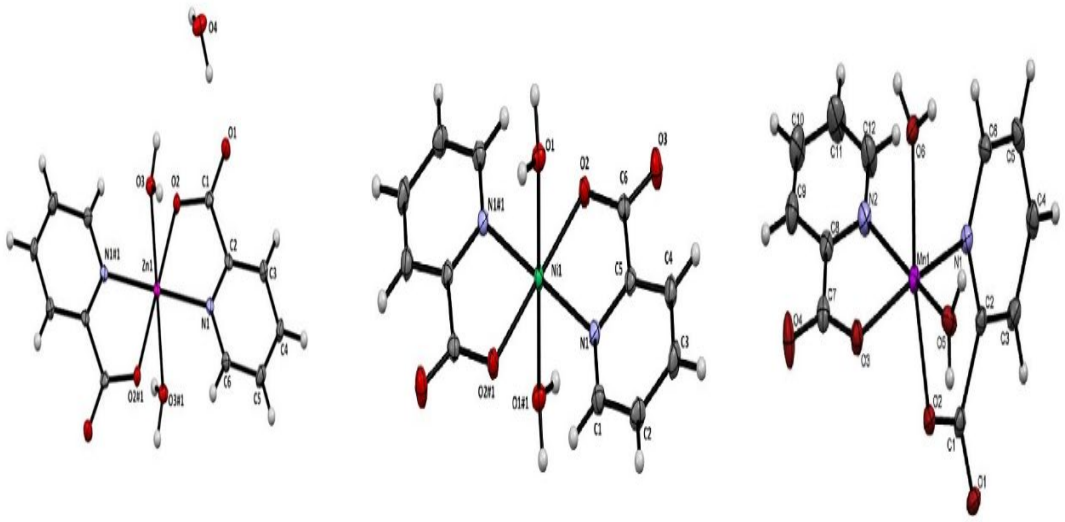

Şekil 2.9. Piridin-2-karboksilik asit içeren Zn(II), Ni(II) ve Mn(II) kompleksleri.

Tamer ve arkadaşları 2016 yılında gerçekleştirdiği çalışmada, Mn(II)-pikolinat Mn (II)-pikolinat kompleksine 1,10-fenantrolin gibi π-konjuge bir yardımcı ligand ilave ederek yeni bir kompleks sentezlemişler, kristal yapısı ve spektroskopik özellikleri detaylı biçimde incelenmiş; elde edilen deneysel veriler, yoğunluk fonksiyonel teorisi (DFT) hesaplamalarıyla desteklenmiştir. Elde edilen kompleksin Birinci mertebe yüksek kutuplanabilirlik (β) değerlerinin 26.004×10^{-30} esu olarak hesaplamışlar ve β değeri, standart bir NLO referansı olan p-nitroanilininkine kıyasla yaklaşık 22 kat daha yüksek bulunmuştur. Bu sonuç, HOMO-LUMO enerji farkının daraltılmasının ve sistemdeki π-konjugasyonun artırılmasının NLO performansını olumlu yönde etkilediğini göstermektedir (Şekil 2.10) [44].

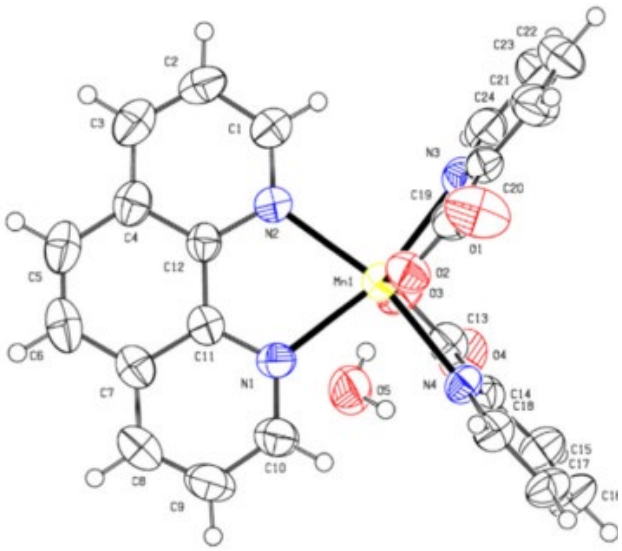

Şekil 2.10. $[Mn(pic)_2(phen)]\cdot H_2O$ (pic: piridin2-karboksilik asit) kompleksi görseli

Tamer ve arkadaşları 2017 yılında gerçekleştirdiği çalışmada Cu(II) pikolinat kompleksine 1,10-fenantrolin gibi π-konjuge bir yardımcı ligand ilave ederek yeni bir kompleks sentezlemişler, IR, UV-Vis, elementel analiz ve X-ışını kırınım (XRD) teknikleri ile bu bileşiğin yapısal karakterizasyonunu kapsamlı şekilde gerçekleştirmiştir. Birinbi dereceden yüksek kutuplanabilirlik değeri olan β değerini 2629.08×10^{-33} esu olarak bularak DFT ile yapılan teorik hesaplamalar, bu kompleksin güçlü bir NLO yanıtı sergileyebileceğini doğrulamış ve piridin-2-karboksilik asit temelli koordinasyon bileşiklerinin optoelektronik uygulamalarda değerlendirilebileceğini bir kez daha desteklemiştir (Şekil 2.11) [45].

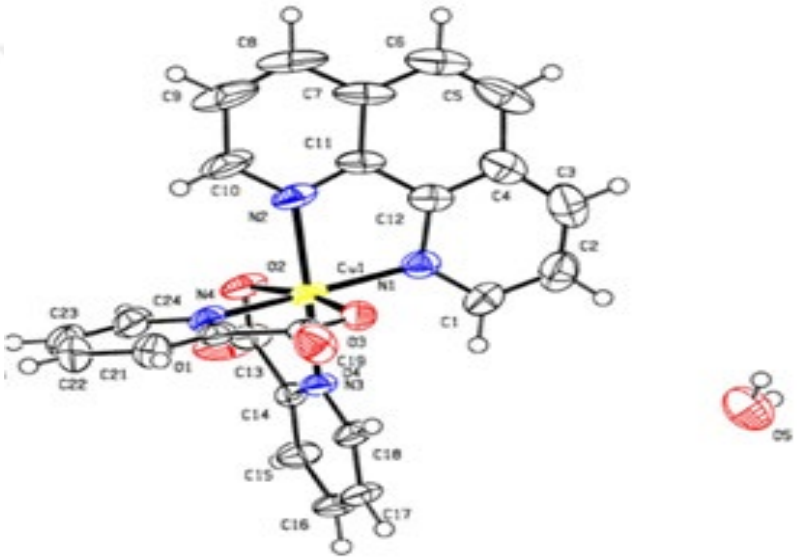

Şekil 2.11. [Cu(pic)$_2$(phen)]·H$_2$O (pic: piridin-2-karboksilik asit) kompleksi görseli

Öte yandan, Uğurlu 2018 yılında gerçekleştirilen hesaplamalı bir çalışmada, piridin-2-karboksilik asit ve çeşitli türevlerinin moleküler yapıları detaylı olarak incelenmiş; dipol moment, kutuplanabilirlik (α) ve Birinci mertebe yüksek kutuplanabilirlik (β) gibi elektriksel özellikleri hem DFT/B3LYP hem de HF seviyelerinde sistematik olarak analiz edilmiştir. Elde edilen veriler, piridin-2-karboksilik asit türevlerinin β değerlerinin moleküler konformasyonlarına, özellikle de torsiyonel açılarına yüksek derecede duyarlı olduğunu göstermiştir. Bunun yanı sıra, bu tür ligandların düşük HOMO–LUMO enerji farklarına sahip olması ve elektron yoğunluğunun sistem genelinde dengeli dağılması, onları doğrusal olmayan optik (NLO) materyal tasarımında son derece ilgi çekici hale getirmektedir[46].

Altürk ve çalışma arkadaşları 2019 yılında gerçekleştirdiği çalışmada, ligand sistemleri olarak piridin-2-karboksilik asit (picH) ve 6-metilpiridin-2-karboksilik asit (6-MepicH) içeren iki farklı Co(II) kompleksini başarıyla sentezlemişlerdir. Sentezlenen yapıların kristalografik analizleri X-ışını kırınım tekniğiyle gerçekleştirilmiş, spektral karakterizasyonları yapılmış ve biyolojik aktiviteleri detaylı biçimde değerlendirilmiştir. Araştırmada, zaman-bağımlı yoğunluk fonksiyonel teorisi (TD-DFT) kullanılarak komplekslerin ikinci ve üçüncü dereceden doğrusal olmayan optik (NLO) parametreleri hesaplanmıştır. HSEh1PBE fonksiyoneli ve 6-311G(d,p) baz setiyle yapılan teorik çalışmalar ikinci mertebe yüksek kutuplanabilirlik değeri olan γ parametresini 106.6-101.4×10^{-36} esu bulmuşlar ve bunu sonucunda bu komplekslerin belirgin NLO yanıtı gösterdiğini ortaya koymuştur. Ayrıca, biyolojik açıdan yapılan analizler bu yapıların α-glukozidaz enzimini inhibe etme potansiyeline sahip olduğunu göstermiş, böylece hem biyofarmasötik hem de fotonik uygulamalar açısından bu tür kobalt komplekslerinin dikkate değer adaylar olduğunu ortaya koymuştur (Şekil 2.12) [47].

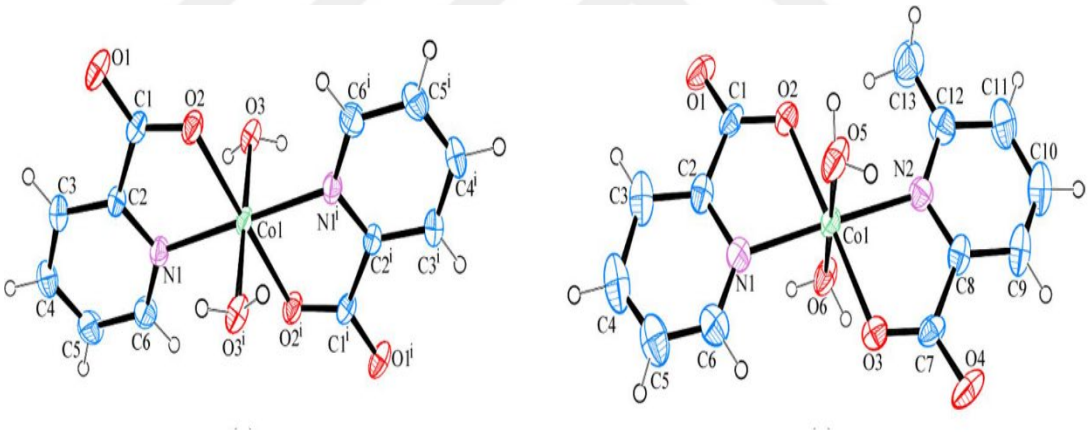

Şekil 2.12. [Co(6-Mepic)(pic)·2H_2O] (6-Mepic: 6-metoksi-2-piridin-karbokdilik asit, pic: 2-piridin karboksilik asit) kompleksleri görseli

Rekha 2019 yılında gerçekleştirdiği çalışmada, piperazinyum bis(pikolinat) PPPA tek dişli yapısını tek kristal X-ışını kırınım yöntemi ile inceleyerek, bu kompleksin yapısal özelliklerini detaylı biçimde ortaya koymuşlardır. Ayrıca, gerçekleştirilen deneysel Z-scan ölçümleri ile bu yapının üçüncü dereceden doğrusal olmayan optik (NLO) özellikleri 1.70×10^{-6} esu olarak belirlenmiş ve piridin-2-karboksilik asit bazlı sistemlerin NLO aktif yeni malzeme tasarımlarında değerlendirilebileceği yönünde önemli kanıtlar elde edilmişti (Şekil 2.13) [48].

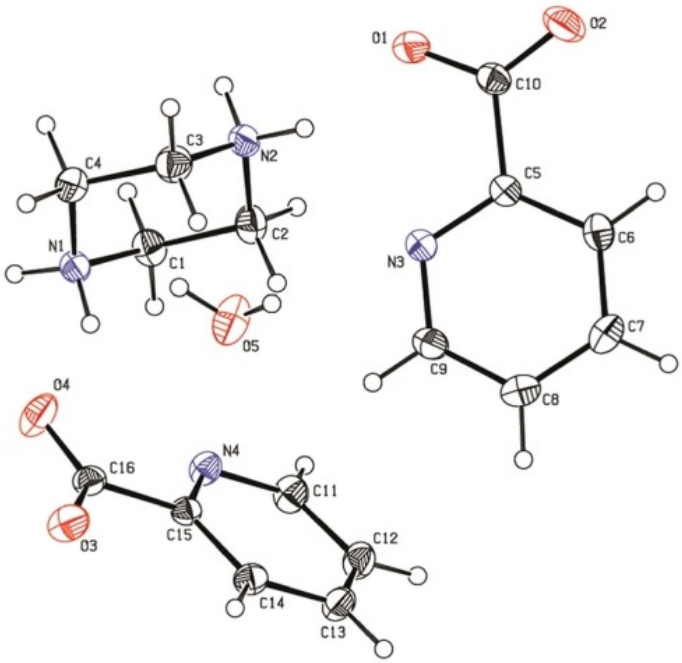

Şekil 2.13. Piperazinyum bis(pikolinat) PPPA tek dişli yapısının tek kristal görseli.

Rejan ve arkadaşları tarafından 2019 yılında yürütülen başka bir çalışmada ise Co (II) iyonu ile oluşturulan bir pikolinat kompleksinin hem spektroskopik hem de teorik yöntemlerle kapsamlı analizleri gerçekleştirilmiştir. Özellikle ligandın bidentat koordinasyon modunun ve kompleksin şelat tipi yapısının, deneysel ve teorik olarak NLO yanıtını anlamlı düzeyde artırdığı tespit edilmiştir. Bu bulgular, ligand bağlanma biçiminin ve moleküler geometri düzeninin doğrusal olmayan optik performans üzerinde belirleyici bir rol oynadığını göstermektedir (Şekil 2.14) [49].

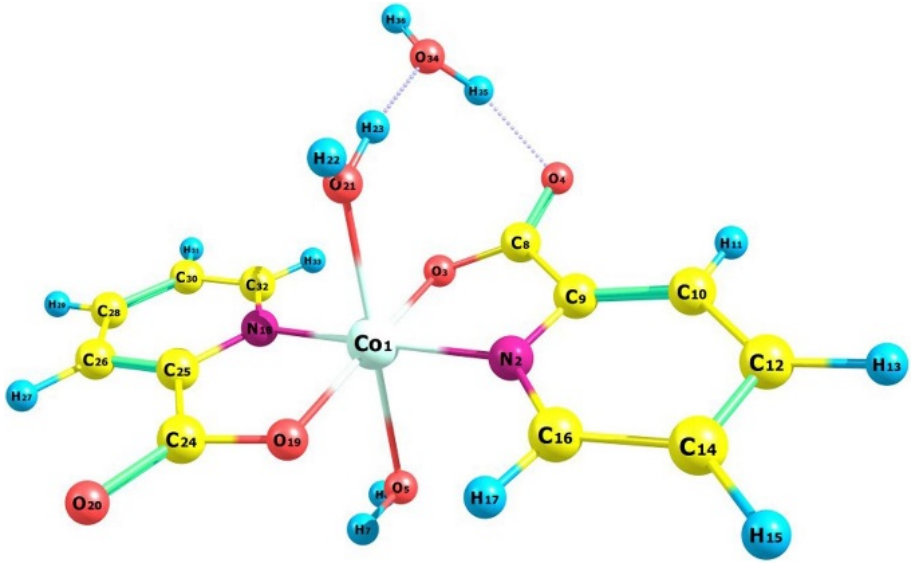

Şekil 2.14.PCOH (trans-diaqua-bis(piridin-2-karboksilato)-cobalt(II) dihidratin) kompleksinin görseli

Chinnasamy ve çalışma arkadaşları 2019 yılında gerçekleştirdiği çalışmada, Zn-pikolinat dihidrat kristalini inceleyerek bu yapının ikinci harmonik üretim (SHG) kapasitesine sahip olduğunu ve geniş optik bant aralığı sayesinde doğrusal olmayan optik (NLO) aygıtlar için potansiyel bir malzeme adayı olduğunu rapor etmişlerdir Şekil 2.15) [50].

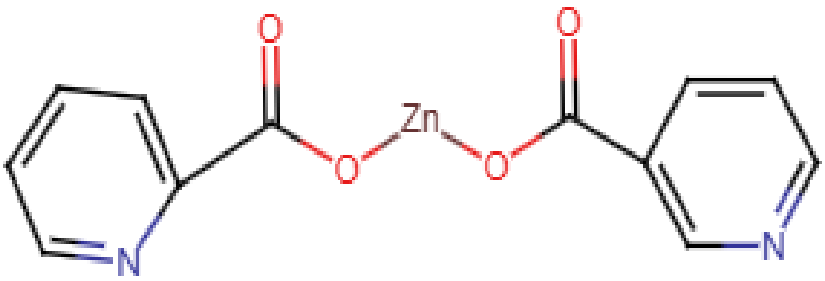

Şekil 2.15. Piridin-2-karboksilik ast ligandı ile elde edilmiş Zn pikolinat dihidrat (ZPD) kristalinin şeması

Tamer ve arkadaşlarının 2020 yılında yaptıkları çalışmada, 4MeOPA ve 4,4-Dimetil-2,2-dipiridil ligandları kullanılarak Mn(II) ve Cd(II) metal merkezli karışık organometalik yeni kompleksler sentezlenmiştir. Bu yapıların spektroskopik özelleri deneysel ve teorik olarak sunulmuştur. Buna ek olarak çalışmada sentezlenen metal organik komplekslerin doğrusal olmayan optik (NLO) özellikleri teorik olarak araştırılmış ve karışık Mn(II) kompleksi için β parametresi 332.97×10^{-30} esu bulunurken eşlenmemiş elektrona sahip olmayan Cd(II) kompleksi elektron çekici ve sağlayıcı ligandların karşılıklı yerleşmesi sonucu 3.2828×10^{-30} esu olarak hesaplanmıştır. Tüm bu sonuçlar ele alındığında elektron alıcı ve verici gruplara sahip olan komplekslerin dolu orbitali olmasa dahi NLO malzeme olarak aktif özellikler sergilediği görülmektedir (Şekil 2.16) [51].

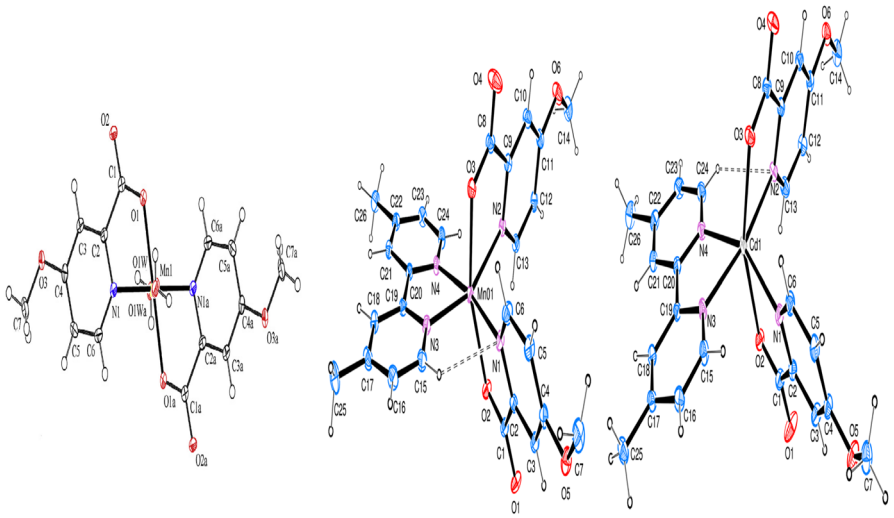

Şekil 2.16. 4-metoksipiridin-2-karboksilik asit içeren Mn(II) ve Cd(II) kompleksleri.

Andriychenko ve arkadaşları 2021 yılında gerçekleştirdiği daha güncel bir çalışmada ise, Cu (II) ve Zn (II) metal iyonları ile piridin-2-karboksilik asit kullanılarak elektrokimyasal sentez yoluyla yeni mononükleer kompleksler elde edilmiştir. Elde edilen komplekslerin spektroskopik karakterizasyonu gerçekleştirilmiş ve pikolinat ligandının hem azot hem de oksijen donor atomları üzerinden metal merkezine koordinasyon sağladığı gösterilmiştir. Araştırmacılar, çalışmalarını B3LYP fonksiyoneli kullanarak teorik hesaplamalarla desteklemiş ve hem deneysel hem de kuramsal açıdan kapsamlı bir değerlendirme sunmuşlardır. Ayrıca, bu tür komplekslerin belirli sentetik koşullar altında kolaylıkla üretilebileceği de vurgulanmıştır (Şekil 2.17) [52].

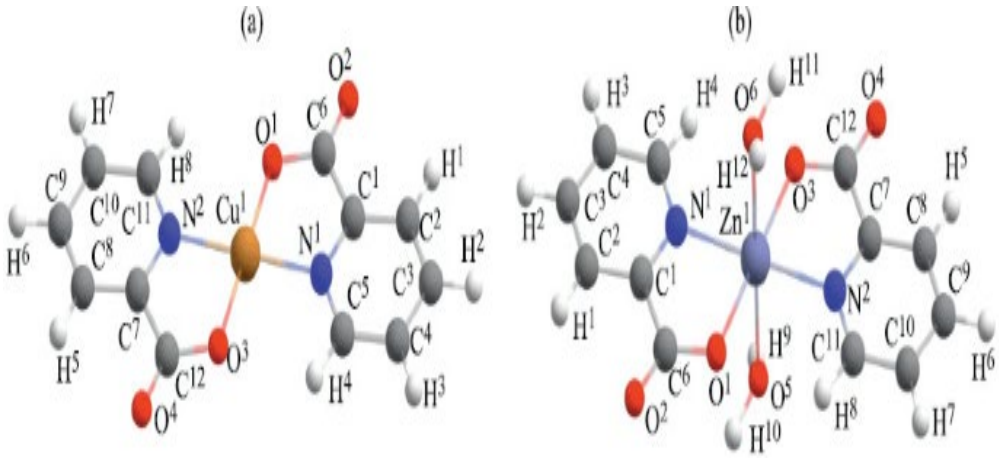

Şekil 2.17. a) [$CuPic_2$] ve b) [$ZnPic_2(H_2O)_2$] kompleksleri (Pic: Piridin-2-karboksilik asit)

Avcı ve arkadaşlarının 2021 yılında yaptıkları çalışmada, 6-kloropiridin-2-karboksilik asit (6-ClPAH) ve 6-bromopiridin-2-karboksilik asit (6-BrPAH) lilgandlarını kullanarak Mn(II), Cr(II), Ni(II), Cu(II), Zn(II), Fe(II), Cd(II), Co(II) ve Hg(II) metal iyonları merkezli yeni metal organik kompleksler sentezlemişler ve bu komplekslerin spektroskopik özelliklerini deneysel ve teorik olarak araştırmışlardır. Bu araştırma sonucunda verilen değerlerin literatürle ve deneysel-teorik olarak uyum içerisinde olduğunu sunmuşlardır. Ek olarak bu komplekslerin NLO özelliklerini detaylı olarak teorik hesaplamalar ile hesaplamışlardır. Birinci mertebe yüksek kutuplanabilirlik değerlerini β statik olarak Mn(II) kompleksi için 22.2×10^{-30} esu ve Hg(II) kompleksi için 13×10^{-30} esu olarak hesaplamışlarıdr. Sonuç olarak en yüksek β değerini en yüksek spin durumuna sahip Mn(II) kompleksi için bulmuşlar ve Hg(II) kompleksinde atomun eşlenmemiş elektrona sahip olmamasına rağmen kayda değer sonuçlar verdiğini bularak sonuçların hem komplekslerin simetrisinden hemde elektron sağlayıcı ve çekici ligandların varlığının NLO aktif malzemeler üstünde etkinliğini artırdığını sunmuşlardır (Şekil 2.18) [53].

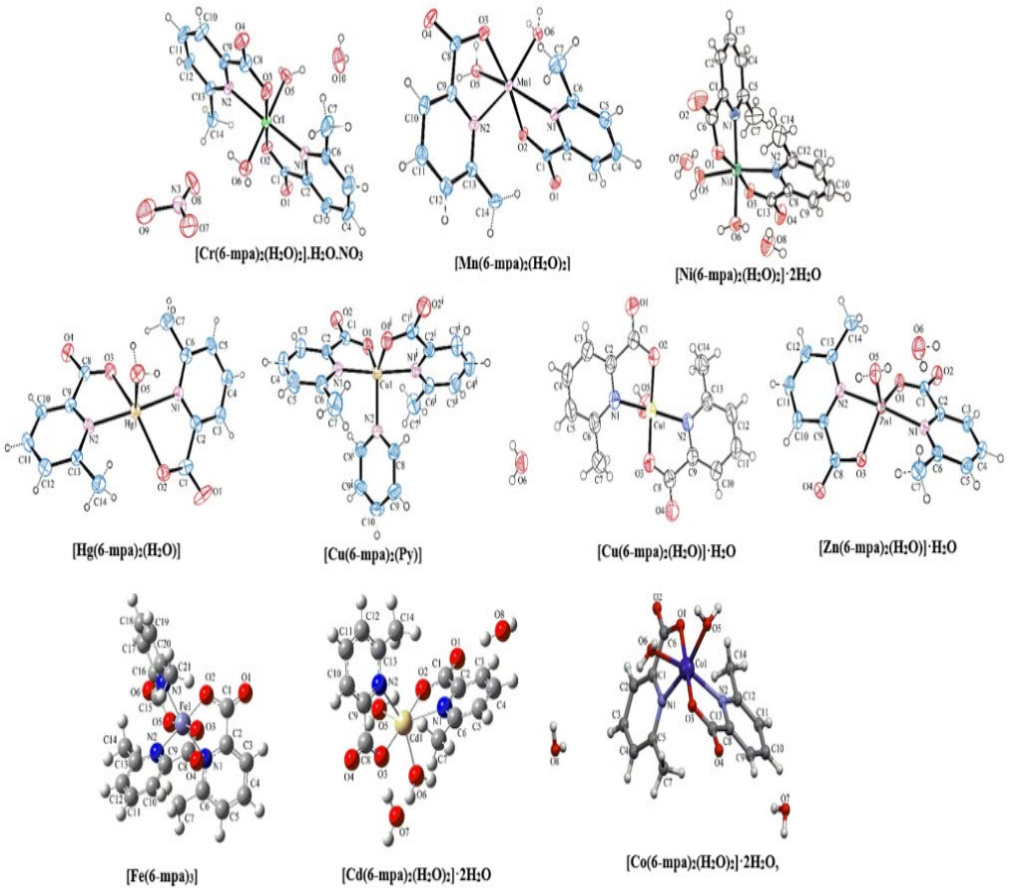

Şekil 2.18. 6-metilpiridin-2-karboksilik asit içeren kompleksler

Prema ve Rose 2022 yılında gerçekleştirdiği çalışmada, piridin-2-karboksilik asit ile beş farklı metal (II) tuzu arasında gerçekleştirdikleri reaksiyonlar sonucunda yeni koordinasyon kompleksleri elde etmişlerdir. Sentezlenen bu bileşiklerin yapısal, elektronik ve doğrusal olmayan optik (NLO) özellikleri hem spektroskopik analizler hem de kuantum kimyasal yöntemler kullanılarak detaylı biçimde incelenmiştir. Çalışma bulguları, komplekslerin birinci mertebe yüksek kutuplanabilirlik (β) değerlerinin oldukça yüksek olduğunu ve bu yapıların NLO teknolojilerinde değerlendirilme potansiyeline sahip olduklarını göstermektedir (Şekil 2.19) [54].

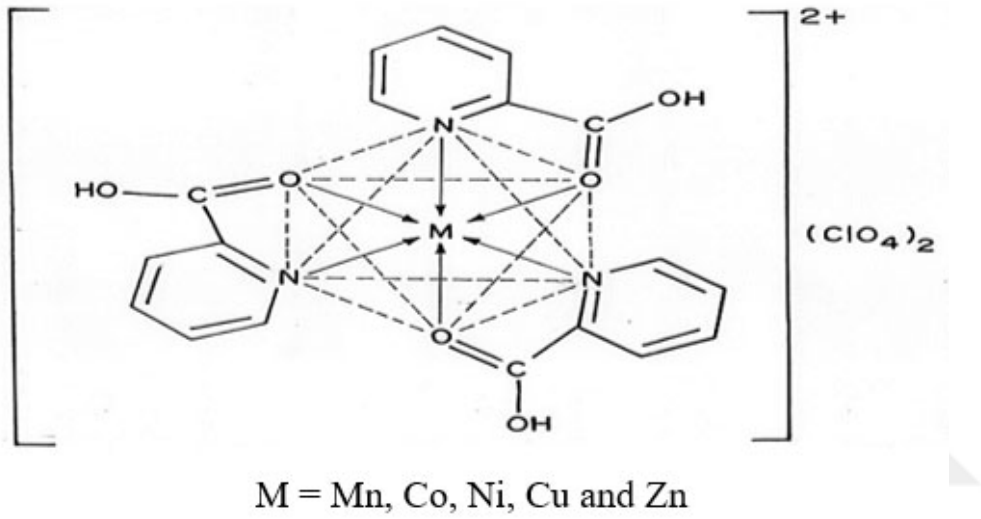

Şekil 2.19. Piridin-2-karboksilik asit içeren Metal(II) perklorat komplekslerinin yapısı

Rendosova ve arkadaşları 2023 yılında gerçekleştirdiği çalışmada, çeşitli Ga(III)-piridin karboksilat kompleksleri (GaPic(pic:pikolinik asit)), GaDpic(Dpic: dipikolinik asit), GaChel (Chel: kelidamik asit) ve GaCldpic(Cldpic: klorodipikolinik asit)) tek adımlı bir yöntemle sentezlenmiş ve IR, elementel analiz, TGA ve X-ışını difraksiyonu ile karakterize edilmiştir. Komplekslerin yapısal kararlılıkları potansiyometrik ve ^{1}H NMR analizleriyle belirlenmiş; çözeltideki türleri ve kararlılık sabitleri saptanmıştır. GaDpic ve GaCldpic'in dirençli P. aeruginosa suşlarına karşı güçlü antimikrobiyal etkileri gözlenirken, GaPic özellikle çeşitli kanser hücre hatlarında yüksek sitotoksisite göstermiştir. Ayrıca, serum albümin ile bağlanma davranışları floresans spektroskopisiyle değerlendirilmiştir (Şekil 2.20) [55].

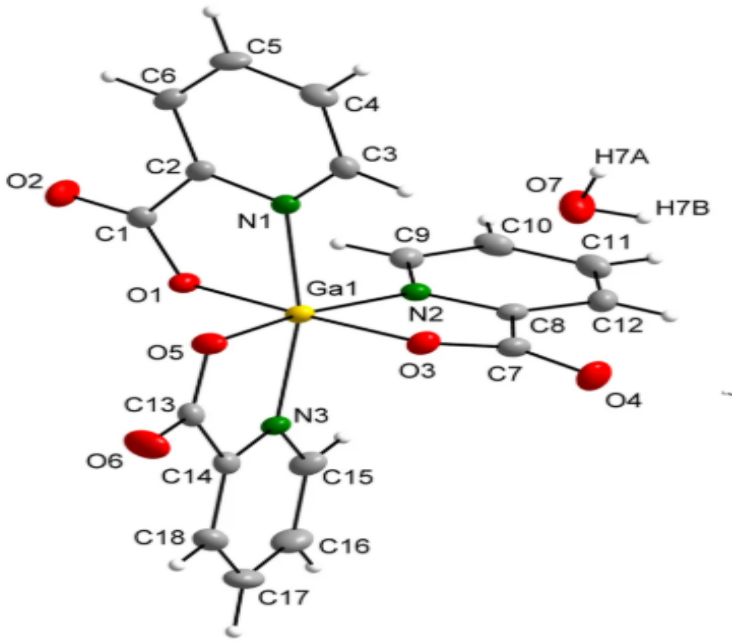

Şekil 2.20. $[Ga(Pic)_3]\cdot H_2O$ (Pic: piridin-2-karboksilik asit) için moleküler yapı için çizilmiş %50 olasılık düzeyinde elipsoidler.

Avcı ve arkadaşları tarafından 2023 yılında yapılan çalışmada, 2-piridinkarboksaldehitin metilamin ve izotiyosiyanat ile kondenzasyonuyla elde edilen Schiff bazı türevi L_1'in Mn(II), Co(II) ve Ni(II) kompleksleri sentezlenmiş ve spektral/optik özellikleri detaylı olarak araştırılmıştır. XRD ve LC-HRMS ile karakterize edilen komplekslerin FT-IR, UV-Vis ve Hirshfeld yüzey analizleri yapılmıştır. DFT/TD-DFT yöntemleri ile teorik spektroskopik ve optik parametreler hesaplanmış; komplekslerin özellikle NLO (doğrusal olmayan optik) özellikleri değerlendirilmiştir. Üçüncü mertebeden yüksek kutuplanabilirlik değerini $[Mn(L_1)_2(NCS)_2]$ kompleksi için 51.65×10^{-13} olarak rapar etmişlerdir. Elde edilen bulgular, Mn(II) kompleksinin yüksek üçüncü dereceden NLO yanıtı ile gelecekte optoelektronik uygulamalarda kullanılabilecek potansiyele sahip olduğunu ortaya koymuştur (Şekil 2.21) [56].

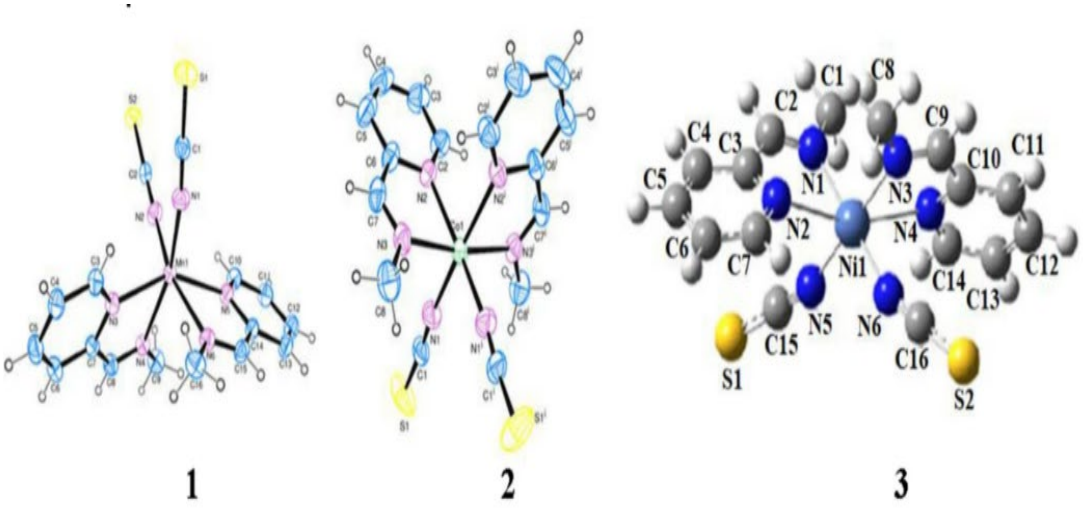

Şekil 2.21. DFT/CAM-B3LYP seviyesi kullanılarak $[Mn(L_1)_2(NCS)_2]$ komleksi ve $[Co(L_1)_2(NCS)_2]$ kompleklsinin 'nin tek kristal yapıları ve $[Ni(L_1)_2(NCS)_2]$ (L_1:piridin-2-karboksilik asit) kompleksinin teorik olarak optimize edilmiş yapısı.

Tamer ve arkdaşları tarafından 2023 yılında yapılan çalışmada, metoksi-piridin-2-karboksilik asit (MeOpic) ligandı kullanılarak $[Zn(MeOPic)_2(H_2O)_2]$ ve $[Ni(MeOPic)_2(H_2O)_2]$ şeklinde iki yeni Zn(II) ve Ni(II) kompleksi sentezlenmiş ve XRD, FTIR ve UV-Vis yöntemleriyle karakterize edilmiştir. Kristal yapı analizleri, ligandın metal merkezine N ve O atomlarıyla iki dişli olarak bağlandığını ve komplekslerin bozulmuş oktahedral geometriye sahip olduğunu göstermiştir. DFT hesaplamaları, UV-Vis ve NBO analizleri, metal-ligand ve ligand-ligand yük aktarımı olduğunu ortaya koymuştur. ikinci dereceden elektro-optik Kerr etkisi γ (-ω;ω,0,0) ve elektrik alanı kaynaklı ikinci harmonik üretim γ (-2ω;ω,ω,0) parametrelerini Ni(II) kompleksi için $13,04\times10^{-36}$ esu ve $2258,9\times10^{-36}$ esu olarak hesaplanmıştır. Tüm bu sonuçlar ele alındığında Ni(II) kompleksinin üçüncü dereceden NLO uygulamaları için potansiyel taşıdığı belirlenmiştir (Şekil 2.22)[57].

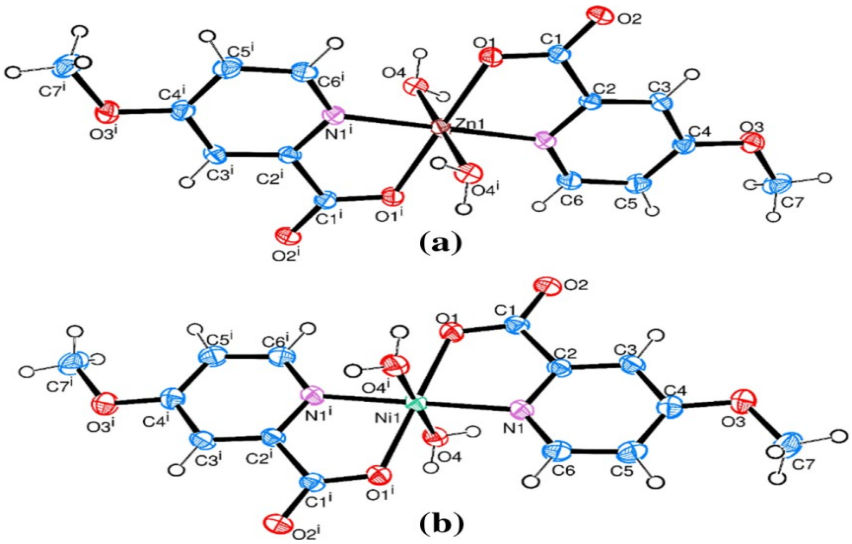

Şekil 2.22. a) $[Zn(MeOPic)_2 \cdot (H_2O)_2]$ kompleksi b) $[Ni(MeOPic)_2 \cdot (H_2O)_2]$ kompleksi (MeOPic: 4-metoksipiridin-2-karboksilik asit)

Matlou ve çalışma arkadaşları 2023 yılında gerçekleştirdiği çalışmada ise, Re(I) trikarbonil çekirdeği ile piridin-2-karboksilik asit türevlerinden oluşan toplam 15 farklı kompleks sentezlemiş ve bu bileşiklerin kristal yapılarının yanı sıra, akciğer kanseri hücre hatları üzerindeki in vitro biyolojik aktivitelerini incelemiştir. Özellikle piridin-2-karboksilik asit (Pico) ile flor içeren türevler olan 3,5-difloropiridin- 2 -karboksilik asit (Dfpc) ve 3-triflorometil-piridin-2-karboksilik asit (Tfpc) kullanılılan komplekslerin, yalnızca sitotoksik etkiler değil, aynı zamanda koordinasyon çevresindeki varyasyonlara bağlı olarak gösterdikleri NLO davranışları da analiz edilmiştir. Elde edilen veriler, piridin-2-karboksilik asit temelli ligandların hem farmakolojik hem de optoelektronik açıdan işlevsel özellikler taşıdığını bir kez daha ortaya koymuştur (Şekil 2.23)[58].

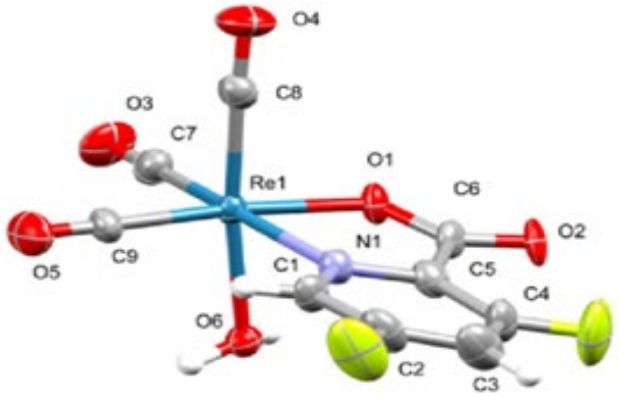

Şekil 2.23. 3,5-difloropiridin- 2 -karboksilik asit ligandı ile elde edilen Re(I) komleksi

Ma ve çalışma arkadaşları 2023 yılında gerçekleştirdiği çalışmada, solvotermal yöntemle sentezlenen yeni bir iki boyutlu çinko bazlı koordinasyon polimeri olan $\{Zn(HL)(H_2O)_2\}_n$ (burada HL = 4-(2,4-dikarboksifenil-piridin-2-karboksilik asit), görünür ışık altında güçlü fotokatalitik performans sergileyerek sulu çözeltilerden Rodamin B ve Metil Oranj gibi organik boyaları etkin bir şekilde uzaklaştırmışlardır. Fotokatalitik süreçte rol oynayan aktif radikal türleri, üç farklı radikal kapan tuzağı kullanılarak deneysel olarak analiz edilmiş; mekanizmanın ayrıntıları yoğunluk fonksiyonel teorisi (DFT) hesaplamalarıyla desteklenerek ortaya konmuştur. Bu çalışma, söz konusu koordinasyon polimerinin çevresel kirleticilerin giderilmesinde potansiyel bir fotokatalizör olarak değerlendirilebileceğini göstermektedir (Şekil 2.24) [59].

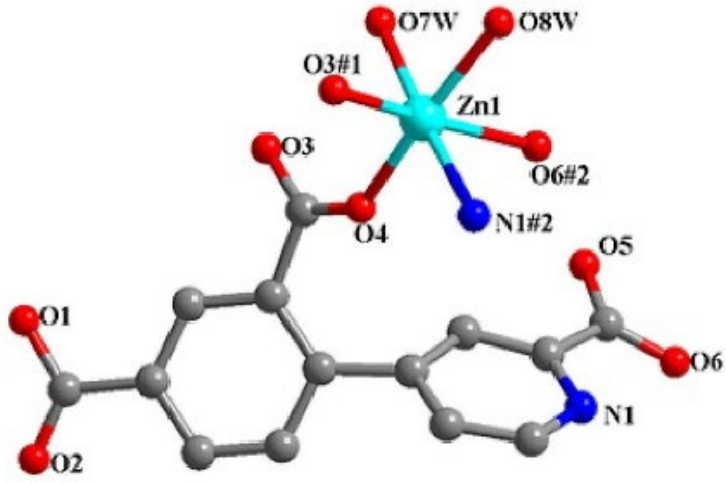

Şekil 2.24. $\{Zn(HL)(H_2O)_2\}_n$ (HL = 4-(2,4-dikarboksifenil-piridin-2-karboksilik asit) kompleksi

Li ve çalışma arkadaşları 2023 yılında gerçekleştirdiği çalışmada çalışmada, $FAPbI_3$ bazlı perovskit güneş hücrelerinin (PeSC) verimlilik ve kararlılığını artırmak amacıyla, 4-hidroksipiridin-2-karboksilik asit (4HPA) aracılığıyla perovskit/delik taşıyıcı katman arayüzü düzenlenmiştir. DFT hesaplamaları, 4HPA'nın yüzeyle güçlü elektronik etkileşim kurduğunu ve yük geçişini kolaylaştırdığını göstermektedir. 4HPA, hidrojen bağları ile birlikte Pb–O ve Pb–N koordinatif bağları oluşturarak tuzak yoğunluğunu düşürmekte ve radyasyonsuz rekombinasyonu baskılamaktadır. Sonuç olarak, daha saf α-faz kristal yapısı ve iyileştirilmiş enerji seviyeleri elde edilmiştir. Bu strateji ile geliştirilen PeSC'ler, yüksek verim (%23,28) ve modül düzeyinde (%19,26) istikrarlı performans sergilemiştir[60].

Areas ve arkadaşlarının 2024 yılında gerçekleştirdiği başka bir araştırma kapsamında, kadmiyum pikolinat esaslı bir koordinasyon polimeri başarıyla sentezlenmiş ve yapısı çeşitli analiz teknikleriyle detaylı olarak incelenmiştir. Teorik ve deneysel bulgular, bu yapının yalnızca optik ve elektronik özellikler açısından değil, aynı zamanda gaz adsorpsiyonu ve NLO uygulamaları bakımından da dikkat çekici potansiyele sahip olduğunu ortaya koymaktadır. Özellikle yoğunluk fonksiyonel teorisi ve moleküler simülasyonlara dayanan hesaplamalar, malzemenin H_2S gibi hedef moleküllerle güçlü etkileşimler kurabildiğini göstermiştir. Bu da materyalin çevresel sensör uygulamaları için umut verici bir aday olduğunu düşündürmektedir (Şekil 2.25) [61].

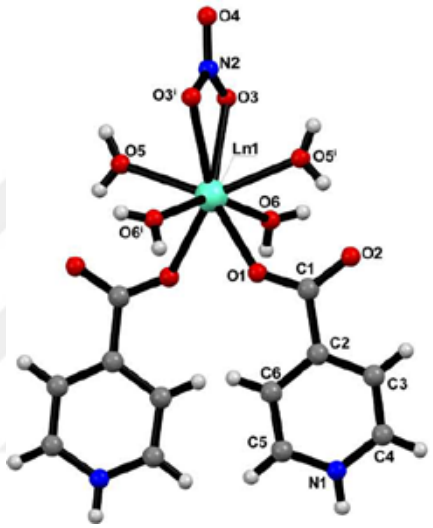

Şekil 2.25. $[L_n(NO_3)(4picH)_2(H_2O)_4](NO_3)_2$ (4picH: 4-pikolinik sit) kristal yapısı

Garcia ve arkadaşları 2024 yılında yaptıkları araştırma kapsamında, 5-nitropiridin-2-karboksilik asit (5-npic) kullanılarak farklı geçiş metalleriyle (Mn, Cd, Cu, Co, Ni, Zn) altı yeni metal kompleksinden oluşan bir seri sentezlemişleridir. Bu komplekslerin yapısal çeşitliliği, ligandın farklı koordinasyon davranışlarından kaynaklanmış ve 1D, 2D ya da mononükleer düzenlemeler ortaya koymuşlardır. Kristal yapıları ve spektral özellikleri detaylı olarak incelemişler; özellikle Cd (II) içeren kompleksin hem antikanser hem de anti-inflamatuar etkiler açısından belirgin biyolojik aktivite gösterdiği raporlanmıştır. Bu bulgular, biyolojik açıdan aktif metal komplekslerinin geliştirilmesine yönelik yeni bir katkı sunmaktadır (Şekil 2.26)[62].

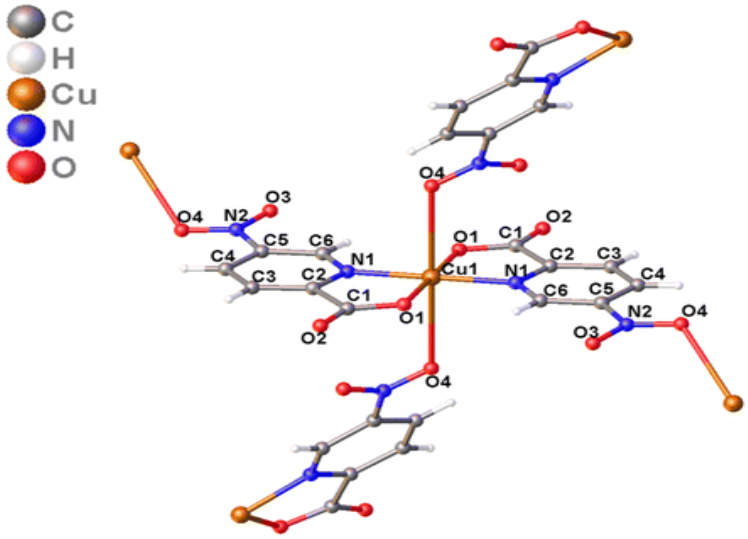

Şekil 2.26. $[Cu(5\text{-npic})_2]_n$ (5-npic: 5-nitropiridin-2-karboksilik asit) kompleksi

Manopradha ve çalışma grubunun 2024 yılında yaptıkları çalışmada, benzotriazol ve piridin-2-karboksilik asit türevi olan BTPCA bileşiğinin kristalleri yavaş buharlaşma yöntemiyle büyütmüşler ve kristal yapısını toz X-ışını kırınımı ile doğrulamışlardır. FT-IR ve UV spektrumlarını deneysel olarak rapor etmişlerdir. Teorik incelemeler ise yoğunluk fonksiyonel teorisi (DFT) kullanılarak gerçekleştirilmiş; HOMO–LUMO enerji seviyeleri ile doğal bağ orbital analizleri doğrusal olmayan optik (NLO) özellikler açısından değerlendimişlerdir. B3LYP/6-311++G(d,p) temel seti ile yürütülen hesaplamalar, molekülün hem doğrusal hem de doğrusal olmayan optik tepkilerini açıklamıştır. SHG verimliliği Kurtz-Perry tekniği ile ölçülmüş, mavi bölgede ışıma gösterdiği floresans analizleriyle ortaya konmuştur. Ek olarak, mekanik dayanım özellikleri Wooster ilişkisinden yararlanılarak analiz edilmiştir. Bu kapsamlı çalışma, BTPCA bileşiğinin NLO malzeme geliştirme açısından potansiyelini ortaya koymuşlardır (Şekil 2.27) [63].

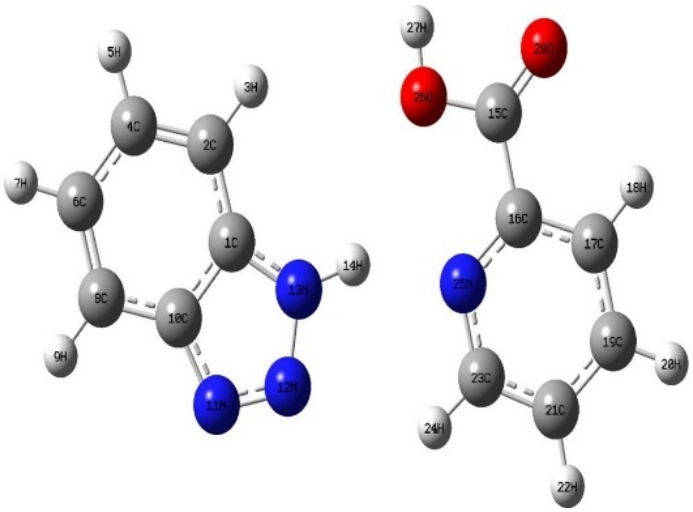

Şekil 2.27. BTPCA (Benzotrial piridin-2-karboksilik asit)'nın optimize edilmiş moleküler yapısı

Randhawa ve arkadaşlarının 2024 yılında yaptıkları çalışmada, piridin karboksilik asit liganlarıyla kullanılarak H_2macropa isimli makrosiklik şelatlayıcının azot içeren yapısının kükürt atomları ile kademeli olarak değiştirilmesiyle elde edilen yeni ligandların, $^{203}Pb^{2+}$ ve $^{213}Bi^{3+}$ iyonlarıyla kompleksleşme davranışlarını değerlendirilmektedir. Sentezlenen ligandların türevlerinin koordinasyon özellikleri; potansiyometrik titrasyon, NMR ve UV-vis spektroskopileri, X-ışını kristalografisi ve DFT hesaplamaları gibi çok yönlü analiz yöntemleriyle ayrıntılı olarak incelenmiş ve elde edilen bulgular, ligand yapısındaki kükürt atomlarının artmasının komplekslerin hem kararlılığını hem de kinetik dayanıklılığını azalttığını göstermiştir. Bununla birlikte, model bileşiklerle yapılan hesaplamalar, S-donörlerin Pb^{2+} ve Bi^{3+} iyonlarına karşı daha yüksek bağlanma eğilimi sergilediğini ortaya koymuştur. Radyoaktif işaretleme deneyleri sonucunda, H_2macropa'nın hem $203Pb^{2+}$ hem de $213Bi^{3+}$ iyonlarıyla yüksek etiketleme verimi sunduğu, H_2S_4macropa'nın ise yalnızca Bi^{3+} ile kompleks oluşturabildiği belirlenmiştir. Ayrıca, bu komplekslerin serum stabilitesi oldukça yüksek bulunmuştur (Şekil 2.28) [65]

Şekil 2.28. Randhawa ve arkadaşları tarafından sentezlenen yeni ligandların görselleri

Hu ve arkadaşlarının 2024 yılında yaptıkları çalışmada, moleküler düzeyde yük taşınımının yalnızca π-orbitaller üzerinden değil, uygun yapısal koşullarda σ-orbitaller üzerinden de gerçekleşebileceği göstermişlerdir. STM-BJ tekniğiyle yapılan deneysel analizler, meta-bağlantılı piridin-2-karboksilik asit, para-bağlantılı izomerine kıyasla çok daha yüksek iletkenlik sergilediğini ortaya koymuştur. Titreşim analizi ve DFT hesaplamaları, bu beklenmedik iletkenliğin, molekülün σ-sisteminin taşıyıcı yol oluşturmasıyla ilişkili olduğunu doğrulamışlardır. Elde edilen veriler, σ-elektronlarının konjuge moleküler yapılarda da etkin taşıyıcılar olabileceğini göstererek, moleküler ölçekli elektronik aygıtların tasarımında yeni bir yaklaşımın önünü açmaktadır [66].

Cao ve arkadaşlarının 2024 yılında yaptıkları çalışmada, teorik hesaplamalarla birlikte, bir iki dişli piridin-2-karboksilik asit (**Pic**) ligandının ve onun beş dişli piridin-2-karboksilik asit türevinin (H_2dpa) uranil bağlama yetenekleri araştırılmıştır. H_2dpa 'nın düzlemsel N_3O_2-donör konfigürasyonu, uranilin tipik beşgen bipiramidal koordinasyon geometrisine uyduğunu ve böbreklerde uranil için dikkate değer bir uzaklaştırma tercihi olduğunu göstermişlerdir [67].

Jamgohari ve arkadaşlarının 2024 yılında yaptıkları çalışmada, etilendiamin ve 2-piridin karboksilat içeren yeni bir Pd(II) kompleksi sentezlenmiş ve Pt(II) analoğu ile birlikte yapısal, spektroskopik ve biyolojik özellikleri incelemişlerdir. Yapılar FT-IR, UV-Vis, NMR ve X-ışını kristalografisi ile karakterize edip, DNA ile etkileşimleri ve antikanser etkileri değerlendirmişlerdir. Bileşiklerin DNA'ya moleküler bağlanması göstererek, Pd(II) ve Pt(II) kompleksleri kanser hücrelerinde seçici toksisite etkisine sahip olduğunu göstermişlerdir (Şekil 2.29) [68].

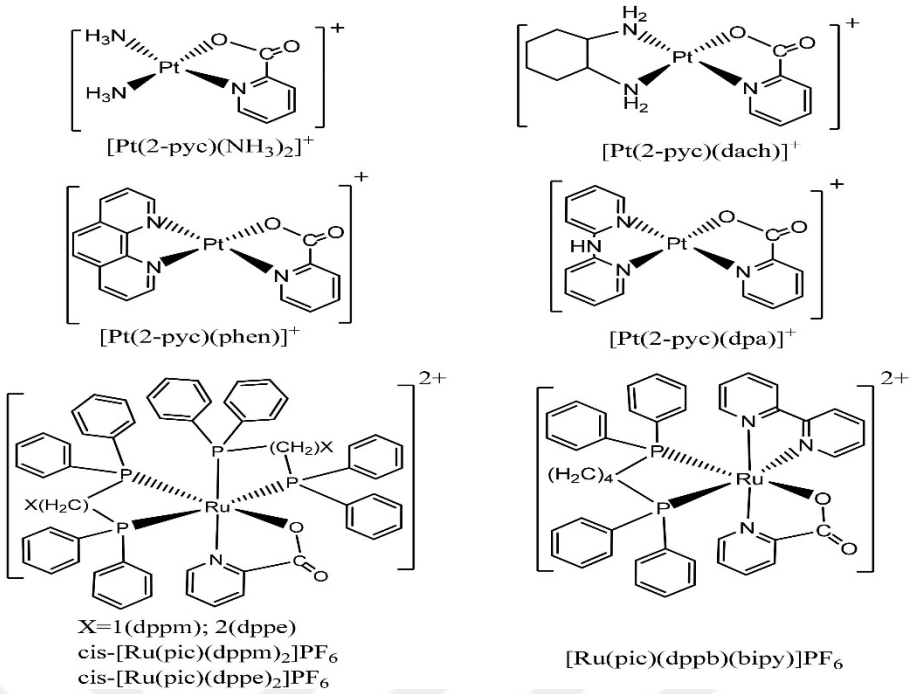

Şekil 2.29. Jamgohari ve arkadaşları tarafından sentezlenen piridin-2-karboksilik asit içeren metal kompleksleri

David ve arkadaşları tarafından 2025 yılında yapılan Platin (II) merkezli komplekslerin fotofiziksel özellikleri ve ışığa duyarlı biyolojik etkileri üzerine yapılan güncel bir çalışmada, dört farklı pikolinat ligandı içeren yapısındaki bileşikler sentezlenmiş ve çok yönlü olarak değerlendirilmiştir. Kristal yapılarının X-ışını kırınım analizleri, özellikle kompleks 1 ve 3'ün düzenli zincirsel yapılanma eğiliminde olduğunu ortaya koymuştur. Bu komplekslerin fotofiziksel davranışları, emisyon karakteristiklerinin temel olarak ligand içi yük transferi (ILCT) geçişlerine dayandığını göstermiştir. Z-scan yöntemiyle belirlenen singlet oksijen üretim verimleri (%13–17) ve in vitro biyolojik testler, özellikle kompleks 3'ün ışık varlığında belirgin fototoksik etki gösterdiğini ortaya konmuştur. Ayrıca bu kompleksin, protein etkileşimi ve NADH fotooksidasyonu gibi biyolojik mekanizmalarla ilişkilendirilebilecek aktiviteler sergilediği belirtilmiştir.

Olawale ve arkadaşları tarafından 2025 yılında gerçekleştirilen araştırmada, piridin-2-karboksilik asit ile kadmiyum asetat dihidrat [$Cd(CH_3COO)_2.2H_2O$] arasındaki reaksiyon sonucu CP-2 adlı yeni bir koordinasyon polimeri başarıyla elde etmişler. Sentezlenen yapı, çeşitli spektroskopik analizler, elementel bileşim tayini ve toz X-ışını kırınımı kullanılarak kapsamlı şekilde karakterize edilmiştir. Elde edilen bulgular, kristalin oluşumunun başarılı olduğunu açıkça ortaya koymuşlardır. Malzemenin elektronik ve optik davranışları, yoğunluk fonksiyonel teorisi (DFT) ve zamana bağlı

DFT (TD-DFT) hesaplamalarıyla detaylandırarak; özellikle yüksek mertebe kutuplanabilirlik değerleri sayesinde doğrusal olmayan optik (NLO) uygulamalar açısından dikkat çekici bir performans sergilediği belirlemişlerdir. Bunun yanı sıra, Monte Carlo ve moleküler dinamik simülasyonları CP-2'nin H_2S başta olmak üzere bazı endüstriyel gazlarla güçlü adsorptif etkileşimler geliştirdiğini göstermişlerdir [70].

Gomez ve arkadaşları tarafından 2025 yılında gerçekleştirilen çalışmada, Me_2N-pbt (-(4-dimetilaminofenil-benzotiazolat) ana ligandı ile dört farklı pikolinat türevi içeren yeni Pt (II) kompleksleri sentezlenmiş ve bu bileşiklerin fotofiziksel özellikleri, singlet oksijen üretim kapasiteleri ile biyolojik etkileri değerlendirilmiştir. X-ışını analizleri, komplekslerin katı hâlde bir boyutlu zincirler oluşturduğunu ortaya koyarken, emisyon özelliklerinin ligand-tabanlı geçişlere dayandığı belirlenmiştir. Özellikle şekilde verilen kompleks, ışığa duyarlı antiproliferatif etkisiyle öne çıkmış, biyokimyasal süreçlerde yüksek aktivite göstermiştir. Bulgular, bu tür komplekslerin fototerapi potansiyeline sahip olduğunu ortaya koymaktadır (Şekil 2.30) [71].

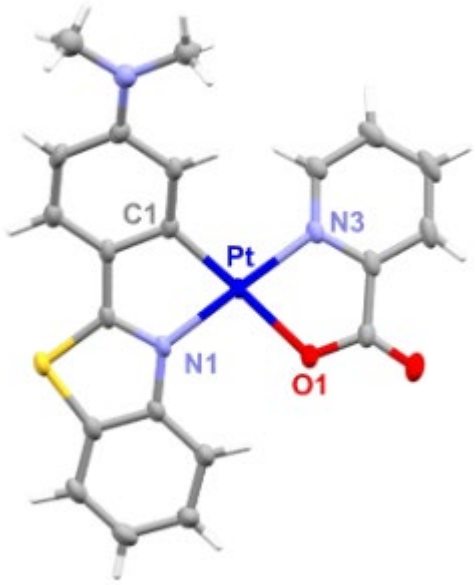

Şekil 2.30. Me_2N-pbt (-(4-dimetilaminofenil-benzotiazolat) ana ligandı kullanılarak elde edilen Pt(II) kompleksi.

Li ve arkadaşları tarafından 2025 yılında yapılan çalışmada, demir kompleksleri ile çeşitli peroksitler arasındaki etkileşimlerin, Fenton ve benzeri tepkimelerde hangi aktif oksidan türlerinin üretildiğini belirlemede önemli rol oynadığını ortaya koymuştur. Bu kapsamda Fe(III)-pikolinat kompleksi örnek alınarak yürütülen deneysel ve teorik

çalışmalar, kullanılan peroksit türüne bağlı olarak farklı oksidanların oluştuğunu göstermiştir. Özellikle H_2O_2 ve bazı organik hidroperoksitlerin radikal üretimini başlattığı, buna karşılık perasetik asit ve benzeri bileşiklerin yüksek değerlikli Fe (IV) türlerini oluşturduğu belirlenmiştir. Hesaplamalar, bu farkın, peroksit grubunun elektron etkisiyle demir merkezindeki bağların zayıflamasına veya güçlenmesine bağlı olduğunu ortaya koymuştur (Şekil 2.31) [72].

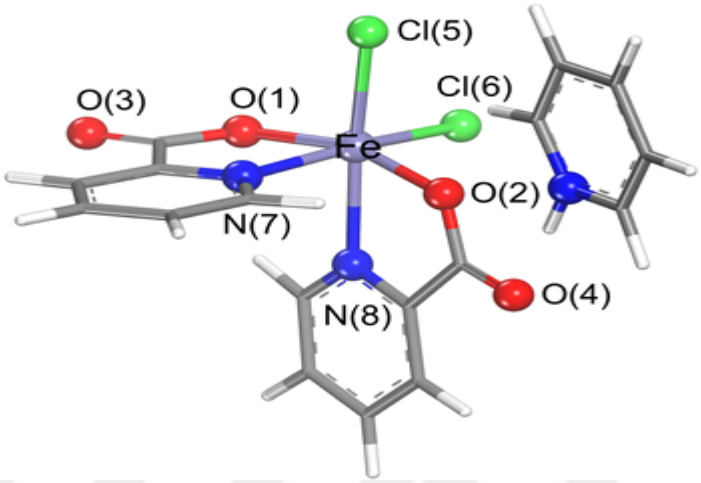

Şekil 2.31. Piridin-2-karboksilik asit ve peroksit liganları kullanılarak elde edilen Fe(III) kompleksi.

3. BULGULAR VE TARTIŞMA

3.1. 6-kloropiridin-2-karboksilik Asidin Zn (II) ve Cu (II) Kompleksleri İçin Yapısal, Spektroskopik (FT-IR ve UV-Vis), Doğrusal Olmayan Optik ve Moleküler Yerleştirme Analizlerine İlişkin Deneysel ve Teorik Yaklaşımlar

Necmi, D., Ömer, T.,Merve, Ş., Davut, A., Mavişe, Y.,Adil, B., ve Yusuf, A. (2022). 6-kloropiridin-2-karboksilik Asidin Zn (II) ve Cu (II) Kompleksleri İçin Yapısal, Spektroskopik (FT-IR ve UV-Vis), Doğrusal Olmayan Optik ve Moleküler Yerleştirme Analizlerine İlişkin Deneysel ve Teorik Yaklaşımlar. *Applied Organometallic Chemistry*, *36*(6), e6678. https://doi.org/10.1002/aoc.6678

Bu çalışmada, 6-kloropiridin-2-karboksilik asit ligandının Zn(II) ve Cu(II) metal iyonlarıyla kompleksleşmesi sonucunda elde edilen yeni koordinasyon bileşiklerinin sentezi, yapısal özellikleri ve elektronik davranışları kapsamlı olarak araştırılmıştır. Sentez aşamasında, 2 mmol oranında çözülen ligandlar etanol-su karışımı içinde hazırlanmış, ardından 1 mmol oranında metal tuzları ilave edilerek 50 °C'de 2 saat boyunca oda sıcaklığında sürekli karıştırıldı. Daha sonra renksiz çözelti süzüldü ve 2 hafta boyunca oda sıcaklığında buharlaşmaya bırakıldı. Elde edilen renksiz ve beyaz tonlarında kristaller daha sonra X-ışını kırınımı deneylerinde kullanıldı

Kristal yapının belirlenmesi amacıyla tek kristal X-ışını kırınım (SC-XRD) analizi gerçekleştirilmiş ve elde edilen veriler, SHELXT programı ile çözülmüştür. Kristalografik analiz sonucunda Zn(II) kompleksinin monoklinik kristal sisteminde $P2_{1/C}$ uzay grubunda bozulmuş oktahedral geometriye, Cu(II) kompleksinin ise triklinik kristal sisteminde P-1 uzay grubunda bozulmuş trigonal bipiramidal geometriye sahip olduğunu ortaya koymuştur. Elde edilen bağ uzunlukları ve bağ açıları, teorik hesaplamalarla büyük ölçüde örtüşmüş; özellikle eksenel bağlardaki kısalmalar Jahn-Teller etkisine bağlanmıştır. Bu bulgular, koordinasyon modlarının doğrulanmasında yapısal verilerle teorik verilerin uyumunu gözler önüne sermiştir. Her iki kompleks için hidrojen bant geometrisi parametreleri de sunulmuştur. Kristaller içinde, C—H···O ve O—H···O moleküller arası H bağları moleküllerin üç boyutlu bir ağ oluşturmasını sağlar. Zn (II) kompleksinde en güçlü H bağı (O3—H3B···O5, H···A = 1.87 Å, D···A=2.669 Å) $-x + 1, -y + 1, -z + 1$ simetri

koduyla gözlenir. Cu (II) kompleksinde ise en güçlü H bağı (O3—H3B···O5, H···A = 1.94 Å, D···A = 2.712 Å x - 1, y , z simetri koduyla gösterilir .

Komplekslerin FT-IR spektrumları, 4000-400 cm^{-1} aralığında kaydedilmiş ve DFT hesaplamalarından elde edilen verielerle karşılaştırılmıştır. H_2O ligandındaki O-H gerilme titreşimleri Zn(II) kompleksinde 3239 cm^{-1}, Cu(II) kompleksinde ise 3188 cm^{-1} civarında gözlemlenmiş ve bu değerler teorik hesaplamalarla da desteklenmiştir. Simetrik ve asimetrik karboksilat grubu (COO^-) titreşimleri sırasıyla 6-kloropiridin-2-karboksilik asit ligandında 1040 cm^{-1}, Zn (II) kompleksi için 1641 ve 1249 cm^{-1}'de ve Cu(II) kompleksi için 1621 ve 1252 cm^{-1}'de gözlendi . Simetrik ve asimetrik ν (COOH) titreşimleri arasındaki farkın, FT-IR spektrumlarında 392 ve 369 cm^{-1} olarak gözlendi ve hesaplanan IR spektrumlarında 404 ve 435 cm^{-1} olarak bulundu. Serbest piridin-2-karboksilik asit türevlerinin IR spektrumlarında bu fark 620–642 cm^{-1} bölgesinde elde edildi. COOH asimetrik ve simetrik titreşim bantları arasındaki farktaki azalma, piridin-2-karboksililat ligandının karboksil grubu O atomu üzerinden Zn(II) ve Cu(II) metallerine tek dişli ligand olarak koordine olduğunu göstermektedir. Serbest piridin halkasında 989 cm^{-1} civarında bildirilen halka soluklanma bandının, piridin halkasının Zn(II) ve Cu(II) iyonlarına ayrı ayrı koordinasyonu üzerine 1008 cm^{-1}'e kaydığı gözlemlenmiştir.

Yüksek enerjili π→π * ve n→π* geçişleri Zn(II) iyonuna koordine edildiğinde 230/217 ve 274/253 nm'de ve Cu(II) iyonuna koordine edildiğinde 231/254 ve 273/306 nm'de gözlendi Ligant-metal yük transferi (LMCT) geçişine atanan daha zayıf ve daha az enerjik tepeler sırasıyla Zn(II) ve Cu(II) kompleksleri için 326 ve 373 nm'de de gözlendi. d^{10} elektronik konfigürasyonuna sahip Zn(II) kompleksinde d-d elektronik yük transferi göstermezken, d^9 elektronik konfigürasyonuna sahip Cu(II) kompleksinde 840/938 nm'de938 nm'de d - d yük geçişi olarak atanan bir soğurma bandı gözlendi.

Ayrıca, her iki kompleksin SARS-CoV-2 ana proteazı (PDB ID: 6LU7) ile potansiyel biyolojik etkileşimleri moleküler kenetlenme yöntemleriyle analiz edilmiştir. Zn(II) kompleksinin bağlanma enerjisinin-5.24 kcal/mol ve inhibasyon sabitinin (K_i) 144.6 μM olduğu, Cu(II) kompleksinin ise sırasıyla-4.14 kcal/mol ve 925.95 μM değerlerine sahip olduğu belirlenmiştir. Bu sonuçlar, yerleştirme prosedüründen, bağlanma enerjisinin negatif değerleri kompleks Zn(II) ve Cu(II) 'nin kararlı olduğunu ve hedef SARS-CoV-2 ana proteazının boşluğunda başarılı bir şekilde bağlandığını ve Zn(II)

kompleksinin daha yüksek bağlanma afinitesi gösterdiğini ve SARS-CoV-2 ana proteazını inhibe etme potansiyelinin daha yüksek olduğunu göstermektedir.

Komplekslerin HOMO-LUMO enerji aralıkları ile NLO parametreleri arasındaki ilişki de önemlidir. HOMO-LUMO enerji farkı, sırasıyla LH, Zn(II) ve Cu(II) kompleksleri için 5.52, 4.64 ve 3.41 eV olarak hesaplanmıştır. Bu değerlerin düşüklüğü, moleküler sistemin daha kolay uyarılabilir olduğunu ve böylelikle yüksek polarizabilite ve hiperpolarizabiliteye olanak sağladığını göstermektedir. Cu(II) kompleksinde gözlenen dar enerji aralığı <ΔE> ile yüksek <β> değeri arasındaki ters orantılı ilişki, bu moleküllerin yumuşak (soft) elektronik yapıda olduğunu ve hızlı elektronik cevap verebildiklerini göstermektedir.

Çalışmada son olarak, komplekslerin NLO özellikleri yoğunluk fonksiyonel teorisi (DFT) kapsamında B3LYP fonksiyoneli ve 6-311++G(d,p)/LanL2DZ karma baz seti kullanılarak hesaplanmıştır. Elde edilen sonuçlara göre, Zn(II) kompleksinin β(0;0,0) değeri 0.88×10^{-30} esu iken, Cu(II) kompleksinin β(0;0,0) değeri 10.40×10^{-30} esu olarak bulunmuştur. Bu fark, esas olarak merkezdeki metal iyonlarının elektronik konfigürasyonundan kaynaklanmaktadır. Zn(II) iyonu, tam dolu bir d^{10} konfigürasyonuna sahip olup küresel simetri gösterir; bu nedenle elektron yoğunluğu transferi sınırlıdır ve sistemin kutuplanabilirlik düşüktür. Buna karşılık, Cu(II) iyonu, d^9 konfigürasyonuna sahip olduğundan, özellikle ligand-metal veya metal-ligand yük transferi mekanizmalarına izin vererek elektron yoğunluğunun daha kolay yeniden dağılmasına ve daha yüksek bir β(0;0,0değerine yol açmaktadır. Bu bağlamda, özellikle Cu(II) kompleksi, ikinci dereceden NLO uygulamaları (örneğin ikinci harmonik üretimi, elektro-optik modülasyon ve optik anahtarlama) için potansiyel bir aday olarak değerlendirilebilir.

3.2. 3-hidroksi ve 4-kloro ikameli piridin-2-karboksilik asidin yeni bir karışık ligand çinko(II) kompleksi: Sentez, karakterizasyon, NLO özellikleri ve DFT hesaplaması

Merve, Ş., Ömer, T., Necmi, D., Davut, A., Hayatullah. M. ve Yusuf, A. (2024). 3-hidroksi ve 4-kloro ikameli piridin-2-karboksilik asidin yeni bir karışık ligand çinko(II) kompleksi: Sentez, karakterizasyon, NLO özellikleri ve DFT hesaplaması. *Materials Today Communications*, 38, 108021. https://doi.org/10.1016/j.mtcomm.2024.108021

Bu çalışmada sentezlenen Zn(II) metal kompleksi, çinko asetat metal tuzu ile 3-hidroksipiridin-2-karboksilik asid ve 4-kloropiridin-2-karboksilik asidin etanol-su karışımı içinde karıştırılmasıyla elde edilmiştir. Elde edilen çözelti 50 °C'de 2 saat boyunca sürekli karıştırıldı. Daha sonra renksiz çözelti süzüldü ve 2 hafta boyunca oda sıcaklığında buharlaşmaya bırakıldı. Elde edilen renksiz kristaller daha sonra X-ışını kırınımı deneylerinde kullanıldı. Kristal yapının belirlenmesi amacıyla tek kristal X-ışını kırınım (SC-XRD) analizi gerçekleştirilmiş ve elde edilen veriler SHELXT programı ile çözülmüştür. Kristalografik analiz sonucunda yapının monoklinik kristal sisteminde ve P_n uzay grubunda kristalleştiği belirlenmiştir. Kompleks yapı içerisinde Zn(II) metal iyonunun bozulmuş bir oktahedral koordinasyon küresinin merkezine yerleştiği sonucuna ulaşılmıştır. Ayrıca kristal yapıda H···H, O···H/H···O, C···H/H···C, O···C/C···O, ve C···C gibi kovalent olmayan etkileşimlerin kompleksin istiflenmesinde aktif rol oynadıkları tespit edilmiştir.

[Zn(3OHpca)(4Clpca)(H_2O)$_2$] kompleksinin FT-IR spektrumda yaklaşık 3287 cm^{-1} civarında geniş bir OH gerilme bandı gözlemlenmiş olup, bu bant yapıda yer alan ve Zn(II) metal merkezine koordine olan H_2O molekülünü işaret etmektedir. Simetrik ve asimetrik karboksilat grubu (COO^-) titreşimleri sırasıyla 3OHpca, 4Clpca ve Zn(II) kompleksleri için 1678–1273 cm^{-1}, 1734–1305 cm^{-1} ve 1659–1300 cm^{-1}'de tespit edildi. Aynı bant Zn(II) kompleksi için 1662–1289 cm^{-1}'de B3LYP seviyesi kullanılarak da hesaplandı. Bu sonuçlardan görülebileceği gibi, asimetrik ve simetrik COOH titreşimleri arasındaki fark 3OHpca ligandı için 405 cm^{-1} ve 4Clpca ligandı için 429 cm^{-1}'dir. Asimetrik ve simetrik COO^-gerilme titreşimi arasındaki farka gelince, 359 cm^{-1} deneysel olarak ölçülmüş ve 373 cm^{-1} teorik olarak hesaplanmıştır. COOH asimetrik ve simetrik titreşim bantları arasındaki farktaki azalma, metal-ligand kompleksimizin O atomu aracılığıyla Zn metaline tek dişli ligand olarak koordine

olduğunu göstermektedir. Serbest piridin halkasında yaklaşık 1000 cm^{-1} civarında bildirilen halka soluklanma bandının, piridin halkasının Zn(II) iyonuna koordinasyonu üzerine 1054 cm^{-1}'e kaydığı gözlemlenmiştir.

Yüksek enerjili π→π * ve n→π* geçişleri 3OHpca için 225 ve 291 nm'de gözlendi. Aynı soğurma bantları 4Clpca için 228 ve 266 nm'de gözlendi. Bu ligandlar Zn(II) iyonuna koordine edildiğinde, ligandlar arası ve ligand içi π→π∗ ve n→π * geçişleri 201, 225, 265, 273 ve 299 nm'ye kaydığı tespit edilmiştir. Ligand metal yük transferi etkileşimleri ayrıca 341 nm'de gözlenen zayıf banttan da sorumlu olduğu sonucuna ulaşılmıştır.

Zn(II) kompleksinin HOMO ve LUMO enerjileri sırasıyla -6.5678 eV ve -2.4275 eV olarak belirlendi. Ligandlar ve Zn(II) kompleksi için HOMO–LUMO enerji aralığı sırasıyla 4.8595, 4.9999 ve 4.7358 eV olarak hesaplandı. HOMO ve LUMO arasındaki enerji aralığının ligandlar ve kompleks için 4Clpca>3OHpca>Zn(II) kompleksi şeklinde azalan bir düzende olduğu gözlemlenmiştir. Bu veriler elektronik konfigürasyonun değişimine karşı ligandların daha dirençli olduğunu gösteriyor. Kimyasal olarak yumuşak moleküller sert moleküllerden daha kolay polarize olduğundan, Zn(II) kompleksi kolayca polarize olabilir. Bu durum, bileşiğin elektrooptik özelliklerinin güçlü olduğunu ve fotonik uygulamalarda kullanılabilirliğini göstermektedir.

Sentezlenen kompleksin doğrusal olmayan optik (NLO) özellikleri, yoğunluk fonksiyonel teorisi (DFT) çerçevesinde B3LYP fonksiyoneli ve LanL2DZ baz seti kullanılarak teorik olarak değerlendirilmiştir. Yapılan hesaplamalar, molekülün kutuplanabilirlik ⟨α⟩, birinci mertebe yüksek kutuplanabilirlik ⟨β⟩ ve ikinci mertebe yüksek kutuplanabilirlik ⟨γ⟩ parametreleri açısından yüksek NLO performansı sergilediğini ortaya koymuştur.

B3LYP/6–311 + +G(d,p)/LanL2DZ seviyesindeki hesaplamalara göre, statik birinci mertebe yüksek kutuplanabilirlik parametresi β(0;0,0) sırasıyla 15382×10^{-34}, 36131×10^{-34} ve 4.5200×10^{-34} esu'dur. Zn(II) kompleksi ve ligandlar için statik ikinci mertebe yüksek kutuplanabilirlik parametresi γ(0;0,0,0) sırasıyla 3.1169×10^{-36}, 4.1968×10^{-36} ve 39.106×10^{-36} esu olarak hesaplanmıştır. Bu sonuçlardan da görüleceği üzere, statik birinci mertebe yüksek kutuplanabilirlik parametresi değeri

Zn(II) kompleksi için daha düşük iken, statik ikinci mertebe yüksek kutuplanabilirlik parametresi Zn(II) kompleksi için daha yüksektir.

Frekansa bağlı birinci mertebe yüksek kutuplanabilirlik parametreleri, elektro-optik Pockels etkisi β(-ω;ω,0) ve elektrik alanı kaynaklı ikinci harmonik üretim (EFSHG) β(−2ω;ω,ω) incelenmesini içerir. Frekansa bağlı ikinci mertebe yüksek kutuplanabilirlik çalışmalarına gelince, dc-Kerr etkisi γ(-ω;ω,0,0) ve EFSHG γ(−2ω;ω,ω,0) hesaplamaları yapılır. Zn(II) kompleksi için β(-ω;ω,0) ve β(−2ω;ω.ω) sırasıyla 1.6044×10^{-34} ve 49.720×10^{-34} esu olarak elde edilmiştir. Bu sonuçlar, Zn(II) kompleksinin statik ve frekansa bağlı birinci mertebe yüksek kutuplanabilirlik parametrelerinin oldukça düşük olduğunu göstermektedir. Zn(II) kompleksi için dc-Kerr etkisi γ(-ω;ω,0,0) ve EFSHG γ(−2ω;ω,ω,0) değerleri de sırasıyla 13.04×10^{-36} ve 2258.9×10^{-36} esu olarak hesaplanmıştır. Sonuç olarak, Zn(II) kompleksinin ikinci dereceden NLO özellikleri, benzer yapılar için literatürde bildirilenlerden daha düşük elde edilirken, üçüncü dereceden NLO özellikleri önemli ölçüde dikkate değerdir.

3.3. Kompleks Oluşumun Statik Ve Frekansa Bağlı Doğrusal Olmayan Optik Özellikler Üzerindeki Etkisi: Birleşik Deneysel Ve Teorik Araştırma

Ömer, T., Merve, Ş., Necmi, D., Davut, A. ve Yusuf, A. (2025). Kompleks oluşumun statik ve frekans bağımlı doğrusal olmayan optik özellikler üzerindeki etkisi: Birleştirilmiş deneysel ve teorik araştırma. *Spectrochimica Acta Part A Molecular and Biomolecular Spectroscopy*, 325, 125138. https://doi.org/10.1016/j.saa.2024.125138

Bu çalışmada, 6-bromopiridin-2-karboksilik asit (6Brpca) ve 4,4′-dimetil-2,2′-dipiridil (Dmdpy) ligandları ile Mn(II) iyonu kullanılarak, $[Mn(6Brpca)_2Dmdpy]\cdot CH_3OH$ kimyasal formüllü yeni bir karışık ligandlı geçiş metali kompleksi başarıyla sentezlenmiştir. Sentez prosedüründe, 6Brpca öncelikle etanol/su (1:1) çözeltisi içinde çözülmüş ve bu çözeltiye $(CH_3COO)_2Mn.4H_2O$ metal tuzu ilave edilmiştir. Homojen karışım elde edildikten sonra, nötr yardımcı ligand olarak Dmdpy eklenmiş ve karışım 50 °C'de 2 saat boyunca sürekli karıştırılarak sentez süreci tamamlanmıştır. Daha sonra renksiz çözelti 2 hafta boyunca oda sıcaklığında buharlaşmaya bırakılmıştır. Oluşan sarı renkli kristaller, hedeflenen kompleksin başarılı bir şekilde elde edildiğini göstermiştir.

Kristal yapının belirlenmesi amacıyla tek kristal X-ışını kırınım (SC-XRD) analizi gerçekleştirilmiş ve elde edilen veriler SHELXT programı ile çözülmüştür.

Kristalografik analiz sonucunda yapının monoklinik sistemde $P2_1/n$ uzay grubunda kristalleştiği belirlenmiştir. Merkezi Mn(II) iyonu, iki adet 6Brpca ve bir adet Dmdpy ligandıyla koordinasyon yaparak bozulmuş oktahedral bir geometri oluşturmaktadır. Kristal, molekülleri O—H···O ve C—H···O moleküller arası H bağları aracılığıyla üç boyutlu bir ağ oluşturur. Kompleksin istiflenmesinden sorumlu tüm etkileşimler güçlü hidrojen bağları gibi görünmektedir ve bu nedenle kompleksin termal kararlılığının yüksek olduğu sonucuna varılabilir

Mn(II) kompleksi kristal yapısında serbest bir CH_3OH molekülü içerir. FT-IR spektrumunda 3427 cm^{-1}'de gözlenen titreşim bandının CH_3OH molekülündeki OH gerilmesinden kaynaklandığı açıktır. B3LYP/LanL2DZ seviyesi kullanılarak elde edilen teorik spektrumdaki karşılık gelen titreşim bandı ise 3287 cm^{-1}'de bulunmuştur.

6Brpca için COO^- grubu asimetrik ve simetrik CO gerilme titreşimleri 1695 ve 1174 cm^{-1}'de gözlenmiştir. Mn(II) kompleksi için ise karşılık gelen bantlar 1609 ve 1291 cm^{-1}'de gözlenmiştir. Karboksilat grupları için asimetrik ve simetrik CO gerilme titreşimleri arasındaki farkın merkezi metal iyonlarına koordinasyonun önemli bir göstergesi olduğu iyi bilinmektedir. Serbest 6Brpca için 521 cm^{-1} ve Mn(II) kompleksi için 318 cm^{-1} olarak elde edilen fark, 6Brpca ligandının O atomları aracılığıyla Mn(II) iyonuna koordine olduğunu göstermektedir. Bu frekans farkı, karboksilat gruplarının O atomu aracılığıyla tek dişli koordinasyon modunda olduğunu göstermektedir

Halka solunum titreşimleri, aromatik ve heterosiklik bileşiklerin karakterizasyonunda önemli bir rol oynayan belirgin titreşim modlarıdır. Mevcut çalışmada, 986 ve 988 cm^{-1}'de gözlemlenen titreşim bantları sırasıyla 6Brpca ve Dmdpy ligandları için halka solunum titreşimleri olarak atanmıştır. Ligandlar merkezi Mn(II) iyonuna koordine edildikten sonra, bu titreşim bandı 1010 cm^{-1}'e kayarak piridin halkası N atomu aracılığıyla koordinasyonun olduğunu göstermektedir.

Yüksek enerjili $\pi \rightarrow \pi^*$ ve $n \rightarrow \pi^*$ geçişleri 6Brpca için 207, 222 ve 275 nm'de gözlendi. Aynı soğurma bantları Dmdpy için 209, 239 ve 281 nm'de gözlendi. Bu ligandlar Mn(II) iyonuna koordine edildiğinde, ligandlar arası ve ligand içi $\pi \rightarrow \pi*$ ve $n \rightarrow \pi^*$ geçişleri 206, 2225 ve 263 nm'ye kaydığı tespit edilmiştir. Ligand metal yük transferi etkileşimleri ayrıca 307 nm'de gözlenen zayıf banttan da sorumlu olduğu sonucuna ulaşılmıştır.

Mn(II) kompleksinin HOMO ve LUMO enerjileri sırasıyla -4.7379 eV ve -2.3129 eV olarak belirlendi. Dmdpy, 6Brpca ve Mn(II) kompleksi için HOMO–LUMO enerji aralığı sırasıyla 5.3079, 4.1401 ve 2.4250 eV olarak hesaplandı. HOMO ve LUMO arasındaki enerji aralığının ligandlar ve kompleks için Dmdpy>6Brpca>Mn(II) kompleksi şeklinde azalan bir düzende olduğu gözlemlenmiştir. Bu veriler elektronik konfigürasyonun değişimine karşı ligandların daha dirençli olduğunu gösteriyor. Kimyasal olarak yumuşak moleküller sert moleküllerden daha kolay polarize olduğundan, Mn(II) kompleksi kolayca polarize olabilir. Bu durum, bileşiğin elektrooptik özelliklerinin güçlü olduğunu ve fotonik uygulamalarda kullanılabilirliğini göstermektedir.

Sentezlenen kompleksin doğrusal olmayan optik (NLO) özellikleri, yoğunluk fonksiyonel teorisi (DFT) çerçevesinde B3LYP fonksiyoneli ve LanL2DZ baz seti kullanılarak hesaplanmıştır. B3LYP/LanL2DZ seviyesindeki hesaplamalara göre, statik birinci mertebe yüksek kutuplanabilirlik parametresi Dmdpy, 6Brpca ligandları ve Mn(II) kompleksi için β(0;0,0) sırasıyla 0.1801×10^{-30}, 3.5792×10^{-30} ve 62.498×10^{-30} esu'dur. Mn(II) kompleksi ve Dmdpy, 6Brpca ligandları için statik ikinci mertebe yüksek kutuplanabilirlik parametresi γ(0;0,0,0) sırasıyla 387.88×10^{-36}, 15.006×10^{-36} ve 6.1678×10^{-36} esu olarak hesaplanmıştır. Bu sonuçlardan da görüleceği üzere, statik birinci mertebe yüksek kutuplanabilirlik parametresi ve statik ikinci mertebe yüksek kutuplanabilirlik parametresi Mn(II) kompleksi için daha yüksektir.

Frekansa bağlı birinci mertebe yüksek kutuplanabilirlik parametreleri, elektro-optik Pockels etkisi β(-ω;ω,0) ve elektrik alanı kaynaklı ikinci harmonik üretim (EFSHG) β(−2ω;ω,ω) incelenmesini içerir. Frekansa bağlı ikinci mertebe yüksek kutuplanabilirlik çalışmalarına gelince, dc-Kerr etkisi γ(-ω;ω,0,0) ve EFSHG γ(−2ω;ω,ω,0) hesaplamaları yapılır. Mn(II) kompleksi için β(-ω;ω,0) ve β(−2ω;ω.ω) sırasıyla 15.12×10^{-30} (0.085628**)** ve 5663.8×10^{-30} esu (0.085628**)** olarak elde edilmiştir. Mn(II) kompleksi için dc-Kerr etkisi γ(-ω;ω,0,0) ve EFSHG γ(−2ω;ω,ω,0) değerleri de sırasıyla (0.085628**)** -360157×10^{-36} ve 153.776×10^{-36} esu olarak hesaplanmıştır. Sonuç olarak, Zn(II) kompleksinin ikinci dereceden ve üçüncü dereceden NLO uygulamaları için çok ümit verici bir aday olduğu sonucuna varılmıştır.

3.4. 4-kloro-Piridin-2-Karboksilik asit içeren Co(II) kompleksinin belirgin yüksek statik/dinamik birinci ve ikinci mertebe yüksek kutuplanabilirliği üzerinde kompleks oluşumunun etkisinin araştırılması

Merve, Ş., Ömer, T., Necmi, D., Davut, A. ve Yusuf, A. (2025). 4-kloro-Piridin-2-Karboksilik asit içeren Co(II) kompleksinin belirgin yüksek statik/dinamik birinci ve ikinci mertebe yüksek kutuplanabilrliği üzerinde kompleks oluşumunun etkisinin araştırılması. *Materials Science in Semiconductor Processing*, 188 (33), 109179. https://doi.org/10.1016/j.mssp.2024.109179

Bu çalışmada, 4-kloropiridin-2-karboksilik asit ligandı ile Co(II) iyonu kullanılarak $[Co(4Clpca)_2(H_2O)_2]$ kimyasal formüllü yeni bir geçiş metal kompleksi başarıyla sentezlenmiştir. Sentez prosedüründe, 2 mmol 4-kloropiridin-2-karboksilik asidin (4Clpca) 30 mL 1:1 etanol ve su karışımında çözüldü ve bu çözeltiye $Co(CH_3COO)_2{\cdot}2H_2O$ metal tuzu ilave edilmiş ve karışım 50 °C'de 2 saat boyunca sürekli karıştırılarak kristalizasyon süreci tamamlanmıştır. Daha sonra turuncu renkte elde edilen çözelti iki hafta boyunca oda sıcaklığında buharlaşmaya bırakıldı.

Kristal yapının belirlenmesi amacıyla tek kristal X-ışını kırınım (SC-XRD) analizi gerçekleştirilmiştir ve elde edilen veriler SHELXT programı ile çözülmüştür. Kristalografik analiz sonucunda yapının monoklinik kristal sisteminde ve C2/c uzay grubunda kristallenmiş olup, Co(II) iyonunun bozulmuş oktahedral geometriye sahip olduğu tespit edilmiştir. Kristal molekülleri O—H···O, C—H···O ve C—H···Cl moleküller arası H bağları ile üç boyutlu bir ağ oluştururlar. Kompleksin istiflenmesinden sorumlu tüm etkileşimler güçlü hidrojen bağları gibi görünmektedir ve bu nedenle kompleksin termal kararlılığının yüksek olduğu sonucuna varılabilir.

Yeni sentezlenen $[Co(4Clpca)_2(H_2O)_2]$ kompleksinde, H_2O ligandından kaynaklanan OH gerilmesi için titreşim bandı deneysel olarak 3245 cm^{-1}'de ölçülmüştür. Bu titreşim bandı için karşılık gelen teorik veriler, B3LYP ve CAM-B3LYP seviyeleri için 3693 ve 3741 cm^{-1} olarak hesaplanmıştır. Özellikle OH gerilme titreşimlerinde teorik olarak elde edilen titreşim frekansının deneysel değerlerden yüksek olduğu bilinmektedir. Bu durumun deneysel spektrumlar, moleküller arası etkileşimlerin baskın olduğu katı fazda kaydedilirken, teorik spektrum, moleküller arası etkileşimlerin oldukça zayıf olduğu izole gaz fazında hesaplanmasından kaynaklanmaktadır.

Mevcut çalışmada, asimetrik ν CO gerilme titreşimi 1619 cm^{-1}'de gözlenmiştir ve B3LYP/CAM-B3LYP seviyesi kullanılarak 1584/1636 cm^{-1}'de hesaplanmıştır. Simetrik ν CO gerilme titreşim bandı da 1256 cm^{-1}'de gözlemlendi. 4-Kloro-piridin-2-karboksilik asit ligandının FT-IR spektrumunda, asimetrik ve simetrik ν CO bantları 1698 ve 1226 cm^{-1}'de gözlemlenmiş ve aralarındaki fark 472 cm^{-1} olarak bulunmuştur. Co(II) için simetrik ve asimetrik ν CO bantları arasındaki dalga sayısı farkı 363 cm^{-1} olarak bulunmuştur ve bu da 4-Kloro-piridin-2-karboksilik asit ligandının karboksilat grubu O atomu aracılığıyla Co(II) iyonuna koordine olduğunu göstermektedir.

Ayrıca, 4-Kloro-piridin-2-karboksilik asit ligandının FT-IR spektrumunda piridin halkasal titreşimlerine ait soluklanma bandı 998 cm^{-1}'de ölçülmüş olup, Co(II) kompleksi için aynı bant 1036 cm^{-1}'de belirlenmiştir. B3LYP ve CAM-B3LYP seviyeleri kullanılarak ise 1011 ve 1035 cm^{-1}'de hesaplanmıştır. Halka soluklanma titreşimleri bandındaki serbest liganda göre oluşan kayma ligandın piridin N atomu aracılığıyla Co(II) iyonuna koordine olduğunu gösterir.

$[Co(4Clpca)_2(H_2O)_2]$ kompleksinin deneysel UV-Vis spektrumunda, 206 ve 259 nm'de gözlenen bantlar $\pi \rightarrow \pi*$ ve $n \rightarrow \pi*$ elektronik geçişleri olarak atanmıştır. Teorik spektrumdaki karşılık gelen veriler sırasıyla CAM-B3LYP seviyesi kullanılarak 226 ve 278 nm'de hesaplandı. B3LYP seviyesi ayrıca sırasıyla 235 ve 274 nm'de bu elektronik soğurma bantlarını tahmin etti. 305 nm'de gözlenen en yüksek deneysel soğurma bandı, B3LYP ve CAM-B3LYP seviyeleri kullanılarak 294 ve 295 nm olarak hesaplandı ve bu soğurma bandları ligand metal yük transfer geçişleri olarak atanmıştır.

B3LYP seviyesi sonuçlarına göre, HOMO ve LUMO enerjileri sırasıyla -6.4494 ve -2.4672 eV olarak hesaplandı. Bu enerjiler, Co(II) kompleksinin elektronik özellikleri ve reaktifliği hakkında önemli bilgiler sağlar. HOMO ve LUMO arasındaki enerji boşluğu (ΔE = 3.9823 eV), kompleksin elektronik yük transfer yeteneğini yansıtır.

Co(II) kompleksinin HOMO ve LUMO B3LYP/LanL2DZ ve CAM-B3LYP/LanL2DZ seviyeleri kullanılarak hesaplanmıştır. Bu enerjiler sırasıyla -6,4494 ve -2,4672 eV olarak hesaplandı. 4Clpca ligandı ve Co(II) kompleksi için HOMO–LUMO enerji aralığı B3LYP/LanL2DZ seviyesi ile 4.9999 ve 3.9823 eV olarak elde edilmiştir. Daha küçük bir ΔE, Co(II) kompleksini içeren redoks reaksiyonlarında alakalı olabilecek daha kolay bir elektron transferini gösterir. Bu

durumda nispeten küçük ΔE, elektron transferini içeren elektronik geçişlerin kolayca meydana gelme olasılığını gösterir. Daha düşük bir HOMO enerjisi, daha güçlü ligand alanı etkilerini gösterir ve ligandlara daha yüksek derecede elektron delokalizasyonu anlamına gelir. Bu durum, metal-organik koordinasyon bileşiğinin yalnızca 4Clpca ligandına göre elektrooptik özelliklerinin güçlü olduğunu ve fotonik uygulamalarda kullanılabilirliğini göstermektedir.

$[Co(4Clpca)_2(H_2O)_2]$ kompleksinin doğrusal olmayan optik (NLO) özellikleri hem statik hem de frekans bağımlı koşullar altında detaylı biçimde teorik olarak hesaplanmıştır. Bu bağlamda, kompleksin kutuplanabilirlik (<α>), Yönelime bağlı kutuplanabilirlik (Δα), birinci mertebe yüksek kutuplanabilirlik (<β>) ve ikinci mertebe yüksek kutuplanabilirlik (<γ>) değerleri, DFT-B3LYP ve CAM-B3LYP fonksiyonelleri ile LanL2DZ temel seti kullanılarak hesaplanmıştır.

B3LYP/LanL2DZ ve CAM-B3LYP/LanL2DZ seviyelerindeki hesaplamalara göre, statik birinci mertebe yüksek kutuplanabilirlik parametresi 4Clpca ligandı ve Co(II) kompleksi için β(0;0,0) sırasıyla $4.1969 \times 10^{-30} - 3.0532 \times 10^{-30}$ ve $0{,}0018 \times 10^{-30} - 0{,}0007 \times 10^{-30}$ esu'dur. Co(II) kompleksi için elde edilen β (0;0,0) parametreleri karşılaştırıldığında, 4Clpca ligandı Co(II) iyonuna bağlandıktan sonra, merkezi simetrik yapının oluşması nedeniyle β (0;0,0) parametreleri azalır. Co(II) kompleksi ve 4Clpca ligandı için statik ikinci mertebe yüksek kutuplanabilirlik parametresi B3LYP/LanL2DZ ve CAM-B3LYP/LanL2DZ seviyerindeki hesaplamalar için sırasıyla γ(0;0,0,0) sırasıyla $60.891 \times 10^{-36} - 30.805 \times 10^{-36}$ ve $1.1892 \times 10^{-36} - 3.2938 \times 10^{-36}$ esu olarak hesaplanmıştır. Bu sonuçlardan da görüleceği üzere, statik birinci mertebe yüksek kutuplanabilirlik parametresi Co(II) kompleksi için daha küçükken, statik ikinci mertebe yüksek kutuplanabilirlik parametresi Co(II) kompleksi için daha yüksektir. Bu artış, metal-ligand etkileşimleri sonucu oluşan yük dağılımı yeniden organizasyonu ve molekül içerisindeki π-elektron delokalizasyonunun artmasına bağlanmaktadır. Kompleksleşme ile molekülde meydana gelen orbital yeniden düzenlemeler, özellikle HOMO'dan LUMO'ya olan geçişlerdeki yük transfer mekanizmalarını güçlendirerek üçüncü mertebeden NLO tepkisini belirgin şekilde artırmaktadır.

Frekansa bağlı birinci mertebe yüksek kutuplanabilirlik parametreleri, elektro-optik Pockels etkisi β(-ω;ω,0) ve elektrik alanı kaynaklı ikinci harmonik üretim (EFSHG) β(−2ω;ω,ω) incelenmesini içerir. Co(II) kompleksi için β(-ω;ω,0) ve β(−2ω;ω.ω)

değerleri B3LYP/LanL2DZ ve CAM-B3LYP/LanL2DZ seviyerindeki hesaplamalar için sırasıyla $0.0118\times10^{-30} - 0.0250\times10^{-30}$ ve $0.0950\times10^{-30} - 0.0600\times10^{-30}$ esu olarak elde edilmiştir. Co(II) kompleksi için dc-Kerr etkisi γ(-ω;ω,0,0) değerleri de B3LYP/LanL2DZ ve CAM-B3LYP/LanL2DZ seviyerindeki hesaplamalar için sırasıyla 329.59×10^{-36} – 10.043×10^{-36} esu olarak hesaplanmıştır. Sonuç olarak, Co(II) kompleksinin ikinci dereceden düşük NLO değeri sergilesede ve üçüncü dereceden NLO uygulamaları için ümit vaad eden bir aday olduğu sonucuna varılmıştır.

3.5. 6-floropiridin-2-karboksilik asidin yeni bir Cu(II) kompleksinin yapısal, titreşimsel, termal ve doğrusal olmayan optik özelliklerinin araştırılması

Ömer, T., Merve, Ş., Davut, A.,Adil, B., Mebarek, B., Mohamed, B., Necmi, D. ve Yusuf, A. (2025). 6-floropiridin-2-karboksilik asidin yeni bir Cu(II) kompleksinin yapısal, titreşimsel, termal ve doğrusal olmayan optik özelliklerinin araştırılması. *Journal of Molecular Structure*, 1342 ,142707. https://doi.org/10.1016/j.molstruc.2025.142707

Bu çalışmada, 6-floropiridin-2-karboksilik asit (6Fpca) ligandı ile Cu(II) iyonu kullanılarak [$Cu(6Fpca)_2(H_2O)$] formülünde yeni bir, geçiş metal kompleksi başarıyla sentezlenmiştir. Sentez prosedüründe, 0.2 mmol 6-floropiridin-2-karboksilik asit (6Fpca) 30 mL 1:1 etanol ve su karışımında çözüldü ve bu çözeltiye $Cu(CH_3COO)_2{\cdot}2H_2O$ metal tuzu ilave edilmiş ve karışım 50 °C'de 2 saat boyunca sürekli karıştırılarak sentez süreci tamamlanmıştır. Daha sonra mavi renkte elde edilen çözelti iki hafta boyunca oda sıcaklığında buharlaşmaya bırakıldı. Mavi renkli kristaller toplanarak soğuk ethanolde yıkanmıştır.

Kristal yapının belirlenmesi amacıyla tek kristal X-ışını kırınım (SC-XRD) analizi gerçekleştirilmiştir ve elde edilen veriler SHELXT programı ile çözülmüştür. Kristalografik analiz sonucunda yapının ortorombik kristal sisteminde ve *Pbca* uzay grubunda kristallenmiş olup, Cu(II) iyonunun bozulmuş bozulmuş tetragonal piramidal geometriye sahip olduğu tespit edilmiştir. Kristal O-H···O, C—H···F, C-H···N ve C-H···O moleküller arası H bağları vasıtasıyla üç boyutlu bir ağ oluşturur.

Kompleksin istiflenmesinde güçlü hidrojen bağları etkin olduğu için, kompleksin termal kararlılığının yüksek olduğu sonucuna varılabilir.

FT-IR analizinde, serbest 6Fpca ligandına ait teorik OH gerilme titreşimi 3390 cm^{-1}'de hesaplanmışken, bu titreşim koordinasyon sonrası ortadan kalkmış ve kompleks

yapıda, Cu(II) ile koordineli H_2O molekülüne ait yeni OH titreşimi 3449 cm^{-1}'de gözlemlenmiştir. Bu bant kompleks yapısında su moleküllerinin varlığına işaret etmektedir. Karboksilat grubunun (COO^-) karakteristik asimetrik ve simetrik gerilme titreşimleri ligand ve Cu(II) kompleksi için sırasıyla 1639 ve 1274 cm^{-1}'de belirlenmiş ve bu iki pik arasındaki 419 cm^{-1}'lik fark, karboksilat grubunun O atomu üzerinden tek dişli koordinasyonunu işaret etmektedir.

Ayrıca, 6Fpca ligandı için piridin halkasına ait soluklanma bandı 998 cm^{-1}'de ölçülmüş olup, Co(II) kompleksi için aynı bant 1020 cm^{-1}'de belirlenmiş olup B3LYP seviyesi kullanılarak 1007 cm^{-1}'de hesaplanmıştır. Halka soluklanma titreşimleri bandındaki serbest liganda göre oluşan kayma ligandın piridin N atomu aracılığıyla Cu(II) iyonuna koordine olduğunu gösterir.

Yüksek enerjili $\pi \rightarrow \pi^*$ ve $n \rightarrow \pi^*$ geçişleri deneysel olarak Cu(II) kompleksi için 213 ve 263 nm'de gözlendi. Aynı soğurma bantları teorik olarak sırasıyla 209, 227 ve 244 nm'de hesaplandı. Ligant metal yük transferi (LMCT) etkileşimleri deneysel ve teorik olarak sırasıyla 369 ve 383 nm'de gözlenen zayıf banttan da sorumlu olduğu sonucuna ulaşılmıştır.

Cu(II) kompleksinin HOMO ve LUMO enerjileri B3LYP/LanL2DZ seviyesi kullanılarak hesaplanmıştır. Bu enerjiler sırasıyla-6.8244 ve -3.5151 eV olarak hesaplandı. 6Fpca ligandı ve Cu(II) kompleksi için HOMO–LUMO enerji aralığı sırasıyla 4.5398 ve 3.3094 eV olarak hesaplandı. Bu enerji boşlukları, 6Fpca ligandının karşılık gelen Cu(II) kompleksinden daha yüksek kararlılığa ve daha düşük reaktiviteye sahip olduğunu gösterir.

$[Cu(6Fpca)_2(H_2O)]$ kompleksinin NLO özellikleri hem statik hem de frekansa bağlı yüksek mertebe kutuplanılabilirlik parametreleri üzerinden derinlemesine incelenmiştir. Bu bağlamda, kompleksin moleküler polarizabilite (α), birinci mertebe yüksek kutuplanabilirlik (β) ve ikinci mertebe yüksek kutuplanabilirlik (γ) değerleri, koordinasyon sonucunda önemli ölçüde artış göstermiştir.

B3LYP/LanL2DZ seviyesindeki hesaplamalara göre, statik birinci mertebe yüksek kutuplanabilirlik parametresi 6Fpca ligandı ve Cu(II) kompleksi için $\beta(0;0,0)$ sırasıyla 1.6537×10^{-30} ve 3.0188×10^{-30} esu'dur. Cu(II) kompleksi ve ligandın statik ikinci mertebe yüksek kutuplanabilirlik parametresi $\gamma(0;0,0,0)$ sırasıyla 3.5860×10^{-36} ve 19.667×10^{-36} esu olarak hesaplanmıştır. Bu sonuçlardan da görüleceği üzere, statik

birinci mertebe yüksek kutuplanabilirlik parametresi liganda oranla daha düşük sonuçlar vermişken ve statik ikinci mertebe yüksek kutuplanabilirlik parametresi Mn(II) kompleksi için daha yüksektir. . Bu artış, kompleksin elektron bulutunun koordinasyon sonrası daha kolay kutuplanabildiğini göstermektedir.

Frekans bağımlı NLO parametreleri, iki farklı radyasyon frekansında (ω = 0.0856252 ve 0.0428126 a.u.) hesaplanmıştır, Cu(II) kompleksi için en yüksek β(-ω;ω,0) değeri 22.265×10^{-30} esu ile 0.0856252 a.u. frekansında elde edilmiştir ve β(−2ω;ω.ω) değeri ise 14.206×10^{-30} esu(0.085628 a.u.**)** olarak elde edilmiştir. Mn(II) kompleksi için dc-Kerr etkisi γ(-ω;ω,0,0) ve EFSHG γ(−2ω;ω,ω,0) değerleri de sırasıyla 147.552×10^{-36} ve 169.670×10^{-36} esu olarak hesaplanmıştır. Cu(II) kompleksi için γ (-ω; ω,0,0) ve γ (−2 ω;ω,ω,0) değerlerindeki artış, kompleksin daha büyük elektronik sistemine ve koordinasyon kaynaklı elektron delokalizasyonuna atfedilebilen üçüncü dereceden NLO özelliklerinde önemli bir gelişmeyi göstermektedir. Bu nedenle, bozulma ve su molekülünün ek koordinasyonu tarafından ortaya çıkarılan asimetri, kompleks içindeki elektron delokalizasyonunu ve yük transferini artırarak serbest 6Fpca ligandına kıyasla daha yüksek polarize edilebilirlik ve hiperpolarize edilebilirlik değerlerine yol açmaktadır. Metal merkez ile ligandlar arasındaki güçlü donör-akseptör etkileşimleri, kompleksin NLO tepkisini indüklemede önemli bir rol oynamaktadır.

4. SONUÇLAR VE TARTIŞMA

Bu kapsamlı araştırma çerçevesinde, 6-klor, 6-flor, 3-hidroksi, ve 4-klor ikameli piridin-2-karboksilik asit türevleriyle tasarlanmış Zn(II), Cu(II), Co(II) ve Mn(II) merkezli toplam altı farklı kompleksin yapısal, spektroskopik ve optoelektronik özellikleri detaylı biçimde değerlendirilmiştir. Kristal yapılar üzerinden yapılan analizler, koordinasyon geometrilerinin metal iyonunun elektronik konfigürasyonuna ve bağlanan ligandların sterik/elektronik özelliklerine bağlı olarak farklılaştığını göstermektedir. [Zn(6Clpca)$_2$·(H$_2$O)$_2$],[Co(4Clpca)$_2$·(H$_2$O)$_2$], Mn(6Brpca)$_2$(Dmdpy)]· CH$_3$OH$_2$ ve [Zn(4Clpca)(3OHpca)·(H$_2$O)$_2$] komplekslerinin kristal yapıları bozulmuş oktahedral bir geometri sergilemiş; altı koordinasyon noktasında ligandların piridin azotu ve karboksilat oksijen atomları ile bağlandığı belirlenmiştir. Benzer şekilde, [Cu(6Fpca)$_2$(H$_2$O)] ve [Cu(6Clpca)$_2$(H$_2$O)] komplekslerinde ise tetragonal piramidal koordinasyon geometrisi sergilediği belirlenmiştir.

Spektroskopik açıdan değerlendirildiğinde, FT-IR verileri hem ligandların koordinasyon durumunu doğrulayan hem de yapısal dönüşümleri izlemeyi mümkün kılan karakteristik bant değişimlerini ortaya koymuştur. O-H gerilme titreşimleri, [Zn(6Clpca)$_2$(H$_2$O)$_2$] için 3239 cm^{-1}, [Cu(6Clpca)$_2$(H$_2$O)] için 3188 cm^{-1}, [Zn(3OHpca)(4Clpca)$_2$.H$_2$O] için 3287 cm^{-1}, [Mn(6Brpca)$_2$Dmdpy].CH$_3$OH için 3427 cm^{-1}, [Co(4Clpca)$_2$(H$_2$O)$_2$] için 3245 cm^{-1} ve [Cu(6Fpca)$_2$(H$_2$O)] için 3449 cm^{-1} olarak kaydedilmiştir. Karboksilat gruplarının simetrik ve asimetrik gerilme frekansları arasındaki Δν farkı, sırasıyla [Zn(6Clpca)$_2$(H$_2$O)$_2$] için 392 cm^{-1}, [Cu(6Clpca)$_2$(H$_2$O) için 369 cm^{-1}, [Mn(6Brpca)$_2$(Dmdpy)]. CH$_3$OH için 318 cm^{-1}, [Co(4Clpca)$_2$(H$_2$O)$_2$] için 363 cm^{-1} , [Zn(3OHpca)(4Clpca)$_2$.H$_2$O] için 359 cm^{-1} ve [Cu(6Fpca)$_2$(H$_2$O)] için 419 cm^{-1} olup, ligandların çoğunlukla tek dişli koordinasyon sergilediğini göstermektedir. Ayrıca, piridin halkasının soluklanma titreşimleri de [Zn(6Clpca)$_2$(H$_2$O)$_2$] ve [Cu(6Clpca)$_2$(H$_2$O)] komplekslerinde 1008 cm^{-1}, [Mn(6Brpca)$_2$Dmdpy].CH$_3$OH'de 986–1010 cm^{-1}, [Co(4Clpca)$_2$(H$_2$O)$_2$]'de 1036 cm^{-1} [Zn(3OHpca)(4Clpca)$_2$.H$_2$O] kompleksinde 1054 cm^{-1} ve [Cu(6Fpca)$_2$(H$_2$O)]'de 1032 cm^{-1}'de gözlemlenmiştir. Bu sonuçlar, metal merkezinin elektron yoğunluğuna

etkisiyle birlikte ligandın rezonans yapısını yeniden şekillendirdiğini ve buna bağlı olarak moleküler simetri ile polarizasyon davranışlarının değiştiğini göstermektedir.

UV-Vis spektral analizler, her bir kompleksin özgün elektronik geçiş davranışlarını ortaya koymuştur. $[Cu(6Fpca)_2(H_2O)]$ kompleksinde $\pi \rightarrow \pi^*$ geçişine karşılık gelen bant 263 nm'de, ligand-metal yük transfer (LMCT) geçişi ise 369 nm'de gözlemlenmiştir. $[Mn(6Brpca)_2(Dmdpy)]\cdot CH_3OH$ kompleksinde ise ligand içi geçişler 209, 227 ve 244 nm civarında (LMCT) geçişi ise 383 nm'de kaydedilmiştir. $[Cu(6Clpca)_2(H_2O)]$ kompleksinde $[Zn(6Clpca)_2(H_2O)_2$ kompleksinde UV geçişleri daha yüksek enerjiye karşılık gelen 253-274 nm civarındayken (LMCT) geçişi ise 310 nm civarındadır. $[Zn(3OHpca)(4Clpca)_2.H_2O]$ kompleksinde 201-285 nm aralığında $\pi \rightarrow \pi^*$ geçişine karşılık gelen bantlar gözlenmiş ve MLCT yük geçişi gözlenmemişken, $[Co(4Clpca)_2(H_2O)_2]$ kompleksinde teorik olarak 305 ve 356 nm'de MLCT karakterli geçişler saptanmıştır.

NLO parametreleri açısından değerlendirildiğinde, her kompleksin moleküler polarizabilite ($<\alpha>$), birinci mertebe yüksek kutuplanabilirlik ($<\beta>$) ve ikinci mertebe yüksek kutuplanabilirlik ($<\gamma>$) değerleri sistematik olarak hesaplanmış ve hem statik hem de dinamik koşullar altında karşılaştırılmıştır. Özellikle $[Mn(6Brpca)_2(Dmdpy)].CH_3OH$ kompleksinin statik $<\beta>$ değeri 62.498×10^{-30} esu, frekans-bağımlı $<\beta>$ değeri ise $11,448\times10^{-30}$ esu olarak tespit edilmiş; buna karşılık $<\gamma>$ değeri statik koşullarda 387.88×10^{-36} esu, dinamik koşullarda (532 nm, ω=0.0856252 a.u.) ise 680.035×10^{-36} esu olarak hesaplanmıştır. Bu değerler, literatürdeki geleneksel NLO referanslarından (örneğin p-nitroanilin $<\beta> = 8\times10^{-30}$ esu ve üre $<\beta>=0,130\times10^{-30}$ esu) yüksek olup, bu kompleksin üçüncü derece NLO uygulamalarında (üçüncü harmonik üretimi, Kerr etkisi, iki foton absorpsiyon vb.) son derece güçlü bir aday olduğunu göstermektedir. $[Cu(6Clpca)_2(H_2O)]$ kompleksinde $<\beta>$ değeri 10.40×10^{-30} esu, dipol moment 4.0259 Debye, $<\alpha>$ değeri ise 1.19×10^{-23} esu olarak belirlenmiştir. Bu parametreler, Cu(II) iyonunun d^9 konfigürasyonu ve ligand-metal arasında etkin yük transferi sayesinde güçlü ikinci mertebe yüksek kutuplanabilirlik NLO yanıtın elde edildiğini ortaya koymaktadır. $[Zn(6Clpca)_2(H_2O)_2]$ kompleksinde ise $<\beta>$ değeri yalnızca 0.88×10^{-30} esu olup, Zn(II)'nin tam dolu d^{10} yapısına bağlı olarak yük transfer kapasitesinin sınırlı olduğu anlaşılmıştır. Aynı zamanda dipol momentin düşük olması (Debye) ve kutuplanabilirlik (1.79×10^{-23} esu) Cu(II) kompleksine kıyasla daha yüksek olmasına

rağmen <β> değerinin düşük kalması, doğrusal olmayan yanıtın yönlenmiş yük dağılımı ve asimetriyle yakından ilişkili olduğunu göstermektedir. $[Co(4Clpca)_2(H_2O)_2]$ kompleksinde ise iki farklı hesaplama yöntemiyle yapılmış olan hesaplamalarda dikkat çekici bir biçimde değerler B3LYP hesaplama yöntemi ile yapılan hesaplamalarda daha iyi sonuç vermiştir. Bu sonuçlara bakıldığında statik <β> değeri 0.0018×10^{-30} esu ve frekansa bağlı <β> değeri 0.0950×10^{-30} esu gibi ihmal edilebilir düzeyde olmasına karşın, statik <γ> değeri 60.891×10^{-36} esu ve frekansa bağlı <γ> değeri ise 433.93×10^{-36} esu ile oldukça yüksek bulunmuştur. Bu sonuç, kristalin simetrik yapısı nedeniyle birinci mertebe yüksek kutuplanabilirlik NLO yanıtın baskılanırken, ikinci mertebe yüksek kutuplanabilirlik cevapların (özellikle frekans bağımlı γ parametrelerinin) orbital yeniden düzenlenme ile kuvvetlendiğini göstermektedir. Koordinasyon sonucu oluşan π-delokalizasyon ve azalan HOMO-LUMO farkı (ΔE = 3.98 eV) bu yüksek mertebe kutuplanabilirliğin önemli sebeplerindendir. $[Cu(6Fpca)_2(H_2O)]$ kompleksinde statik <β> değeri 3.0188×10^{-23} esu, <γ> değeri ise 19.667×10^{-36} esu olarak hesaplanmıştır. Frekans bağımlı ölçümlerde β(-ω;ω,0) değeri 22.265×10^{-30} esu, γ(-ω;ω,0,0) değeri ise 111.07×10^{-36} esu (ω=0.0856252 a.u.) olarak bulunmuştur. Bu sonuçlar, özellikle kompleksin metal merkezine koordine olmuş su molekülüyle birlikte kazandığı asimetrik yapı sayesinde ikinci mertebe yüksek kutuplanabilirlik NLO performansında belirgin bir iyileşme sağladığını göstermektedir. Son olarak $[Zn(3OHpca)(4Clpca)_2 \cdot H_2O]$ kompleksinin statik <β> değeri 4.5200×10^{-34} esu, <γ> değeri ise 39.106×10^{-36} esu olarak hesaplanmıştır. Frekans bağımlı ölçümlerde β(-2ω;ω,ω) değeri 49.720×10^{-30} esu, γ(-ω;ω,ω,0) değeri ise 22.589×10^{-36} esu (ω=0.0856252 a.u.) olarak bulunmuştur.

Doğrusal olmayan optik (NLO) yanıtlar açısından değerlendirildiğinde, çalışmada incelenen tüm kompleksler için moleküler polarizabilite (<α>), birinci mertebe yüksek kutuplanabilirlik (<β>) ve ikinci mertebe yüksek kutuplanabilirlik (<γ>) parametreleri detaylı şekilde hesaplanmış ve hem statik hem de belirli dalga boyunda frekans-bağımlı koşullarda yorumlanmıştır. Tüm bu veriler birlikte değerlendirildiğinde, komplekslerdeki doğrusal olmayan optik özelliklerin yalnızca HOMO–LUMO enerji farkı veya ligand yapısıyla sınırlı olmadığı, aynı zamanda yapısal asimetri, elektron donör-akseptör dizilimi, yük transfer yolları ve kristal simetrisi gibi çok sayıda etkileşimli faktörün kombinasyonu ile ortaya çıktığı anlaşılmaktadır. Bu bağlamda, $[Mn(6Brpca)_2(Dmdpy)] \cdot CH_3OH$, $[Zn(3OHpca)(4Clpca)_2.H_2O]$ ve $[Cu(6Fpca)_2(H_2O)]$

gibi kompleksler, sahip oldukları düşük enerji aralığı, yüksek mertebe kutuplanılabilirlik değerleri ve elektronik olarak yönlenmiş yapıları sayesinde, hem birinci hem de ikinci derece NLO cihaz uygulamaları için son derece uygun moleküler adaylar olarak öne çıkmaktadır. Bu bulgular, moleküler düzeyde NLO özelliklerin rasyonel ligand tasarımı ve uygun metal seçimleriyle optimize edilebileceğini, böylece ileri düzey fotonik ve elektro-optik teknolojilerde yeni nesil fonksiyonel malzeme geliştirme açısından güçlü bir temel oluşturduğunu ortaya koymaktadır.

5. ÖNERİLER

Bu kapsamlı araştırma, metal-organik komplekslerin doğrusal olmayan optik (NLO) özellikleriyle geometrik yapıları arasındaki ilişkinin anlaşılması ve yönlendirilmesine yönelik literatürde önemli bir temel oluşturmuştur. Elde edilen teorik NLO verileri ışığında, bu yapıların NLO davranışlarını daha iyi anlamak ve potansiyel uygulamalara uyarlamak amacıyla ileriye dönük birtakım öneriler aşağıda sunulmuştur.

Öncelikle, ligand yapılarında gerçekleştirilecek olan fonksiyonel gruplandırma ve yapısal modifikasyonların, moleküllerin polarizasyon kapasitesini artırarak <β> ve <γ> gibi NLO parametrelerinin optimize edilmesine katkı sunacağı sonucuna ulaşılmıştır. Tez çalışmasında, diğer komplekslere daha üstün NLO parametrelerine sahip olan Mn(II) ve Cu(II) iyonu içeren kompleksler göz önüne alarak, bu metal iyonlarını içeren daha sonraki yapılacak olan çalışmaların daha üstün NLO parametrelerine sahip olabileceği düşünülmektedir.

Ayrıca, yapısal ve elektronik olarak asimetriyi sağlayan ikincil nötral ligandların kompleks yapıya koordine olmasıyla NLO davranışındaki belirgin iyileşme bu tez kapsamında bizzat tespit edilmiştir. Daha sonra yapılacak olan benzer çalışmalarda, kompleks içerisinde ikincil nötral ligandların da yer alması daha iyi NLO malzemlerinin elde edilmesini sağlayabilir.

Ayrıca, metal kompleksinin karşılıklı kenarlarında elektron sağlayıcı ve elektron çekici fonksiyonel grupların bulunması bir D-π-A yapısı oluşturarak NLO yanıtlarının daha üstün olmasına olanak sağladığı bilinmektedir. Bu Bağlamda, elektron sağlayıcı ve elektron çekici fonksiyonel grup veya atomların kompleksin harşılıklı kenarlarında olacak şekilde yerleşmesi komplekslere NLO özellikleri açısından önemli bir avantaj sağlayacaktır. Bu bağlamda, yeni çalışmalarda ligand seçimi yaparken bu duruma dikkat edilmesi gerekmektedir.

Bu tez çalışmasında yürütülen teorik NLO hesaplamalarına ek olarak, ileri dönem çalışmalarında NLO özelliklerinin deneysel olarak ölçülmesinde kullanılan Z-scan yöntemindan faydalanarak daha kapsamlı bir analiz yapılabilir. Bu sayede hem

deneysel hemde teorik metotlar kullanılarak, ilgili yapıların NLO davranışları hakkında çok daha detaylı bir bilgi elde edilebilir.

KAYNAKLAR

[1] Chemla DS, Zyss J (1987) Nonlinear optical properties of organic molecules and crystals

[2] Boyd RW (2008) Nonlinear Optics, 3rd ed. Academic Press, Burlington, MA

[3] Marder SR, Perry JW, Schaefer WP (1989) Synthesis of Organic Salts with Large Second-Order Optical Nonlinearities. Science (1979) 245:626

[4] Prasad PN (2004) Introduction to Nonlinear Optical Effects in Molecules and Polymers. Wiley-Interscience, Hoboken, NJ

[5] Nikogosyan DN (2005) Nonlinear Optical Crystals: A Complete Survey. Springer, Berlin

[6] Dmitriev VG, Gurzadyan GG, Nikogosyan DN (1999) Handbook of Nonlinear Optical Crystals. Springer, Berlin

[7] Ghosh S, Bharadwaj PK (2004) Structure of a Discrete Hexadecameric Water Cluster in a Metal-Organic Framework. Inorg Chem 43:5180–5182. https://doi.org/10.1021/ic049461j

[8] Tamer Ö, Tamer SA, İdil Ö, et al (2018) Antimicrobial activities, DNA interactions, spectroscopic (FT-IR and UV-Vis) characterizations, and DFT calculations for pyridine-2-carboxylic acid and its derivates. J Mol Struct 1152:399–408. https://doi.org/10.1016/J.MOLSTRUC.2017.09.100

[9] Manjunatha KB, Rajarao R, Poornesh P, et al (2019) Enhanced photostability and optical nonlinearity of nickel and cobalt organometallic complexes. Opt Mater (Amst) 89:494–497. https://doi.org/https://doi.org/10.1016/j.optmat.2019.01.076

[10] Siji Narendran NK, Soman R, Arunkumar C, Chandrasekharan K (2015) Third-order nonlinear optical investigations of meso-tetrakis(2,3,5,6-tetrafluoro-N,N-dimethyl-4-anilinyl) porphyrin and its metal complexes. Spectrochim Acta A Mol Biomol Spectrosc 136:838–844. https://doi.org/https://doi.org/10.1016/j.saa.2014.09.102

[11] Chai J, Liu Y, Dong J, et al (2017) Synthesis, structure, chemical and bioactivity behavior of eight chromium (III) picolinate derivatives Cr(R-pic)3. Inorganica Chim Acta 466:151–159. https://doi.org/10.1016/j.ica.2017.05.041

[12] Cotton FA, Wilkinson G, Murillo CA, Bochmann M (1999) Advanced Inorganic Chemistry, 6th ed. Wiley-Interscience, New York

[13] Braga D, Grepioni F (2000) Organometallic Polymorphism and Phase Transitions. Chem Soc Rev 29:229–238. https://doi.org/10.1039/A909042H

[14] Desiraju GR (2011) A Bond by Any Other Name. Angewandte Chemie International Edition 50:52–59. https://doi.org/10.1002/anie.201002960

[15] Long QQ, Hu ZB, Wang HS, et al (2018) Field-induced single molecule magnet behavior of a DyIII-NaI one-dimensional chain extended by acetate ions. Inorg Chem Commun 98:127–131. https://doi.org/10.1016/j.inoche.2018.10.006

[16] Prasad PN, Williams DJ (1991) Introduction to Nonlinear Optical Effects in Molecules and Polymers. Wiley-Interscience, New York

[17] Clayden J, Greeves N, Warren S (2012) Organic Chemistry. Oxford University Press, Oxford

[18] Housecroft CE, Sharpe AG (2018) Inorganic Chemistry, 5th ed. Pearson Education, Harlow

[19] Liu SY, Sun WY (2017) Design and application of carboxylic acid-functionalized ligands in coordination chemistry. CrystEngComm 19:4231–4244. https://doi.org/10.1039/C7CE00615A

[20] Manandhar E, Wallace KJ (2012) Host–guest chemistry of pyrene-based molecular receptors. Inorganica Chim Acta 381:15–43. https://doi.org/10.1016/J.ICA.2011.09.021

[21] She S, Bian S, Hao J, et al (2014) Aliphatic Organoimido Derivatives of Polyoxometalates Containing a Bioactive Ligand. Chem—Eur J 20:16987

[22] Evans OR, Lin W (2002) Crystal engineering of NLO materials based on metal--organic coordination networks. Acc Chem Res 35:511–522. https://doi.org/10.1021/ar0001012

[23] Kinik FP, Ortega-Guerrero A, Ongari D, et al (2021) Pyrene-based metal organic frameworks: From synthesis to applications. Chem Soc Rev 50:3143–3177. https://doi.org/10.1039/D0CS00424C

[24] Tamer Ö (2016) 2-Piridinkarboksilik Asit Içeren Bazı Geçiş Metal Komplekslerinin Sentezi, Yapılarının Analizi Ve Doğrusal Olmayan Optik Özelliklerinin Incelenmesi. 224

[25] Figgis BN, Raston CL, Sharma RP, White AH (1978) Crystal structure of Tris (pyridine-2-carboxylato) manganese (III) monohydrate. Aust J Chem 31:2545–2548. https://doi.org/10.1071/CH9782545

[26] Musilek P, Krömer P, Bartoň T (2015) Review of nature-inspired methods for wake-up scheduling in wireless sensor networks. Swarm Evol Comput 25:100–118. https://doi.org/10.1016/j.swevo.2015.07.007

[27] Chang SC, Ma JTH, Wang JT, Li NC (1972) Picolinate metal complexes of Cr(III) ions. J Coord Chem 2:31–38. https://doi.org/10.1080/00958977208076910

[28] Loiseleur H (1972) Structure du picolate de nickel, tétrahydrate. Acta Crystallogr B 28:816–820. https://doi.org/10.1107/S0567740872003255

[29] Faure R, Loiseleur H, Thomas-David G (1973) Nouvel affinement de la structure cristalline du bis(pyridine-2-carboxylato) cuivre(II) hydraté. Acta Crystallogr B 29:1890–1893. https://doi.org/10.1107/S0567740873005716

[30] Lumme P, Lundgren G, Mark W (1969) The Crystal Structure of Zinc Picolinate Tetrahydrate. Acta Chem Scand 23:3011–3022. 201602002041245352

[31] Takenaka A, Utsumi H, Ishihara N, et al (1970) Molecular and crystal structures of trans-diaquo-bis-(picolinato) Nickel (II) dihydrate, Ni(H2O)2(Pc)2·2H2O, and trans-diaquo-bis-(picolinato) Zinc (II) dihydrate, Zn(H2O)2(Pc)2·2H2O. Nippon Kagaku Zasshi 91:921

[32] Deloume JP, Loiseleur H (1974) Structure cristalline du pyridine-2-carboxylate de cadmium. Acta Crystallogr B 30:607–609. https://doi.org/10.1107/S0567740874003396

[33] Deloume JP, Loiseleur H, Thomas G (1973) Structure du picolate de magnésium dihydraté. Acta Crystallogr B 29:668–673. https://doi.org/10.1107/S0567740873003146

[34] Alvarez-Larena A, Piniella JF, Pons J, et al (1994) Crystal structure of catena {bis[μ-(2-pyridinecarboxilato-μ-O2, O1, N)] mercury (II)}, Hg((C5H4N)(CO2))2. Zeitschrift für Kristallographie 209:695. https://doi.org/10.1524/zkri.1994.209.8.695

[35] Huang D, Wang W, Zhang X, et al (2004) Synthesis, Structural Characterizations and Magnetic Properties of a Series of Mono-, Di-and Polynuclear Manganese Pyridinecarboxylate Compounds. Eur J Inorg Chem 2004:1454–1464. https://doi.org/10.1002/ejic.200300586

[36] Heren Z, (2006). Z Anorg Allg Chem 632:1309–1313.

[37] Wu AQ, Guo GH, Zheng FK, et al (2005) [SmNi(pic)3(H2O)5]n(ClO4)2n · 3nH2O, the first Sm–Ni heterometallic complex of picolinic acid ligand showing novel basket weave topology: Synthesis, structure and magnetics. Inorg Chem Commun 8:1078–1081. https://doi.org/10.1016/J.INOCHE.2005.08.014

[38] Novitskii G, Borta A, Ganzhu D, et al (2009) Chemical transformations of lanthanide nitrate complexes: Synthesis and X-ray diffraction analysis. Russian Journal of Coordination Chemistry 35:381–388. https://doi.org/https://doi.org/10.1134/S107032840905011X

[39] Wang Q, Yu Z, Wang Q, et al (2012) Synthesis, crystal structure and DNA-binding properties of a mononuclear copper complex with pyridine-2-carboxylate ligand. Inorganica Chim Acta 383:230–234. https://doi.org/https://doi.org/10.1016/j.ica.2011.11.013

[40] Ghadermazi M, Soleimannejad J, Sheshmani S, et al (2012) Characterization, crystal structures and solution studies of Zn(II), Cd(II) and Mg(II) complexes obtained from a proton transfer compound including pyridine-2-carboxylic acid and piperazine. Journal of the Iranian Chemical Society 9:579–589. https://doi.org/10.1007/s13738-012-0071-x

[41] Li D, Zhong Guoq, Zang Q (2016) Solid–Solid Synthesis, Crystal Structure and Thermal Decomposition of Cooper (II) Complex of 2 Picolinic Acid. https://doi.org/10.30492/IJCCE.2016.23551

[42] Celestine MJ, Bullock JL, Boodram S, et al (2015) Interesting properties of p-, d-, and f-block elements when coordinated with dipicolinic acid and its derivatives as ligands: their use as inorganic pharmaceuticals. Reviews in Inorganic Chemistry 35:57–67. https://doi.org/10.1515/revic-2014-0004

[43] Tamer Ö, Avci D, Atalay Y (2015) Synthesis, X-ray structure, spectroscopic characterization and nonlinear optical properties of Nickel (II) complex with picolinate: A combined experimental and theoretical study. J Mol Struct 1098:12–20. https://doi.org/10.1016/J.MOLSTRUC.2015.05.035

[44] Tamer Ö, Avcı D, Atalay Y (2016) Synthesis, X-Ray crystal structure, photophysical characterization and nonlinear optical properties of the unique manganese complex with picolinate and 1,10 phenantroline: toward the designing of new high NLO response crystal. Journal of Physics and Chemistry of Solids 99:124–133. https://doi.org/10.1016/J.JPCS.2016.08.013

[45] Tamer Ö, Avcı D, Atalay Y (2017) A novel Cu(II) Complex of Picolinate and 1,10-Phenanthroline: Preparation, Crystal Structure Determination, Spectroscopic Characterization and Nonlinear Optical Studies. J Inorg Organomet Polym Mater 27:700–713. https://doi.org/10.1007/s10904-017-0513-0

[46] UĞURLU G (2018) Theoretical Investigation of The Molecular Structure, Conformational and Nonlinear Optical Properties of Picolinic Acid and Its Derivatives. Journal of the Institute of Science & Technology/Fen Bilimleri Estitüsü Dergisi 8:

[47] Altürk S, Avcı D, Başoğlu A, et al (2018) Copper(II) complex with 6-methylpyridine-2-carboxyclic acid: Experimental and computational study on the XRD, FT-IR and UV–Vis spectra, refractive index, band gap and NLO parameters. Spectrochim Acta A Mol Biomol Spectrosc 190:220–230. https://doi.org/10.1016/j.saa.2017.09.041

[48] Rekha P, Chakkaravarthi G, Mohan Kumar R, et al (2019) Growth, structural and optical limiting property of a new third order nonlinear optical material: piperazinium bis (2-carboxypyridine) monohydrate. Journal of Materials Science: Materials in Electronics 30:9471–9488. https://doi.org/10.1007/s10854-019-01279-z

[49] Rajan R V, Gowri S, Manopradha N, et al (2019) Growth, structural, third order nonlinear optical properties, dielectric properties, conductivity mechanisms and spectroscopic characterization of a luminescent material trans-diaqua-bis (pyridine-2-carboxylato)-cobalt (ii) dihydrate for optoelectronic applications. Opt Laser Technol 119:105664. https://doi.org/10.1016/j.optlastec.2019.105664

[50] Chinnasamy E, Arulmani S, Deepa K, et al (2019) Growth, Spectral, Optical, Studies of A Zinc Picolinate Dihydrate NLO Single Crystal. Mater Today Proc 8:264–270. https://doi.org/10.1016/j.matpr.2019.02.110

[51] Tamer Ö, Mahmoody H, Feyzioğlu KF, et al (2020) Synthesis of the first mixed ligand Mn (II) and Cd (II) complexes of 4-methoxy-pyridine-2-carboxylic acid, molecular docking studies and investigation of their anti-tumor effects in vitro. Appl Organomet Chem 34:e5416. https://doi.org/10.1002/aoc.5416

[52] Andriychenko EO, Zelenov VI, Bespalov A V, et al (2021) Electrochemical Synthesis and Characterization of Copper (II) and Zinc (II) Coordination Compounds with Nicotinic and Picolinic Acids. Russ J Gen Chem 91:1697–1705. https://doi.org/10.1134/S1070363221090139

[53] Avcı D, Altürk S, Sönmez F, et al (2021) Novel metal complexes containing 6-methylpyridine-2-carboxylic acid as potent α-glucosidase inhibitor: synthesis, crystal structures, DFT calculations, and molecular docking. Mol Divers 25:171–189. https://doi.org/10.1007/s11030-020-10037-x

[54] Prema S, Leema RA (2022) A Study of Metal Complexes of 2-Picolinic Acid. Oriental Journal of Chemistry 38:753. http://dx.doi.org/10.13005/ojc/380328

[55] Rendošová M, Gyepes R, Sovová S, et al (2023) Ga(III) pyridinecarboxylate complexes: potential analogues of the second generation of therapeutic Ga(III) complexes? JBIC Journal of Biological Inorganic Chemistry 28:591–611. https://doi.org/10.1007/s00775-023-02012-2

[56] Avcı D, Özge Ö, Başoğlu A, et al (2023) Synthesis, crystal structures, and DFT calculations: novel Mn(II), Co(II) and Ni(II) complexes of N-(pyridin-2-ylmethylene) methanamine with isothiocyanate as promising optical materials. Opt Quantum Electron 55:408. https://doi.org/10.1007/s11082-023-04668-1

[57] Tamer Ö, Dege N, Avcı D, Atalay Y (2023) The static and frequency-dependent second- and third-order nonlinear optical properties of Zn(II) and Ni(II) complexes of 4-methoxypyridine-2-carboxylic acid: A detailed experimental and theoretical study. Appl Organomet Chem 37:e7206. https://doi.org/10.1002/aoc.7206

[58] Matlou ML, Malan FP, Nkadimeng S, et al (2023) Exploring the in vitro anticancer activities of Re (I) picolinic acid and its fluorinated complex derivatives on lung cancer cells: a structural study. JBIC Journal of Biological Inorganic Chemistry 28:29–41. https://doi.org/10.1007/s00775-022-01971-2

[59] Ma S, Yang P, Wu Z, et al (2023) Construction of a novel two-dimensional coordination polymer based on picolinic acid-containing ligand for the effective elimination of organic dyes from wastewater. Polyhedron 238:116427. https://doi.org/10.1016/j.poly.2023.116427

[60] Li F, Huang X, Ma C, et al (2023) Tailoring the Interface with a Multifunctional Ligand for Highly Efficient and Stable FAPbI3 Perovskite Solar Cells and Modules. Advanced Science 10:2301603. https://doi.org/10.1002/advs.202301603

[61] Areas ES, Rodrigues BP, Nascimento ACC do, et al (2024) Photoluminescent and Magnetic Properties of Mononuclear Lanthanide-Based Compounds Containing the Zwitterionic Form of 4-Picolinic Acid as a Ligand. J Braz Chem Soc 35(4). https://doi.org/10.21577/0103-5053.20230160

[62] García-García A, Medina-O'donnell M, Rojas S, et al (2024) Modulating anti-inflammatory and anticancer properties by designing a family of metal-complexes based on 5-nitropicolinic acid. Dalton Transactions 53:8988–9000. https://doi.org/10.1039/D4DT00265B

[63] Manopradha N, Gowri S, Selvaraju K, Kirubavathi K (2024) Experimental and quantum computational studies of benzotriazole pyridine-2-carboxylic acid crystals. Chem Phys 585:112368. https://doi.org/https://doi.org/10.1016/j.chemphys.2024.112368

[64] Khera M, and Goel N (2024) Noncovalent Interactions, Structure Elucidation and Docking Studies of anti-Fungal Pyridine Carboxamide Derivatives of Co(II), Ni(II), Cu(II) & Zn(II). Polycycl Aromat Compd 44:4416–4429. https://doi.org/10.1080/10406638.2023.2250053

[65] Randhawa P, Kadassery KJ, McNeil BL, et al (2024) The H2Sx macropa Series: Increasing the Chemical Softness of H2macropa with Sulfur Atoms to Chelate Radiometals [213Bi]Bi3+ and [203Pb]Pb2+ for Radiopharmaceutical Applications. Inorg Chem 63:21177–21193. https://doi.org/10.1021/acs.inorgchem.4c03498

[66] Hu Y, Zhou Y, Ye J, et al (2024) σ-dominated charge transport in sub-nanometer molecular junctions. Fundamental Research 4:1128–1136. https://doi.org/https://doi.org/10.1016/j.fmre.2022.06.021

[67] Cao D, Chen B, Xu Y, et al (2024) Efficient removal of uranium from the kidneys by a picolinate-based pentadentate chelator. New Journal of Chemistry 48:7552–7556. https://doi.org/10.1039/D4NJ00986J

[68] Jamgohari N, Hassan M-T, Effat D, et al (2024) Synthesis, crystal structure, cytotoxicity, in-detail experimental and computational CT-DNA interaction studies of 2-picolinate Pd(II) and Pt(II) complexes. J Biomol Struct Dyn 42:8937–8957. https://doi.org/10.1080/07391102.2023.2249106

[69] George M, John JS, Gowri S, et al (2025) Third-order nonlinear optical studies and investigation of the hydrogen bond network in 2-picolinic perchloric acid using neutron diffraction. Journal of Materials Science: Materials in Electronics 36:665. https://doi.org/10.1007/s10854-025-14693-3

[70] Olawale MD, Ojo ND, Oyeneyin OE, et al (2025) Synthesis, Electronic, Dynamic Optical and Adsorption (Monte Carlo and Molecular Dynamics) Properties of Cadmium Picolinate Coordination Polymer-2 (Cp-2). Journal of Computational Biophysics and Chemistry 1–15. https://doi.org/10.1142/S2737416525500310

[71] Gómez de Segura D, Salmain M, Bertrand B, et al (2025) Structural Features and Photophysical and Antiproliferative Properties of Me2N-pbt-Cycloplatinated Complexes with Picolinate Ligands. Inorg Chem 64:10243–10259. https://doi.org/10.1021/acs.inorgchem.5c01175

[72] Li J, Yang L, Cui Y, et al (2025) Peroxide Directing the Iron Cycling for Tailored Generation of Active Oxidants in Aqueous Fenton Reactions. Environ Sci Technol 59:3316–3324. https://doi.org/10.1021/acs.est.4c12341

EKLER

EK-A1

Received: 30 January 2022 | Revised: 1 March 2022 | Accepted: 20 March 2022
DOI: 10.1002/aoc.6678

RESEARCH ARTICLE

Applied Organometallic Chemistry WILEY

Experimental and theoretical approaches on structural, spectroscopic (FT-IR and UV-Vis), nonlinear optical, and molecular docking analyses for Zn (II) and Cu (II) complexes of 6-chloropyridine-2-carboxylic acid

Necmi Dege[1] | **Ömer Tamer**[2] | **Merve Şimşek**[2] | **Davut Avcı**[2] | **Mavişe Yaman**[1] | **Adil Başoğlu**[2] | **Yusuf Atalay**[2]

[1]Department of Physics, Faculty of Arts and Sciences, Ondokuz Mayıs University, Samsun, Turkey

[2]Department of Physics, Faculty of Arts and Sciences, Sakarya University, Sakarya, Turkey

Correspondence
Ömer Tamer, Department of Physics, Faculty of Arts and Sciences, Sakarya University, Sakarya 54187, Turkey.
Email: omertamer@sakarya.edu.tr

Abstract

Novel transition metal-based complexes that may be of value as biological agents and/or nonlinear optical materials, Zn (II) and Cu (II) transition metal complexes of 6-chloropyridine-2-carboxylic acid (LH), were successfully synthesized. The chemical structure of each complex was characterized using X-ray diffraction (XRD) method and FT-IR spectroscopy. XRD and FT-IR demonstrated that **L** ligand coordinate to central metal ions through the donor N and O atoms. By coordinating two H_2O ligand to Zn (II) ion, a distorted octahedral complex geometry was constructed for **1**. As for **2**, a distorted trigonal bipyramidal coordination geometry was obtained by a H_2O ligand coordination to Cu (II) ion. Theoretical studies using B3LYP/6-311++G(d,p)-LanL2DZ were performed to further validate the proposed structures. The molecular docking of **1** to SARS-CoV-2 main protease (PDB: 6LU7) gives a binding energy of −5.24 kcal/mol and inhibition constant of 144.6 μM, demonstrating that **1** is a more promising candidate to biologically active complexes than **2**. The first-order hyperpolarizability (β) parameter for **1** and **2** was calculated as 0.88×10^{-30} and 10.40×10^{-30} esu, respectively. These β values also demonstrated that **2** exhibits more effective NLO character than **1** due to the electronic configuration and coordination geometry.

KEYWORDS
DFT, molecular docking, NLO, SARS-CoV-2, 6-Chloropyridine-2-carboxylic acid

1 | INTRODUCTION

The interest for organometallic complexes of transition metal ions with different kinds of ligands has been increased by the motivation of their potential use as a promising therapeutic agents[1–3] and optical materials.[4–6] Research in the field of nonlinear optics has increasingly concentrated on the design of new organometallic complexes, since the report in 1987 by Green et al.,[7] in which good second-harmonic generation (SHG) efficiency was revealed for a ferrocenyl derivative. In recent times, organometallic complexes are among the most frequently investigated materials for their nonlinear optical properties.[8–14] The optoelectronic characteristics of these materials are extremely dependent on the *d* electron configuration and energy levels, which can be easily

 © 2022 John Wiley & Sons, Ltd.

modulated through the choose of metal ion and oxidation state as well as the ligand environments. Furthermore, organometallic systems can exhibit metal–ligand or ligand–metal charge transfer bands, improving the second order NLO activity of investigated system. A number of organometallic compounds have low-energy excited states with excited-state dipole moments significantly different from their respective ground-state dipole moments. Most of these excited states involve in electron density transfer between the central metal ions and surrounding ligands with large oscillator strength. This charge transfer will also make a substantial contribution to the second order NLO activity.[15]

On the other hand, the beginning of inorganic medical chemistry goes back to the discovery of cisplatin, a potent antitumor agent, in the 1960s.[16] Platinium-containing therapeutic agents such as carboplatin, oxaliplatin, and picoplatin are also discovered after intensive researches to fight cancer and used effectively in the treatment of patients. The success of these metal-based therapeutic agents is limited due to their poor selectivity, severe side effects, and strong drug resistance.[17] These types of drugs destroy not only cancer cells that grow pathologically in the body but also normal cells that grow rapidly. This is why most cancer drugs also have side effects on bone marrow, blood cells, and tissues containing other rapidly growing cells. Considerable efforts have been made to synthesize novel complexes with non-platinum-based transition metals to overcome these disadvantages.[18–20]

It was reported that some metal ion chelators that have shown promising antitumor activity include heterocyclic carboxaldehyde thiosemicarbazones, analogs of pyridoxal isonicotinoyl hydrazone, and other natural and synthetic chelators.[21,22] Due to the effective complexation ability of the pyridine ring and carboxylic acid group, pyridine-2-carboxylic acid and its derivates have attracted extensive attention as a potential chelating ligand.[22–25] In our previous study, Mn (II) and Cd (II) complexes of 4-methoxy-pyridine-2-carboxylic acid were synthesized and tested on human breast carcinoma cell line MCF-7.[22] The obtained results demonstrated that the final complexes exhibit a higher inhibitory effect than both metal salts and ligands. In another study, it was reported that Ru (II) complexes of pyridine-2-carboxylic acid displayed moderate antiproliferative effects toward colorectal carcinoma (HCT116) and cervix adenocarcinoma (HeLa).[26] Buczkowska et al.[27] performed a comprehensive study about cytotoxic and antimicrobial activities of Cu (II), Co (II), Pt (II), and Zn (II) complexes with N,O-chelating heterocyclic carboxylates and reported that these complexes have interesting cytotoxic activities in various human cancer cell lines. A molybdenum complex of pyridine-2-carboxylic acid synthesized by Joshi et al.[28] and quite promising inhibitory effect against HepG2 (human liver cancer), A549 (human lung cancer), and MCF-7 (human breast cancer) cell lines, respectively, have been found.

6-chloropyridine-2-carboxylic acid is a versatile ligand due to the functional pyridine ring, carboxylic acid group, and Cl atom. It has been reported that these electron-donating and electron-withdrawing groups play an active role in the coordination of the ligand to the biological target.[25,29–31] In a recent study, the Co (II) and Mn (II) complexes of 6-chloropyridine-2-carboxylic acid were synthesized, and their structural, spectroscopic, electronic, and optical properties were investigated. In addition, another study could not be found about the transition metal complexes of 6-chloropyridine-2-carboxylic acid. In our ongoing study, Cu (II) and Zn (II) complexes of 6-chloropyridine-2-carboxylic acid were synthesized and characterized using XRD, FT-IR, and UV-Vis techniques as well as DFT calculations. Nonlinear optical properties and molecular docking analysis to SARS-CoV-2 main protease were also investigated for **1** and **2**.

2 | MATERIALS AND METHODS

2.1 | Synthesis

All chemical reagents were obtained from Sigma Aldrich and used without further purification. The general synthesis scheme is given in Figure 1. Zn $(CH_3COO)_2$–$2H_2O$–(0.1 mmol) and Cu $(CH_3COO)_2$–H_2O (0.1 mmol) were dissolved in 20 ml ethanol and water (1:1) mixture. 6-chloropyridine-2-carboxylic acid (**LH**) (2 mmol) was slowly added to the obtained Zn (II) and Cu (II) solutions with continuous

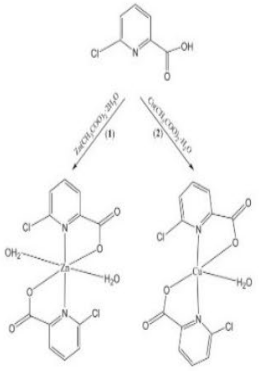

FIGURE 1 The general synthesis for **1** and **2**

stirring for 2 h, and the final solutions were filtered and allowed to evaporate at room temperature for 2 weeks. The colorless and blue crystals of **1** and **2** suitable for X-ray diffraction studies were obtained.

2.2 | Experimental

A Stoe IPDS II diffractometer using Mo-Kα (λ = 0.71073 Å) radiation at 296 K[32] was used to collect data in the X-Ray diffraction measurements. SHELXT[33] and SHELXL[34] were used in the determination of the crystal structure and crystal refining process, respectively. Mercury,[35] PLATON,[36] WinGX,[37] and PublCIF[38] were also utilized to obtain crystal geometries, their drawings, and Crystal Information File (CIF). The detailed crystallographic data and refinement parameters for **1** and **2** were presented in Table 1. FT-IR spectra of the Zn (II) and Cu (II) complexes of 6-chloropyridine-2-carboxylic acid were recorded in the region 4,000–400 cm^{-1} on PERKIN ELMER Spectrum-Two FT-IR spectrophotometer equipped with Perkin Elmer UATR-TWO diamond ATR. The UV-Vis spectra for **1** and **2** were also recorded in the range of 900–200 nm by HITACHI U-2900 UV/VIS spectrophotometer in ethanol solvent with quartz cell of 1 cm.

2.3 | Theoretical background

Gaussian 09, Revision rev. D01[39] and GaussView 5.0[40] were used to obtain ground state geometries, vibrational spectra, frontier molecular orbitals, molecular electrostatic potentials, dipole moment (μ), polarizability (α), and first-order static hyperpolarizability (β) parameters of **1** and **2**. B3LYP level[41,42] of density functional theory in conjunction with the combined basis set of 6-311++G (d,p)/LanL2DZ was utilized to achieve the above calculations. While 6-311++G(d,p) basis set[43] was used to C, O, N, and H atoms, LanL2DZ basis set[44,45] was utilized to Zn (II) and Cu (II) ions. The conductor-like polarizable continuum model (CPCM) was executed to consider solvent effect in the calculation of UV-Vis spectra for **1** and **2**. The important contributions from molecular orbitals to electronic absorption bands observed in UV-Vis spectra were determined by SWIZARD software.[46] The distribution of molecular orbitals on the complexes was investigated in detail with the chemissian program.[47] Molecular docking simulations were implemented by using Autodock version 4.2 software[48] under Lamarckian Genetic Algorithm method (LGA) to predict affinity score and conformations of the complexes with SARS-CoV-2 main protease (PDB: 6 LU7). Autodock version 4.2 was used for protein optimization, by removing water and other atoms and then adding a polar hydrogen group. Autodock 4.2 was supported by Autodock tools and MGL tools. Ligand tethering of the protein was performed by regulating the genetic algorithm (GA) parameters, using 10 runs of the GA criteria. Discovery Studio Visualizer 4.0 software[49] was also used to prepare ligand and target protein and visualize interactions between target and complexes. The grid box dimensions (60 × 60 × 60 Å for both complexes) and spacing parameter (0.586 Å for 1 and 0.664 Å for 2) were determined to cover the whole target binding site and complexes.

TABLE 1 Crystallographic data and refinement parameters for **1** and **2**

Chemical formula	$C_{12}H_{10}Cl_2N_2O_6Zn$ (1)	$C_{12}H_8Cl_2N_2O_5Cu$ (2)
Mr	414.49	394.64
Crystal system, space group	Monoclinic, *P*21/*c*	Triclinic, $P\bar{1}$
Temperature (K)	296	296
α, β, γ (°)	90, 92.742 (4), 90	86.649 (9), 84.923 (9), 77.172 (9)
a, b, c (Å)	7.1296 (3), 12.7214 (8), 16.8829 (8)	6.7891 (8), 9.0625 (10), 11.3269 (12)
V ($Å^3$)	1529.50 (14)	676.30 (13)
Z	4	2
Radiation type	Mo *K*α	Mo *K*α
μ (mm^{-1})	1.99	2.04
Crystal size (mm)	0.78 × 0.66 × 0.55	0.79 × 0.57 × 0.34
Diffractometer	STOE *IPDS* 2 diffractometer	STOE *IPDS* 2 diffractometer
Absorption correction	Integration	Integration
Tmin, Tmax	0.393, 0.513	0.268, 0.562
No. of measured, independent andobserved [I > 2σ(I)] reflections	10,763, 2,994, 2,675	6,190, 2,657, 2,505
R_{int}	0.031	0.033
(sin θ/λ)max ($Å^{-1}$)	0.617	0.617
$R[F^2 > 2\sigma(F^2)]$, *wR* (F^2), *S*	0.028, 0.069, 1.04	0.027, 0.073, 1.04
H-atom treatment	H-atom parameters constrained	H-atom parameters constrained
$\Delta\rho_{max}$, $\Delta\rho_{min}$ (e $Å^{-3}$)	0.38, −0.45	0.38, −0.43

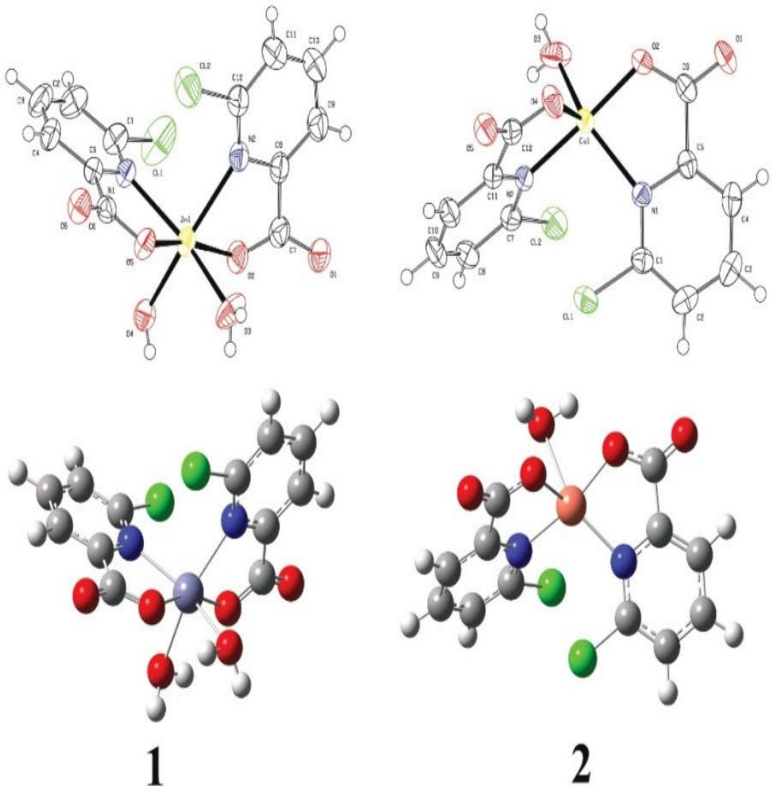

FIGURE 2 The crystal structures and optimized molecular geometries (obtained by B3LYP/6-311++G(d,p)-LanL2DZ) for **1** and **2**

3 | RESULTS AND DISCUSSION

3.1 | Crystal and predicted structures of 1 and 2

The crystal structures of **1** and **2** complexes are presented in Figure 2. Selected bond lengths and angles are also presented in Table 2. The neutral complex of ($ZnL_2[H_2O]_2$) crystallizes in monoclinic crystal system with space group P $2_1/c$. In Zn (II) complex, two deprotaned 6-chloropyridine-2-carboxylic acid ligands coordinate the Zn (II) ion, forming a distorted octahedral complex by the coordination of two-hydrate molecule to the central Zn (II) ion. Two oxygen atoms (O3 and O4) from two H_2O ligands and two nitrogen atoms (N1 and N2) from the 6-chloropyridine-2-carboxylate ligand comprise the equatorial planes. The bond distances in equatorial plane are 2.1063(17) Å (Zn1-O3), 2.1198(16) Å (Zn1-O4), 2.2099(16) Å (Zn1-N1), and 2.2643(18) Å (Zn1-N2). Two oxygen atoms (O2 and O5) of the 6-chloropyridine-2-carboxylate ligand are in axial positions, with the distance from the equatorial plane being 2.0565(15) and 2.0286(14), respectively. The sum of N1-Zn1-O4 (87.20[6]°), O4-Zn1-O3 (92.71[7]°), O3-Zn1-N2 (95.38[8]°), and N2-Zn1-N1 (90.98[6]°) bond angles is 366.15°, which further confirms that the four atoms are nearly coplanar.[29,50,51] When the bond lengths between the central metal ion and the surrounding donor atoms were examined, it was concluded that the bond lengths of Zn1—O2 and Zn1—O5 were shorter due to the Jahn-Teller effect.[50,52] The bond lengths of C—N and C—C in pyridine ring are observed at the range of 1.321 (3)–1.352(3) Å and 1.362(4)–1.381(4) Å, respectively. The corresponding calculated bond lengths are at the region of 1.3262–1.3498 Å and 1.3885–1.3911 Å. The observation and calculation of the N1—C1 and N2—C12 bonds shorter than the N2—C5 and N2—C8 bonds can be easily explained by the bonding of the C1 and C12 atoms to the electronegative Cl atom.

The neutral complex of ($CuL_2[H_2O]$) crystallizes in triclinic crystal system with space group *P*-1. The basal plane consists of one pyridine nitrogen atom (N1), one carboxylate group oxygen atom (O4) atom, and one oxygen atom (O3) from the hydrate molecule. The axial position is occupied by one carboxylate group oxygen atom (O2) and one pyridine nitrogen atom (N2). The bond lengths of Cu1—N1, Cu1—O4, and Cu1—O3 are observed at 2.1103(17), 2.0943(16), and 2.0072(17) Å. As for the

TABLE 2 The experimental and theoretical geometrical parameters (bond lengths and angles) for **1** and **2**

1			2		
Bond length	**XRD**	**B3LYP**	**Bond length**	**XRD**	**B3LYP**
Zn1O5	2.0286 (14)	1.9784	Cu1—O2	1.9094 (15)	1.9145
Zn1O2	2.0565 (15)	1.9785	Cu1—N2	1.9850 (17)	2.0065
Zn1O3	2.1063 (17)	2.2492	Cu1—O3	2.0072 (17)	2.4563
Zn1O4	2.1198 (16)	2.2494	Cu1—O4	2.0943 (16)	1.9747
Zn1N1	2.2099 (16)	2.2022	Cu1—N1	2.1103 (17)	2.1050
Zn1—N2	2.2643 (18)	2.2022	Cl1—C1	1.728 (2)	1.7489
Cl2C12	1.727 (2)	1.7512	Cl2—C7	1.727 (2)	1.7467
Cl1—C1	1.721 (2)	1.7512	O2—C6	1.286 (3)	1.2927
O5—C6	1.274 (2)	1.2869	O4—C12	1.246 (3)	1.2880
O2—C7	1.267 (3)	1.2869	N1—C1	1.324 (3)	1.3312
O6—C6	1.226 (3)	1.2186	N1—C5	1.353 (3)	1.3530
N1—C1	1.321 (3)	1.3262	O5—C12	1.245 (3)	1.2172
N1—C5	1.347 (3)	1.3498	O1—C6	1.209 (3)	1.2150
O1—C7	1.234 (3)	1.2186	N2—C7	1.329 (3)	1.330
N2—C12	1.321 (3)	1.3262	N2—C11	1.351 (3)	1.3505
N2—C8	1.352 (3)	1.3498	C5—C4	1.377 (3)	1.3859
C5—C4	1.376 (3)	1.3885	C5—C6	1.505 (3)	1.5268
C5—C6	1.506 (3)	1.5357	C7—C8	1.372 (3)	1.3885
C8—C9	1.376 (3)	1.3885	C11—C10	1.366 (3)	1.3863
C8—C7	1.505 (3)	1.5357	C11—C12	1.523 (3)	1.5339
C4—C3	1.381 (4)	1.3905	C1—C2	1.382 (3)	1.3906
C9—C10	1.381 (4)	1.3905	C8—C9	1.382 (4)	1.3918
C1—C2	1.378 (3)	1.3911	C4—C3	1.384 (4)	1.3899
C2—C3	1.372 (4)	1.3902	C2—C3	1.369 (4)	1.3900
C12—C11	1.362 (4)	1.3911	C9—C10	1.386 (3)	1.3906
C11—C10	1.362 (4)	1.3902			
O5—Zn1—O2	166.13 (6)	159.92	O2—Cu1—N2	177.11 (7)	162.56
O5— Zn1—O3	85.23 (7)	74.73	O2—Cu1—O3	87.35 (7)	75.38
O2— Zn1—O3	80.94 (7)	91.32	N2—Cu1—O3	89.89 (8)	88.2
O5— Zn1—O4	94.27 (6)	91.32	O2—Cu1—O4	99.21 (7)	100.25
O2— Zn1—O4	85.35 (6)	74.73	N2—Cu1—O4	80.78 (7)	82.61
O3— Zn1—O4	92.71 (7)	92.84	O3—Cu1—O4	107.72 (8)	81.03
O5— Zn1—N1	76.96 (6)	79.48	O2—Cu1—N1	81.45 (7)	81.91
O2— Zn1—N1	116.83 (6)	114.14	N2—Cu1—N1	101.33 (7)	107.57
O3— Zn1—N1	162.13 (7)	154.13	O3—Cu1—N1	144.21 (8)	138.22
O4— Zn1—N1	87.20 (6)	89.75	O4—Cu1—N1	107.59 (7)	138.07
O5— Zn1—N2	105.90 (6)	114.15	C6—O2—Cu1	118.04 (14)	118.45
O2— Zn1—N2	76.64 (6)	79.48	C12—O4—Cu1	113.85 (13)	115.99
O3— Zn1—N2	95.38 (8)	89.7	C1—N1—C5	116.55 (18)	117.87
O4— Zn1—N2	158.79 (7)	154.12	C1—N1—Cu1	134.96 (15)	133.49
N1— Zn1—N2	90.98 (6)	98.99	C5—N1—Cu1	108.26 (13)	108.6
C6—O5—Zn1	120.51 (13)	120.33	C7—N2—C11	118.47 (18)	30.27

(Continues)

TABLE 2 (Continued)

1			2		
Bond length	**XRD**	**B3LYP**	**Bond length**	**XRD**	**B3LYP**
C7–O2–Zn1	114.78 (14)	120.33	C7–N2–Cu1	127.35 (15)	129.6
C1–N1–C5	117.30 (18)	118.4	C11–N2–Cu1	114.19 (14)	111.33
C1–N1–Zn1	131.40 (15)	132.87	N1–C5–C4	123.0 (2)	122.51
C5–N1–Zn1	111.18 (12)	108.66	N1–C5–C6	115.63 (18)	116.26
C12–N2–C8	116.84 (19)	118.4	C4–C5–C6	121.3 (2)	121.19
C12–N2–Zn1	134.49 (15)	132.87	N2–C7–C8	123.4 (2)	123.13
C8–N2–Zn1	108.64 (14)	108.66	N2–C7–Cl2	116.23 (16)	117.28
N1–C5–C4	122.75 (19)	122.04	C8–C7–Cl2	120.29 (17)	119.58
N1–C5–C6	115.83 (16)	117.34	O1–C6–O2	125.8 (2)	127.71
C4–C5–C6	121.42 (19)	120.62	O1–C6–C5	119.6 (2)	118.98
O6–C6–O5	125.68 (19)	128.04	O2–C6–C5	114.61 (18)	113.29
O6–C6–C5	118.96 (18)	118.0	N2–C11–C10	121.8 (2)	121.77
O5–C6–C5	115.35 (17)	113.96	N2–C11–C12	114.84 (18)	115.73
N2–C8–C9	122.7 (2)	122.04	C10–C11–C12	123.3 (2)	122.39
N2–C8–C7	115.35 (18)	117.34	N1–C1–C2	124.3 (2)	123.59
C9–C8–C7	122.0 (2)	120.62	N1–C1–Cl1	118.02 (16)	118.11
O1–C7–O2	126.1 (2)	128.04	C2–C1–Cl1	117.70 (18)	118.27
O1–C7–C8	117.9 (2)	118.0	C7–C8–C9	117.8 (2)	117.8
O2–C7–C8	115.99 (18)	113.95	O5–C12–O4	126.4 (2)	128.62
C5–C4–C3	118.3 (2)	118.78	O5–C12–C11	117.28 (19)	118.23
C8–C9–C10	118.6 (2)	118.78	O4–C12–C11	116.31 (18)	113.1
N1–C1–C2	124.2 (2)	123.77	C5–C4–C3	118.7 (2)	118.73
N1–C1–Cl1	116.43 (17)	117.27	C3–C2–C1	118.3 (2)	118.01
C2–C1–Cl1	119.37 (18)	118.97	C2–C3–C4	119.0 (2)	119.19
C3–C2–C1	117.7 (2)	117.59	C8–C9–C10	119.5 (2)	119.52
N2–C12–C11	124.3 (2)	123.77	C11–C10–C9	119.0 (2)	118.74
N2–C12–Cl2	117.22 (17)	117.27			
C11–C12–Cl2	118.51 (19)	118.97			
C10–C11–C12	118.1 (2)	117.59			
C11–C10–C9	119.5 (2)	119.4			
C2–C3–C4	119.8 (2)	119.4			

Cu1–N2 and Cu1–O2 bond lengths, a compression in the axial position due to the Jahn-Teller effect and these bond lengths are reported at 1.9850(17) and 1.9094(15) Å. The corresponding calculated bond lengths are found at 2.1050, 1.9747, and 2.4563 Å in basal plane, 2.0065 and 1.9145 Å in axial position. The sum of O3–Cu1–O4 (107.72[8]°), O3–Cu1–N1 (144.21[8]°), and O4–Cu1–N1 (107.59[7]°) bond angles is observed as 359.52°. The obtained bond lengths and angles around the central Cu (II) ion demonstrated the complex has a slightly distorted trigonal bipyramidal coordination geometry.[25,53,54] The C–C and C–N bond lengths in pyridine ring are observed at the region of 1.369(4)–1.386 (3) Å and 1.324(3)–1.353(3) Å, respectively. The corresponding bond lengths in the predicted geometric structure are found at the range of 1.3859–1.3906 Å and 1.3300–1.3530 Å, as consistent with the previously reported results for similar complex systems.[55–57]

The crystal packing along with the hydrogen bonds patterns of both crystals is presented in Figure 3. The hydrogen banding geometry parameters for both complexes are also presented in Table 3. Within the crystals, the C–H=O and O–H=O intermolecular H bonds link the molecules into a three-dimensional network. In Zn

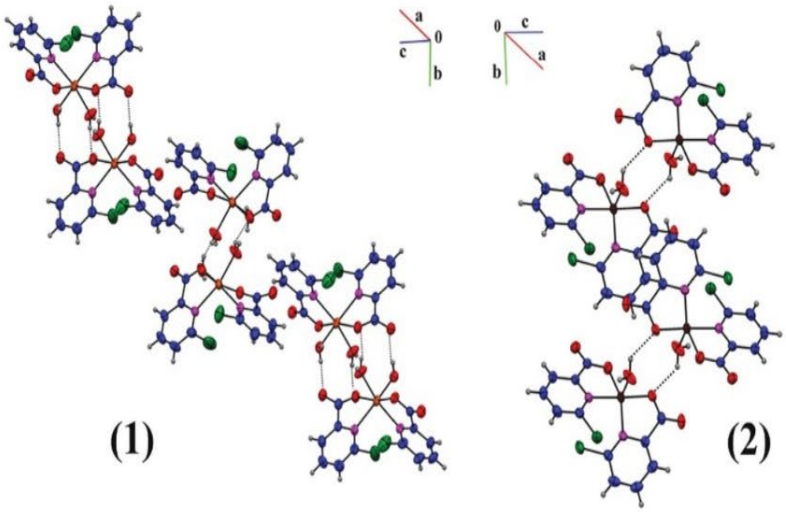

FIGURE 3 View of the crystal packing for **1** and **2**. The C—H≡O hydrogen bonds are shown as dashed lines

TABLE 3 Hydrogen bonds geometries for **1** and **2** complexes

D—H≡A	D—H (Å)	H≡A (Å)	D≡A (Å)	D—H≡A (°)	Symmetry codes
Zn (II) complex					
C4—H4≡O1^{i}	0.93	2.34	3.143 (3)	145	$x+1, -y+3/2, z+1/2$
C2—H2≡O6^{ii}	0.93	2.50	3.225 (3)	135	$-x+1, y+1/2, -z+3/2$
O4—H4A≡O6^{iii}	0.80 (1)	2.04 (1)	2.826 (2)	165 (3)	$x-1, y, z$
O4—H4B≡O1^{iv}	0.81 (1)	1.94 (1)	2.745 (2)	178 (3)	$-x, -y+1, -z+1$
O3—H3A≡O2^{iv}	0.82 (1)	1.98 (1)	2.790 (2)	170 (3)	$-x, -y+1, -z+1$
O3—H3B≡O5^{v}	0.81 (1)	1.87 (1)	2.669 (2)	165 (3)	$-x+1, -y+1, -z+1$
Cu (II) complex					
O3—H3A≡O2^{i}	0.87	2.05	2.751 (2)	137	$-x+1, -y+2, -z+1$
O3—H3B≡O5^{ii}	0.87	1.94	2.712 (2)	146	$x-1, y, z$
C8—H8≡Cl1^{iii}	0.93	2.96	3.826 (2)	156	$-x+1, -y+1, -z+2$
C4—H4≡Cl2^{iv}	0.93	2.98	3.904 (3)	173	$-x+1, -y+1, -z+1$
C2—H2≡O5^{v}	0.93	2.35	3.262 (3)	166	$x, y-1, z$
C10—H10≡O5^{vi}	0.93	2.40	3.187 (3)	142	$-x+2, -y+2, -z+2$

(II) complex, the strongest H bond (O3—H3B≡O5, H≡A = 1.87 [1] Å, D≡A = 2.669 [2] Å) is observed with the symmetry code of $-x+1, -y+1, -z+1$. As for Cu (II) complex, the strongest H bond (O3—H3B≡O5, H≡A = 1.94 Å, D≡A = 2.712 [2] Å) is shown with the symmetry code of $x-1, y, z$.

3.2 | Vibrational spectra

The experimental IR spectra for **1** and **2** were observed at the region of 4,000–400 cm^{-1}, and the obtained vibrational wavenumbers were presented in Table 4, as compared with the corresponding data calculated by B3LYP/6-311++G(d,p)-LanL2DZ level. The experimental IR spectrum for LH ligand was also included in Figure 4 in order to clearly display the vibrational band shifts because of the coordination to the central metal ions. The stretching vibrations of OH group in hydrate ligand were reported at the range of 3,235–3,418 cm^{-1}.[51,58] In this study, this type of vibration was observed at 3,239 and 3,188 cm^{-1} for Zn (II) and Cu (II) complexes. The corresponding bands in the predicted spectra were also found at 3,750–3,577 cm^{-1} and 3,685–3,603 cm^{-1}, respectively. In the IR spectrum of 6-chloropyridine-2-carboxylic acid (**LH**), the stretching vibration of ν

TABLE 4 Selected experimental and theoretical vibrational wavenumbers (cm^{-1}) for **1** and **2**

Assignments with PED	Exp.	B3LYP	Assignments with PED	Exp.	B3LYP
ν OH(90%)		3,750	ν OH(100%)		3,685
ν OH(99%)	3,239	3,577	ν OH(20%)	3,188	3,603
ν CH(92%)		3,096	ν CH(93%)		3,095
ν CH(92%)	3,092	3,096	ν CH(94%)	3,082	3,094
ν CH(93%)		3,092	ν CH(99%)		3,092
ν CH(99%)		3,056	ν CH(98%)		3,060
ν CH(99%)		3,056	ν CH(94%)		3,060
ν OC(77%)	1,641	1,703	ν OC(91%)	1,626	1,706
ν OC(77%)		1,697	ν OC(90%)		1,691
ν CC(36%)	1,585	1,566	ν CC(54%)	1,584	1,570
β HCC(57%)	1,406	1,404	ν CC(14%) + β NCC(12%) + β HCC(54%)	1,412	1,407
ν NC(26%)	1,370	1,383	ν NC(12%) + β HCC(29%)	1,374	1,382
ν NC(26%)	1,355	1,380	ν NC(33%) + β HCC(23%)	1,335	1,379
ν OC(48%)	1,249	1,299	ν OC(22%) + ν NC(15%) + β HCC(10%)	1,252	1,271
ν NC(50%)		1,237	ν NC(42%)		1,235
β HCC(22%)	1,141	1,154	β HCC(22%)	1,157	1,159
τ HCCC(23%) + τ CCCN(27%)	1,008	990	τ HCCC(64%) + τ CCCN(22%)	1,008	990
τ HCCC(89%) + γ OCOC(54%)	767	818	τ HCCC(58%) + γ OOCC(19%)		808
τ HCCC(86%) + γ OCOC(48%)	763	758	τ HCCC(53%) + γ OOCC(31%)	777	753
γ ClNCC(39%)		513	τ NCCC(16%) + γ ClNCC(31%)		505

Note: ν, stretching; β, in-plane bending; γ, out of plane bending; τ, torsion vibration.

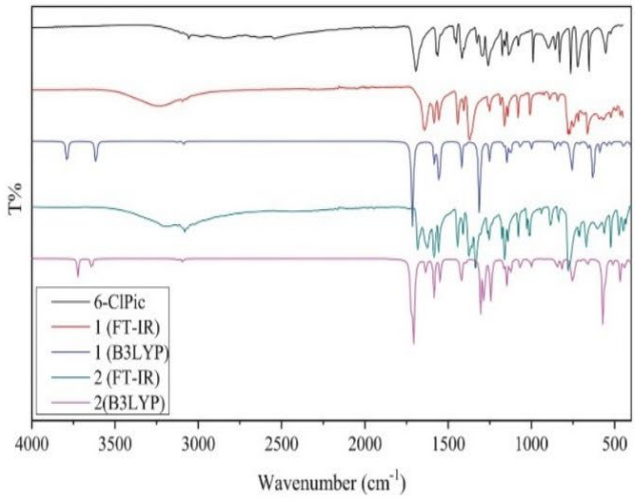

FIGURE 4 The experimental and theoretical IR spectra for **LH**, **1**, and **2**

(COOH) is observed at 989 cm^{-1}, as consistent with previously reported values.[58,59] In Zn (II) and Cu (II) complexes of transition metal complexes of **LH** ligand, the bands derived from the vibrations of the ν (COOH) disappear and another characteristic band assigned as the vibration of carboxylate anion ν ($COOH^-$) occur.[31,55,58] In the present study, the symmetric and asymmetric stretching vibrations of COO^- group was observed at 1,641 and 1,249 cm^{-1} for **1** and 1,621 and 1,252 cm^{-1} for **2**. It is well known that the difference between symmetric and asymmetric ν (COOH) vibrations gives a clue about the coordination around the central metal ion. This difference was observed as 392 and 369 cm^{-1} in FT-IR spectra and found as 404 and 435 cm^{-1} in predicted IR spectra. In the IR spectra of the uncoordinated pyridine-2-carboxylic acid derivatives, this

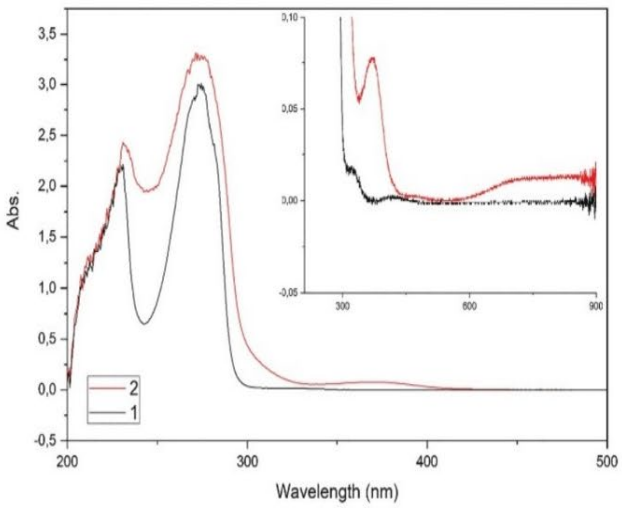

FIGURE 5 The experimental UV-Vis spectra **1** and **2** obtained in ethanol solvent

difference was obtained at the region of 620–642 cm^{-1}.[59] Thus, it is concluded that the LH is coordinated to Zn (II) and Cu (II) ions through the carboxyl group as a monodentate ligand. It is observed that the vibrational wavenumbers of the bands in the spectra of **1** and **2** complexes have a higher value than the corresponding bands from the that of **LH**. The shifts in the vibrational band positions derived from the aromatic system in the spectra of **1** and **2** complexes compared with the spectra of **LH** indicate the changes in the electronic charge distribution in the aromatic ring under the influence of a coordinated metal ions. For example, the ring breathing vibration mode for pyridine ring observed at 989 cm^{-1} for **LH** ligand was obtained at 1,008 cm^{-1} for **1** and **2** complexes, demonstrating that the stabilization of the electron system in the aromatic ring of acid.[60–63] The corresponding bands in the predicted spectra were found at 990 cm^{-1} for both complexes. In this way, the coordination of the pyridine ligand through N atoms to Zn (II) and Cu (II) ions was elucidated in accordance with the X-ray diffraction results.

3.3 | UV-Vis spectra and FMO energies

In UV-Vis spectra of the picolinic acid derivates, the intra-ligand π-π* and *n*-π* electronic transitions related to the C=O, C=N, and C=C are reported in the literature to lie in the region between 224 and 265 nm.[59] The UV-Vis spectra for **1** and **2** recorded in ethanol solvent are presented in Figure 5. As can be seen in Table 5, the π-π* and *n*-π* absorption bands were observed at 230 and 274 nm for **1** and 231 and 273 nm for **2**. The weaker and less energetic peaks assigned to ligand–metal charge transfer (LMCT) transition were also observed at 326 and 373 nm for **1** and **2**, respectively. While the zinc complex (**1**) with d^{10} electronic configuration does not exhibit *d*-*d* electronic charge transfer, an absorption band assigned as *d*-*d* charge transition was observed at 840 nm in the copper complex (**2**) with d^9 electronic configuration.[64,65] TD-B3LYP/CPCM results presented in Table 5 demonstrated that the absorption band calculated at 217 nm is derived from HOMO-5 → LUMO+2 with the main contribution of 74%. Chemissian program[47] results also demonstrated that HOMO-5 mainly localized on COO^- (73%), pyridine ring (16%), and Cl atom (9%), H_2O (1%), while LUMO+2 lies down on pyridine ring (92%), Cl (5%), and COO^- (3%). So the band observed/calculated 230/217 nm is mainly originated as the π electron transitions from COO^- to pyridine ring. Another absorption band observed/calculated at 274/253 nm is mainly derived from HOMO-2 → LUMO(74%). HOMO-2 mainly localized on pyridine ring (52%), Cl(23%), and COO^-(24%), while LUMO strongly lies down on pyridine ring (89%), COO^- (10%), and Cl (1%). So this absorption band is originated by the transitions from COO^- group and Cl atom to pyridine ring. The longest wavelength absorption for **1** (326/310 nm) is HOMO → LUMO (60%) and HOMO-1 → LUMO+1 (35%). Considering that HOMOs localized on pyridine ring (33%), COO^- (61%), Zn (II) (4%), and H_2O (2%), the transitions from COO^- to pyridine ring are responsible for this minimum energy absorption band for **1**. When it comes to UV-Vis spectrum of Cu (II) complex, the bands observed/calculated at 231/254 nm and 273/306 nm were assigned as π-π* and *n*-π* transitions. The other bands observed/calculated at 373/377 nm and 840/938 nm were also assigned as ligand–metal charge transfer (LMCT) and metal–metal charge transfer (MMCT), respectively. The electronic absorption bands calculated at 254 and 283 nm were mainly attributed to transitions from Cl and

TABLE 5 Experimental and theoretical UV-Vis spectral data and their detailed analysis

	Exp.	TD-B3LYP/6-311++G(d,p)/LanL2DZ				
	λ (nm)	λ (nm)	Oscillator Str.	Important contributions		
1	230	217	0.1017	H-5 → L + 2(74%)	H-3 → L + 3(8%)	H-5 [pyr(16%)/Cl(9%)/COO^-(73%)/H_2O (1%)] → L + 2 [pyr(92%)/Cl(5%)/ COO^-(3%)]
	274	253	0.1625	H-2 → L(74%)	H-3 → L + 1(16%)	H-2 [pyr(52%)/Cl(23%)/COO^-(24%)] → L [pyr(89%)/Cl(1%)/COO^-(10%)]
	326	310	0.0002	H → L (60%)	H-1 → L + 1(35%)	H [pyr(33%)/COO^-(61%)/Zn(4%)/H_2O (2%)] → L [pyr(89%)/COO^-(11%)]
2	231	254	0.0995	H-5 → L + 2 β(22%)	H-5 → L + 1 α(16%)	H-5 [pyr(53%)/Cl(27%)/COO^-(17%)/ Cu(4%)] → L + 2 [pyr(88%)/Cl(2%)/ COO^-(9%)/Cu(1%)]
	273	283	0.0043	H → L + 1 β (27%)	H-3 → L + 1 β (9%)	H [pyr(30%)/Cl(1%)/COO^-(56%)/ Cu(11%)/ H_2O(2%)] → L + 1 [pyr(85%)/Cl(1%)/ COO^-(11%)/Cu(2%)/H_2O(1%)]
	373	377	0.0371	H-1 → L β (49%)	H-3 → L β (23%)	H-1 [pyr(41%)/COO^-(60%)/ Cu(7%)/H_2O (3%)] → L [pyr(22%)/Cl(1%)/COO^-(20%)/ Cu(56%)/H_2O(1%)]
	840	938	0.0044	H-3 → L β (29%)	H-0 → L β (19%)	H-7 [pyr(25%)/Cl(1%)/COO^-(52%)/ Cu(18%)/H_2O(4%)] → L [pyr(22%)/Cl (1%)/COO^-(20%)/Cu(56%)/H_2O(1%)]

Abbreviations: COO^-, carboxylate group; Cl, Cl atom; H_2O, water ligand; pyr, pyridine ring.

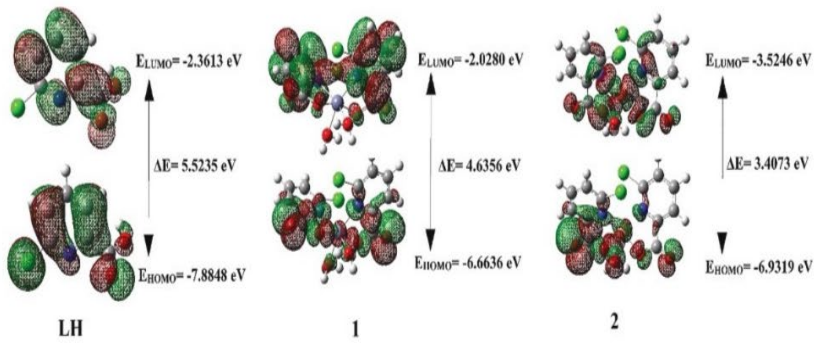

FIGURE 6 The FMO energies for **LH**, **1** and **2**

COO moieties to pyridine ring, while the effect of Cu (II) ion with d^9 electronic configuration are dominant in the absorption bands calculated at 377 and 938 nm.

The 3D fragments of frontier molecular orbitals (FMOs) and their energies were calculated by using time dependent B3LYP level of DFT and 6-311++G(d,p) in conjunction with LanL2DZ basis sets (Figure 6). The TD-B3LYP/CPCM calculations were performed for **1** in singlet spin state and **2** in doublet spin state. Since the β spin electronic transitions were dominant in the UV-Vis spectrum of **2**, HOMO-LUMO energy gap was determined through the β spin molecular orbitals. The HOMO-LUMO energy gap for LH, **1** and **2** complexes were calculated as 5.5235, 4.6356, and 3.4073 eV, respectively. The energy gap between HOMO and LUMO is used as an indicator of stability and/or reactivity, which is related to chemical hardness (η), that indicates the resistance to change, or deformation of the electron cloud.[66] The energy gap values calculated for **LH**, **1**, and **2** demonstrated that the chemical hardness is arranged in descending order of **LH** > **1** > **2**. It is well known that the larger HOMO-LUMO energy gap implies the harder

TABLE 6 The total static dipole moment (μ), the mean polarizability (<α>), the anisotropy of the polarizability (Δα), and the mean first hyperpolarizability (<β>) for **LH**, **1**, and **2**

Property	LH	1	2
μ (Debye)	2.6480	0.7842	4.0259
α (esu)	1.12×10^{-23}	1.79×10^{-23}	1.19×10^{-23}
Δα (esu)	1.73×10^{-23}	2.92×10^{-23}	2.22×10^{-23}
β (esu)	2.74×10^{-30}	0.88×10^{-30}	10.40×10^{-30}
E_{HOMO} (eV)	−7.8848	−6.6636	−6.9319
E_{LUMO} (eV)	−2.3613	−2.0280	−3.5246
ΔE (eV)	5.5235	4.6356	3.4073
χ (eV)	5.1231	4.3459	5.2283
η (eV)	2.7617	2.31781	1.7037

molecules; on the other hand, a smaller HOMO-LUMO gap means small excitation energies to the manifold of excited states; therefore, soft molecules will be more polarizable than hard molecules.[59] When the relationship between HOMO-LUMO energy gaps and β parameters between organometallic complexes **1** and **2** is evaluated, it is seen that **2** complex with a small HOMO-LUMO energy gap has a higher β value. It is also known that the lower HOMO energy implies the more stable molecular structure. So the stability of the investigated systems is arranged as **LH** > **2** > **1** just as the HOMO energies are ordered. As is known, Zn (II) ion has $3d^{10}$ electron configuration, which is fully occupied and spherical symmetry, and its complexes are relatively more stable than those of Cu (II) ion. Table 6 also demonstrated that the coordination of **LH** ligand to Cu (II) ion decreases to HOMO-LUMO energy gap and increases its chemical reactivity.

3.4 | Nonlinear optics

Scientists combining organic ligands with transition metal ions to design new materials with efficient nonlinear optical properties hope to achieve both of the advantages of organic molecules (design flexibility and fast response) and the advantages of inorganic salts (stability and thermal stability). The flexibility of metal–organic complexes is provided by metal variation, ligand variation, different coordination geometry, oxidation state, electron donating/withdrawing capabilities of the metal or ligand, and stabilization of unstable organic fragments. These variables can be modified partially or all at once to obtain materials with targeted NLO properties. In order to investigate NLO properties of **1** and **2** complexes, the mean polarizability (<α>), anisotropy of the polarizability (Δα), and mean first hyperpolarizability (<β>) parameters were calculated by using B3LYP level in conjunction with 6-311++G(d,p)/LanL2DZ basis set. Furthermore, NLO properties of **LH** ligand were also investigated to understand the variation in NLO properties during the coordination of **LH** ligand to Zn (II) and Cu (II) ions. The dipole moment for **LH**, **1**, and **2** complexes was calculated as 2.6480, 0.7842, and 4.0259 Debye, respectively. The mean first-order hyperpolarizability parameter was also calculated as 2.74×10^{-30}, 0.88×10^{-30}, and 10.40×10^{-30} esu, respectively. These results demonstrate that the μ and β parameters have a similar trend for the studied systems. It was also concluded that the coordination of **LH** ligand to Cu (II) ion increases the β parameter due to the d^9 electronic configuration of metal ion. As for the coordination to Zn (II) with the fully occupied and spherically symmetrical electronic configuration, a decrease in the β parameter was obtained. In our previous study, the β parameter for Co (II) and Mn (II) complexes of LH ligand was calculated as 3.45×10^{-30} and 1.71×10^{-30} esu, respectively.[58] In the other studies, the β parameter for Cu (II) complexes of 6-methylpyridine-2-carboxylic acid was also calculated as 1.2×10^{-30} esu[25] and 4.6×10^{-30} esu.[56] So it can be said that 6-chloropyridine-2-carboxylic acid is a good building block to obtain novel NLO crystals. The obtained first hyperpolarizability parameters for **1** and **2** are also compared with those reported for pNA[67] and urea.[68] The β parameter obtained for **1** is 10.5 times smaller than that of pNA (9.2×10^{-30} esu), while the same parameter obtained for **2** is calculated as 1.1 times larger than that of pNA. In both complexes, the β parameter was higher than that reported for urea (0.130×10^{-30} esu). So it can be said that complex **2** can be a promising candidate for effective NLO materials.

3.5 | Natural bond orbital analysis

The NBO investigation is commonly used to understand the chemical interpretation of hyper conjugative interactions and electron density redistribution in numerous bonding and antibonding orbitals. The NBO analysis for **1** and **2** was performed by using B3LYP level and 6-311++G(d,p)/LanL2DZ basis set, and the obtained results were presented in Table 7. Large $E^{(2)}$ value means strong interactions are present between electron–donor and electron–acceptor groups and greater degree of conjugation in the whole system. The natural charge of the Zn (II) ion, which is +2 in the free state, in **1** complex was calculated as +1.68649. NBO analysis also estimated the electronic configuration of Zn (II) ion as [core]

TABLE 7 Second-order perturbation theory analysis of Fock matrix on NBO basis for **1** and **2**

1							2						
Type	Bond	Type	Antibond	E^2 (kcal/mol)	$E(j)-E(i)^b$ (a.u.)	$F(i,j)^o$ (a.u)	Type	Bond	Type	Antibond	E^2 (kcal/mol)[a]	$E(j)-E(i)^b$ (a.u.)[b]	$F(i,j)$ (a.u)[c]
LP(2)	O5	LP*(6)	Zn1	36.07	0.44	0.118	LP(3)	O2	LP*(6)	Cu1	20.43	0.53	0.131
LP(1)	N1	LP*(6)	Zn1	25.03	0.48	0.103	LP(1)	N1	LP*(6)	Cu1	16.51	0.58	0.127
LP(2)	O4	LP*(6)	Zn1	18.69	0.61	0.103	LP(2)	O4	LP*(6)	Cu1	16.81	0.49	0.115
LP(2)	O2	LP*(6)	Zn1	35.08	0.44	0.118	LP(1)	N2	LP*(6)	Cu1	19.33	0.59	0.137
LP(1)	N2	LP*(6)	Zn1	25.03	0.48	0.103	LP(2)	O3	LP*(6)	Cu1	5.66	0.50	0.072
LP(2)	O3	LP*(6)	Zn1	18.68	0.61	0.103	LP(1)	C4	π*	N2—C5	72.40	0.10	0.124
LP(2)	O5	σ*	O6—C6	14.31	1.01	0.110	LP(3)	Cl1	π*	C1—C2	6.99	0.32	0.064
LP(2)	O5	π*	O6—C6	70.80	0.30	0.132	LP(3)	O4	π*	O5—C12	36.54	0.30	0.132
LP(2)	O6	σ*	O5—C6	24.26	0.73	0.121	LP(2)	O5	σ*	O4—C12	12.23	0.73	0.123
LP(2)	O6	σ*	C6—C6	21.21	0.60	0.102	LP(2)	O5	σ*	C11—C12	10.50	0.60	0.102
LP(2)	O2	σ*	O1—C7	14.31	1.01	0.110	LP(1)	C10	π*	C9—C10	36.93	0.13	0.110
LP(2)	O1	π*	O2—C7	24.26	0.73	0.121	LP(2)	O1	σ*	O2—C6	12.68	0.72	0.124
LP(2)	O1	π*	C8—C7	21.21	0.60	0.102	LP(2)	O2	π*	O1—C6	33.67	0.31	0.129
π	N2—C8	π*	C12—C11	27.40	0.32	0.086	LP(2)	O1	π*	O2—C6	12.68	0.72	0.124
π	C12—C11	π*	N2—C8	15.53	0.27	0.060	LP(2)	O1	σ*	C5—C6	10.28	0.61	0.101
π	C9—C10	π*	N2—C8	34.39	0.25	0.084	LP(3)	Cl2	π*	N2—C7	8.72	0.28	0.070
π	C12—C11	π*	C9—C10	19.64	0.31	0.071	LP(2)	O4	σ*	O4—C12	7.20	0.98	0.114
π	N1—C5	π*	C1—C2	27.40	0.32	0.086	π	C1-C2	π*	N1—C5	7.49	0.27	0.058
π	C4—C3	π*	N1—C5	34.40	0.25	0.084	π	N1-C5	π*	C1—C2	13.20	0.33	0.085
π	C4—C3	π*	C1—C2	20.50	0.26	0.006	π	N2-C7	π*	C8—C9	4.95	0.37	0.055
π	C1—C2	π*	C4—C3	19.64	0.31	0.071	π	C8-C9	π*	N2—C7	17.66	0.23	0.083

[a]Hyper conjugative interaction energy.
[b]Energy difference between donor and acceptor NBOs.
[c]Fock matrix element between i and j NBOs.

$4S^{(0.33)}3d^{(9.97)}4p^{(0.01)}$ with 17.99839 core electron, 10.30812 valance electron, 0.00699 Rydberg electron, and 28.31351 total electron. As for Cu (II) ion, its natural charge was calculated as +1.42817, and its total 27.57183 electrons were shared as 17.99723 core electron, 9.56750 valance electron, and 0.00710 Rydberg electron. The electronic configuration of free Cu (II) ion was obtained as $[core]4S^{(0.32)}3d^{(9.24)}4p^{(0.01)}$ in complex **2**. The fact that the calculated natural charges of metal ions in the complex are smaller than the values of free ions indicates that the charge transfers from the ligand to the metal are more dominant than those in the opposite direction.

The high energy interactions of LP O/N → LP*Zn/Cu were presented in Table 7. These intensive interactions are the powerful indicators of six-coordinated Zn (II) and five coordinated Cu (II) centers through the donor N and O atoms. The higher interaction energies imply the more intensive interactions which means that the bond lengths between the interacting atoms is shorter than that of the atoms which have lower interaction energies. For example, the hyperconjugative interaction energies of LP(2) O5 LP*(6) Zn1 and LP(3) O2 → LP*(6) Cu1 calculated as the highest energies (36.07 and 20.43 kcal/mol) among the bonds between central metal ions and donor N/O atoms. X-ray diffraction results also demonstrated that these bond lengths are the lowest coordination bonds (Zn—O5, 2.0286[14] Å and Cu1—O2 1.9094[15]). Moreover, the Jahn-Teller compression determined for **1** and **2** crystals was also confirmed by NBO analysis. In complex **1**, the intensive interactions of LP(2) O5 → π* O6—C6, π C9—C10 → π* N2—C8, and π C4—C3 → π* N1—C5 were determined by the higher energies of 70.80, 34.39, and 34.40 kcal/mol. In complex **2**, the hyperconjugation energies of LP(1) C4 → π* N2—C5, LP(3) O4 → π* O5—C12, and LP(2) O2 → π* O1—C6 were calculated as 72.40, 36.54, and 33.67 kcal/mol, demonstrating the stabilization of **2**.

3.6 | MEP surfaces

The molecular electrostatic potential (MEP) surfaces for **1** and **2** were simulated by using B3LYP/6-311++G(d,p)/LanL2DZ level. According to MEP surfaces presented in Figure 7, the highest negative potential implemented in red color is found around the uncoordinated O atoms of carboxyl group. The highest positive potential also lies down around the hydrate ligand H atom and aromatic H atoms. The electrostatic potential scale for **2** (±7.940 e−2) is calculated as higher than that of **1** (±6.901 e−2). The more electrostatic potential gap between the highest and lowest points implies that the system under investigation can be easily polarized and exhibits better first order hyperpolarizability (β). The MEP originated in space around a molecule by the charge distribution is very helpful in understanding the reactive sites for nucleophilic and electrophilic attack in hydrogen bonding interaction and in biological recognition process. The electrophilic and nucleophilic sites give information about the region from where the compound can have intra or intermolecular interactions and metallic bonding. So **1** and **2** can participate in new interaction through the highest negative or positive potential regions.

3.7 | Molecular docking

Molecular docking study was used to estimate the interactions of **1** and **2** complexes with SARS-CoV-2 main protease (PDB: 6LU7) at the atomic level, which allow us to characterize the behavior of the investigated complexes

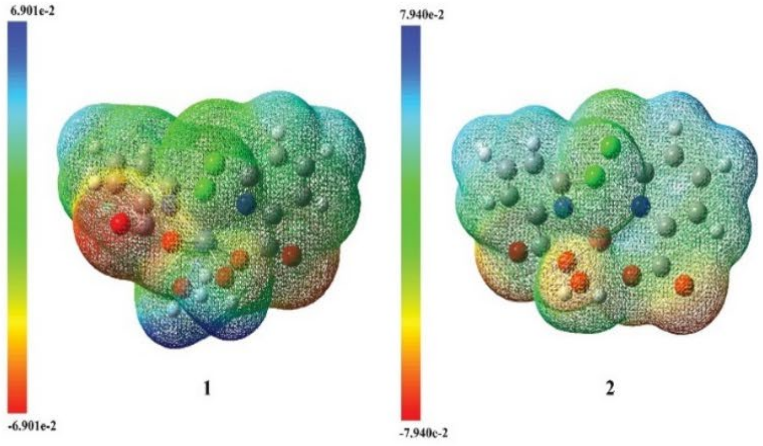

FIGURE 7 Molecular electrostatic potential (MEP) surfaces for 1 and 2 obtained by B3LYP/6-311++G(d,p)/LanL2DZ

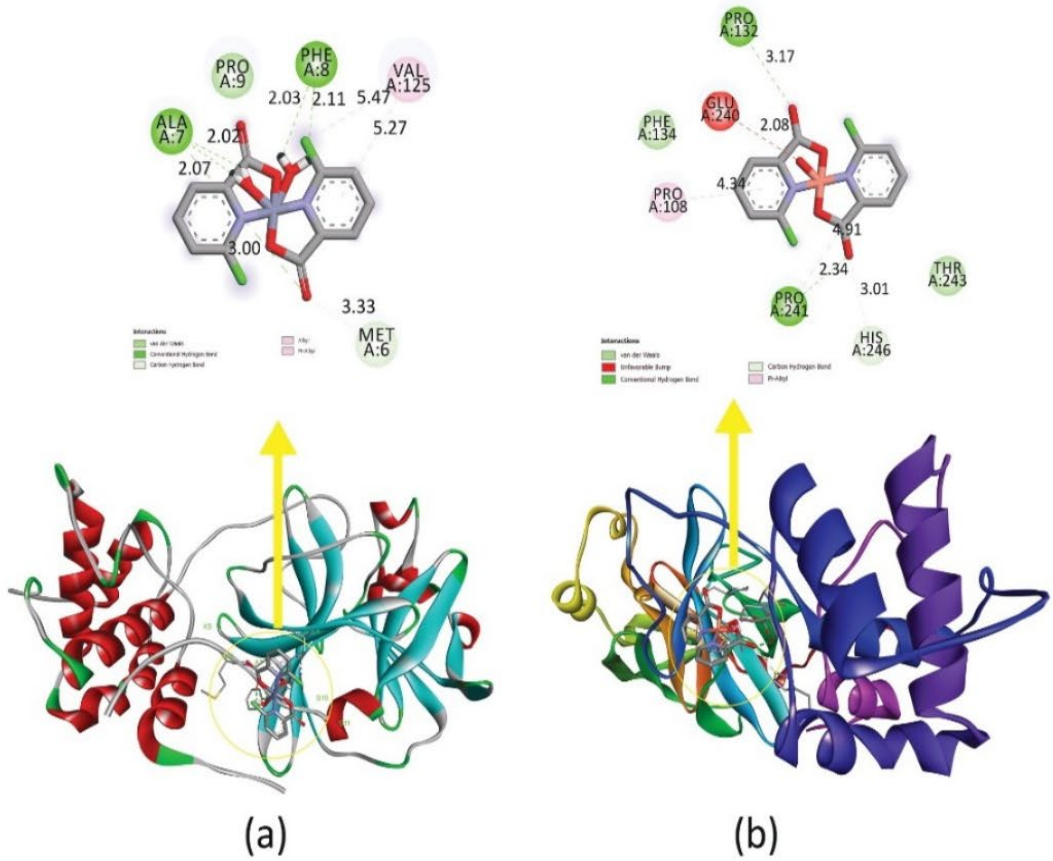

FIGURE 8 Three- and two-dimensional molecular interaction of (a) **1** and (b) **2** for inhibitor to SARS-CoV-2 main protease (PDB: 6LU7)

in the binding site of target structure. According to molecular docking results summed up in Figure 8, it was clearly observed that complex **1** could form conventional H bonding interactions with ALA A:7 and PHE A:8 with the interaction length range of 2.02–3.00 Å. Another important interaction is van der Waals interaction found between carboxyl group O atom and MET A:6 with the interaction length of 3.333 Å. As for complex **2**, the conventional H bonding interactions of carboxylate O atoms with PRO A:132 and PRO A:241 were predicted with the interaction bond lengths of 3.17 and 2.34 Å. The van der Waals and π-Alkyl interactions play active roles in the interaction of **2** complex with target structure. The docking results also explain the relative performance of stabilization and binding energy of the complexes. The molecular docking of **1** and **2** complexes to SARS-CoV-2 main protease (PDB: 6LU7) gives a binding energy of −5.24 and −4.14 kcal/mol, respectively. Molecular docking analysis also estimated inhibition constant as 144.6 and 925.95 μM. From the docking procedure, the negative values of the binding energy demonstrate that complexes **1** and **2** are stable and successfully binding in the cavity of target SARS-CoV-2 main protease. When the results of molecular docking are examined, it is seen that complex **1** has superior binding ability than complex **2**.

4 | CONCLUSION

Novel Zn (II) and Cu (II) transition metal complexes of 6-chloropyridine-2-carboxylic acid (**1** and **2**) were successfully synthesized, and their crystal structures and spectroscopic properties were determined by XRD method, FT-IR, and UV-Vis spectroscopies. Both XRD and FT-IR results demonstrated that **1** crystalizes as a distorted octahedral complex, while **2** crystalizes in a distorted trigonal bipyramidal coordination geometry. The n-π^*, π- π^*, LMCT, and d-d electronic absorption bands arise in the UV-Vis spectrum of **2** observed in ethanol solvent. Since

the *d* orbital was fully occupied, *d-d* absorption band was not observed in that of **1**. The HOMO-LUMO energy gaps were obtained in the order of **LH** > **1** > **2**. The first-order static hyperpolarizability parameters (β) were also calculated in the order of **1** < **LH** < **2**. So it was demonstrated that the LMCT and *d-d* electronic transitions induce β while the fully occupied d electron configuration decreases β. When it comes to molecular docking study, both the binding ability and inhibition constant of **1** to SARS-CoV-2 main protease are found as more effective than **2**. The main source of this difference is thought to be the nature of the metal ions, the coordination geometries of complexes, and the additional H_2O molecule. In summary, among the newly synthesized and characterized **1** and **2** complexes, **2** has superior NLO properties compared to **1**, while **1** has superior inhibition constant and binding affinity against SARS-CoV-2 main protease.

AUTHOR CONTRIBUTIONS

Necmi Dege: Data curation; investigation; methodology; project administration; software; supervision. **Ömer Tamer:** Data curation; investigation; methodology; project administration; software; supervision. **Merve Şimşek:** Data curation; software. **Davut Avcı:** Data curation; investigation; methodology; software. **Mavise Yaman:** Data curation; investigation; software. **Adil Başoğlu:** Data curation; investigation; software; validation. **Yusuf Atalay:** Data curation; investigation; methodology; software; visualization.

DATA AVAILABILITY STATEMENT

The data that support the findings of this study are available from the corresponding author upon reasonable request.

ORCID

Necmi Dege https://orcid.org/0000-0003-0660-4721
Ömer Tamer https://orcid.org/0000-0002-2241-789X
Merve Şimşek https://orcid.org/0000-0002-6921-6526
Davut Avcı https://orcid.org/0000-0002-9011-6191
Mavişe Yaman https://orcid.org/0000-0001-5239-1478
Adil Başoğlu https://orcid.org/0000-0002-5973-8419
Yusuf Atalay https://orcid.org/0000-0001-8578-5801

REFERENCES

[1] C. X. Zhang, S. J. Lippard, *Curr. Opin. Chem. Biol.* **2003**, *7*, 481.
[2] A. Y. Louie, T. J. Meade, S. Lippard, *Chem. Rev.* **1999**, *99*, 2711.
[3] C.-M. Che, F.-M. Siu, *Curr. Opin. Chem. Biol.* **2010**, *14*, 255.
[4] C. Wang, T. Zhang, W. Lin, *Chem. Rev.* **2012**, *112*, 1084.
[5] C. Wang, D. Liu, W. Lin, *J. Am. Chem. Soc.* **2013**, *135*, 13222.
[6] L. Mingabudinova, V. Vinogradov, V. Milichko, E. Hey-Hawkins, A. Vinogradov, *Chem. Soc. Rev.* **2016**, *45*, 5408.
[7] M. L. Green, S. R. Marder, M. E. Thompson, J. A. Bandy, D. Bloor, P. Kolinsky, R. Jones, *Nature* **1987**, *330*, 360.
[8] S. Taboukhat, N. Kichou, J.-L. Fillaut, O. Alévêque, K. Waszkowska, A. Zawadzka, A. El-Ghayoury, A. Migalska-Zalas, B. Sahraoui, *Sci. Rep.* **2020**, *10*, 1.
[9] S. D. Bella, *Chem. Soc. Rev.* **2001**, *30*, 355.
[10] S. D. Cummings, L.-T. Cheng, R. Eisenberg, *Chem. Mater.* **1997**, *9*, 440.
[11] S. A. Abdel-Latif, H. Moustafa, *Appl. Organomet. Chem.* **2017**, *31*, e3876.
[12] S. A. Abdel-Latif, A. A. Mohamed, *J. Mol. Struct.* **2017**, *1134*, 307.
[13] A. F. Darweesh, N. A. A. El-Fatah, S. A. Abdel-Latif, I. A. Abdelhamid, A. H. Elwahy, M. E. Salem, *ARKIVOC: J. Org. Chem.* **2021**, *2021*, 23.
[14] Y. M. Issa, S. A. Abdel-Latif, A. L. El-Ansary, H. B. Hassib, *New J. Chem.* **2021**, *45*, 1482.
[15] N. J. Long, *Angew. Chem. Int. Ed.* **1995**, *34*, 21.
[16] B. Rosenberg, L. Van Camp, T. Krigas, *Nature* **1965**, *205*, 698.
[17] R. Oun, Y. E. Moussa, N. J. Wheate, *Dalton Trans.* **2018**, *47*, 6645.
[18] I. U. Amarasena, S. Chatterjee, J. A. Walters, R. Wood-Baker, K. M. Fong, *Cochrane Database Syst. Rev.* **2015**, *2015*.
[19] I. Ott, R. Gust, *Int. J Pharm. Med. Chem.* **2007**, *340*, 117.
[20] P. Köpf-Maier, *Eur. J. Clin. Pharmacol.* **1994**, *47*, 1.
[21] J. L. Buss, F. M. Torti, S. V. Torti, *Curr. Med. Chem.* **2003**, *10*, 1021.
[22] Ö. Tamer, H. Mahmoody, K. F. Feyzioğlu, O. Kılınç, D. Avci, O. Orun, N. Dege, Y. Atalay, *Appl. Organomet. Chem.* **2020**, *34*, e5416.
[23] H. Hao, X. Liu, X. Ge, Y. Zhao, X. Tian, T. Ren, Y. Wang, C. Zhao, Z. Liu, *J. Inorg. Biochem.* **2019**, *192*, 52.
[24] S. W. Leuthauser, L. W. Oberley, T. D. Oberley, *J. Natl. Cancer. Inst.* **1982**, *68*, 123.
[25] D. Avcı, S. Altürk, F. Sönmez, Ö. Tamer, A. Başoğlu, Y. Atalay, B. Z. Kurt, N. Dege, Mol Divers, **2021**, *25*, 171.
[26] S. Nikolić, L. E. Mihajlović-Lalić, M. Vidosavljević, S. Aranđelović, S. Radulović, S. Grgurić-Šipka, *J. Organomet. Chem.* **2019**, *902*, 120966.
[27] M. Buczkowska, A. Bodtke, U. Lindequist, M. Gdaniec, P. J. Bednarski, *Arch. Pharm.* **2011**, *344*, 605.
[28] A. Joshi, R. Gupta, D. Sharma, M. Singh, *Dalton Trans.* **2021**, *50*, 1253.
[29] D. Avcı, Y. Saeedi, A. Başoğlu, N. Dege, S. Altürk, Ö. Tamer, Y. Atalay, *Appl. Organomet. Chem.* **2021**, *35*, e6125.
[30] Ö. Tamer, D. Avcı, N. Dege, Y. Atalay, *J. Mol. Struct.* **2020**, *1202*, 127288.
[31] D. Avcı, S. Altürk, F. Sönmez, Ö. Tamer, A. Başoğlu, Y. Atalay, B. Z. Kurt, N. Dege, *JBIC J. Biol. Inorg. Chem.* **2019**, *24*, 747.
[32] C. Stoe, Stoe&Cie, Darmstadt, Germany, **2002**.
[33] G. M. Sheldrick, *Acta Crystallogr. A: Found. Adv.* **2015**, *71*, 3.
[34] G. M. Sheldrick, *Acta Crystallogr. C: Struct. Chem.* **2015**, *71*, 3.
[35] C. F. Macrae, P. R. Edgington, P. McCabe, E. Pidcock, G. P. Shields, R. Taylor, M. Towler, J. Streek, *J. Appl. Crystallogr.* **2006**, *39*, 453.
[36] A. Spek, *J. Appl. Crystallogr.* **2003**, *36*, 7.
[37] L. J. Farrugia, *J. Appl. Crystallogr.* **1999**, *32*, 837.
[38] S. P. Westrip, *J. Appl. Crystallogr.* **2010**, *43*, 920.

[39] M. Frisch, G. Trucks, H. B. Schlegel, G. E. Scuseria, M. A. Robb, J. R. Cheeseman, G. Scalmani, V. Barone, B. Mennucci, G. Petersson, Gaussian Inc., Wallingford CT, **2009**, 201.
[40] R. Dennington, T. Keith, J. Millam, **2009**.
[41] A. D. Becke, *J. Chem. Phys.* **1993**, *98*, 1372.
[42] C. Lee, W. Yang, R. G. Parr, *Phys. Rev. B* **1988**, *37*, 785.
[43] R. Ditchfield, W. J. Hehre, J. A. Pople, *J. Chem. Phys.* **1971**, *54*, 724.
[44] P. J. Hay, W. R. Wadt, *J. Chem. Phys.* **1985**, *82*, 299.
[45] P. J. Hay, W. R. Wadt, *J. Chem. Phys.* **1985**, *82*, 270.
[46] S. Gorelsky, University of Ottawa, Ottawa, Canada, **2010**.
[47] L. Skripnikov, V. Chemissian, 4.01, Visualization Computer Program, **2014**.
[48] G. M. Morris, D. S. Goodsell, R. S. Halliday, R. Huey, W. E. Hart, R. K. Belew, A. J. Olson, *J. Comput. Chem.* **1998**, *19*, 1639.
[49] D. S. Biovia, Discovery studio modeling environment, in, Release, **2017**.
[50] Ö. Tamer, D. Avcı, E. Çelikoğlu, Ö. İdil, Y. Atalay, *Appl. Organomet. Chem.* **2018**, *32*, e4540.
[51] D. Avcı, S. Altürk, F. Sönmez, Ö. Tamer, A. Başoğlu, Y. Atalay, B. Z. Kurt, J Mol Struct, **2020**, *1205*, 127655.
[52] F. A. Cotton, G. E. Lewis, C. A. Murillo, W. Schwotzer, G. Valle, *Inorg. Chem.* **1984**, *23*, 4038.
[53] K. D. Karlin, J. C. Hayes, S. Juen, J. P. Hutchinson, J. Zubieta, *Inorg. Chem.* **1982**, *21*, 4106.
[54] A. Patra, *J. Chem. Soc. Dalton Trans.* **1999**, 2461.
[55] D. Avcı, S. Altürk, F. Sönmez, Ö. Tamer, A. Başoğlu, Y. Atalay, B. Z. Kurt, N. Dege, *Tetrahedron Lett.* **2018**, *74*, 7198.
[56] S. Altürk, D. Avcı, A. Başoğlu, Ö. Tamer, Y. Atalay, N. Dege, *Spectrochim. Acta A: Mol. Biomol. Spec.* **2018**, *190*, 220.
[57] Ö. Tamer, B. Sarıboğa, I. Ucar, *Struct. Chem.* **2012**, *23*, 659.
[58] N. Dege, Ö. Tamer, M. Yaman, A. Başoğlu, D. Avcı, Y. Atalay, *Applied Physics A* **2021**, *127*, 1.
[59] Ö. Tamer, S. A. Tamer, Ö. İdil, D. Avcı, H. Vural, Y. Atalay, *J. Mol. Struct.* **2018**, *1152*, 399.
[60] Ö. Tamer, *J. Mol. Struct.* **2017**, *1144*, 370.
[61] Ö. Tamer, D. Avcı, Y. Atalay, *J. Inorg. Organomet. Polym. Mater.* **2017**, *27*, 700.
[62] Ö. Tamer, D. Avcı, Y. Atalay, *J. Phys. Chem. Solids* **2016**, *99*, 124.
[63] S. Altürk, D. Avcı, Ö. Tamer, Y. Atalay, O. Şahin, *J. Phys. Chem. Solids* **2016**, *98*, 71.
[64] F. K. Camellia, A. Al Mahmud, M. J. Pramanik, K. Nahar, M. M. Haque, M. Kudrat-E-Zahan, *J. Chil. Chem. Soc.* **2021**, *66*, 5295.
[65] M. Shakir, N. Shahid, N. Sami, M. Azam, A. U. Khan, *Spectrochim. Acta A: Mol. Biomol. Spec.* **2011**, *82*, 31.
[66] R. G. Pearson, *J. Am. Chem. Soc.* **1963**, *85*, 3533.
[67] L. T. Cheng, W. Tam, S. H. Stevenson, G. R. Meredith, G. Rikken, S. R. Marder, *J. Phys. Chem.* **1991**, *95*, 10631.
[68] C. Adant, M. Dupuis, J. Bredas, *Int. J. Quantum Chem.* **1995**, *56*, 497.

How to cite this article: N. Dege, Ö. Tamer, M. Şimşek, D. Avcı, M. Yaman, A. Başoğlu, Y. Atalay, *Appl Organomet Chem* **2022**, *36*(6), e6678. https://doi.org/10.1002/aoc.6678

Materials Today Communications 38 (2024) 108021

Contents lists available at ScienceDirect

Materials Today Communications

journal homepage: www.elsevier.com/locate/mtcomm

A new mixed-ligand zinc(II) complex of 3-hydroxy and 4-chloro substituted pyridine-2-carboxylic acid: Synthesis, characterization, NLO properties and DFT calculation

Merve Şimşek [a], Ömer Tamer [a,*], Necmi Dege [b], Davut Avcı [a], Hayatullah Mahmoody [c], Yusuf Atalay [a]

[a] Sakarya University, Faculty of Science, Department of Physics, Sakarya, Türkiye
[b] Ondokuz Mayıs University, Faculty of Art and Science, Department of Physics, Türkiye
[c] Sar-e-pul Higher Education Institute, Department of Physics, Sarepul, Afghanistan

ARTICLE INFO

Keywords:
Zn(II) complex
Pyridine-2-carboxylic acid derivative
FT-IR
UV-Vis
Dc-Kerr effect and EFSHG

ABSTRACT

Molecular engineering of metal-organic frameworks has recently attracted increasing attention due to their potential technological applications in the fields of optics and photonics. In addition to improved optical properties, the incorporation of metal ions into organic ligands makes it possible to control the intensity and polarization of the incident laser light. This makes organometallic complexes valuable and suitable candidates for nonlinear optical applications. In this study, a novel Zn(II) complex was synthesized by using 4-chloropyridine-2-carboxylic acid (4-Clpca) and 3-hydroxypyridine-2-carboxylic acid (3OHpca). The structural and spectroscopic properties of the Zn(II) complex were examined through XRD, FT-IR and UV-Vis techniques. The HOMO-LUMO energy range for the Zn(II) complex was found to be 4.7358 eV. Nonlinear optical parameters of Zn(II) complex were investigated as static and frequency-dependent ($\omega = 0.0856453887$ au) methods. The dc-Kerr effect $\gamma(-\omega;\omega,0,0)$ and EFSHG $\gamma(-2\omega;\omega,\omega,0)$ parameters were calculated as 13.04×10^{-36} esu and 2258.9×10^{-36} esu, respectively. The newly synthesized Zn(II) complex, which has weak second-order NLO properties due to the fully occupied electronic configuration of the Zn(II) ion, is quite promising in terms of its third-order optical properties.

1. Introduction

The need for new functional materials with the desired nonlinear optical (NLO) efficiency is increasing day by day, due to their potential for usage in a variety of fields, including optical data storage, optical switching, optical communication, optical computing, and other laser devices [1–7]. In the past, the search for new NLO materials in order to meet the needs of constantly developing technology has focused on many different types of NLO materials including inorganic, organic, organometallic, semiconductor and so on [8–11]. For nonlinear optics applications, the advantages of organic materials are described as large nonlinear optical coefficient, structural flexibility, and short optical response time, but they also suffer from low thermal stability, low mechanical strength, and limited operating temperature ranges [12–14]. Inorganic crystals such as $LiNbO_3$ are one of the most common materials used for nonlinear electro-optical applications, and have good thermal and temporal stability properties. However, inorganic materials also have disadvantages such as the cost of obtaining and processing single crystals is more expensive, less flexible than organic materials, and difficult to grow as single crystals [15]. Metal organic coordination complexes represent a novel class of hybrid materials that seamlessly blend the remarkable characteristics of inorganic and organic components. These materials exhibit a substantial nonlinear optical index, rapid optical response, versatility in integrating and modifying organic compounds, and excellent thermal stability inherent to inorganic substances [6,7].

In the pursuit of discovering various organometallic materials with strong non-linear optical properties, scientists have recently focused on pyridine-carboxylic acid derivatives. This is due to the presence of donor atoms N and O, their flat geometries, and coordination potential with metal ions. To date, 4-methoxy-pyridine-2-carboxylic acid [16,17], 4-(trifluoromethyl) pyridine-2-carboxylic acid [18],

* Corresponding author.
E mail address: omertamer@sakarya.edu.tr (Ö. Tamer).

https://doi.org/10.1016/j.mtcomm.2024.108021
Received 4 November 2023; Received in revised form 27 December 2023; Accepted 31 December 2023
Available online 6 January 2024
2352-4928/© 2024 Elsevier Ltd. All rights reserved.

6-chloropyridine-2-carboxylic acid [19], 5-(trifluoromethyl) pyridine-2-carboxylic acid [20], 6-methylpyridine-2-carboxylic acid [21], 6-bromopyridine-2-carboxylic acid [22] ligands have been coordinated to different metal ions, and the obtained coordination complexes were investigated in view of NLO properties. In the present study, an interesting coordination complex with non-centrosymmetric structure was synthesized by coordinating the ligands of 4-chloropyridine-2--carboxylic acid and 3-hydroxypyridine-2-carboxylic acid to Zn(II) ion. In particular, in the case of substitution of electron donor and acceptor groups or atoms to the opposite sides of metal complexes, the metal center may act as the donor, or as the acceptor, or even as the bridge of a donor–acceptor network. Moreover, it is clear that the electronic charge mobility of the complex will increase due to the coordination of the acceptor and donor groups to opposite ends, and therefore an improvement in the NLO properties will be observed.

The crystal structure of the synthesized [Zn(3OHpca)(4Clpca)$(H_2O)_2$] complex was determined through the use of X-ray diffraction methods. FT-IR and UV-Vis spectrum were used to provide a detailed spectral characterization. Finally, Density Functional Theory (DFT) calculations were carried out to gain a thorough comprehension of the structural, spectroscopic, and electronic characteristics of the Zn(II) complex. Additionally, the nonlinear optical properties of Zn(II) complexes were evaluated by calculating the first and second order nonlinear hyperpolarizabilities. In NLO calculations, both static and frequency-dependent (ω = 0.0856453887 au) methods were considered.

2. Materials and methods

2.1. Synthesis

All of the chemical reagents used to obtain Zn(II) crystal were acquired from Sigma Aldrich and utilized without any subsequent purification. The synthesis procedure is presented in Fig. 1. 4-chloropyridine-2-carboxylic acid (4ClPpca) (1 mmol) and 3-hydroxypyridine-2-carboxylic acid (3OHpca) (1 mmol) were solved in 30 mL ethanol/water mixture (1:1). After that, $Zn(CH_3COO)_2$•2 H_2O (1 mmol) was also dissolved in the last mixture to obtain Zn(II) complex. The resulting solution was stirred continuously at 50 °C for a duration of 2 h. Afterward, the colorless solution was filtered and allowed to evaporate at room temperature over a period of 2 weeks. The resulting colorless crystals were subsequently employed in X-ray diffraction experiments.

2.2. Experimental

A Stoe IPDS II diffractometer was utilized to collect crystallographic data using Mo-Kα (λ = 0.71073 Å) radiation at 296 K [23]. The crystal structure determination was performed using SHELXT [24], the crystal refinement was conducted via SHELXL [24]. Mercury[25], PLATON [26], WinGX [27], and PublCIF [28] to obtain crystal geometries, their drawings, and the Crystal Information File (CIF). Table 1 presents the information about the obtained crystallographic data and used refinement parameters for the Zn(II) complex. The FT-IR spectrum for Zn(II) complex including4Clpca and 3OHpca were obtained between 4000 and 400 cm^{-1} using the PERKIN ELMER Spectrum-Two FT-IR spectrophotometer. The UV-Vis spectrum for Zn(II) complex was recorded using a HITACHI U-2900 UV/VIS spectrophotometer in ethanol solvent at the range of 900–200 nm.

2.3. Theoretical methods

Gaussian 16 Revision rev. D01 [24] was employed to obtain the ground state geometry, vibrational spectrum, highest occupied and lowest unoccupied molecular orbitals, molecular electrostatic potential surface, dipole moment (μ), polarizability (α), first- and second-order static/dynamic hyperpolarizability (β and γ) parameters of for the Zn

Table 1
Crystallographic data and refinement parameters for Zn(II) complex.

CCDC	2296286
Chemical formula	$C_{12}H_{11}ClN_2O_7Zn$
M_r	396.05
Crystal system, space group	Monoclinic, P_{21}
Temperature (K)	293
a, b, c (Å)	5.1943 (6), 23.319 (3), 6.6173 (7)
β (°)	108.913 (8)
V (Å^3)	758.24 (16)
Z	4
Radiation type	Mo Kα
μ (mm^{-1})	1.83
Crystal size (mm)	0.78 × 0.66 × 0.55
Diffractometer	STOE IPDS 2 diffractometer
Absorption correction	Integration
T_{min}, T_{max}	0.393, 0.513
Independent and observed [I > 2σ(I)] reflections	4490, 2361, 1855
R_{int}	0.047
$(sin\ \theta/\lambda)_{max}$ (Å^{-1})	0.583
Refinement R[F^2 > 2σ(F^2)], wR(F^2), S	0.075, 0.202, 1.01
Number of reflections	2361
Number of parameters	216
Number of restraints	4
H atom treatment	H atom parameters constrained
$\Delta\rho_{max}$, $\Delta\rho_{min}$ (e Å^{-3})	0.78, −0.61

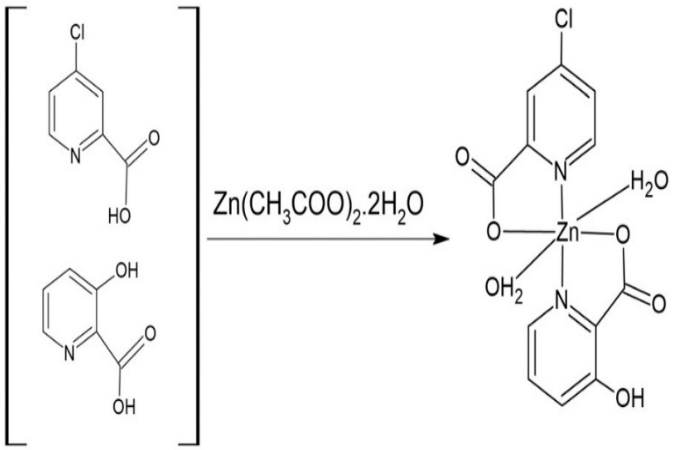

Fig. 1. The general synthesis scheme for Zn(II) complex.

(II) complex. GaussView 6.0 [25] program was also executed to reveal the obtained results visually. B3LYP level [25] of DFT was utilized, along with the combined basis sets of 6–311 + +G (d,p) and LanL2DZ to conduct the aforementioned calculations. While the LanL2DZ basis set was used for the modeling of the Zn(II) ion [28], the 6–311 + +G(d,p) basis set was used for the modeling of the C, O, N, and H atoms [26]. The CPCM was utilized to account for the solvent effect in calculating of UV-Vis spectrum of Zn(II). The SWIZARD software [29] was utilized to identify the significant roles of molecular orbitals in electronic absorption bands observed in UV-Vis spectrum.

3. Results and discussion

3.1. Crystal and optimized structures of Zn(II) complex

Table 2 displays the selected theoretical and experimental bond lengths for the Zn(II) complex. The crystal structure and optimized molecular geometry of the Zn(II) complex are shown in Fig. 2a-b. Single crystal X-ray diffraction analysis shows that the Zn (II) complex crystallizes in a monoclinic Pn space group. The asymmetric unit comprises one Zn(II) central ion, one partially deprotonated 4-chloropyridine-2-carboxylic acid and one partially deprotonated 3-hydroxypyridine-2-carboxylic acid ligand. Both 4Clpca and 3OHpca ligands coordinated with the central Zn(II) ion by forming five-membered chelate rings. The Zn(II) ion is coordinated with two dentate ligands, 4Clpca and 3OHpca, through both pyridine N atoms and carboxylate O atoms, as described in the synthesis scheme. Fig. 2 shows that the coordination sphere of the distorted octahedral geometry of the Zn(II) complex is constructed by the coordination of two aqua ligands to the central metal ion. Fig. 2 also illustrates that 4Clpca, 3OHpca, and central Zn(II) ion were present in the equatorial plane, whereas two aqua ligands and Zn(II) ion were present in the axial plane. The equatorial plane bond lengths are determined experimentally and theoretically to be 2.084(13) Å and 2.0413 Å (Zn1-O1), 2.122(12) Å and 2.0269 Å (Zn1-O1'), 2.106(12) Å and 2.1292 Å (Zn1-N1), and 2.093(12) Å and 2.1310 Å (Zn1-N1'). Meanwhile, the axial plane bond distances are experimentally and theoretically found to be 2.123(13) Å and 2.3453 Å (Zn1-O3'), 2.181 (12) Å and 2.3403 Å (Zn1-O3). The experimental reports show that Zn–O and Zn–N bond distances range from 2.009(3)–2.193(3) Å and 2.038(4)–2.054(3) Å, respectively. In a similar Zn(II) complex, bond lengths for Zn-N and Zn-O were reported in the ranges of 2.2099 (16)–2.2643 (18) and 2.0286 (14)–2.1198 (16) Å, respectively. N1-Zn1-O1' (101.4(5)°), O1'-Zn1-O1 (91.1(5)°), O1-Zn1-N1' (92.8(5)°) and N1'-Zn1-N1 (178°).

Table 2
Experimental and theoretical bond lengths (Å) and angles (°) for the Zn(II) complex.

Bond Lengths	XRD	B3LYP	Bond Lengths	XRD	B3LYP
N1–Zn1	2.106(12)	2.1292	N1'–Zn1	2.093(13)	2.1310
O3'–Zn	2.123(13)	2.3453	Zn1–O3	2.181(13)	2.3403
Zn1–O1	2.084(13)	2.0413	O1'–Zn1	2.122(12)	2.0279
N1'–C5'	1.330(2)	1.3340	N1'–C2'	1.364(18)	1.3424
C6–N1	1.320(2)	1.3398	C2–N1	1.358(19)	1.3411
C6–C5	1.370(2)	1.3888	C2'–C1'	1.500(2)	1.5171
C6–H6	0.9300	1.0844	C4'–C3'	1.390(3)	1.3854
C5–C4	1.380(3)	1.3939	C4'–H4'	0.9300	1.0833
C5–H5	0.9300	1.0815	C3'– C2'	1.380(2)	1.4032
C4–C2	1.430(3)	1.3893	C3'–O4	1.340(2)	1.3329
C4–Cl1	1.770(2)	1.7467	C3'–H3'	0.930	1.0836
C3–C2	1.390(2)	1.3915	C1–O2	1.267(18)	2.2170
C3–H3	0.9300	1.0812	C1–O1	1.260(2)	1.2909
C2–C1	1.490(2)	1.5396	O1'–C1'	1.240(2)	1.2742
C5'–C4'	1.370(3)	1.3962	C5'–H5'	0.9300	1.0836
C2'–C3'	1.390(2)	1.4095	O2'–C1'	1.276(19)	1.2440
O3'–H3'A	0.8501	0.9659	O3'–H3'B	0.8500	0.9632
O3'–H3'B	0.8501	0.9654	O3–H3A	0.8498	0.9632
O4–O4H	0.8200	1.0026			
Bond Angles	**XRD**	**B3LYP**	**Bond Angles**	**XRD**	**B3LYP**
N1–Zn1–N1'	178.7 (6)	175.95	N1'–Zn1–O1	101.4 (5)	103.97
N1–Zn1–O3	88.0 (5)	89.404	N1'–Zn1–O1'	79.7 (5)	80.909
N1–Zn1–O3'	92.1 (5)	93.973	N1'–Zn1–O3	92.8 (5)	90.587
N1–Zn1–O1	79.6 (5)	80.030	N1'–Zn1–O3'	87.1 (5)	87.200
N1–Zn1–O1'	99.2 (5)	95.101			

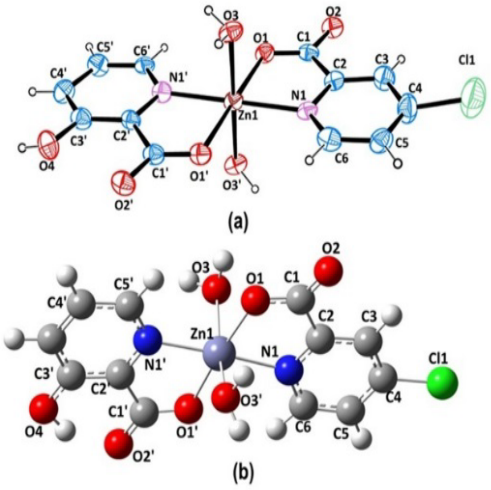

Fig. 2. a) The crystal structure and b) the optimized molecular geometry (obtained by B3LYP/6–311 ++G(d,p)-LanL2DZ) for Zn(II) complex.

When examining the bond angles presented, it is apparent that the Zn atom and 2-picolinic acid complex in our structures are in an octahedral configuration [30]. According to the experimental XRD data, the C-N and C-C bond lengths in the pyridine ring were found to be between 1.320 (3) – 1.364 (3) Å and 1.370 (4) – 1.500 (4) Å, respectively. Technical terms are defined when first mentioned. Theoretically, bond lengths of 1.3398–1.3411 Å and 1.3854–1.5396 Å have been calculated. The N1-C2 bond is shorter compared to other N-C bond lengths due to the presence of the C1 atom in the same ring as the electronegative atom Cl. Similarly, the N1 and N2 atoms are in the equatorial plane with the Zn atom, as evidenced by the bonds and bond angles between N1-Zn1 and N1'-Zn1. The Zn-N1 bond angle and length are shorter than Zn-N1' due to the electronegativity of the Cl atom. Upon comparing our results with the existing literature, it becomes apparent that our findings are consistent with the literature [31].

3.2. Hirshfeld surface exploration

Non-covalent interactions play a pivotal role in the field of crystal engineering as they determine the arrangement of crystalline units. To explore and study these interactions, we performed Hirshfeld surface (HS) analysis utilizing Crystal Explorer 17.5 software [32]. Hirshfeld Surface (HS) exploration is an important way used to evaluate the atomic and molecular interactions in the single crystals. Hirshfeld surface, constructed on the normalized distance (d_{norm}), is utilized in order to provide a visual representation of the intermolecular interactions by color coding [33]. When comparing hydrogen bond interactions to van der Waals radii, shorter bonds are depicted by a red cloud, those of similar length by a white cloud, and longer bonds by a blue cloud. Fig. 3 visually demonstrates both shorter and longer contacts for the Zn(II) complex. The red cloud found on the HS near one of the H-atom of aqua ligand and O-atom of carboxyl group demonstrate that these atoms are involve in H-bonding interactions as can be seen in Fig. 3. The non-coordinated O atom of carboxylate group, Cl atom and some of the H-atom of pyridine ring are also engaged in H-bonding interactions. The three-dimensional HS [34] of the Zn(II) complex mapped over the d_{norm} has the spanning range of −0.6406 to 1.5578 au. Additionally, the HS map reveals light red dots, indicative of relatively weak C—H…O

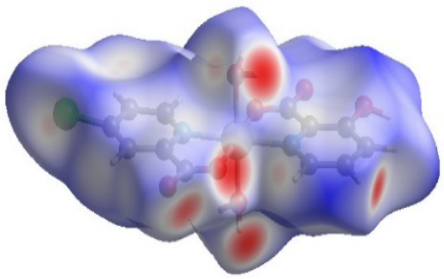

Fig. 3. Hirshfeld surface (HS) plotted over d_{norm} for Zn(II) complex in the range of −0.6406–1.5578 a.u.

interactions within the crystalline arrangement of Zn(II) crystals.

To comprehensively analyze the non-covalent interactions that underpin the stabilization of the crystal packing within the Zn(II) complex, a two-dimensional fingerprint depiction is employed as can be seen in Fig. 4. Fig. 4 vividly illustrates key interactions, including H…H, O…H/H…O, C…H/H…C, O…C/C…O, and C…C, and demonstrates their interplay across the surfaces. The strength of each interatomic contact is quantitatively calculated by aggregating decoupled mutual interactions. Notably, interatomic contacts involving H-H and O-H are the predominant contributors to the crystal packing, with corresponding contribution percentages of 26.6% and 33.6%, respectively. Other important contact points, O-C, H-Cl, C-Cl, C-C, C-O, O-Cl, O-N interactions, were found to be 10.5% −10.4–5% - 4.1–3.5% −3.5% and 2.8%, respectively.

3.3. Thermal analysis

We assessed the change in sample weight as a function of temperature under controlled gas atmosphere and temperature for the Zn(II) complex through TG–DTA analysis using the NETZSCH STA 449 F1 analyzer. The TG and DTA curves for Zn(II) complex are presented in Fig. 5. The thermally decomposition process of Zn(II) complex is mainly consisted of two stages. The first stage occurring at the region of 110–140 °C corresponds to the removing of coordinated H_2O ligands. The process is resulted by the weight loss of 9.16%. The weight loss for the same process was calculated as 9.08%. The solid skeleton structure remains thermally stable up to 216 °C. When continued heating, the second decomposition process occurs between 216–762 °C. In this process, the weight loss is observed as 69.84%, and calculated as 70.36%. The final solid product with the weight of 21% (experimental) and 20.55% (calculated) is likely to ZnO when the temperature is higher than 762 °C.

3.4. Vibrational spectrum

The experimental FT-IR spectrum for the Zn(II) complex was recorded at the range of 4000–400 cm^{-1}. DFT/B3LYP level in conjunction with the combined 6–311 + +G(d,p)/LanL2DZ basis set was operated to provide a deep explanation of the vibrational modes. DFT methods calculate wavenumbers slightly larger than their corresponding experimental values due to the anharmonicity, electron correlation and basis set deficiency. Therefore, the wavenumbers obtained by B3LYP/6–311 + +G(d.p)/LanL2DZ were multiplied by the scale factor of 0.96 and brought closer to the experimental data. In order to make a detailed comparison, the experimental FT-IR spectra of 4Clpca and 3OHpca ligands were also recorded and presented in Fig. 6 as compared with that of Zn(II) complex.

Previous studies for similar crystals have shown that the IR bands observed at 3239–3188 cm^{-1} are due to the OH stretching vibrations of the H_2O ligand and the IR bands observed at 3092–3082 cm^{-1} are due to the CH stretching vibrations [19]. In this study, the OH vibrational band was observed at 3287 cm^{-1} and calculated at 3743 cm^{-1}. The CH vibration band was observed at 3097 cm^{-1} and calculated at 3095 cm^{-1}.

Information about both the coordination environment of metal ions and their electronic structures has been evaluated by using the infrared spectrum of Zn(II) complex. The frequency range between the symmetric and asymmetric stretching vibrations of the carboxyl group provides a powerful information about the coordination of the carboxyl group to the metal ion, while the intensity of these vibration peaks indicates high charge mobility and polarizability within the synthesized crystal [17,21,35–40]. Symmetric and asymmetric carboxylate group (COO^-) vibrations were detected at 1678–1273 cm^{-1}, 1734–1305 cm^{-1} and 1659–1300 cm^{-1} for 3OHpca, 4Clpca and Zn(II) complex, respectively. The same band for Zn(II) complex was also calculated at 1662–1289 cm^{-1} using the B3LYP level. As can be seen from these results, the difference between asymmetric and symmetric COOH vibrations is 405 cm^{-1} for the 3OHpca ligand and 429 cm^{-1} for the 4Clpca ligand. As for the difference between asymmetric and symmetric COO^- stretching vibration, 359 cm^{-1} was experimentally measured and 373 cm^{-1} theoretically calculated. The decrease in the difference between COOH asymmetric and symmetric vibrational bands indicates that our metal-ligand complex coordinates to Zn metal as a monodentate ligand via O atom.

The ring breathing band, which is approximately reported around 1000 cm^{-1} in the free pyridine ring [31], is observed to shift to 1054 cm^{-1} upon coordination of the pyridine ring to the Zn(II) ion [22]. In the FT-IR spectrum obtained for the Zn(II) complex, the CC stretching vibrations are observed in the range of 1585–1080 cm^{-1}, and calculated at the range of 1567–1082 cm^{-1}. The in-plane C-H bending vibrations are detected in the range of 1451–1032 cm^{-1}. The out of plane bending vibrations of the C-H bonds are found in the range of 964–541 cm^{-1}, as consistent with the similar structures [41–44].

The experimental FT-IR spectrum closely aligns with the theoretical IR spectrum when comparing the complex formed with ligands. Any minor disparities between the experimental and theoretical data can be attributed to the fact that experimental measurements are conducted on a solid-state material, characterized by strong intermolecular interactions, while theoretical calculations are performed on isolated gas phase molecules.Table 3.

3.5. UV-Vis spectrum and FMO energies

The experimental UV-Vis spectrum was recorded in ethanol solvent within the range of 900–200 nm for the synthesized Zn (II) complex. However, since no band has been observed at high wavelengths, it has been given within the range of 200–400 nm. Furthermore, theoretical UV-Vis spectrum was calculated using the TD-B3LYP/CPCM method in ethanol solvent on the basis of optimized molecular structure. The obtained experimental and calculated electronic absorption spectrum were presented in Fig. 7.

High energy $\pi \rightarrow \pi^*$ and $n \rightarrow \pi^*$ transitions were observed at 225 and 291 nm for 3OHpca. The same absorption bands were observed for 4Clpca at 228 and 266 nm. When these ligands were coordinated to Zn (II) ion, the inter- and intra-ligand $\pi \rightarrow \pi^*$ and $n \rightarrow \pi^*$ transitions shifted to 201, 225, 265, 273 and 299 nm. Ligand metal charge transfer interactions are also responsible for the weak band observed at 341 nm. The corresponding electronic absorption bands in the theoretical UV-Vis spectrum were calculated at the range of 201 and 285 nm. Swizard program [45] was used to understand which molecular orbitals plays important roles in UV-Vis spectrum.

HOMO-9→LUMO+ 1 (38%), HOMO→LUMO+ 5 (19%), HOMO-→LUMO+ 3 (18%), HOMO-9→LUMO (5%) electronic transitions are the source of the calculated electronic absorption band at 201 nm. HOMO-7→LUMO (32%), HOMO→LUMO+ 3 (18%), HOMO-6→LUMO+ 1 (9%), HOMO-5→LUMO+ 1 (6%), HOMO-9->LUMO+ 1 (6%), HOMO-5→LUMO (6%) electronic transitions are the source of the calculated electronic absorption band at 225 nm. HOMO-4→LUMO

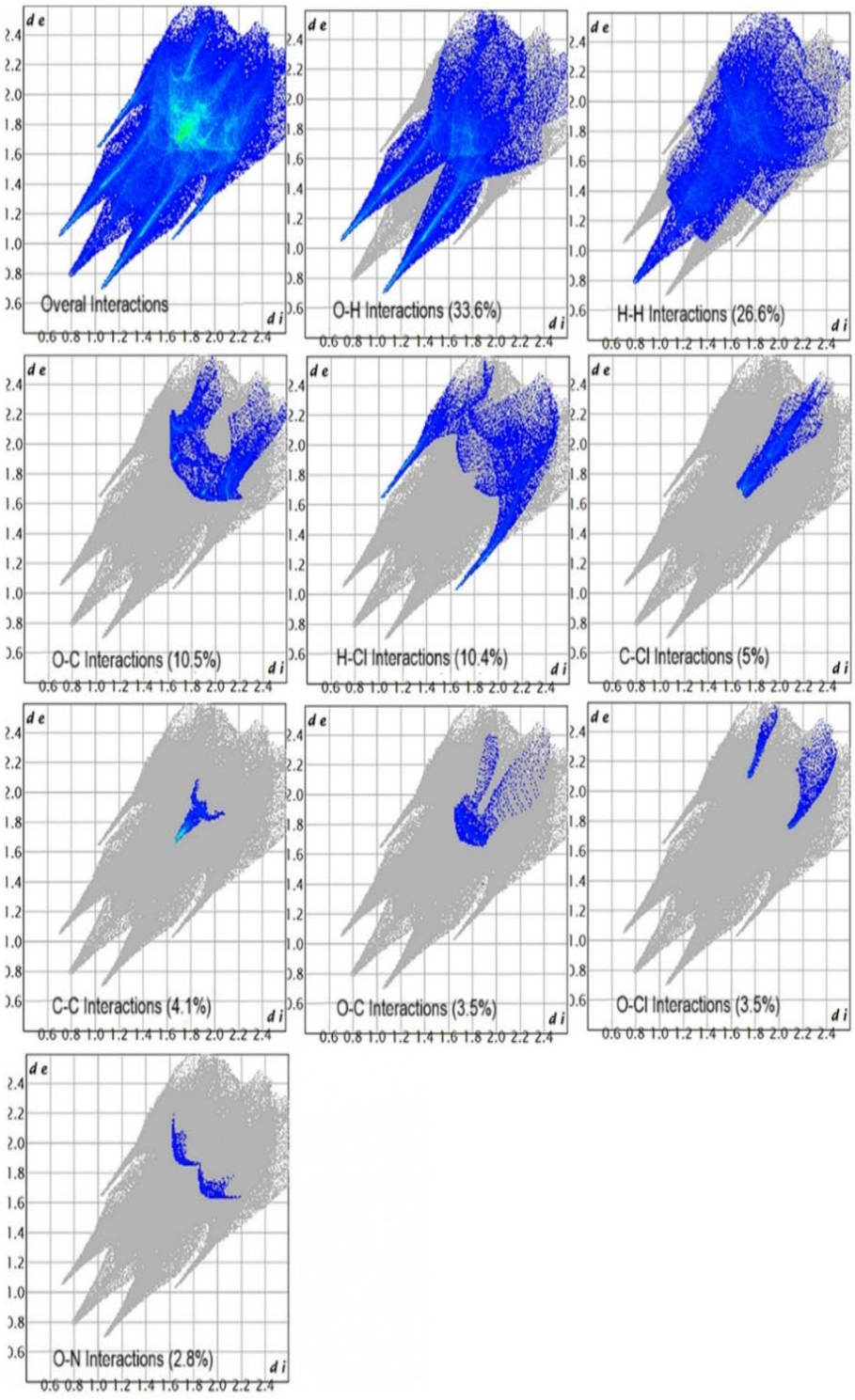

Fig. 4. . 2D fingerprint graphs of Zn(II) complex for dominant individual interactions.

(34%), HOMO-2→LUMO (30%) and HOMO-2→LUMO+ 1 (11%) electronic transitions are the source of the calculated electronic absorption band at 263 nm. The source of the electronic absorption band calculated at 276 nm is HOMO→LUMO+ 1 (60%), HOMO→LUMO (39%), while the source of the electronic absorption band calculated at 299 nm is HOMO→LUMO (58%), HOMO→LUMO+ 1 (36%).

Since the Zn(II) atom is a colorless material, the theoretical calculation of the complex does not give a peak in the visible region, while the experimental calculation shows an absorption band at 341 nm as a result of small charge transitions due to Van der Waals interaction. As can be clearly seen from all these results and Fig. 8, there is a charge transfer from 3OHpca to 4Clpca in Zn(II) complex. Singlet-singlet spin transitions for the $[Zn(3OHpca)(4Clpca)(H_2O)_2]$ complex were calculated in ethanol solvent. In these calculations, the solvent effect (ethanol) was taken into account using the PCM model and is given in Table 4.

Frontier molecular orbitals play a pivotal role in shaping the optical

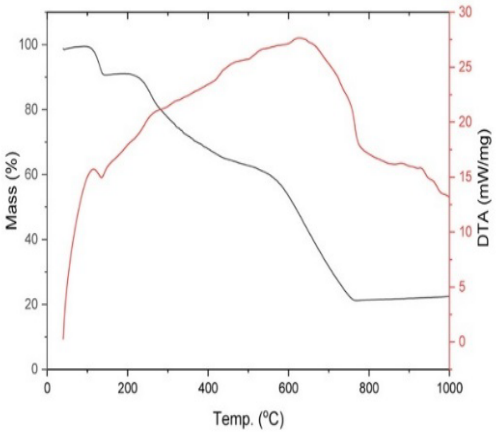

Fig. 5. TG-DTA curves for Zn(II) complex.

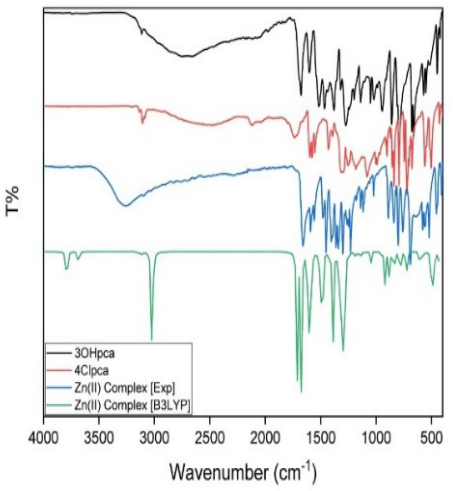

Fig. 6. Experimental and theoretical IR spectrum for 3OHpca, 4Clpca and Zn (II) complex.

Table 3
Selected experimental and theoretical vibrational wavenumber (cm^{-1}) for Zn(II) complex.

Assignments and PED Analysis	EXP. (cm^{-1})	B3LYP (cm^{-1})
ν O-H (97%)	3287	3743
ν C H (100%)	3097	3095
ν O═C (78%)	1659	1662
ν C═C (73%)	1585	1567
β HCC (55%)	1451	1480
ν O-C (73%)	1300	1289
ν N-C (30%)	1229	1233
ν C C (99%)	1080	1082
γ OCOC (59%)	808	812
τ HCCC (21%)+ τ CCCN (13%)	698	707
γ ClCCC (36%)	535	541

and electrical properties of materials, as well as in UV-Vis spectroscopy. The energy difference between the Highest Occupied Molecular Orbital (HOMO) and Lowest Unoccupied Molecular Orbital (LUMO) serves as a key criterion for characterizing factors like chemical reactivity, kinetic stability, and biological activity of materials. Systems with a narrow HOMO-LUMO energy gap, often referred to as 'soft molecules,' are renowned for their heightened chemical reactivity and reduced kinetic stability. The parameter of chemical hardness (η) illustrates the ability of chemical systems to resist changes in their electronic distributions. The

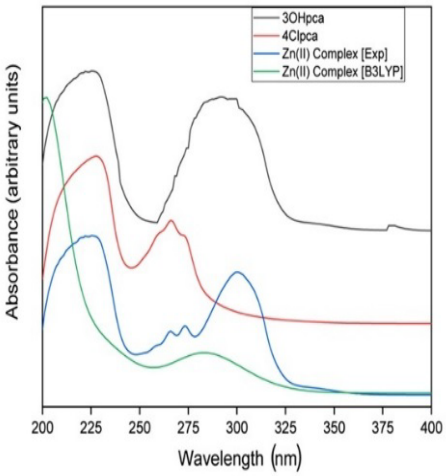

Fig. 7. Experimental UV-Vis spectrum of 3OHpca, 4Clpca, Zn(II) complexes and theoretical UV-Vis spectrum of Zn(II) complex.

parameters χ and η are indicators of chemical reactivity and system stability. The chemical potential (φ) characterizes the tendency for electron release from a system in equilibrium and is associated with the rearrangement of electronic charge during chemical processes. As seen from Table 5, the χ parameter exhibits the opposite behavior to η, whereby χ determines which of the molecular systems is more electronegative when compared with each other.

The frontier molecular orbital energies of the Zn(II) complex with an octahedral coordination geometry were computed at the B3LYP/6–311 + +G(d,p)/LanL2DZ level of theory. This was performed while accounting for a restricted closed-shell electron configuration. The HOMO and LUMO energies of the Zn(II) complex were determined to be −6.5678 eV and −2.4275 eV respectively. The values of η, χ, and S may be ascertained by utilizing the energies of the frontier molecular orbitals (HOMO and LUMO) [33]. As can be seen in Table 5, the HOMO–LUMO energy gap for the ligands and the Zn(II) complex was calculated as 4.8595, 4.9999, and 4.7358 eV, respectively. The energy gap between HOMO and LUMO is observed to be in decreasing order as 4Clpca> 3OHpca > Zn(II) complex for the ligands and complex, which shows the resistance to the change of electronic configuration, and since soft molecules are more polarized than hard molecules, the Zn(II) complex could be easily polarized [35,46]. The literature provides values of 4.1003 eV and 0.4078 eV^{-1} for the parameters χ and S of the Zn(II) complex, respectively [33]. In this study, the χ, η and W parameters were found to be 4.6617 eV, 2.3679 eV and 4.5890 eV for Zn(II) complex, respectively. The S parameter is also calculated as 0.2112 eV^{-1} for Zn((II) complex.

3.6. Molecular electrostatic potential (MEP)

The MEP surface for the Zn(II) complex was generated using the B3LYP/6–311 + +G(d,p)/LanL2DZ level. Fig. 9 shows the MEP surfaces, indicating the positive and negative potential regions over the Zn (II) complex. The electrostatic potential is calculated at the range of −7.087 – 7.087 e^{-2} a.u. for Zn(II) complex. The negative potential represented by red color is mainly found over the non-coordinated oxygen-atom of carboxylate group and slightly negative potential is also found around the oxygen-atom of hydroxyl group. When it comes to positive electrostatic potential represented by dark blue color, it is mainly detected around the hydrogen-atom of aqua ligands, slightly positive electrostatic potential is also found around the hydrogen-atoms of pyridine rings. Lastly, approximately zero potential illustrated by green color is calculated over the chlorine-atom. Thus, it can be inferred that in the event of the Zn(II) complex participating in any reaction, the

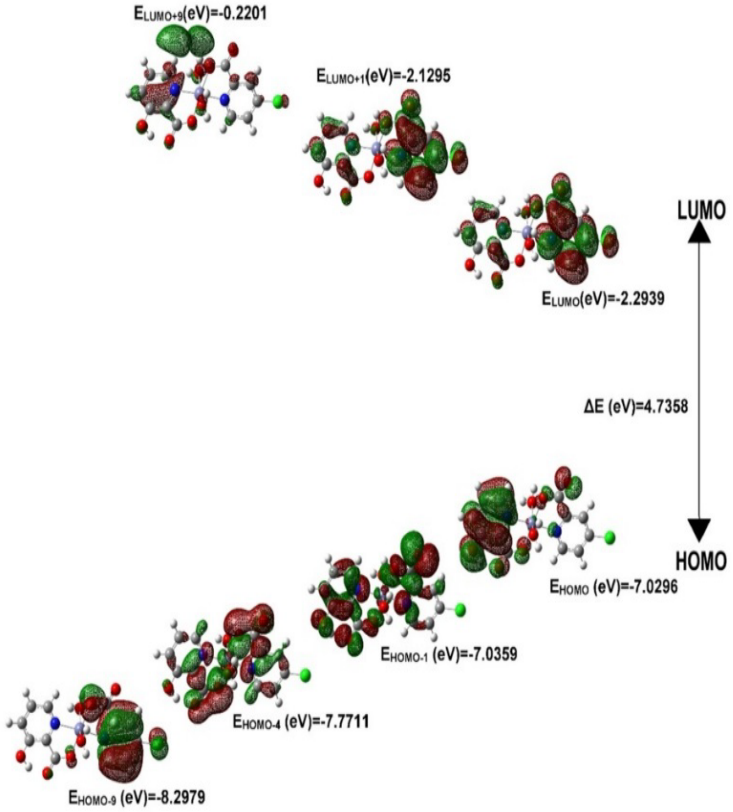

Fig. 8. Frontier molecule orbitals and their energies for the Zn(II) complex.

Table 4
Experimental and theoretical wavelengths, oscillator intensities and selected important contributions for the Zn(II) complex.

Exp. λ (nm)	B3LYP λ (nm)	Oscillator str.	Important contr.
202	201	0.3885	H-9→L+ 1(38%), H→L+ 5(19%), H→L+ 3(18%)
225	224	0.0360	H-7→L(32%), H→L+ 3(18%), H-6→L+ 1(9)
265	263	0.0001	H-4→L(34%), H-2→L(+30%), H-2→L+ 1(11%)
273	276	0.0200	H→L+ 1(60%), H→L(39%)
299	285	0.1672	H→L(58%), H→L+ 1(36%)
341	-	-	-

Table 5
The chemical hardness (η), electronegativity (χ), electrophilicity index (W), chemical softness (S) and FMO energies for Zn(II) obtained by B3LYP/LanL2DZ levels.

Parameter	3OHpcA	4Clpca	Zn (II) Complex
E_{HOMO} (eV)	-7.2456	-7.5517	-7.0296
E_{LUMO} (eV)	-2.3861	-2.5518	-2.2939
ΔE (eV)	4.8595	4.9999	4.7358
χ (eV)	4.8158	5.0518	4.6617
η (eV)	2.4297	2.4999	2.3679
W(eV)	4.7726	5.1041	4.5890
$S(eV^{-1})$	0.2058	0.2000	0.2112

carboxylate group oxygen atoms and H_2O ligand hydrogen atoms are the most reactive regions which are prone to participate in interactions such as intermolecular hydrogen bonding. It is likely that new covalent bonds or hydrogen bonding interactions could be formed through these atoms.

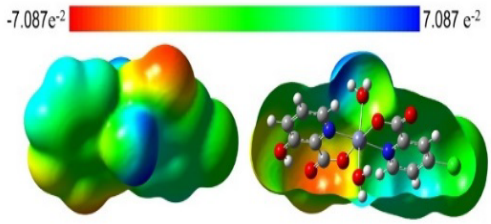

Fig. 9. MEP surface for Zn(II) complex.

3.7. Nonlinear optical properties (NLO)

It is well known that one of the frequently used methods to obtain NLO materials with desired properties is to combine the advantages of organic and inorganic structures. Changing the central metal ion, ligand, oxidation level or coordination geometry is effectively used to improve the NLO properties of metal organic hybrid materials [19]. To obtain materials with the desired NLO properties, these variables can be partially or fully modified simultaneously. It is known that substitution of opposite sides of metal-organic coordination complexes with groups and/or atoms having different characteristics in terms of electronegativity affinity improves the NLO properties of the material. The presence of the OH group on one side of the Zn(II) complex and the Cl atom on the other side increases the ground state charge asymmetry and therefore improves the NLO properties. Especially, Zn(II) complexes also attract attention in terms of third-order nonlinear optical properties due to the their closed d^{10} shell and therefore with a high transparency in the UV region.

In order to investigate the NLO properties of the Zn(II) complex, the linear optical parameters (α and Δα), the first and second order hyperpolarizability parameters (β and γ), known as nonlinear optical param-

eters, are calculated using the B3LYP level and the 6–311 + +G(d,p)/LanL2DZ basis set in the gas phase using Eqs. 1–5 [47–51].

$$\alpha = \frac{(\alpha_{xx} + \alpha_{yy} + \alpha_{zz})}{3} \quad (1)$$

$$\Delta\alpha = \left\{ \frac{1}{2} \left[(\alpha_{xx} - \alpha_{yy})^2 + (\alpha_{yy} - \alpha_{zz})^2 + (\alpha_{zz} - \alpha_{xx})^2 \right] \right\}^{1/2} \quad (2)$$

$$\beta_a = Sum(\beta_{ajj} + \beta_{jaj} + \beta_{jja}) \quad (3)$$

$$\beta = \left[(\beta_x)^2 + (\beta_y)^2 + (\beta_z)^2 \right]^{1/2} \quad (4)$$

$$\gamma = \frac{1}{5} \left[\gamma_{xxx} + \gamma_{yyy} + \gamma_{zzz} + 2(\beta_{xyy} + \beta_{xzz} + \beta_{yyzz})^2 \right] \quad (5)$$

Table 6 shows that the calculated total dipole moment values for Zn (II) complex and the ligands are 8.69312, 1.80735 and 1.009116 Debye, respectively. According to calculations at the B3LYP/6–311 + +G(d,p)/LanL2DZ level, the value of the static first-order hyperpolarization parameter β (0;0,0) is 15382×10^{-34}, 36131×10^{-34} and 4.5200×10^{-34} esu, respectively. The static second-order hyperpolarization γ(0;0,0,0) for the Zn(II) complex and ligands was calculated as 3.1169×10^{-36}, 4.1968×10^{-36} and 39.106×10^{-36} esu, respectively. As can be seen from these results, while the static first-order hyperpolarization parameter is lower, the static second-order hyperpolarization parameter value increases for the Zn(II) complex.

The frequency-dependent nonlinear optical studies includes the investigation of electro-optical Pockels effect β(-ω;ω,0) and electric field induced second harmonic generation (EFSHG) β(−2ω;ω,ω). When it comes to the dynamic second hyperpolarizability studies, the calculation of thedc-Kerr effect γ(-ω;ω,0,0) and EFSHG γ(−2ω;ω,ω,0) are performed. The β(-ω;ω,0) and β(−2ω;ω.ω) are obtained as 1.6044×10^{-34} and 49.720×10^{-34} esu, respectively. These results indicate that the static and dynamic first-order hyperpolarizability parameters of the Zn (II) complex are quite low. The dc-Kerr effect γ(-ω;ω,0,0) and EFSHG γ(−2ω;ω,ω,0) for Zn(II) complex were also calculated as 13.04×10^{-36} and 2258.9×10^{-36} esu, respectively. According to Table 6, the second-order NLO properties of the Zn(II) complex are obtained lower than those reported in the literature for similar structures, while the third-order NLO properties are significantly noteworthy [19,30].

4. Conclusion

The newly synthesized Zn(II) complex including 4Clpca and 3OHpca ligands was reported for the first time. The coordination sphere of central Zn(II) ion is observed as a distorted octahedron. By evaluating the FT-IR spectra of 4Clpca, 3OHpca and Zn(II) complex together, the crystal structure results of the Zn(II) complex were further supported. In the recorded UV-Vis spectrum of Zn(II) complex, the absorption bands observed at 225, 265, 273 and 299 nm were assigned as high energy n→π * and π→π * , while the band observed at 341 nm was assigned as LMCT interaction. Zn(II) complex does not exhibit*d*–*d*electronic transitions since this type of transitions are both spin and orbital forbidden in Zn(II) ion. HOMO and LUMO illustrations also demonstrated that the electronic transitions from HOMO to LUMO are originated from the charge movement from 3OHpca to 4Clpca, as would be expected. Considering the nonlinear optical (NLO) properties of the synthesized Zn (II) complex, the first-order hyperpolarizability parameters were determined to be quite weak in both static and frequency-dependent methods. However, the dc-Kerr effect γ(-ω;ω,0,0) and EFSHG γ(−2ω;ω,ω,0) parameters calculated as 13.04×10^{-36} esu and 2258.9×10^{-36} esu demonstrated that Zn(II) complex is a highly promising material for third order NLO application.

Table 6
The μ (Debye), α, ($\times 10^{-23}$ esu), Δα ($\times 10^{-23}$ esu), β ($\times 10^{-34}$ esu), and γ ($\times 10^{-36}$ esu) for 3OHpca, 4Clpca and Zn(II) complex.

Parameter	3OHpca	4Clpca	Zn (II) complex
μ	8.69312	1.80735	1.009116
α(0;0)	6.7181	6.7276	2.9300
Δα(0;0)	11.201	10.799	4.4836
α (-ω;ω)	7.0589	7.0667	3.8407
Δα(-ω;ω)	11.847	11,429	2.9544
β(0;0,0)	15,382	36,131	4.5200
β(-ω;ω,0)	34,229	59,872	1.6044
β(−2ω;ω,ω)	737.290	384.62	49.720
γ(0;0.0,0)	3.1169	4.1968	39.106
γ(-ω;ω,0,0)	6.0701	10.9505	13.04
γ(−2ω;ω,ω,0)	380.90	460.12	2258.9

Funding

This work was supported by the Scientific Research Projects Unit of Sakarya University (Project Number: 2023-19-44-48).

CRediT authorship contribution statement

Avcı Davut: Formal analysis, Investigation, Software, Supervision, Writing – review & editing. **Dege Necmi:** Data curation, Formal analysis, Investigation. **Tamer Ömer:** Conceptualization, Methodology, Software, Visualization, Writing – review & editing. **Şimşek Merve:** Formal analysis, Investigation, Visualization, Writing – original draft. **Atalay Yusuf:** Software, Supervision, Writing – review & editing. **Mahmoody Hayatullah:** Investigation, Software, Visualization.

Declaration of Competing Interest

The authors declare that they have no known competing financial interests or personal relationships that could have appeared to influence the work reported in this paper.

Data availability

Data will be made available on request.

References

[1] D.R. Kanis, M.A. Ratner, T.J. Marks, Design and construction of molecular assemblies with large second-order optical nonlinearities. Quantum chemical aspects, Chem. Rev. 94 (1994) 195–242, https://doi.org/10.1021/cr00025a007.
[2] F. Meyers, S.R. Marder, B.M. Pierce, J.L. Brédas, J. Am. Chem. Soc. 116 (1994) 10703.
[3] M. Nakano, H. Fukui, T. Minami, K. Yoneda, Y. Shigeta, R. Kishi, B. Champagne, E. Botek, T. Kubo, K. Ohta, K. Kamada, (Hyper)polarizability Density Analysis for Open-Shell Molecular Systems Based on Natural Orbitals and Occupation Numbers, Theor. Chem. Acc. (2011).
[4] B. Kirtman, B. Champagne, D.M. Bishop, Electric field simulation of substituents in donor-acceptor polyenes: a comparison with ab initio predictions for dipole moments, polarizabilities, and hyperpolarizabilities, J. Am. Chem. Soc. 122 (2000) 8007.
[5] S. Di Bella, Second-order nonlinear optical properties of transition metal complexes, Chem. Soc. Rev. 30 (2001) 355–366, https://doi.org/10.1039/b100820j.
[6] V. Guerchais, H. Le Bozec, in: H. Bozec, V. Guerchais (Eds.), Metal Complexes Featuring Photochromic Ligands BT - Molecular Organometallic Materials for Optics, Springer Berlin Heidelberg, Berlin, Heidelberg, 2010, pp. 171–225, https://doi.org/10.1007/978 3 642 01866 4 6.
[7] B.J. Coe, Switchable nonlinear optical metallochromophores with pyridinium electron acceptor groups, Acc. Chem. Res. 39 (2006) 383–393, https://doi.org/10.1021/ar050225k.
[8] O.R. Evans, W. Lin, Crystal engineering of NLO materials based on metal–organic coordination networks, Acc. Chem. Res. 35 (2002) 511–522, https://doi.org/10.1021/ar0001012.
[9] S. Muhammad, H.-L. Xu, R.-L. Zhong, Z.-M. Su, A.G. Al-Sehemi, A. Irfan, Quantum chemical design of nonlinear optical materials by sp2 hybridized carbon nanomaterials: issues and opportunities, J. Mater. Chem. C 1 (2013) 5439–5449, https://doi.org/10.1039/C3TC31183J.

[10] F.Q. Jiang, Mh, Organic and semiorganic nonlinear optical materials, Adv. Mater. 11 (1999) 51.
[11] C. Chen, Y. Wang, B. Wu, K. Wu, W. Zeng, L. Yu, Design and synthesis of an ultraviolet-transparent nonlinear optical crystal Sr2Be2B2O7, Nature 373 (1995) 322–324, https://doi.org/10.1038/373322a0.
[12] Z. Xiao, Y. Shi, R. Sun, J. Ge, Z. Li, Y. Fang, X. Wu, J. Yang, M. Zhao, Y. Song, Ultrafast broadband optical limiting in simple pyrene-based molecules with high transmittance from visible to infrared regions, J. Mater. Chem. C 4 (2016) 4647–4653, https://doi.org/10.1039/C5TC04047G.
[13] I. Pintre, J. Serrano, B. Ros, J. Martínez-Perdiguero, I. Alonso Villanueva, J. Ortega, C. Folcia, J. Etxebarria, R. Alicante, B. Villacampa, Bent core liquid crystals in a route to efficient organic nonlinear optical materials, J. Mater. Chem. 20 (2010) 2965, https://doi.org/10.1039/B923616C.
[14] H. Motiei, A. Jafari, R. Naderali, Third-order nonlinear optical properties of organic azo dyes by using strength of nonlinearity parameter and Z-scan technique, Opt. Laser Technol. 88 (2017) 68–74, https://doi.org/10.1016/j.optlastec.2016.09.011.
[15] L.B. Innocenzi P, Organic–inorganic hybrid materials for non linear optics. J. Mater. Chem. 15 (2005) 31.
[16] Ö. Tamer, H. Mahmoody, K. Feyzioğlu, O. Kılınç, D. Avci, O. Orun, N. Dege, Y. Atalay, Synthesis of the first mixed ligand Mn (II) and Cd (II) complexes of 4 methoxy-pyridine-2-carboxylic acid, molecular docking studies and investigation of their anti-tumor effects in vitro: first mixed ligand complexes of 4-methoxy-pyridine-2-carboxylic ac, Appl. Organomet. Chem. 34 (2019) e5416, https://doi.org/10.1002/aoc.5416.
[17] Ö. Tamer, A unique manganese (II) complex of 4-methoxy-pyridine-2-carboxylate: synthesis, crystal structure, FT-IR and UV–Vis spectra and DFT calculations, J. Mol. Struct. 1144 (2017) 370–378, https://doi.org/10.1016/j.molstruc.2017.05.077.
[18] H. Vural, M. Orbay, Synthesis, crystal structure, spectroscopic investigations and DFT calculations of the copper(II) complex of 4-(Trifluoromethyl)pyridine-2-carboxylic acid, J. Mol. Struct. 1146 (2017), https://doi.org/10.1016/j.molstruc.2017.06.056.
[19] N. Dege, Ö. Tamer, M. Şimşek, D. Avcı, M. Yaman, A. Başoğlu, Y. Atalay, Experimental and theoretical approaches on structural, spectroscopic (FT-IR and UV-Vis), nonlinear optical, and molecular docking analyses for Zn (II) and Cu (II) complexes of 6-chloropyridine-2-carboxylic acid, Appl. Organomet. Chem. 36 (2022) e6678.
[20] J. Sun, G. Wang, C. Liu, Y. Shi, M. Zhao, Synthesis of four pyrene-containing chalcone derivatives: achieving excellent third-order nonlinear optical properties by optimizing halopyridines, Opt. Laser Technol. 109 (2019) 600–607, https://doi.org/10.1016/j.optlastec.2018.08.038.
[21] D. Avcı, S. Altürk, F. Sönmez, Ö. Tamer, A. Başoğlu, Y. Atalay, B.Z. Kurt, N. Dege, Three novel Cu(II), Cd(II) and Cr(III) complexes of 6−Methylpyridine−2−carboxylic acid with thiocyanate: synthesis, crystal structures, DFT calculations, molecular docking and α-Glucosidase inhibition studies, Tetrahedron 74 (2018) 7198–7208, https://doi.org/10.1016/j.tet.2018.10.054.
[22] D. Avci, Y. Saeedi, A. Başoğlu, N. Dege, S. Altürk, Ö. Tamer, Y. Atalay, Novel Mn(II) and Zn(II) complexes of 6-bromopicolinic acid as a potential optical material: synthesis, spectral characterizations, linear, and nonlinear optical properties and density functional theory calculations, Appl. Organomet. Chem. 35 (2020), https://doi.org/10.1002/aoc.6125.
[23] C. Stoe. Stoe&Cie. Darmstadt., C. Stoe. Stoe&Cie. Darmstadt. Germany. 2002., (2002).
[24] Gaussian, B. Revision, M.J. Frisch, G.W. Trucks, H.B. Schlegel, P.M.W. Gill, B. G. Johnson, M.A. Robb, J.R. Cheeseman, T. Keith, G.A. Petersson, J. A. Montgomery, K. Rhagavachari, M.A. Al-Laham, V.G. Zakrzewski, J.V. Ortiz, J. B. Foresman, J. Cioslowski, B.B. Stefanov, A. Nanayakkara, M. Challacombe, C. Y. Peng, P.Y. Ayala, W. Chen, M.W. Wong, J.L. Andres, E.S. Replogle, R. Gomperts, R.L. Martin, D.J. Fox, J.S. Binkley, D.J. Defrees, J. Baker, J.P. Stewart, M. Head-Gordon, C. Gonzalez, J.A. Pople, Gaussian (1995).
[25] C. Lee, W. Yang, R.G. Parr, Development of the Colle-Salvetti correlation-energy formula into a functional of the electron density, Phys. Rev. B Condens. Matter 37 (1988) 785–789, https://doi.org/10.1103/physrevb.37.785.
[26] W.J. Hehre, R. Ditchfield, J.A. Pople, Self—consistent molecular orbital methods. XII. Further Extensions of gaussian—type basis sets for use in molecular orbital studies of organic molecules, J. Chem. Phys. 56 (2003) 2257–2261, https://doi.org/10.1063/1.1677527.
[27] P.J. Hay, W.R. Wadt, Ab initio effective core potentials for molecular calculations. Potentials for K to Au including the outermost core orbitals, J. Chem. Phys. 82 (1985) 299–310, https://doi.org/10.1063/1.448975.
[28] P.J. Hay, W.R. Wadt, Ab initio effective core potentials for molecular calculations. Potentials for the transition metal atoms Sc to Hg, J. Chem. Phys. 82 (1985) 270–283, https://doi.org/10.1063/1.448799.
[29] S..Gorelsky, SWizard program, universty, Canada/ottowa, 2010.
[30] M.X. Li, B. Wang, J. Song, H. Wu, H. Chen, X, ynthesis, crystal structure, and BSA interaction with a new Co (II) complex based on 5-(trifluoromethyl) pyridine-2-carboxylic acid. J. Coord. Chem. 72 (2019) 73.
[31] N. Dege, Experimental and theoretical approaches on structural, spectroscopic (FT-IR and UV-Vis), nonlinear optical, and molecular docking analyses for Zn (II) and Cu (II) complexes of 6-chloropyridine-2-carboxylic acid, (2022) 1–16. (https://doi.org/10.1002/aoc.6678).
[32] D. Jayatilaka, S. Wolff, D. Grimwood, J. McKinnon, M. Spackman, CrystalExplorer: a tool for displaying Hirshfeld surfaces and visualising intermolecular interactions in molecular crystals, Acta Crystallogr. Sect. A - Acta Crystallogr A 62 (2006), https://doi.org/10.1107/S0108767306098199.
[33] Ö. Tamer, N. Dege, D. Avcı, Y. Atalay, The static and frequency-dependent second- and third order nonlinear optical properties of Zn(II) and Ni(II) complexes of 4 methoxypyridine-2-carboxylic acid: A detailed experimental and theoretical study, Applied Organometallic Chemistry. n/a (n.d.) e7206. https://doi.org/https://doi.org/10.1002/aoc.7206.
[34] M.A. Spackman, D. Jayatilaka, Hirshfeld surface analysis, CrystEngComm 11 (2009) 19–32, https://doi.org/10.1039/B818330A.
[35] Ö. Tamer, S.A. Tamer, Ö. İdil, D. Avcı, H. Vural, Y. Atalay, Antimicrobial activities, DNA interactions, spectroscopic (FT-IR and UV-Vis) characterizations, and DFT calculations for pyridine 2 carboxylic acid and its derivates, J. Mol. Struct. 1152 (2018) 399–408, https://doi.org/10.1016/J.MOLSTRUC.2017.09.100.
[36] Ö. Tamer, D. Avcı, Y. Atalay, Synthesis, X Ray crystal structure, photophysical characterization and nonlinear optical properties of the unique manganese complex with picolinate and 1,10 phenantroline: toward the designing of new high NLO response crystal, J. Phys. Chem. Solids 99 (2016) 124–133, https://doi.org/10.1016/J.JPCS.2016.08.013.
[37] Ö. Tamer, D. Avcı, Y. Atalay, Synthesis, crystal structure, spectroscopic characterization and nonlinear optical properties of Co(II)- picolinate complex, Mater. Chem. Phys. 168 (2015) 138–146, https://doi.org/10.1016/J.MATCHEMPHYS.2015.11.013.
[38] Ö. Tamer, H. Mahmoody, K.F. Feyzioğlu, O. Kılınç, D. Avcı, O. Orun, N. Dege, Y. Atalay, Synthesis of the first mixed ligand Mn (II) and Cd (II) complexes of 4-methoxy-pyridine-2-carboxylic acid, molecular docking studies and investigation of their anti-tumor effects in vitro, Appl. Organomet. Chem. 34 (2020) e5416, https://doi.org/10.1002/aoc.5416.
[39] H. Pir, N. Gunay, O. Tamer, D. Avci, Y. Atalay, Theoretical investigation of 5 (2 Acetoxyethyl)-6-methylpyrimidin-2, 4-dione: conformational study, NBO and NLO analysis, molecular structure and NMR spectra, Spectrochim. Acta Part A Mol. Biomol. Spectrosc. 112 (2013) 331–342, https://doi.org/10.1016/j.saa.2013.04.063.
[40] H.P. Günüş, Ö. Tamer, D. Avci, Y. Atalay, Effects of donor–accceptor groups on the structural and electronic properties of 4-(methoxymethyl)-6-methyl-5-nitro-2-oxo-1,2-dihydropyridine-3-carbonitrile, Spectrochim. Acta Part A Mol. Biomol. Spectrosc. 132 (2014) 183–190, https://doi.org/10.1016/J.SAA.2014.04.128.
[41] N. Dege, Ö. Özge, D. Avcı, A. Başoğlu, F. Sönmez, M. Yaman, Ö. Tamer, Y. Atalay, B. Zengin Kurt, Concentration effects on optical properties, DFT, crystal characterization and α-glucosidase activity studies: Novel Zn(II) complex, Spectrochim. Acta Part A Mol. Biomol. Spectrosc. 262 (2021) 120072, https://doi.org/10.1016/J.SAA.2021.120072.
[42] D. Avcı, S. Altürk, F. Sönmez, Ö. Tamer, A. Başoğlu, Y. Atalay, B. Zengin Kurt, N. Dege, Novel metal complexes containing 6-methylpyridine-2-carboxylic acid as potent α-glucosidase inhibitor: synthesis, crystal structures, DFT calculations, and molecular docking, Mol. Divers. 25 (2021) 171–189, https://doi.org/10.1007/s11030-020-10037-x.
[43] Ö. Tamer, D. Avcı, E. Çelikoğlu, Ö. İdil, Y. Atalay, Crystal growth, structural and spectroscopic characterization, antimicrobial activity, DNA cleavage, molecular docking and density functional theory calculations of Zn(II) complex with 2-pyridinecarboxylic acid, Appl. Organomet. Chem. 32 (2018) e4540, https://doi.org/10.1002/aoc.4540.
[44] Ö. Tamer, D. Avcı, Y. Atalay, Quantum chemical characterization of N-(2-hydroxybenzylidene)acetohydrazide (HBAH): a detailed vibrational and NLO analysis, Spectrochim. Acta Part A Mol. Biomol. Spectrosc. 117 (2014) 78–86, https://doi.org/10.1016/J.SAA.2013.07.112.
[45] S.L..Gorelsky, SWizardProgramRevision4.5, (2010). (http://www.sg.chem.net/).
[46] R.G. Pearson, Hard and soft acids and bases, J. Am. Chem. Soc. 85 (1963) 3533–3539, https://doi.org/10.1021/ja00905a001.
[47] D. Avcı, Second and third order nonlinear optical properties and molecular parameters of azo chromophores: semiempirical analysis, Spectrochim. Acta Part A Mol. Biomol. Spectrosc. 82 (2011) 37–43, https://doi.org/10.1016/j.saa.2011.06.037.
[48] Y. Zhang, C.-Y. Zhao, W.-H. Fang, X.-Z. You, A molecular design view on the first hyperpolarizability of salicylidenceaniline derivatives, Theor. Chem. Acc. 96 (1997) 129–134, https://doi.org/10.1007/s002140050213.
[49] J.L. Oudar, J. Zyss, Structural dependence of nonlinear-optical properties of methyl (2,4 dinitrophenyl) aminopropanoate crystals, Phys. Rev. A 26 (1982) 2016–2027, https://doi.org/10.1103/PhysRevA.26.2016.
[50] J.L. Oudar, Optical nonlinearities of conjugated molecules. Stilbene derivatives and highly polar aromatic compounds, J. Chem. Phys. 67 (2008) 446–457, https://doi.org/10.1063/1.434888.
[51] M. Benscbaa, M. Boukelkoul, Ö. Tamer, Y. Atalay, D. Avcı, Theoretical Investigation of Structural, Spectroscopic (IR, 1H and 13C NMR), Static, and Frequency-Dependent Nonlinear Optical Properties of 4-[(1E)-3-(4-Methoxyphenyl)-3-Oxoprop-1-en-1-yl]Phenyl 4-Methylbenzene-1-Sulfonate, Polycyclic Aromatic Compounds. (n.d.) 1–19. (https://doi.org/10.1080/10406638.2023.2254906).

Spectrochimica Acta Part A: Molecular and Biomolecular Spectroscopy 325 (2025) 125138

Contents lists available at ScienceDirect

Spectrochimica Acta Part A:
Molecular and Biomolecular Spectroscopy

journal homepage: www.journals.elsevier.com/spectrochimica-acta-part-a-molecular-and-biomolecular-spectroscopy

The effect of complex formation on the static and frequency-dependent nonlinear optical properties: A combined experimental and theoretical investigation

Ömer Tamer [a,*], Merve Şimşek [a], Necmi Dege [b], Davut Avcı [a], Yusuf Atalay [a]

[a] Sakarya University, Faculty of Science, Department of Physics, Sakarya 54147, Türkiye
[b] OndokuzMayıs University, Faculty of Science, Department of Physics, Samsun 55139, Türkiye

HIGHLIGHTS

- The newly synthesized mixed ligand Mn (II) complex were optimized by B3LYP/LanL2DZ.
- IR and UV–Vis spectra were evaluated.
- SOMO and SUMO energies were investigated.
- Mn(II) complex has higher static and frequency-dependent β and γ than 6Brpca and Dmdpy ligands.
- The variations in μ, ΔE, β, and γ were comprehensively evaluated.

GRAPHICAL ABSTRACT

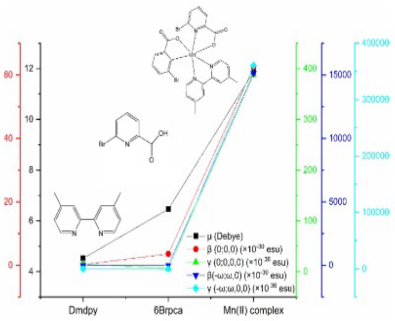

ARTICLE INFO

Keywords:
6 Bromopyridine 2 carboxylic acid
XRD
FT IR and UV–Vis Spectra
Frequency-dependent hyperpolarizability
DFT

ABSTRACT

A novel mixed ligand Mn(II) complex of 6-Bromopyridine-2-carboxylic acid (6Brpca) and 4,4′-dimethyl-2,2′-dipyridyl has been prepared and structurally characterized using single-crystal X-ray diffraction. The spectroscopic properties were also analyzed by using FT-IR and UV–Vis spectral techniques. The coordination complexes having transition metal ions are known to have promising optical nonlinearity behavior. Therefore, B3LYP level density functional theory was used to investigate first- and second-order hyperpolarizabilities (β and γ) and provide a deep understanding of the relation between the structure and NLO properties. The calculations of frequency-dependent α, β, and γ at frequencies of ω = 0.0856252 and 0.0428126 au. for 6Brpca and Dmdpy ligands as well as Mn(II) complex have been also carried out using B3LYP/LanL2DZ level. Especially second harmonic generation (SHG) first and second hyperpolarizabilities (β(−2ω;ω,ω) and γ (−2ω;ω,ω,0)) parameters for Mn(II) complex have been calculated as 11448 × 10^{-30} and 680035 × 10^{-36} esu, respectively. It has been determined that there is a tremendous increase in β and γ parameters when 6Brpca and Dmdpy ligands coordinate to the high spin multiplicity Mn(II) ion. Theoretical calculations revealed that the large first- and second-order hyperpolarizabilities are caused by strong intramolecular charge transfer between the transition metal and the coordinated ligands. These results indicate that the the organometallic complex under investigation is valuable candidate for optoelectronic and photonic applications.

* Corresponding author.
E-mail address: omertamer@sakarya.edu.tr (Ö. Tamer).

https://doi.org/10.1016/j.saa.2024.125138
Received 2 August 2024; Received in revised form 26 August 2024; Accepted 12 September 2024
Available online 15 September 2024
1386-1425/© 2024 Elsevier B.V. All rights are reserved, including those for text and data mining, AI training, and similar technologies.

1. Introduction

Transition-metal complexes have properties that can be carefully tuned through ligand design and metal selection for the control of spin and oxidation state as well as electronic or optical properties [1,2]. Transition metal complex-based nonlinear optical (NLO) materials exhibit unique properties that contribute to their nonlinear optical behavior, such as robustness, physical and chemical stability, and tunability. These materials are meticulously designed to control optical nonlinearity, enhancing the intensity and polarization of incident laser light, making them highly suitable for nonlinear optical applications [3]. Transition metal complex-based NLO materials demonstrate promising microscopic second and third-order nonlinear optical features, making them ideal for optoelectronics and telecommunication applications. The presence of transition metal ions significantly induces the magnitude of hyperpolarizability, confirming their excellent nonlinear optical property. The characterization of these materials reveals large NLO coefficients, a desired optically transparent range, and a high laser damage threshold, making them suitable for advanced optoelectronic devices [4–6]. However, synthesizing transition metal complex-based NLO materials with optimized properties poses several challenges. These materials need to meet stringent criteria, including a non-centrosymmetric structure, large NLO coefficients, and a high laser damage threshold. The influence of various factors, such as metal ion, ligand and coordination geometry, on the nonlinear optical properties of metal complexes has been studied to understand their contributions and address the challenges in synthesizing optimized materials [7,8].

One of the common strategies to obtain new NLO materials with large first- and second-order hyperpolarizabilities is to coordinate organic ligands to metal ions [9–11]. Accordingly, the coordination of electron-donating and/or withdrawing substituents to provide polarization of the π-electrons in organic systems, thereby creating the possibility of a second and third-order NLO response, has been extended to metal complexes consisting of conjugated donor–acceptor systems [12]. However, the majority of the metal coordination complexes reported for the search for ideal NLO materials have centrosymmetric crystal structures. In such structures where the dipole moments cancel each other out, the magnitude of the total dipole moment and, hence, the first-order hyperpolarizability are very low [13,14]. One of the most common ways to overcome the centrosymmetric structure challenge is to coordinate a secondary neutral ligand to the corresponding metal–organic coordination compounds [15]. In the search for potential NLO materials, 1,10-Phenanthroline, and Neocuproine structures are frequently reported to be used as secondary neutral ligands [16–19]. It is known that such large molecular materials, which have electron donating and/or withdrawing groups, conjugated bridges between these groups, and can easily coordinate to metal ions, significantly improve the nonlinear optical properties.

In the search for potential nonlinear optical candidate materials, pyridine-2-carboxylic acid, and its derivatives have been frequently used recently. Previous studies have examined a number of coordination complexes that include pyridine-2-carboxylic acid derivatives coordinated to various metal ions [13,20–36]. In a recent study, the Mn(II) and Zn(II) complexes of 6-bromo-pyridine-2-carboxylic acid were synthesized and their first- and second-order hyperpolarizability parameters were examined. Among the complexes with similar crystal structures, the Mn(II) ion with higher spin multiplicity has been reported to have higher NLO parameters ($\beta = 66.94 \times 10^{-30}$ esu., $\gamma = 558.23 \times 10^{-36}$ esu.) [37]. It is our main motivation that the high spin multiplicity of the Mn(II) metal ion, π-electron density and electron donating/withdrawing ability of 6-bromo-pyridine-2-carboxylic acid ligand as well as the coordination of the secondary neutral ligand 4,4′-Dimethyl-2,2′-dipyridyl provides the non-centrosymmetric structure, and a larger complex where electrons can freely move, thus resulting in a significant increase in NLO properties. In the present study, a novel mixed ligand Mn(II) complex of 6-bromo-pyridine-2-carboxylic acid and 4,4-dimethyl-2,2-dipyridyl was synthesized, and its crystal structure was solved by the XRD method. FT-IR and UV–Vis spectra were used to characterize the spectroscopic properties of the Mn(II) complex. Finally, static and frequency-dependent first- and second-order hyperpolarizability parameters were examined by using B3LYP/lanL2DZ level.

2. Experimental and theoretical Procedures

2.1. Synthesis of [Mn(6Brpca)$_2$dmdpy]•CH$_3$OH

All chemicals used in the present paper were obtained from Merck and used without any further purification. Initially, 6-bromo-pyridine-2-carboxylic acid (0.2 mmol) was dissolved in a 20 mL mixture of ethanol/water, ca 1:1 (v/v). To the resulting solution, $(CH_3COO)_2Mn{\cdot}4H_2O$ (1 mmol) was added and stirred until completely dissolved. Subsequently, 4,4-dimethyl-2,2-dipyridyl (0.1 mmol) was introduced as a secondary neutral ligand to the obtained mixture. The final reaction mixture was maintained at a constant temperature of 50 °C under continuous stirring to ensure thorough interaction of all ligands and metal salt. This synthesis process resulted in the formation of yellow-colored single crystals, indicating the successful creation of the desired octahedral coordination complex. The synthesis procedure for the Mn(II) complex is shown in Fig. 1.

2.2. Experimental methods

The crystal structure determination of the mixed ligand Mn(II) complex was carried out using a Stoe IPDS II diffractometer [38]. The initial structure solution was achieved using SHELXT [39], a powerful software for resolving crystal structures. Subsequent refinement was performed with SHELXL [40], ensuring accurate modeling of the atomic positions and thermal parameters. The visualization and analysis of the molecular structures were conducted using Mercury[41], which provided clear and detailed images of the Mn(II) complex. To validate and analyze the crystal structures further, PLATON [42] was employed, offering additional checks and detailed insights into the crystallographic data. The entire process was managed and integrated using WinGX [43]. Finally, the crystallographic information was compiled and prepared for publication using PublCIF [44], ensuring that all necessary data were accurately presented in the Crystallographic Information File (CIF) format.

The FT-IR spectra of the 6-bromo-pyridine-2-carboxylic acid and 4,4-dimethyl-2,2-dipyridyl ligands and Mn(II) complex were recorded using a Perkin ELMER Spectrum-Two FT-IR spectrophotometer. This instrument is capable of scanning the 4000 to 400 cm^{-1} range, providing detailed information on the molecular vibrations and functional groups present in the ligands and complex. Ultraviolet–visible (UV–Vis) spectrum of the 6-bromo-pyridine-2-carboxylic acid and 4,4-dimethyl-2,2-dipyridyl ligands, as well as Mn(II) complex, were recorded using a HITACHI U-2900 UV/Vis spectrophotometer. The measurements were performed in the 200–900 nm range with ethanol as the solvent. The use of ethanol as the solvent ensures good solubility and stability of the

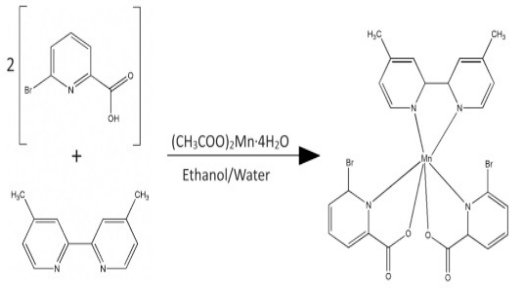

Fig. 1. Synthesis schema for [Mn(6Brpca)$_2$dmdpy]•CH$_3$OH complex.

complexes during the measurements.

2.3. Computational Details

All quantum chemical calculations in this study were carried out using the Gaussian 16 software package [45]. The initial molecular geometries were constructed, visualized, and manipulated using GaussView 6.0.[46], providing an intuitive graphical interface for the preparation and examination of input files and results. The geometry optimizations and frequency calculations for the Mn(II) complex were performed using the B3LYP functional, a widely used hybrid functional that combines Becke's three-parameter exchange functional [47] with the Lee-Yang-Parr correlation functional [48]. This functional is well-regarded for its balance between accuracy and computational efficiency. The LanL2DZ basis set [49] was employed, which includes effective core potentials for heavier elements, reducing the computational cost while maintaining good accuracy for transition metals. Vibrational frequency calculations were conducted to ensure that the optimized structures correspond to true minima on the potential energy surface. A scaling factor of 0.96 was applied to the calculated vibrational frequencies [50]. This scaling factor corrects for the systematic overestimation of vibrational frequencies by the B3LYP/LanL2DZ level of theory, accounting for anharmonicity and other deficiencies in the computational method. The potential energy distribution (PED) was analyzed using the VEDA software [51], which aids in the assignment of vibrational modes by determining the contribution of each internal coordinate to the vibrational frequencies. Time-dependent DFT (TD-DFT) calculations were performed using the TD-B3LYP method to investigate the electronic excitation properties. Solvent effects were accounted for using the Conductor-like Polarizable Continuum Model (CPCM) [52,53]. The origin of electronic absorption bands in the UV–Vis spectrum was investigated by SWizard [54]. Crystal Explorer program [55] was used for Hirschfield surface analysis.

3. Results and Discussion

3.1. Geometric structure

The crystal structure of the complex $[Mn(6Brpca)_2Dmdpy]\cdot CH_3OH$ was determined and refined, providing comprehensive insight into its molecular architecture. The complex crystallizes in the monoclinic space group $P2_1/n$ with the following unit cell dimensions: a = 11.7430(9) Å, b = 12.2786(6) Å, and c = 19.9105(15) Å. The unit cell angles are α = 90 (5)°, β = 101.780(6)°, and γ = 90(5)°, resulting in a unit cell volume of 2810.4(3) $Å^3$. There are four formula units per unit cell (Z=4), which is indicative of the complex packing within the crystal lattice (Table 1).

Fig. 2 demonstrates that the Mn(II) complex consists of a central Mn (II) ion coordinated by two bidentate 6Brpca ligands and a bidentate Dmdpy ligand. This coordination leads to the formation of three five-membered chelate rings, involving the metal ion binding to two nitrogen atoms from Dmdpy and both nitrogen and oxygen atoms from the 6-Brpca ligands. The coordination sphere around the central Mn(II) ion was also detected as a distorted octahedral geometry. The Mn-O3/O1 and Mn-N4/N3 bonds occupy the equatorial plane, while Mn-N2/N1 bonds occupy the axial plane. In Mn(II) complexes, the bond lengths between the Mn(II) ion and the surrounding O and N atoms are crucial parameters that define the structural properties of the complex. In a previous study, the crystal structures of Mn(II) and Cd(II) complexes containing 4-methoxypyridine-2-carboxylic acid and 4,4-dimethyl-2,2-dipyridyl were reported. The Mn(II)-N (Dmdpy) bond lengths were reported as 2.247 (2) and 2.257 (2) Å. The Mn(II)-N bond lengths were reported as 2.259 (2) and 2.261 (2) Å, while Mn(II)-O bond lengths were found as 2.1307(17) and 2.1573(19) Å for 4-methoxypyridine-2-carboxylic acid group [20]. In the case of the $[Mn(6Brpca)_2Dmdpy]\cdot CH_3OH$] complex, the Mn-N2 and Mn-N4 bond lengths were measured at 2.363 (4) Å and 2.259 (4) Å, respectively. These values are consistent with

Table 1
Structural refinement and crystal parameters for $[Mn(6Brpca)_2Dmdpy]\cdot CH_3OH$ complex.

Crystal data	
CCDC	2,358,815
Chemical formula	$C_{24}H_{18}Br_2MnN_4O_4\cdot CH_3O$
M_r	673.22
Crystal system, space group	Monoclinic, $P2_1/n$
Temperature (K)	293
a, b, c (Å)	11.7430 (9), 12.2786 (6), 19.9105 (15)
α, β, γ (°)	90 (5), 101.780 (6), 90(5)
V ($Å^3$)	2810.4 (3)
Z	4
Radiation type	Mo Kα
μ (mm^{-1})	3.35
F (000)	1372
Crystal size (mm)	0.36 × 0.23 × 0.14
Diffractometer	STOE IPDS 2
Absorption correction	Integration (X-RED32; Stoe&Cie, 2002)
T_{min}, T_{max}	0.317, 0.629
No. of measured, independent andobserved [I>2σ(I)] reflections	20948, 6452, 3963
R_{int}	0.081
$(\sin\theta/\lambda)_{max}$ ($Å^{-1}$)	0.650
R [$F^2 > 2\sigma(F^2)$], wR(F^2), S	0.058, 0.162, 0.98
No. of reflections	6452
No. of parameters	338
H-atom treatment	H-atom parameters constrained
Δρmax, Δρmin (e $Å^{-3}$)	1.17, −0.63

theoretical calculations, which reported lengths of 2.1277 Å and 2.0003 Å, respectively. The bond lengths of Mn-O3 and Mn-O2 were experimentally found as 2.127 (3) and 2.131 (3) Å, and theoretically calculated as 1.9765 and 1.9571 Å. The variations in bond lengths between Mn(II) and the surrounding O and N atoms may indicate the degree of distortion in the complex and the presence of the Jahn-Teller effect [13,20,33]. Table 2 clearly demonstrates that a Jahn-Teller elongation is detected at the bond lengths of Mn(II)–N2 and Mn(II)-N1. Avcı et al. reported the Cu(II) complex of 6-bromo-pyridine-2-carboxylic acid and 4,4-dimethyl-2,2-dipyridyl ligands. The C-Br bond lengths were reported as 1.901 (8) and 1.922 (8) [56]. In the present study, the C-Br bond lengths were observed as 1.904 (5) and 1.910 (5) Å.

The chelate ring angles, N3-Mn-N4, N2– Mn –O3 and N1- Mn –O2, were observed at 72.30(13), 73.90 (13) and 73.20 (13)°, respectively. The corresponding theoretical results were also obtained as 79.733, 80.819 and 81.333°, respectively. Avcı et al. reported the same bon angles for a Cu(II) complex at 84.4(2), 74.4(2) and 80.3(3)° [56]. The bond angles of N2-Mn-N4, O2-Mn-N2, N4- Mn –O3 and N3– Mn –O2 observed as 87.58 (14), 93.97 (14), 92.37 (13) and 94.03 (14) are the important indicators of distorted octahedral geometry of Mn(II) complex. The bond lengths and angles for mixed ligand Mn(II) complex obtained by experimental and theoretical methods are consistent with the previously reported similar complexes [37,56–58].

Table 3 presents the parameters of hydrogen bonding geometry for the mixed ligand Mn(II) complex. Fig. 3 presents the crystal packing diagram for the mixed ligand Mn(II) complex, indicating the H-bonding interaction with the red lines. The crystal deconstructs the molecules into a three-dimensional network through O—H···O and C—H···O intermolecular H bonds. All interactions responsible for the stacking of the complex appear to be strong hydrogen bonds, and therefore it can be concluded that the thermal stability of the complex is high. The H-bonding interaction of O25—H25···O1 is the strongest one in Mn(II) crystal with the symmetry code of − x + 1, −y + 1,-z + 1 [H···A=2.12 Å, D···A=2.919 Å].

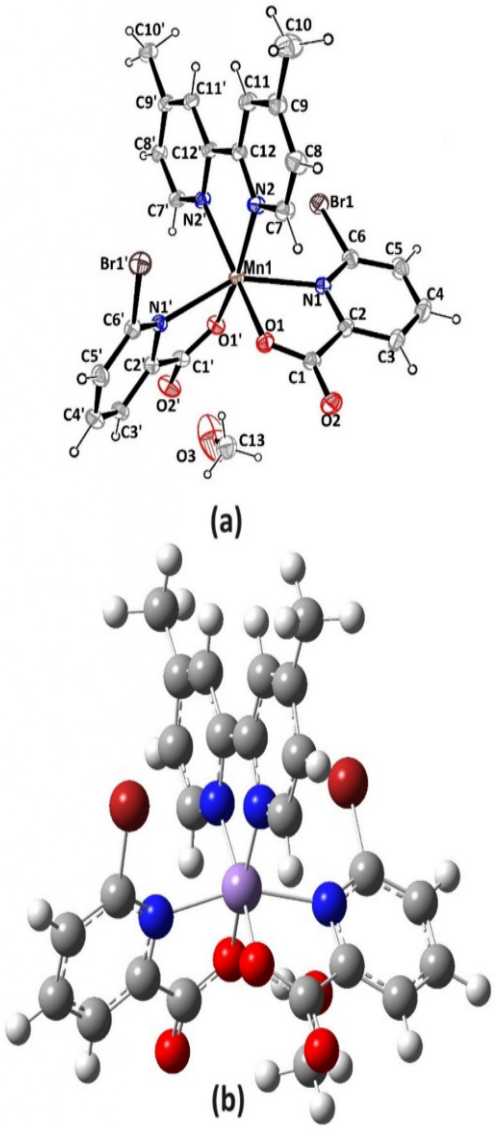

Fig. 2. (a) Crystal structure, and (b) theoretical structure obtained by B3LYP/LanL2DZ level for [Mn(6Brpca)$_2$Dmdpy]•CH$_3$OH.

3.2. Hirshfeld surface analysis

Hirshfeld surface analysis is an advanced method employed to investigate molecular interactions and topological properties in crystal structures. This analysis generates surfaces by considering all the interactions among the ligands within the crystal structure. These surfaces then permit the visualization of intermolecular interactions [26,34–36,59–61]. The Hirshfeld surface determines and visualizes the interaction region of the molecule by calculating the internal and external contributions of the electron density of the molecule. Hirshfeld surface analysis is a widely used technique in a number of scientific disciplines, including crystal packaging analysis, drug design, materials science and molecular recognition studies. It provides an in-depth understanding of molecular interactions. This method makes significant contributions to scientific research and industrial applications by evaluating the interaction patterns and stability of crystal structure [62,63].

The intermolecular interactions and interaction distances in [Mn(6Brpca)$_2$Dmdpy]·CH$_3$OH complex were evaluated by using the Crystal Explorer software [55]. The 3D Hirshfeld surfaces, namely, d_{norm}, shape-index, and curvedness for the newly synthesized mixed ligand Mn(II) complex are presented in Fig. 4. The d_{norm} illustration uses a color scale where red color indicates the interactions shorter than Van der Waals radii, blue color indicates the interactions longer than Van der Waals radii, and white displays the interactions of approximately the same length as Van der Waals radii. According to Fig. 4(a), the intense red spots on the noncoordinated O atom of carboxylate group, oxygen atom of CH$_3$OH group, Br atoms as well as C14 atom of dmdpy clearly indicate a strong H-bonding interactionthrough these atoms [64,65]. The d_{norm} values for the Mn(II) complex range from −0.3397 (red) to 1.9331 (blue) au. The shape index of the Hirshfeld surface obtained for mixed ligand Mn(II) complex (see in Fig. 4(b)) is used to reveal the π–π stacking interactions by the presence of adjacent triangles in blue and red colour [66]. Fig. 4(b) displays that Mn(II) complex has red triangles on the pyridine rings, but has no blue triangle, indicating the absence of the π–π stacking interactions in the crystal under consideration. Fig. 4(c) also reveals that 6Brpca and Dmdpy ligands and chelate rings are defined as regions of low surface curvature, while the regions around the CH3OH ligand and the border ends of the Mn(II) complex are defined as regions of very sharp surface curvature [65,67].

The surface is defined by two parameters, d_e (outer distance) and d_i (inner distance). The nature and strength of the interactions are analyzed in detail through 2D fingerprint plots [33,34]. Further insight into the nature of intermolecular interactions can be derived from the analysis of 2D fingerprint (FP) plots. Fig. 5 illustrates the primary interactions that contribute more strongly to crystal packing. The

Table 2
The experimental and theoretical bond lengths (Å, °) of [Mn(6Brpca)$_2$Dmdpy]·CH$_3$OH complex.

Bond Lengths	XRD	B3LYP	Bond Angles	XRD	B3LYP
Mn-N2	2.363 (4)	2.1277	N2-Mn-N1	148.00 (13)	157.88
Mn –N1	2.362 (4)	2.1281	N2 Mn N4	87.58 (14)	90.923
Mn –O3	2.127 (3)	1.9765	N3-Mn-N2	113.96 (14)	106.67
Mn –O2	2.131 (3)	1.9571	N4 Mn N1	112.20 (15)	106.71
Mn –N4	2.259 (4)	2.0003	N3 Mn N1	96.42 (13)	89.893
Mn –N3	2.245 (3)	1.9954	N3-Mn-N4	72.30(13)	79.733
O3 C7	1.282 (6)	1.3266	N2 Mn O3	73.90 (13)	80.819
O2-C1	1.267 (6)	1.3239	N1-Mn-O3	80.14 (125)	84.576
C7-O4	1.224 (5)	1.2550	N1-Mn-O2	73.20 (13)	81.333
C1-O1	1.267 (6)	1.2557	O2-Mn-N2	93.97 (14)	82.845
N4-C23	1.349 (6)	1.3491	N4-Mn-O3	92.37 (13)	94.222
N1-C6	1.329 (6)	1.3799	N4-Mn-O2	165.54 (13)	169.85
N2-C8	1.371 (6)	1.3789	N3-Mn-O2	94.03 (14)	94.337
N1-C2	1.357 (6)	1.3799	O2-Mn-O3	101.88 (14)	92.688
N4-C19	1.349 (5)	1.3736	Mn-N2-C12	132.0 (3)	133.55
N3-C18	1.352 (6)	1.3735	Mn N2 C8	110.6 (3)	108.69
N4 23	1.349 (6)	1.3621	Mn–N4 C23	124.5 (3)	124.71
N3-C13	1.349 (6)	1.3621	Mn-N1 –C2	109.7 (3)	108.52
C19 C20	1.387 (7)	1.4069	Mn N1 –C6	129.7 (3)	134.09
C6-C5	1.376 (7)	1.4049	C7-O3-Mn	122.1 (3)	118.09
C18 C19	1.485 (6)	1.4672	C1-O2 Mn	121.8 (3)	118.52
C12 Br2	1.904 (5)	1.9634	N2 C12 Br2	116.0 (4)	120.50
C6-Br1	1.910 (5)	1.9632	N1-C6-Br1	115.8 (4)	120.51
O25 C25	1.473 (9)	1.4527	N2 C8 C9	121.6 (5)	123.21

Table 3
Experimentally determined hydrogen bond geometry of the [Mn(6Brpca)$_2$Dmdpy]·CH$_3$OH molecule (values in Å and °).

D—H···A	D—H	H···A	D···A	D—H···A
C17—H17···O2^{i}	0.93	2.62	3.329 (6)	134
C20—H20···O2 ^{i}	0.93	2.76	3.503 (6)	138
C20—H20···O2 ^{i}	0.93	2.64	3.536 (7)	162
C14—H14···O4^{ii}	0.93	2.47	3.337 (6)	155
C5—H5···O25	0.93	2.80	3.489 (11)	132
C3—H3···O3^{iii}	0.93	2.73	3.382 (6)	128
C3—H3···O4^{iii}	0.93	2.76	3.337 (7)	121
O25—H25···O1^{iii}	0.82	2.12	2.919 (10)	165

Symmetry codes: (i) − x + 3/2, y − 1/2, −z + 1/2; (ii) x + 1, y, z; (iii) − x + 1, −y + 1,-z + 1.

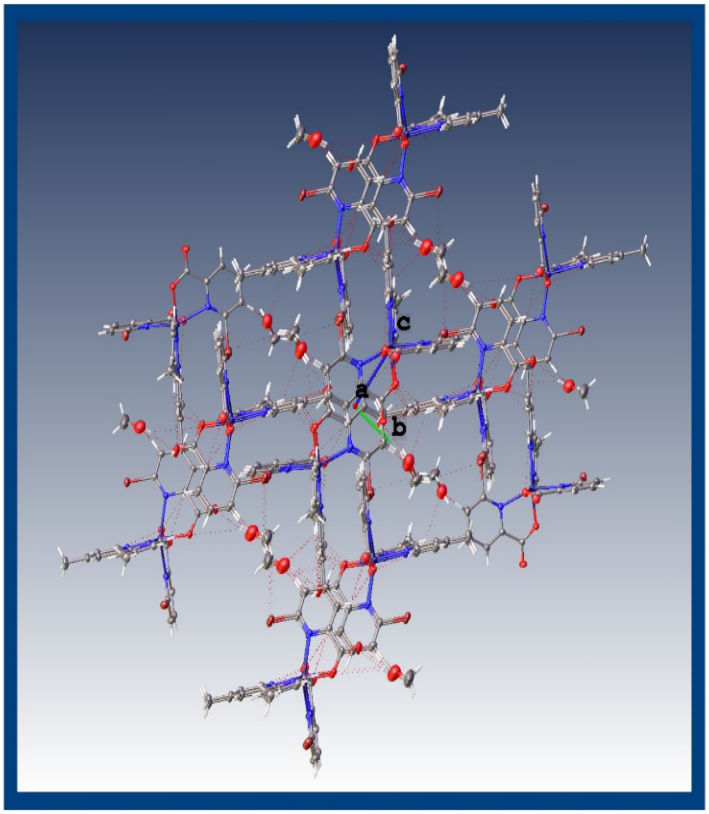

Fig. 3. Crystal packing diagram for $[Mn(6Brpca)_2Dmdpy]\bullet CH_3OH$, indicating the H-bonding interactions with red lines.

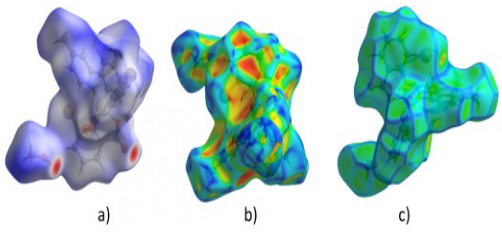

Fig. 4. Hirschfeld surface (HS) plotted over (a) dnorm, (b) shape-index, and (c) curvedness for $[Mn(6Brpca)_2Dmdpy]\cdot CH_3OH$.

contributions of the following intermolecular interactions to crystal packing were determined to be as follows: 37.4 % for H···H, 22.7 % for O···H, 19.4 % for C···H, 9 % for Br···H, 4.5 % for Br···C and 2.2 % for Br···Br. Other interactions that contribute less than 5 % to crystal packing are Br···Br with a contribution percentage of 2.2 %, C···C with 1.6 %, N···H with 1.5 %, Br···N with 1, O···C with 0.4 % and O···O with 0.3 %.

3.3. Vibrational analysis

The vibrational spectrum is used to determine the vibrational modes of investigated system and examine the functional groups and coordination geometry [68]. The vibrational frequencies obtained in the present study reflect the specific vibrational modes of various functional groups and give some clues about the crystal geometry of Mn(II) complex. The experimental vibrational spectrum of the $[Mn(6Brpca)_2Dmdpy]\cdot CH_3OH$ complex has been recorded in the range of 4000–400 cm^{-1}, and calculated in the same wavenumber region by using B3LYP/LanL2DZ level. The obtained FT-IR and theoretical IR spectra were presented in Fig. 6, while the selected vibrational modes and corresponding wavenumbers were presented in Table 4. Theoretical calculations performed using the B3LYP method have shown substantial agreement with experimental results. This compatibility underscores the reliability of theoretical models in predicting molecular vibrations.

The aromatic ring C–H stretching vibrations for the transition metal complexes of pyridine-2-carboxylic acid derivatives are reported at the frequency range of 3071–3070 cm^{-1} [20], 3107–3071 cm^{-1} [56] and 3068–2967 cm^{-1} [69]. In the present study, the C–H stretching vibrations for free 6Brpca ligand were observed at 3048–2839, while those for free Dmbpy ligand were observed at 2991–2896 cm^{-1}. In Mn(II) complex, the vibrational bands observed at 3095–3059 cm^{-1} are due to the aromatic C–H stretching vibrations, while those observed at 2969–2915 cm-1 are due to the methyl group C–H stretching vibrations. The C–H stretching vibrations in the theoretical spectrum were calculated at the range of 3135–2881 cm^{-1}, as consistent with the FT-IR spectrum of Mn (II) complex. The Mn(II) complex contains a free CH_3OH molecule in its crystal structure. It is clear that the vibration band observed at 3427 cm^{-1} in the FT-IR spectrum originates from the OH stretching in the CH_3OH molecule. In a previous study, it was reported that the bands at 3347 cm^{-1} are due to the stretching vibration of methanol molecules [70]. The corresponding vibrational band in the theoretical spectrum was found at 3287 cm^{-1}.

The COO^- group asymmetric and symmetric CO stretching vibrations for 6Brpca were observed at 1695 and 1174 cm^{-1}. The corresponding bands for the Mn(II) complex were observed at 1609 and 1291 cm^{-1}. It is well known that the difference between the asymmetric and symmetric CO stretching vibrations for carboxylate groups is an important indicator of coordination to central metal ions [71–73]. The difference obtained as 521 cm^{-1} for free 6Brpca and 318 cm^{-1} for the Mn(II) complex demonstrates that the 6Brpca ligand coordinates to the Mn(II) ion through the O atoms. This frequency difference indicates that the carboxylate groups are in a monodentate coordination mode through the O atom [74]. The aromatic ring stretching vibrations known as

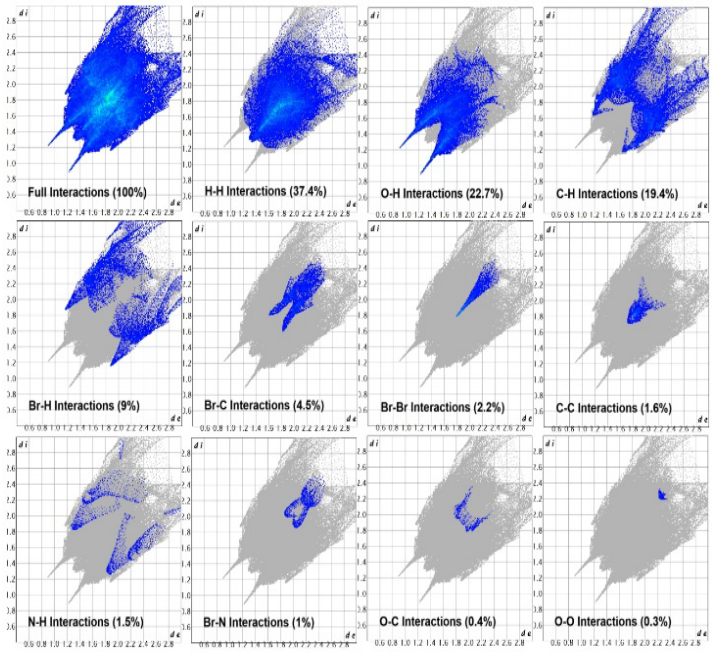

Fig. 5. Hirshfeld surface fingerprint plots of the nearest internal distance (d_i) versus the nearest external distance (d_e) for [Mn(6Brpca)$_2$Dmdpy]·CH$_3$OH complex.

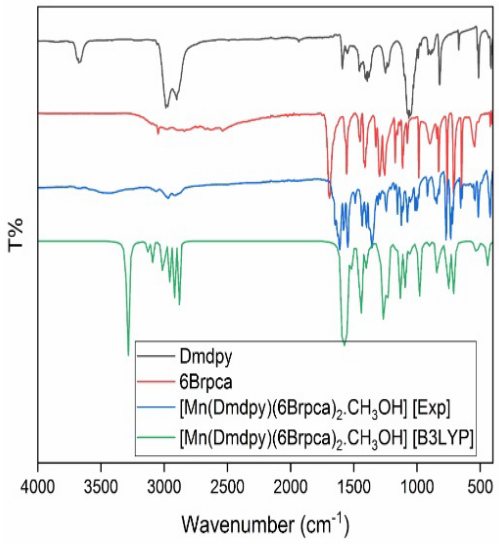

Fig. 6. The FT-IR and theoretical IR spectra for Dmdpy, 6Brpca and [Mn(6Brpca)$_2$Dmdpy]·CH$_3$OH complex.

highly characteristic vibrational bands are important in the spectrum of pyridine and its derivatives. The aromatic ring C–C stretching vibrations were reported in the region 1430–1625 cm^{-1} [75]. In the present study, the vibrational bands at the range of 1648–1204 cm^{-1} were assigned as the aromatic C–C stretching vibrations. The corresponding vibrations in the predicted spectrum were detected 1594–1207 cm^{-1}.

Ring breathing vibrations are distinct vibration modes that play a crucial role in the characterization of aromatic and heterocyclic compounds. For example, in a recent study [20], the ring breathing vibration bands were detected at 1014 cm^{-1} and 990 cm^{-1} for free 4mpic and dmdpy ligands, respectively. Upon coordination of the ligands to central ions, these bands were observed to shift to 1034 cm^{-1} and 1033 cm^{-1} for both complexes, respectively [20]. In the present study, the vibration bands observed at 986 and 988 cm^{-1} were assigned as ring breathing vibrations for 6Brpca and Dmdpy ligands, respectively. After the ligands were coordinated to the central Mn(II) ion, this vibration band shifted to 1010 cm^{-1}, demonstrating that the coordination through the ring N atom.

The in plane CH bending (β HCH and β HCC) vibrations were observed in the region of 1433–1076 cm^{-1}, while the same vibration bands were calculated at the range of 1526–1082 cm-1 with the PED contributions 100–10 %. The identifying of the C-N stretching vibrations is a quite difficult task since the overleaping with the other vibration bands. Sundaraganesan et al. [76] assigned C-N stretching vibration at 1391 cm^{-1} for 2-amino-5-iodopyridine. In the present study, the C-N stretching bands were observed at the range of 1378–1245 cm^{-1}, and calculated in the region of 1524–1237 cm^{-1}.

3.4. Frontier molecular orbital analysis

Understanding of the electronic characteristics of metal–organic coordination compounds is essential for evaluating their electronic behaviors and reactivity. Hence, the frontier molecular orbitals, their energies, and some related quantum chemical parameters for the 6Brpca and Dmdpy ligands as well as Mn(II) complex were computed employing the B3LYP/LanL2DZ methodology. The B3LYP calculations for the UV–Vis spectrum were conducted for the restricted closed-shell model, while the calculations for the 6Brpca and Mn(II) complex were executed for the unrestricted open-shell model. So, the HOMO and LUMO orbitals were considered Dmdpy, and SOMO and SUMO orbitals were considered for 6Brpca and Mn(II) complex. The HOMO, LUMO, SOMO and SUMO for α- and β-spin MOs were provided in Fig. 7. The FMO energies and some related quantum chemical parameters were also provided in Table 5.

The highest occupied molecular orbital (HOMO) and the lowest unoccupied molecular orbital (LUMO) energies of Dmdpy are −6.5159 eV and −1.2079 eV, respectively, resulting in an energy gap (ΔE) of 5.3079 eV. This relatively large ΔE suggests that Dmdpy is a stable molecule with low reactivity. The chemical hardness (η) of Dmdpy is 2.6540 eV, indicating its resistance to deformation of the electron cloud, while its electronegativity (χ) is 3.8619 eV, and its electrophilic index (W) is 2.8097 eV. The chemical softness (S) is calculated to be 0.1884 eV^{-1}. For 6Brpca, the energies of the singly occupied molecular orbitals

Table 4
Selected experimental and theoretical vibrational wavenumbers (cm^{-1}) for [Mn(6Brpca)$_2$Dmdpy]·CH_3OH complex.

Assignments with potential energy distribution (PED)	FT IR	B3LYP/LanL2DZ	
ν OH (98 %)	3427	3287	732.05
ν CH (94 %)		3135	3.1628
ν CH (85 %)	3095	3095	6.9822
ν CH (89 %)	3059	3087	9.769
ν CH (96 %)	2969	2989	21.654
ν CH (100 %)	2915	2919	44.025
ν CH (99 %)		2881	99.814
ν CC (26 %)	1648	1594	106.09
ν CC (30 %)	1628	1590	5.3525
ν OC (64 %)	1609	1584	483.04
ν OC (46 %) + ν CC (12 %)	1578	1577	247.64
ν OC (22 %) + ν CC (18 %)	1547	1558	178.70
ν CC (20 %) + ν NC (22 %)		1524	26.703
β HCH (78 %)	1488	1466	7.2743
β HCH (100 %)	1433	1429	1.1870
β HCC (57 %) + β CCN (11 %)	1399	1405	19.561
ν NC (25 %) + β HCC (26 %)	1378	1389	0.7463
ν CC (10 %) + β HCC (20 %)	1355	1357	6.3188
β HCC (50 %)	1309	1304	7.4209
ν NC (11 %) + ν OC (23 %) + ν CC (14 %)	1291	1289	5.6286
ν NC (20 %) + ν OC (11 %) + ν CC (10 %) + β HCC (11 %)	1245	1273	184.02
ν NC (30 %) + ν OC (19 %) + ν CC (21 %)		1237	109.11
ν CC (30 %) + β HCC (28 %)	1204	1207	0.1230
β HCC (80 %)	1175	1174	6.3785
β HCC (80 %)	1155	1159	10.377
β HCC (29 %)	1122	1127	46.219
β HCC (37 %)	1111	1104	1.9087
β HCC (64 %)	1076	1082	7.0245
τ HCCC (55 %)	1051	1054	0.5921
τ HCCC (61 %) + τ CCCC (22 %) + τ NCCC (10 %)	1012	1006	1.3525
τ HCCC (80 %)	1010	1006	1.5223
τ HCCN (19 %) − τ HCCC (51 %) + τ CCNMn (15 %)	986	988	0.5707
τ HCCC (100 %)	918	937	0.9633
τ HCCN (24 %) − τ HCCC (56 %)	845	845	0.4681
τ HCCN (30 %) − τ HCCC (46 %)	824	841	68.073
β CNC (22 %)	719	728	8.1849
β CCN (56 %)	654	660	0.5957
ν MnN (12 %) + β CCC (30 %)	544	546	1.7370
γ CCCC (27 %) + γ CMnCN (12 %)	514	520	10.678
γ CMnCN (29 %)		455	4.5763
ν CC (24 %) + β NCC (14 %)	422	434	11.656
β CNMn (15 %) + β CCC (10 %)		394	3.1835

(SOMO and SUMO) are −7.9801 eV and −3.8399 eV, which gives ΔE of 4.1401 eV. This smaller energy gap compared to Dmdpy indicates higher reactivity. The η is 2.0701 eV, showing it is less hard compared to Dmdpy. The χ parameter for 6Brpca is 5.9100 eV, indicating a strong ability to attract electrons. The S parameter for 6Brpca is 0.2415 eV^{-1}. When considering the Mn(II) complex [Mn(6Brpca)$_2$Dmdpy]·CH_3OH, the SOMO and LUMO energy is −4.7379 eV and −2.3129 eV, with a ΔE of 2.4250 eV. This much smaller energy gap suggests that the complex is more reactive than the individual ligands. The η parameter for the Mn (II) complex is 1.2125 eV, reflecting a greater ease in electron cloud deformation compared to both Dmdpy and 6Brpca. The χ of the complex is 3.5254 eV, and W is 5.1251 eV. The S of the complex is higher at 0.4124 eV^{-1}, further indicating its increased reactivity. In summary, the frontier molecular orbital analysis shows that the Mn(II) complex [Mn(6Brpca)$_2$Dmdpy]·CH_3OH exhibits higher reactivity compared to its individual ligands, with a significantly smaller energy gap and greater chemical softness. These properties suggest that the complex may participate more readily in chemical reactions.

3.5. Uv–vis spectra

The UV–Vis spectrum of Mn(II) complexes containing pyridine-2-carboxylic acid exhibits electronic transitions such as ligand–ligand charge transfer (LLCT), ligand-to-metal charge transfer (LCMT), and d-d spin forbidden transitions [11,13,77,78]. The LMCT interactions occur in the Mn(II) complex, indicating the transfer of charge from the ligand to the metal ion or vice versa [11]. The UV–Vis spectrum also shows charge transfer bands and d-d spin forbidden transitions, which are characteristic of the electronic transitions in the Mn(II) complex [13]. The UV–Vis spectra for 6Brpca, Dmdpy, and Mn(II) complex were recorded in ethanol solvent at the range of 200–900 nm. Theoretical calculations using the B3LYP/LanL2DZ-CPCM method have been employed to support the experimental results, providing insights into the electronic structure, charge transfer, and nonlinear optical properties of the Mn(II) complex [11,13,78].

When examining the electronic absorption bands and wavelength values in the UV–Vis spectrum (Fig. 8), the experimental data of the [Mn(6Brpca)$_2$Dmdpy]·CH_3OH complex shows three main values where significant absorption bands are observed. According to Fig. 8, the electronic absorption bands at 206, 225 and 263 nm are observed at the experimental UV–Vis spectrum of Mn(II) complex. When it comes to the single ligands' spectra, 6Brpca has absorption bands at 207, 222 and 275 nm, Dmdpy has absorption bands at 209, 239, 281 nm. All of these absorption bands observed for 6Brpca, Dmdpy and Mn(II) complex are assigned as π → π* and n → π* transitions. Another very weak absorption band was observed at 307 nm in the experimental UV–Vis spectrum of Mn(II) complex is also assigned as metal–ligand charge transfer (MLCT) interaction. Table 6 demonstrates that the the lowest wavelength electronic absorption band is observed at a wavelength of 262.9 nm and characterized by an oscillator strength of 0.0270. Significant

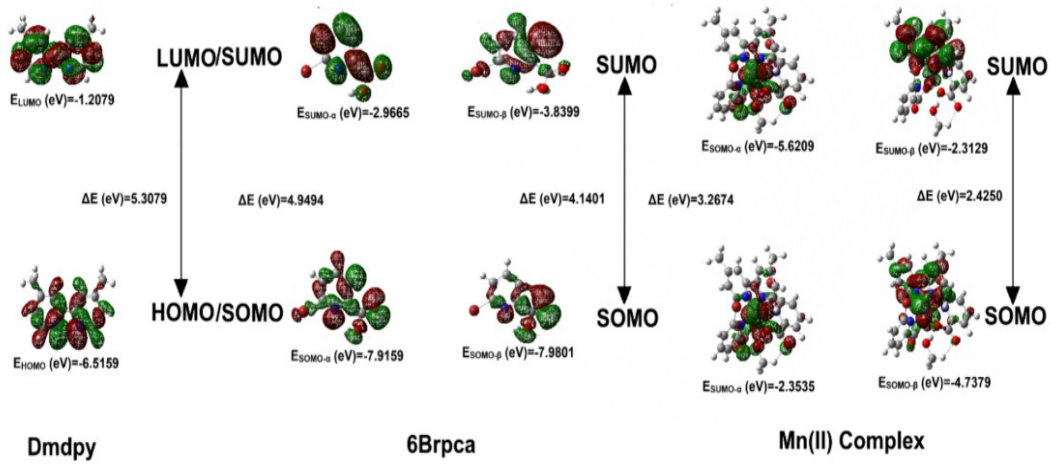

Fig. 7. Frontier molecular orbitals (FMOs) for [Mn(6Brpca)$_2$dmdpy]·CH_3OH complex.

Table 5
The chemical hardness (η), electronegativity (χ), electrophilic index (W), chemical softness (S), and FMO energy for 6Brpca and Dmdpy ligands, $Mn(6Brpca)_2Dmdpy]\cdot CH_3OH$ complex obtained by B3LYP/LanL2DZ levels.

Dmdpy Parameter		6Brpca Parameter	α spin	β −spin	$[Mn(6Brpca)_2Dmdpy]\cdot CH_3OH$		
					Parameter	α-spin	β −spin
E_{HOMO} (eV)	−6.5159	E_{SOMO} (eV)	−7.9159	−7.9801	E_{SOMO} (eV)	−5.6209	−4.7379
E_{LUMO} (eV)	−1.2079	E_{SUMO} (eV)	−2.9665	−3.8399	E_{SUMO} (eV)	−2.3535	−2.3129
ΔE (eV)	5.3079	ΔE (eV)	4.9494	4.1401	ΔE (eV)	3.2674	2.4250
χ (eV)	3.8619	χ (eV)	5.4411	5.9100	χ (eV)	3.9872	3.5254
η (eV)	2.6540	η (eV)	2.4747	2.0701	η (eV)	1.6337	1.2125
W(eV)	2.8097	W(eV)	5.9819	8.4366	W(eV)	4.8654	5.1251
$S(eV^{-1})$	0.1884	$S(eV^{-1})$	0.2020	0.2415	$S(eV^{-1})$	0.3060	0.4124

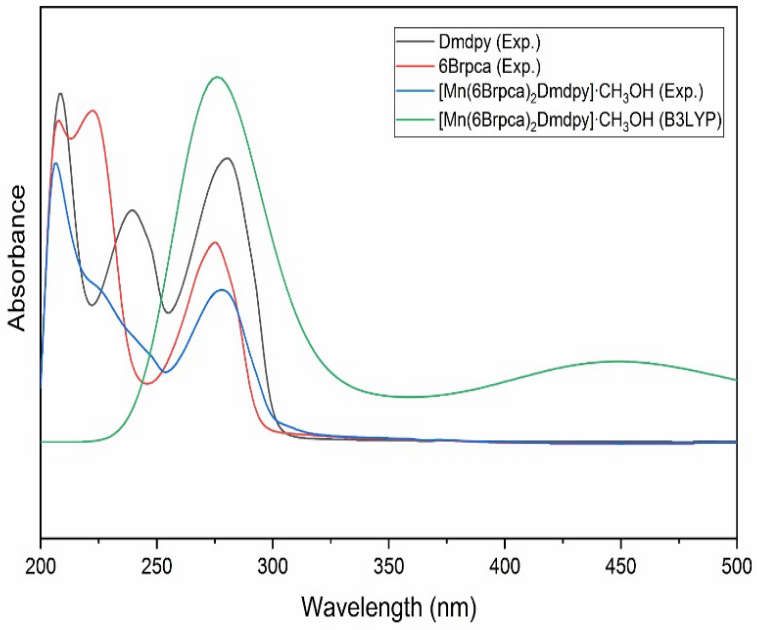

Fig. 8. Experimental and theoretical UV–Vis spectrum of $[Mn(6Brpca)_2Dmdpy]\bullet CH_3OH$ complex.

contributions to this absorption band include the transitions SOMO-7 → SUMO+1 β (40 %), SOMO-6 → SUMO+1 β (29 %). These transitions explain the high-energy absorption band in the complex's UV–Vis spectrum. According to Table 6, the highest intensity electronic absorption band for mixed ligand Mn(II) complex was calculated at 275.6 nm with the oscillator strength of 0.1151. This main theoretical absorption band is originated from the SOMO-2 → SUMO+5 α (31 %), SOMO-4 → SUMO+1 α (7 %) transitions.

The highest wavelength electronic absorption band for Mn(II) complex was found at 479.4 nm with the contributions of SOMO-1 → SUMO α (34 %), SOMO→SUMO+1 α (17 %).

Table 6
The theoretical electronic absorption wavelength, oscillator intensities, and significant contributions for the $[Mn(6Brpca)_2Dmdpy]\cdot CH_3OH$ complex.

λ (nm)	Oscillator str.	Important contr.
262.9	0.0270	SOMO 7 → SUMO+1 β (40 %), SOMO 6 → SUMO+1 β (29 %)
275.6	0.1151	SOMO 2 → SUMO+5 α (31 %), SOMO 4 → SUMO+1 α (7 %)
479.4	0.0341	SOMO-1 → SUMO α (34 %), SOMO→SUMO+1 α (17 %)

3.6. MEP surface

Molecular electrostatic potential (MEP) is a crucial property that helps in understanding the reactive behavior of molecules by examining the distribution of electrostatic potential around the investigated system. It also plays an important role in predicting how molecules interact with each other, particularly in biochemical systems [79]. MEP surface helps in understanding the reactivity, hydrogen bonding, and other properties of molecules [80]. Fig. 9 gives a 3D representation of the MEP surface for 6Brpca, Dmdpy, and Mn(II) complex, illustrating the distribution of electrostatic potential across the molecular surface to provide insights into reactive sites. The color scale ranges from $-9.729e^{-2}$ (the lowest negative potential) to $9.729e^{-2}$ (the highest positive potential), with red regions indicating high negative potential (electron-rich sites) where electrophiles are likely to attack, and blue regions indicating high positive potential (electron-deficient sites) where nucleophiles are likely to interact. When the MEP surfaces calculated for 6Brpca and Dmdpy ligands are examined, it is seen that there is a negative potential on the electron donor N and O atoms, represented by red color. So, it can be said that 6Brpca attack ligands attacks to the nucleophilic center (Mn(II) ion) through the nucleophile sides (O and N atoms). The red color in the MEP surface represents high electron density (electronegative potential), primarily on the non-coordinated O atoms in carboxylate groups. A less intense negative potential, represented by the yellow color, is

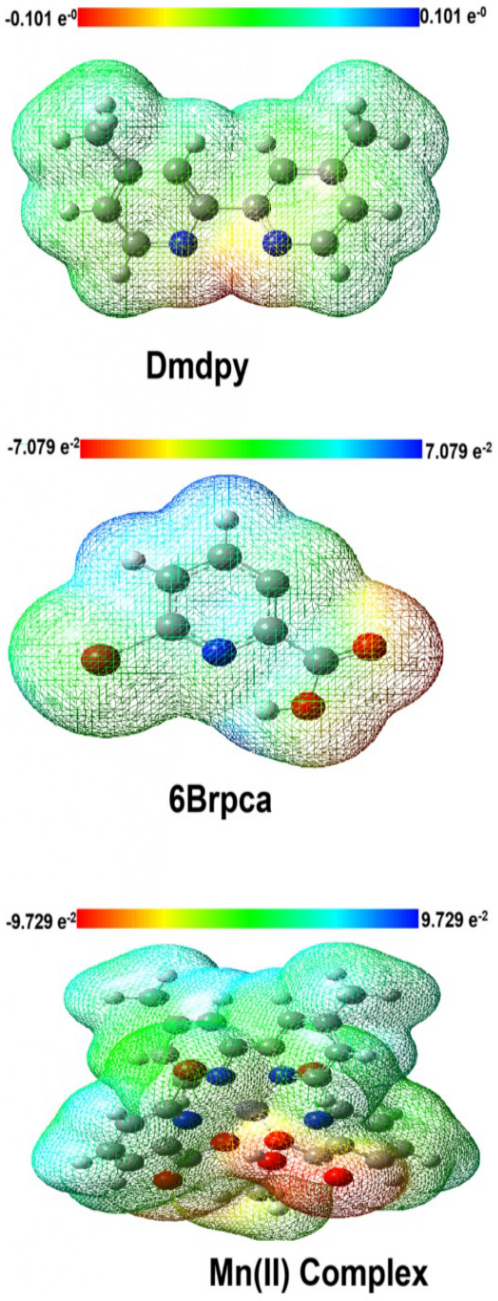

Fig. 9. 3D Molecular electrostatic potential for $[Mn(6Brpca)_2dmdpy]\cdot CH_3OH$ complex.

observed around the Br atoms in 6Brpca ligand. On the other hand, the blue color represents the low electron density (electropositive potential) around the methyl group protons and aromatic ring protons. These results indicate that Mn(II) complex could interact with other molecular systems through the O atoms in carboxylate groups, forming either hydrogen or covalent bonds. Similarly, Mn(II) complex could also interact with other molecular systems through the Br atoms and H atoms via H bonding interactions.

3.7. Natural bonding analysis

Natural bond orbitals (NBO) analysis is a method used in quantum chemistry calculations to study in detail the bond structures and electronic properties of molecules. It plays an important role in determining critical parameters such as the polarization of bonds, donor–acceptor interactions, and stabilization energies, which contribute to a deeper understanding [59,81,82]. To identify the coordination environment of the complex and its intermolecular interactions, NBO analysis was performed by using DFT levels B3LYP/LanL2DZ basis set. The calculated NBO analyses of the mixed ligand Mn(II) complex are presented in Table 7. The electronic configuration and calculated natural charge for the Mn(II) complex ion is [core]4S(0.20)3d(5.83)4p(0.44)4d(0.03)5p (0.01) and + 0.50446. After the formation of the complex, it is observed that the natural charge for the Mn(II) center ions decreases to a smaller value than that of the free ions. This result indicates that charge transfers also occur in the complex and even that these charge transfer interactions from ligand to metal are more dominant than those from metal to ligand [69,83]. The higher energy hyper-conjugative interactions of LP N/O→LP* Mn were also presented in Table 7. These high energy interactions also supports the six-coordinated distorted octahedral Mn(II) center, with the donor N and O atoms. Higher interaction energies represent more intense interactions, which means that bond lengths between interacting atoms are shorter than those of atoms with lower interaction energies. When we look carefully at Table 7, the hyper-conjugative interaction energies for LP(2) O3 → LP*(3) Mn, LP(2) O2 → LP*(3) Mn, LP(1) N2 → LP*(4) Mn, LP(1) N1 → LP*(4) Mn, LP(1) N4 → LP*(3) Mn and LP(1) N3 → LP*(3) Mn are calculated in the range of 17. 55, 23.77, 19.13, 20.8, 30.45 and 27 kcal/mol, respectively. These significant interaction energies are indicators that the donor coordinates to the metal center through N and O, as indicated by XRD analysis. NBO analysis could be also used to demonstrate the presence of H-bonding interaction in the investigated system. In the present study, the interaction of LP (1) O1 → σ*O25-OH25 with the interaction energy of 7.72 kcal/mol, demonstrates that there is a H-bonding interaction of O25—H25···O1.

3.8. Static NLO properties

The incorporation of metal ions into organic ligands allows for control over the first- and second-order hyperpolarizabilities, making these complexes valuable candidates for NLO applications [71]. To evaluate the changes in the NLO properties with the incorporation of Mn (II) metal ion to the 6Brpca and Dmbpy ligands, the dipole moment (μ), polarizability (α), anisotropy of polarizability (Δα), first-order hyperpolarizability (β) and second-order hyperpolarizability (γ) parameters were calculated for the ligands and the Mn(II) complex with the B3LYP/LanL2DZ level. The obtained μ, α, Δα, β, and γ parameters in the absence of an external electromagnetic field were provided in Table 8. The μ parameter for Dmdpy, 6Brpca and Mn(II) complex were calculated as 4.5244, 6.4652 and 11.878 Debye, respectively. Similarly, the β parameters were also obtained as 0.1801×10^{-30}, 3.5792×10^{-30} and 62.498×10^{-30} esu, respectively. In a previous study, it was reported that the incorporation of Mn(II) and Zn(II) to Bis(4-(triazol-5-yl) phenyl)-diazene does not have a clear effect on NLO properties, while the incorporation of Cd(II) markedly changed the nonlinear optical properties [84]. The present study demonstrated that the incorporation of Mn(II) ion to the ligands increased the dipole moment and first- and second-order hyperpolarizability parameters (β, γ). The main disadvantage of metal complexes containing pyridine-2-carboxylic acid derivatives in terms of nonlinear optical properties, especially the first-order hyperpolarizability parameter, is that their dipole moment value is quite low due to their high symmetry and therefore, their NLO properties are low. Bensbaa et al. reported that the β parameters for the centrosymmetric Co(II) and Cd(II) complexes were calculated as 0.0002 $\times 10^{-30}$ esu. The incorporation of a second neutral ligand, such as the Dmdpy ligand, into transition metal complexes containing pyridine-2-carboxylic acid provides additional flexibility in the charge transfer transitions between the metal and ligands and a longer conjugated

Table 7
High-energy interactions obtained by the B3LYP method for the Mn(6Brpca)2Dmdpy]·CH3OH the complex.

Type	Bond	Type	Antibond	E^2(kcal/mol)	$E(j)-E(i)^b$(a.u)	$F(i,j)^a$(a.u)
LP (2)	O2	LP*(3)	Mn	23.77	0.39	0.132
LP (1)	N1	LP*(4)	Mn	20.8	0.32	0.107
LP (1)	N4	LP*(3)	Mn	30.45	0.29	0.128
LP (1)	N3	LP*(3)	Mn	27	0.29	0.121
LP (2)	O3	LP*(3)	Mn	17.55	0.4	0.116
LP (1)	N2	LP*(4)	Mn	19.13	0.32	0.104
LP (3)	O3	π*	O4-C7	33.8	0.27	0.121
LP (2)	O4	σ*	O3-C7	12.33	0.65	0.115
LP (1)	C10	π*	C12-C11	38.2	0.12	0.108
LP (3)	O1	π*	O2-C1	35.35	0.27	0.123
LP (2)	O2	σ*	O1-C1	12.18	0.65	0.114
LP (1)	C3	π*	N1-C2	84.2	0.08	0.123
π	N2-C8	LP*(1)	C9	13.27	0.2	0.08
π	N2-C8	π*	C12-C11	12.4	0.32	0.08
π	C12 C11	LP* (1)	C10	23.47	0.16	0.092
π	N1-C2	LP (1)	C3	12.74	0.21	0.079
π	N1 C2	π*	C6-C5	12.28	0.32	0.081
π	C5 C6	LP*(1)	C4	24.31	0.16	0.093
π	N4-C19	π*	C23-C22	11.01	0.34	0.078
π	N3 C18	π*	C13-C14	11.01	0.34	0.078
π	C20-C21	π*	N4-C23	16.21	0.23	0.082
π	C17 –C15	π*	N3-C13	16.19	0.23	0.082
π	C23 C22	π*	C21 C20	11.21	0.29	0.072
π	C13-C14	π*	C17 –C15	11.23	0.29	0.072
LP (1)	O1	σ*	O25-OH25	7.72	0.99	0.112

Table 8
The dipole moment (Debye), static polarizability ($\times10^{-23}$esu), anisotropy of polarizability ($\times10^{-23}$esu), first-order hyperpolarizability ($\times10^{-30}$esu), and second-order hyperpolarizability (10^{-36} esu) of the Dmdpy and 6Brpca ligands, [Mn(6Brpca)$_2$Dmdpy]·CH$_3$OH complex obtained by using B3LYP/LanL2DZ levels.

Parameter	Dmdpy	6Brpca	Mn(II) Complex
μ (Debye)	4.5244	6.4652	11.878
α (0;0)	2.0392	1.1007	5.1914
Δα (0;0)	1.5469	1.5028	0.5133
β (0;0,0)	0.1801	3.5792	62.498
γ (0;0,0,0)	15.006	6.1678	387.88

pathway through which electrons can move freely, resulting in a higher NLO response [20,85]. When it comes to the γ parameter, the highest magnitude of γ was obtained for the Mn(II) complex, demonstrating that there is a dramatic increment after the complex formation.

3.9. Frequency-dependent NLO properties

The radiation frequency has a significant effect on the first- and second-order hyperpolarizabilities (β and γ) of metal complexes, with valance electrons of transition metals being more efficient in enhancing the magnitude of first- and second-order hyperpolarizabilities. Moreover, frequency-dependent hyperpolarizability is crucial for the development of nonlinear optical (NLO) materials with applications in electro-optical devices and optical communications [56,71,72,86]. The frequency-dependent NLO properties for Mn(II) complex were calculated by using B3LYP/LanL2DZ level in the external electrical fields (ω = 0.085628 and 0.042814 au.). The obtained results are presented Table 9.

Table 9 demonstrates the enhancement of frequency-dependent NLO parameters depending on the applied external electric field. Table 9 also demonstrates that the frequency-dependent β and γ values for the Mn(II) complex are dramatically higher than the corresponding static NLO parameters. In general, the β and γ parameters for 6Brpca and Dmdpy ligands are calculated higher at the frequency of 0.085628 a.u. than those obtained at 0.042814 au. The electro-optic Pockel's effect (EOPE) β(ω;ω,0) for Mn(II) complex was calculated as 15128 × 10^{-30} and 6125.8 × 10^{-30} esu at the frequency of 0.085628 and 0.042814 au., respectively. The electric field-induced second harmonic generation (ESHG) β(−2ω;ω,ω) parameter for Mn(II) complex was also calculated as 5663.8 × 10^{-30} and 11448 × 10^{-30} esu, respectively. In a previous study, the frequency-dependent γ (−2ω;ω,ω,0) values at ω = 0.042827 a.u. for Fe(II) and Ru(II) complexes were reported at the range of 54.369–212.420 × 10^{-30} esu. [17]. For the second-order hyperpolarizability (γ), the dc-Kerr effect γ(−ω;ω,0,0) and second harmonic generation γ(−2ω;ω,ω,0) were calculated for Mn(II) complex. Table 9 demonstrates that the magnitude of γ(−ω;ω,0,0) parameter at the frequency of 0.085628 a.u., calculated as −360157 × 10^{-36} esu, higher than the corresponding data (314140 × 10^{-36} esu) calculated at 0.042814 au. As in first-order hyperpolarizability, the magnitude of second harmonic generation γ (−2ω;ω,0,0) calculated as 680035 × 10^{-36} esu at the frequency of 0.042814 au. is higher than that calculated at the frequency of 0.085628 a.u. Considering especially β(−2ω;ω,ω) and γ (−2ω;ω,ω,0) values calculated for previously reported metal–organic coordination complexes [17,87–90], it is concluded that the Mn(II)

Table 9
The dipole moment (debye), frequency-dependent polarizability ($\times10^{-23}$esu), anisotropy of polarizability ($\times10^{-23}$esu), first-order hyperpolarizability ($\times10^{-30}$esu), second-order hyperpolarizability ($\times10^{-36}$ esu) for [Mn(6Brpca)$_2$Dmdpy]·CH$_3$OH, Dmdpy ligand and 6Brpca ligand obtained by B3LYP/LanL2DZ levels.

Parameter	Dmdpy 0.085628 a.u	Dmdpy 0.042814 au	6Brpca 0.085628 a.u	6Brpca 0.042814 au	Mn(II) Complex 0.085628 a.u	Mn (II) Complex 0.042814 au
α (−ω;0)	2.1783	2.0705	1.3613	1.2898	644.92	7.6019
Δα (−ω;0)	1.7601	1.5937	1.3964	1.3015	1917.8	2.2825
β(−ω;ω,0)	0.3909	0.3495	8.3178	6.2795	15,128	6125.8
β(−2ω;ω,ω)	0.4005	0.0243	34.512	34.514	5663.8	11,448
γ (−ω;ω,0,0)	28.307	19.865	22.234	11.987	−360157	314,140
γ (−2ω;ω,ω,0)	206.41	25.475	−321.77	16.609	153,776	680,035

complex examined in this study is a very promising candidate for second- and third-order NLO applications (see in Fig. 10).

4. Conclusion

A novel mixed ligand [Mn(6Brpca)$_2$Dmdpy]·CH_3OH complex of 6-Bromopyridine-2-carboxylic acid (6Brpca) and 4,4′-dimethyl-2,2′-dipyridyl has been prepared. The coordination sphere around the central Mn(II) ion was defined as a distorted octahedron. Experimental and theoretical IR spectra also demonstrated that 6Brpca and Dmdpy ligands coordinate to central Mn(II) ion as bidentate ligands, forming five-membered chelate rings. UV–Vis spectra recorded for 6Brpca and Dmdpy ligands only have $\pi \rightarrow \pi^*$ and $n \rightarrow \pi^*$ transitions, while that for mixed ligand Mn(II) complex has additional ligand to metal charge transfer (LMCT) at 307 nm. FMO energies for the ligands and Mn(II) complex have demonstrated that the lowest energy gap is found as

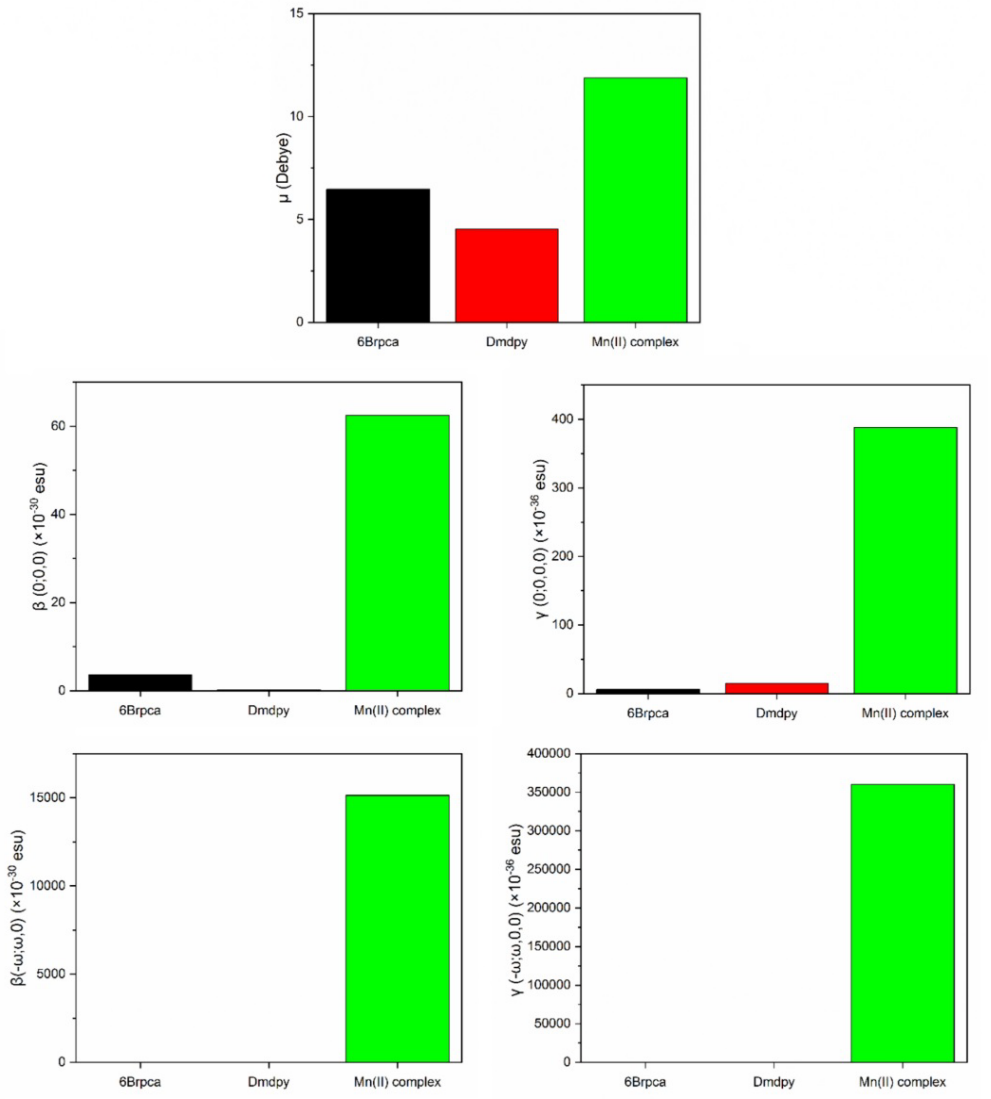

Fig. 10. Graphical representation of the changes in the parameters μ, β (0;0,0), γ (0;0,0,0), β(−ω;ω,0) and γ (−ω;ω,0,0) of the 6Brpca, Dmdpy and Mn(II) complex.

3.2674 eV for Mn(II) complex. So, the mixed ligand Mn(II) complex is more reactive than the free 6Brpca and Dmdpy ligands. In order to examine the difference in the first- and second-order hyperpolarizability for 6Brpca, Dmdpy, and Mn(II) complex, static and frequency-dependent β and γ parameters were calculated. The highest static β (0;0,0) and γ (0;0,0,0) parameters were obtained for the mixed ligand Mn(II) complex as 62.498 × 10^{-30} esu and 387.88 × 10^{-36} esu, respectively. When it comes to the frequency-dependent NLO parameters, γ (−2w;w,w,0) parameter was calculated at 680035 × 10^{-36} esu, 16.609 × 10^{-36} esu and 25.475 × 10^{-36} esu for Mn(II) complex, 6Brpca and Dmdpy ligand, respectively. It was concluded that the Mn(II) complex under investigation especially is a potential candidate for second- and third-order NLO applications.

Funding

This work was supported by the Scientific Research Projects Unit of Sakarya University (Project number: 2023–19–44–48).

Declaration of competing interest

The authors declare that they have no known competing financial interests or personal relationships that could have appeared to influence the work reported in this paper.

Data availability

Data will be made available on request.

References

[1] A. Nandy, C. Duan, M.G. Taylor, F. Liu, A.H. Steeves, H.J. Kulik, Computational discovery of transition-metal complexes: from high-throughput screening to machine learning, Chem. Rev. 121 (2021) 9927–10000.
[2] H.A. Nadeem, M. Imran, S. Saleem, Z. Rafiq, A. Batool, K. Mehmood, M. Pervaiz, S. Hussain, Z. Saeed, U. Younas, GO-Ag-NPs as a promising agent for biomedical, catalytic, electrochemical detection and water treatment technologies; a comprehensive review, Z. Phys. Chem. 237 (2023) 1013–1076.
[3] S. Ranganatha, S. Supriya, D. Ramakrishna, Metal-centric organic compounds: boon to third order nonlinear optical applications, Rev. Inorg. Chem. (2023).
[4] D. Avcı, Ö. Özge, F. Sönmez, A. Başoğlu, Ö. Tamer, Y. Atalay, Novel schiff base-azide metal complexes: Synthesis, spectral, nonlinear optics, and DFT studies, Mater. Sci. Semicond. Process. 179 (2024) 108523.
[5] F. Ahsan, K. Ayub, Transition metalides based on facially polarized all-cis-1, 2, 3, 4, 5, 6 hexafluorocyclohexane–a new class of high performance second order nonlinear optical materials, Phys. Chem. Chem. Phys. 25 (2023) 4732–4742.
[6] H. Li, M. Diao, D.W. Boukhvalov, Y. Ke, M.G. Humphrey, C. Zhang, Z. Huang, Prominent Nonlinear Optical Absorption in SnS2-Based Hybrid Inorganic-Organic Superlattice, Adv. Funct. Mater. 2400077 (2024).
[7] X. Chen, K.M. Ok, Metal oxyhalides: an emerging family of nonlinear optical materials, Chem. Sci. 13 (2022) 3942–3956.
[8] L. Cheng, X. Lü, M. Li, L. Zhang, H. Hou, Study on third-order nonlinear optical properties of functional complexes, Prog. Chem. 25 (2013) 1625.
[9] S.D. Bella, Second-order nonlinear optical properties of transition metal complexes, Chem. Soc. Rev. 30 (2001) 355–366.
[10] J.P. Morrall, G.T. Dalton, M.G. Humphrey, M. Samoc, Organotransition metal complexes for nonlinear optics, Adv. Organomet. Chem. 55 (2007) 61–136.
[11] Ö. Tamer, D. Avcı, Y. Atalay, B. Çoşut, Y. Zorlu, M. Erkovan, Y. Yerli, Synthesis, crystal structure, spectroscopic characterization and nonlinear optical properties of manganese (II) complex of picolinate: A combined experimental and computational study, J. Mol. Struct. 1106 (2016) 98–107.
[12] P.J. Mendes, T.J. Silva, A.P. Carvalho, J.P. Ramalho, DFT studies on thiophene acetylide Ru (II) complexes for nonlinear optics: structure–function relationships and solvent effects, J. Mol. Struct. (Thoechem) 946 (2010) 33–42.
[13] Ö. Tamer, A unique manganese (II) complex of 4-methoxy-pyridine-2-carboxylate: Synthesis, crystal structure, FT-IR and UV–Vis spectra and DFT calculations, J. Mol. Struct. 1144 (2017) 370–378.
[14] Ö. Tamer, D. Avcı, Y. Atalay, Synthesis, crystal structure, spectroscopic characterization and nonlinear optical properties of Co (II)-picolinate complex, Mater. Chem. Phys. 168 (2015) 138–146.
[15] Ö. Tamer, D. Avcı, Y. Atalay, A novel Cu (ii) complex of picolinate and 1, 10 phenanthroline: Preparation, crystal structure determination, spectroscopic characterization and nonlinear optical studies, J. Inorg. Organomet. Polym Mater. 27 (2017) 700–713.
[16] Ö. Tamer, D. Avcı, N. Dege, Y. Atalay, Synthesis, crystal structure, photophysical properties, density functional theory calculations and molecular docking studies on Cd (II) complex of 4, 4′-dimethyl-2, 2′-dipyridyl, J. Mol. Struct. 1202 (2020) 127288.
[17] S. Taboukhat, N. Kichou, J.-L. Fillaut, O. Alévêque, K. Waszkowska, A. Zawadzka, A. El-Ghayoury, A. Migalska-Zalas, B. Sahraoui, Transition metals induce control of enhanced NLO properties of functionalized organometallic complexes under laser modulations, Sci. Rep. 10 (2020) 15292.
[18] S. Das, A. Jana, V. Ramanathan, T. Chakraborty, S. Ghosh, P.K. Das, P. K. Bharadwaj, Design and synthesis of 1, 10 phenanthroline based Zn (II) complexes bearing 1D push-pull NLO-phores for tunable quadratic nonlinear optical properties, J. Organomet. Chem. 691 (2006) 2512–2516.
[19] S. Ayaz, A. Uzer, Y. Dilgin, M.R. Apak, Fabrication of a novel optical glucose biosensor using Copper (II) neocuproine as a chromogenic oxidant and glucose dehydrogenase immobilized magnetite nanoparticles, ACS Omega 8 (2023) 47163–47172.
[20] Ö. Tamer, H. Mahmoody, K.F. Feyzioğlu, O. Kılınç, D. Avci, O. Orun, N. Dege, Y. Atalay, Synthesis of the first mixed ligand Mn (II) and Cd (II) complexes of 4 methoxy-pyridine-2-carboxylic acid, molecular docking studies and investigation of their anti-tumor effects in vitro, Appl. Organomet. Chem. 34 (2020) e5416.
[21] Ö. Tamer, S.A. Tamer, Ö. İdil, D. Avcı, H. Vural, Y. Atalay, Antimicrobial activities, DNA interactions, spectroscopic (FT-IR and UV-Vis) characterizations, and DFT calculations for pyridine 2 carboxylic acid and its derivates, J. Mol. Struct. 1152 (2018) 399–408.
[22] Ö. Tamer, H. Mahmoody, K. Feyzioğlu, O. Kılınç, D. Avci, O. Orun, N. Dege, Y. Atalay, Synthesis of the first mixed ligand Mn (II) and Cd (II) complexes of 4-methoxy-pyridine-2-carboxylic acid, molecular docking studies and investigation of their anti-tumor effects in vitro: First mixed ligand complexes of 4-methoxy-pyridine 2 carboxylic ac, Appl. Organomet. Chem. 34 (2019) e5416.
[23] N.E.A. El-Gamel, G.G. Mohamed, Synthesis, spectral and thermal characterization of 6-hydroxymethyl pyridine-2-carboxylic acid methyl ester and its complexes, J. Therm. Anal. Calorim. 81 (2005) 111–118.
[24] K.S. Małecki J. G., Maroń A.,Penkala M., Synthesis, molecular, spectroscopic and catalytic characterization of ruthenium(II) complexes with pyridine 2 carboxylic acid derivatives ligands, Polyhedron, 48 (2012) 21-30.
[25] H. Vural, M. Orbay, Synthesis, crystal structure, spectroscopic investigations and DFT calculations of the copper(II) complex of 4 (Trifluoromethyl)pyridine 2 carboxylic acid, J. Mol. Struct. 1146 (2017).
[26] M. Şimşek, Ö. Tamer, N. Dege, D. Avcı, H. Mahmoody, Y. Atalay, A new mixed ligand zinc(II) complex of 3-hydroxy and 4-chloro substituted pyridine-2-carboxylic acid: Synthesis, characterization, NLO Properties and DFT Calculation, Materials Today Communications 38 (2024) 108021.
[27] B. Li, J. Wang, H. Song, H. Wu, X. Chen, X. Ma, Synthesis, crystal structure, and BSA interaction with a new Co(II) complex based on 5 (trifluoromethyl)pyridine 2 carboxylic acid, J. Coord. Chem. 72 (2019) 2562–2573.
[28] D.A. Sümeyye Altürk , Ömer Tamer , Yusuf Atalay , Onur Şahin A cobalt (II) complex with 6-methylpicolinate: Synthesis, characterization, second- and third-order nonlinear optical properties, and DFT calculations, Journal of Physics and Chemistry of Solids, 98 (2016) 71 80.
[29] S. Altürk, D. Avcı, A. Başoğlu, Ö. Tamer, Y. Atalay, N. Dege, Copper(II) complex with 6-methylpyridine-2-carboxylic acid: Experimental and computational study on the XRD, FT-IR and UV–Vis spectra, refractive index, band gap and NLO parameters, Spectrochim. Acta A Mol. Biomol. Spectrosc. 190 (2018) 220–230.
[30] D. Avcı, S. Altürk, F. Sönmez, Ö. Tamer, A. Başoğlu, Y. Atalay, B.Z. Kurt, N. Dege, Three novel Cu(II), Cd(II) and Cr(III) complexes of 6–Methylpyridine–2–carboxylic acid with thiocyanate: Synthesis, crystal structures, DFT calculations, molecular docking and α-Glucosidase inhibition studies, Tetrahedron 74 (2018) 7198–7208.
[31] D. Avcı, S. Altürk, F. Sönmez, Ö. Tamer, A. Başoğlu, Y. Atalay, B.Z. Kurt, N. Dege, Novel Cu(II), Co(II) and Zn(II) metal complexes with mixed-ligand: Synthesis, crystal structure, α-glucosidase inhibition, DFT calculations, and molecular docking, J. Mol. Struct. 1197 (2019) 645–655.
[32] D. Avcı, S. Altürk, F. Sönmez, Ö. Tamer, A. Başoğlu, Y. Atalay, B. Zengin Kurt, N. Dege, Novel metal complexes containing 6-methylpyridine-2-carboxylic acid as potent α glucosidase inhibitor: synthesis, crystal structures, DFT calculations, and molecular docking, Mol. Divers. 25 (2021) 171–189.
[33] N. Dege, Ö. Tamer, M. Şimşek, D. Avcı, M. Yaman, A. Başoğlu, Y. Atalay, Experimental and theoretical approaches on structural, spectroscopic (FT-IR and UV-Vis), nonlinear optical, and molecular docking analyses for Zn (II) and Cu (II) complexes of 6-chloropyridine-2 carboxylic acid, Appl. Organomet. Chem. 36 (2022) e6678.
[34] N. Dege, Ö. Özge, D. Avcı, A. Başoğlu, F. Sönmez, M. Yaman, Ö. Tamer, Y. Atalay, B. Zengin Kurt, Concentration effects on optical properties, DFT, crystal characterization and α-glucosidase activity studies: Novel Zn(II) complex, Spectrochim. Acta A Mol. Biomol. Spectrosc. 262 (2021) 120072.
[35] N. Dege, Ö. Tamer, M. Yaman, A. Başoğlu, D. Avcı, Y. Atalay, Crystallographic, spectroscopic, thermal, optical investigations and density functional theory calculations for novel Co(II) and Mn(II) complexes, Appl. Phys. A 127 (2021) 132.
[36] D. Avcı, Y. Saeedi, A. Başoğlu, N. Dege, S. Altürk, Ö. Tamer, Y. Atalay, Novel Mn(II) and Zn(II) complexes of 6-bromopicolinic acid as a potential optical material: Synthesis, spectral characterizations, linear, and nonlinear optical properties and density functional theory calculations, Appl. Organomet. Chem. 35 (2021) e6125.
[37] D. Avcı, Y. Saeedi, A. Başoğlu, N. Dege, S. Altürk, Ö. Tamer, Y. Atalay, Novel Mn (II) and Zn (II) complexes of 6-bromopicolinic acid as a potential optical material: Synthesis, spectral characterizations, linear, and nonlinear optical properties and density functional theory calculations, Appl. Organomet. Chem. 35 (2021) e6125.
[38] C. Stoe, X-area (version 1.18) and X-red32 (version 1.04), Stoe & Cie, Darmstadt, Germany, 2002.

[39] G.M. Sheldrick, SHELXT–Integrated space-group and crystal-structure determination, Acta Crystallographica Section A: Foundations and Advances 71 (2015) 3–8.
[40] G.M. Sheldrick, Crystal structure refinement with SHELXL, Acta Crystallographica Section C, Struct. Chem. 71 (2015) 3–8.
[41] C.F. Macrae, P.R. Edgington, P. McCabe, E. Pidcock, G.P. Shields, R. Taylor, M. Towler, J. Streek, Mercury: visualization and analysis of crystal structures, J. Appl. Crystallogr. 39 (2006) 453–457.
[42] A. Spek, Single-crystal structure validation with the program PLATON, J. Appl. Crystallogr. 36 (2003) 7–13.
[43] L.J. Farrugia, WinGX and ORTEP for Windows: an update, J. Appl. Crystallogr. 45 (2012) 849–854.
[44] S.P. Westrip, publCIF: software for editing, validating and formatting crystallographic information files, J. Appl. Crystallogr. 43 (2010) 920–925.
[45] M.e. Frisch, G. Trucks, H.B. Schlegel, G. Scuseria, M. Robb, J. Cheeseman, G. Scalmani, V. Barone, G. Petersson, H. Nakatsuji, Gaussian 16, in, Gaussian, Inc. Wallingford, CT, 2016.
[46] R. Dennington, T.A. Keith, J.M. Millam, GaussView 6.0. 16, Semichem Inc.: Shawnee Mission, KS, USA, (2016) 143-150.
[47] A.D. Becke, Density-functional thermochemistry. I. The effect of the exchange-only gradient correction, J. Chem. Phys. 96 (1992) 2155–2160.
[48] C. Lee, W. Yang, R.G. Parr, Development of the Colle-Salvetti correlation-energy formula into a functional of the electron density, Phys. Rev. B 37 (1988) 785.
[49] P.J. Hay, W.R. Wadt, Ab initio effective core potentials for molecular calculations, Potentials for the Transition Metal Atoms Sc to Hg, the Journal of Chemical Physics 82 (1985) 270–283.
[50] R.D. Johnson III, NIST 101. Computational chemistry comparison and benchmark database, (1999).
[51] M.H. Jamróz, Vibrational energy distribution analysis (VEDA): scopes and limitations, Spectrochim. Acta A Mol. Biomol. Spectrosc. 114 (2013) 220–230.
[52] V. Barone, M. Cossi, Quantum calculation of molecular energies and energy gradients in solution by a conductor solvent model, Chem. A Eur. J. 102 (1998) 1995–2001.
[53] M. Cossi, N. Rega, G. Scalmani, V. Barone, Energies, structures, and electronic properties of molecules in solution with the C-PCM solvation model, J. Comput. Chem. 24 (2003) 669–681.
[54] S. Gorelsky, SWizard program, University of Ottawa, Ottawa, Canada, 2010.
[55] P.R. Spackman, M.J. Turner, J.J. McKinnon, S.K. Wolff, D.J. Grimwood, D. Jayatilaka, M.A. Spackman, CrystalExplorer: a program for Hirshfeld surface analysis, visualization and quantitative analysis of molecular crystals, J. Appl. Crystallogr. 54 (2021) 1006–1011.
[56] D. Avcı, H.E. Cömert, F. Sönmez, N. Dege, Ö. Tamer, Y. Atalay, Comparative assessment of structure–property relationships of new Cu (II) complex in selected density functionals, Spectrochim. Acta A Mol. Biomol. Spectrosc. 305 (2024) 123489.
[57] A.A. Baroud, L.E. Mihajlović-Lalić, N. Gligorijević, S. Aranđelović, D. Stanković, S. Radulović, K. Van Hecke, A. Savić, S. Grgurić Šipka, Ruthenium (II) bipyridine complexes: from synthesis and crystal structures to electrochemical and cytotoxicity investigation, J. Coord. Chem. 70 (2017) 831–847.
[58] B.-M. Kukovec, Z. Popović, B. Kozlevčar, Z. Jagličić, 3D supramolecular architectures of copper (II) complexes with 6-methylpicolinic and 6-bromopicolinic acid: synthesis, spectroscopic, thermal and magnetic properties, Polyhedron 27 (2008) 3631–3638.
[59] Ö. Tamer, 2-Piridinkarboksilik Asit İçeren Bazı Geçiş Metal Komplekslerinin Sentezi, Yapılarının Analizi Ve Doğrusal Olmayan Optik Özelliklerinin İncelenmesi, (2016) 224.
[60] A. Pekparlak, S.D. Tamer, N. Kanmazalp, M. Berber, D. Arslan, N. Avcı, E. Dege, Y. Tarcan, Atalay, Crystal structure, spectroscopic (FT-IR, 1H and 13C NMR) characterization and density functional theory calculations on Ethyl 2-(dichloromethyl)-4-methyl-1-phenyl-6-thioxo-1,6-dihydropyrimidine-5-carboxylate, J. Mol. Struct. 1171 (2018) 762–770.
[61] M. Bensebaa, M. Boukelkoul, Ö. Tamer, Y. Atalay, D. Avcı, Theoretical Investigation of Structural, Spectroscopic (IR, 1H and 13C NMR), Static, and Frequency-Dependent Nonlinear Optical Properties of 4-[(1E)-3-(4-Methoxyphenyl)-3-Oxoprop-1-en-1-yl]Phenyl 4-Methylbenzene-1-Sulfonate, Polycyclic Aromatic Compounds, 1 19.
[62] P. Akhileshwari, K.R. Kiran, M.A. Sridhar, M.P. Sadashiva, Crystal structure elucidation, Hirshfeld surface analysis, and DFT studies of a N benzyl 3-phenylquinoxalin-2-amine, J. Mol. Struct. 1253 (2022).
[63] P.R. Spackman, M.J. Turner, J.J. McKinnon, S.K. Wolff, D.J. Grimwood, D. Jayatilaka, M.A. Spackman, {\it CrystalExplorer}: a program for Hirshfeld surface analysis, visualization and quantitative analysis of molecular crystals, J. Appl. Crystallogr. 54 (2021) 1006–1011.
[64] Ö. Tamer, N. Dege, D. Avcı, Y. Atalay, The static and frequency-dependent second- and third-order nonlinear optical properties of Zn(II) and Ni(II) complexes of 4-methoxypyridine 2 carboxylic acid: A detailed experimental and theoretical study, Applied Organometallic Chemistry, n/a e7206.
[65] A. Kumar, V. Hüch, V.J. Ram, Partially reduced thiochromene based oxathiahelicenes: crystallographic, computational and Hirschfeld surface analyses, CrstEngComm 15 (2013) 7019–7030.
[66] N.Q. Shikhaliyev, S.T. Çelikesir, M. Akkurt, K.N. Bagirova, G.T. Suleymanova, F. A. Toze, Crystal structure and Hirshfeld surface analysis of (E)-1-(4-chlorophenyl)-2 [2, 2 dichloro-1 (4 fluorophenyl) ethenyl] diazene, Acta Crystallographica Section E: Crystallographic, Communications 75 (2019) 465–469.
[67] R. Yadav, M. Trivedi, G. Kociok Köhn, R. Prasad, A. Kumar, New Ni (II) 1, 2 bis (diphenylphosphino) ethane dithiolates: crystallographic, computational and Hirshfeld surface analyses, CrstEngComm 17 (2015) 9175–9184.
[68] M. Pervaiz, I. Ahmad, M. Yousaf, S. Kirn, A. Munawar, Z. Saeed, A. Adnan, T. Gulzar, T. Kamal, A. Ahmad, Synthesis, spectral and antimicrobial studies of amino acid derivative Schiff base metal (Co, Mn, Cu, and Cd) complexes, Spectrochim. Acta A Mol. Biomol. Spectrosc. 206 (2019) 642–649.
[69] N. Dege, Ö. Tamer, M. Yaman, A. Başoğlu, D. Avcı, Y. Atalay, Crystallographic, spectroscopic, thermal, optical investigations and density functional theory calculations for novel Co (II) and Mn (II) complexes, Appl. Phys. A 127 (2021) 1–17.
[70] P.A. Ajibade, G.A. Kolawole, P. O'Brien, M. Helliwell, J. Raftery, Cobalt (II) complexes of the antibiotic sulfadiazine, the X-ray single crystal structure of [Co (C10H9N4O2S) 2 (CH3OH) 2], Inorg. Chim. Acta 359 (2006) 3111–3116.
[71] M. Şimşek, Ö. Tamer, N. Dege, D. Avcı, H. Mahmoody, Y. Atalay, A new mixed-ligand zinc (II) complex of 3-hydroxy and 4-chloro substituted pyridine-2-carboxylic acid: Synthesis, characterization, NLO Properties and DFT Calculation, Materials Today Communications 38 (2024) 108021.
[72] M. Bensbaa, M. Şimşek, F. Derin, Ö. Tamer, N. Dege, D. Avcı, M. Boukelkoul, Y. Atalay, Influence of Co (II) and Cd (II) Metal Ions on Structural, Electronic and Nonlinear Optical Properties of 4-methoxypyridine-2-carboxylic Acid Complexes: An Experimental and Computational Study, Mater. Today Commun. 109403 (2024).
[73] R. Arivazhagan, C. Sridevi, A. Prakasam, Quantum computational, spectroscopic and molecular docking studies of potent tuberculosis drug 2, 6 dihydroxypyridine-4-carboxylic acid and 2-hydroxy-6-methylpyridine-4-carboxylic acid, J. Mol. Struct. 1250 (2022) 131895.
[74] H. Vural, A novel copper (II) complex containing pyrimidine-4-carboxylic acid: Synthesis, crystal structure, DFT studies, and molecular docking, J. Mol. Struct. 1265 (2022) 133390.
[75] A. Nataraj, V. Balachandran, T. Karthick, M. Karabacak, A. Atac, FT-Raman, FT-IR, UV spectra and DFT and ab initio calculations on monomeric and dimeric structures of 3, 5-pyridinedicarboxylic acid, J. Mol. Struct. 1027 (2012) 1–14.
[76] N. Sundaraganesan, C. Meganathan, B. Anand, B.D. Joshua, C. Lapouge, Vibrational spectra and assignments of 2 amino 5 iodopyridine by ab initio Hartree-Fock and density functional methods, Spectrochim. Acta A Mol. Biomol. Spectrosc. 67 (2007) 830–836.
[77] A.C. Costa Jr, M. Mondragón, G.B. Ferreira, O. Versiane, J. Rangel, G.M. Lima, A. Martin, Molecular structure, natural bond analysis, vibrational and electronic spectra, surface enhanced Raman scattering and Mulliken atomic charges of the normal modes of [Mn (DDTC) 2] complex, Spectrochim. Acta A Mol. Biomol. Spectrosc. 169 (2016) 95–107.
[78] Ö. Tamer, D. Avcı, Y. Atalay, Synthesis, X-Ray crystal structure, photophysical characterization and nonlinear optical properties of the unique manganese complex with picolinate and 1, 10 phenantroline: toward the designing of new high NLO response crystal, J. Phys. Chem. Solids 99 (2016) 124–133.
[79] P. Politzer, P.R. Laurence, K. Jayasuriya, Molecular electrostatic potentials: an effective tool for the elucidation of biochemical phenomena, Environ. Health Perspect. 61 (1985) 191–202.
[80] J.S. Murray, K. Sen, Molecular electrostatic potentials: concepts and applications, (1996).
[81] Y.S. Mary, H.T. Varghese, C.Y. Panicker, T. Thiemann, A.A. Al-Saadi, S.A. Popoola, C. Van Alsenoy, Y. Al Jasem, Molecular conformational analysis, vibrational spectra, NBO, NLO, HOMO-LUMO and molecular docking studies of ethyl 3-(E)-(anthracen-9-yl)prop-2-enoate based on density functional theory calculations, Spectrochimica Acta - Part A: Molecular and Biomolecular Spectroscopy, 150 (2015) 533-542.
[82] F. Weinhold, C.R. Landis, Natural Bond Orbitals and Extensions of Localized Bonding Concepts, Chem. Educ. Res. Pract. 2 (2001) 91–104.
[83] M. Usman, R.A. Khan, A. Alsalme, W. Alharbi, K.H. Alharbi, M.H. Jaafar, M. Abu Khanjer, S. Tabassum, Structural, spectroscopic, and chemical bonding analysis of Zn (II) complex [Zn (sal)](H2O): combined experimental and theoretical (NBO, QTAIM, and ELF) investigation, Crystals, 10 (2020) 259.
[84] X. Yang, Z. Shao, Y. Zhao, Q. Xie, X. Meng, Y. Song, H. Hou, Control of third order nonlinear optical properties by coordination metal change based on a series of metal organic chains, Polyhedron 185 (2020) 114598.
[85] C. Liu, Y. Si, S. Shi, G. Yang, X. Pan, Understanding the photophysical properties of chiral dinuclear Re (I) complexes and the role of Re (I) in their complexes, Dalton Trans. 45 (2016) 7285–7293.

[86] A. Colombo, C. Dragonetti, V. Guerchais, D. Roberto, An excursion in the second-order nonlinear optical properties of platinum complexes, Coord. Chem. Rev. 446 (2021) 214113.
[87] Ö. Tamer, N. Dege, D. Avcı, Y. Atalay, The static and frequency-dependent second- and third-order nonlinear optical properties of Zn (II) and Ni (II) complexes of 4-methoxypyridine-2 carboxylic acid: A detailed experimental and theoretical study, Appl. Organomet. Chem. 37 (2023) e7206.
[88] Y. Chen, Y. Zhang, Y. Shen, Y. Zhao, Y. Q. Qiu, A DFT study of the second order nonlinear optical properties of Ru (ii) polypyridine complexes, Phys. Chem. Chem. Phys. 24 (2022) 18217–18226.
[89] S.K. Hurst, M.P. Cifuentes, J.P. Morrall, N.T. Lucas, I.R. Whittall, M.G. Humphrey, I. Asselberghs, A. Persoons, M. Samoc, B. Luther-Davies, Organometallic complexes for nonlinear optics. 22.1 Quadratic and cubic hyperpolarizabilities of trans-bis (bidentate phosphine) ruthenium σ-arylvinylidene and σ-arylalkynyl complexes, Organometallics, 20 (2001) 4664-4675.
[90] A. Migalska Zalas, Theoretical simulation of the third order nonlinear optical properties of some selected organometallics complexes, Dig. J. Nanomater. Bios. 3 (2008) 1–8.

Materials Science in Semiconductor Processing 188 (2025) 109179

Contents lists available at ScienceDirect

Materials Science in Semiconductor Processing

journal homepage: www.elsevier.com/locate/mssp

Investigation on the effect of complex formation on prominent high static/dynamic first and second hyperpolarizability of Co(II) complex including 4-chloro-Pyridine-2-Carboxylic acid

Merve Şimşek [a], Ömer Tamer [a,*], Necmi Dege [b], Davut Avcı [a], Yusuf Atalay [a]

[a] Sakarya University, Faculty of Science, Department of Physics, Sakarya, 54147, Türkiye
[b] OndokuzMayıs University, Faculty of Science, Department of Physics, Samsun, 55139, Türkiye

ARTICLE INFO

Keywords:
4 Chloro Pyridine 2 Carboxylic acid
Crystal structure
FT-IR and UV–Vis spectra
Frequency dependent hyperpolarizability
DFT

ABSTRACT

Nonlinear optical (NLO) materials with promising first- and second-order hyperpolarizabilities play a crucial role in the fields of electronics and optoelectronics. For the metal-organic coordination complexes, the logical selection of an appropriate ligand and metal ion is vital in designing such materials to enhance their NLO response. In this study, a novel Co(II) complex, including 4-Chloro-pyridine-2-carboxylic acid ligand, was synthesized. The crystal structure and spectroscopic properties were determined by XRD, FT-IR, and UV–Vis spectroscopies. B3LYP and CAM-B3LYP level calculations demonstrated that there is a strong electronic absorption band at 356 nm, originating from the metal-ligand charge transfer (MLCT) transfer in the UV–Vis spectrum. Both XRD and FT-IR data demonstrated that the Co(II) complex has a distorted octahedral coordination geometry. The calculations of static and frequency-dependent α, β, and γat frequencies of $\omega = 0.0856252$ a.u ($\lambda = 532$ nm) and $w = 0.0428126$ au. ($\lambda = 1064$ nm) for 4Clpca and Co(II) complex have been also carried out using B3LYP and CAM-B3LYP levels. The dc-Kerr effect $\gamma(-\omega; \omega,0,0)$ and SHG $\gamma(-2\omega; \omega,\omega,0)$ parameters for Co(II) complex calculated as 329.59×10^{-36} and 433.93×10^{-36} esu are found as dramatically higher those for single pca ligand (6.0267×10^{-36} and 163.70×10^{-36} esu). So, a significant increase was detected in the parameters of frequency-dependent α (-w; 0), β(-w; w,0), and γ (-w; w,0,0) with complex formation.

1. Introduction

The increasing demand for new materials with non-linear optical (NLO) properties in advancing technology has triggered intensive research efforts. These materials have a wide range of applications, including optical data storage, optical switching, optical communication, information processing, and laser devices. To keep up with unstoppable technological advancements, scientists continue to search for materials that meet the demand for various categories of NLO materials [1–8]. In the search for NLO materials with desired properties, organic materials are particularly advantageous due to their large nonlinear optical coefficients, structural flexibility, and short optical response times. On the other hand, inorganic crystals are the preferred choice for linear and non-linear electro-optic applications due to their remarkable thermal stability despite the challenges of mechanical strength and limited operating temperature ranges [9,10]. Inorganic crystals also have disadvantages, such as higher costs and less flexibility compared to organic materials.

Recent scientific research has focused on exploring organometallic materials with strong nonlinear optical responses, especially those derived from derivatives of pyridine-carboxylic acid. Thanks to its donor N and O atoms, the pyridine-carboxylic acid ligand can effectively coordinate with metal ions. In addition, it is possible to tune the non-linear optical properties, especially by adding electron-donating and/or electron-withdrawing functional groups to different edges of the heterocyclic pyridine ring. The information obtained from these efforts plays a crucial role in the future design and development of NLO materials. Recent studies of coordination complexes, including ligands such as pyridine-2-carboxylic acid coordinated with various metal ions, have revealed their nonlinear optical properties. Previous studies have examined coordination complexes that include pyridine-2-carboxylic acid derivative ligands coordinated with various metal ions, such as 4-Methoxy-pyridine-2-carboxylic acid (4Mepca) [11–14], 6-hydroxy-methyl pyridine-2-carboxylic (6OHMepca) [15,16],

* Corresponding author.
E-mail address: omertamer@sakarya.edu.tr (Ö. Tamer).

https://doi.org/10.1016/j.mssp.2024.109179
Received 28 May 2024; Received in revised form 25 November 2024; Accepted 25 November 2024
Available online 3 December 2024
1369-8001/© 2024 Elsevier Ltd. All rights are reserved, including those for text and data mining, AI training, and similar technologies.

4-(Trifluoromethyl)pyridine-2-carboxylic acid (4TFMepca) [17], 4-(4-carboxy-phenyl)-pyridine-2-carboxylic acid (4-4Cppca) [18], imidazo[1,2-a]pyridine carboxylic acid (Impca) [19,20], 3-hydroxy--pyridine-2-carboxylic acid (3Ohpca) [16,21], 5-(trifluoromethyl)pyridine-2-carboxylic acid (5TFMEPCA) [22], 3-methylpicolinic acid (3Mepca) [23,24], 6CHpca, 6-methylpyridine-2-carboxyclic acid (6Mepca) [25–29], 4-chloro-pyridine-2-carboxylic acid (4Clpca) [12, 21], 6-chloro-pyridine-2-carboxylic acid (6Clpca) [30–32], and 6-bromo-pyridine-2-carboxylic acid (6Brpca) [33].

As a result of a detailed literature review, it was determined that there is no experimental or theoretical study on the Co(II) complex containing the 4-Chloro-pyridine-2-carboxylic acid ligand. The idea that the complex containing Cl atoms located on opposite edges of the complex and the Co(II) ion with high spin multiplicity may be particularly strong in terms of the second-order hyperpolarizability parameter motivated the study. In the present study, a novel Co(II) complex of 4-Chloro-pyridine-2-carboxylic acid ligand was synthesized for the first time. The crystal structure, IR, and UV–Vis spectra were analyzed with combined experimental and theoretical methods. Finally, the first and second-order hyperpolarizability parameters (β and γ) were calculated by using B3LYP/LanL2DZ and CAMB3LYP/LanL2DZ levels. The obtained γ parameters demonstrated that the [Co(4Clpca)2(H2O)2] complex is a promising candidate for third-order nonlinear optical applications.

2. Materials and methods

2.1. Synthesis

The Co(II) complex was synthesized using high-quality chemical ligands from Merck. Therefore, no extra purification process was applied to the chemicals used. As depicted in Fig. 1, the synthesis procedure involved dissolving 2 mmol of 4-chloropyridine-2-carboxylic acid (4Clpca) in 30 mL of a 1:1 mixture of ethanol and water. Then, 1 mmol of $[Co(4Clpca)_2(H_2O)_2]$ was added to the constantly stirring solution at 50 °C to form the Co(II) coordination complex. The resulting solution was stirred continuously at 50 °C for 2 h. The final solution was filtered and left to evaporate at room temperature for two weeks. Orange crystals were obtained from the final solution.

2.2. Experimental procedures

A suitable crystal of Co(II) complex was selected for data collection which was performed on a D8-QUEST diffractometer equipped with a graphite-monochromatic Mo-K_α radiation at 293 K. The structure was solved by direct methods using SHELXS-2013 [34] and refined by full-matrix least-squares methods on F^2 using SHELXL-2013 [35]. The H atoms of water molecule were in a difference map and refined freely. The H atoms were located from different maps and then treated as riding atoms with C-H distances of 0.93 Å. The following procedures were implemented in XRD analysis: data collection: Bruker APEX2 [36]; program used for molecular graphics were as follow: MERCURY programs [37]; software used to prepare material for publication: WinGX [38]. Crystallographic data and refinement parameters for the Co(II) complex are presented in Table 1. FT-IR spectrum for the Co(II) complex containing the 4Clpcaligand was recorded in the 4000 to 400 cm^{-1} range using a Perkin ELMER Spectrum-Two FT-IR spectrophotometer. UV–Vis spectrum of the Co(II) complex was obtained in the 800-200 nm range using a HITACHI U-2900 UV/Vis spectrophotometer in ethanol solvent.

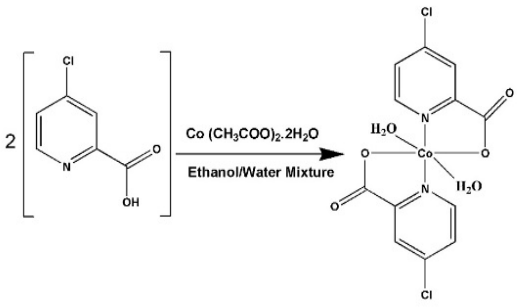

Fig. 1. General synthesis scheme for $[Co(4Clpca)_2(H_2O)_2]$ complex.

2.3. Theoretical methods

The theoretical calculation of the Co(II) complex was obtained using Gaussian 16 software [39]. This software enables comprehensive analysis, including the ground state geometry, vibrational spectrum, frontier molecular orbitals, molecular electrostatic potential surface, dipole moment (μ), polarizability (α), first and second-order static/dynamic hyperpolarizability parameters (β and γ). GaussView 6.0 [40] was also utilized for visualization of the theoretical results. DFT calculations were performed using the B3LYP [40] and CAM-B3LYP [41] levels in conjunction with LanL2DZ basis set [42,43]. The UV–Vis spectrum of the Co(II) complex was calculated with the same basis set, taking into account the effect of ethanol solvent through the CPCM method [44,45]. The identification of molecular orbitals in the electronic absorption bands observed in the UV–Vis spectra was confidently carried out using SWIZARD software [46]. The vibrational wavenumbers were scaled by a factor of 0.96 to eliminate the well-known overestimation of DFT levels [30]. Crystal Explorer program [47] was used to Hirschfield surface analysis. The frequency-dependent nonlinear optical parameters were calculated using the same basis set with frequencies of ω = 0.0856252 and 0.0428126 au.

3. Results and discussion

3.1. Crystal structure analysis

The crystal structure of the Co(II) complex is displayed in Fig. 2. The cell parameters of the $[Co(4Clpca)_2.2H_2O]$ crystal are 24.510 (6), 9.216

Table 1
Structural refinement and crystal parameters table for $[Co(4Clpca)_2(H_2O)_2]$ complex.

Crystal data	
CCDC	2373233
Chemical formula	$C_{12}H_{10}Cl_2CoN_2O_6$
Mr	408.05
Crystal system, space group	Monoclinic, *C*2/*c*
Temperature (K)	293
a, b, c (Å)	24.510 (6), 9.216 (2), 6.9101 (18)
α, β, γ (°)	101.686 (8), 101.686 (8), 101.686 (8)
V (Å^3)	1528.5 (7)
Z	4
Radiation type	Mo Kα
μ (mm ^{1})	1.50
Data collection	
Diffractometer	Bruker APEX3 C
Absorption correction	Multi-scan (Bruker)
T_{min}, T_{max}	0.584, 0.746
No. of measured, independent and observed [I > 2σ(I)] reflections	15819, 1901, 1622
R_{int}	0.029
$(\sin\theta/\lambda)_{max}$ (Å−1)	0.668
Refinement	
R[F2 > 2σ(F2)], w*R*(F2), S	0.025, 0.065, 1.06
No. of reflections	1901
No. of parameters	112
No. of restraints	3
H atom treatment	H atoms treated by a mixture of independent and constrained refinement
$\Delta\rho_{max}$, $\Delta\rho_{min}$ (e Å^{-3})	0.31, −0.24

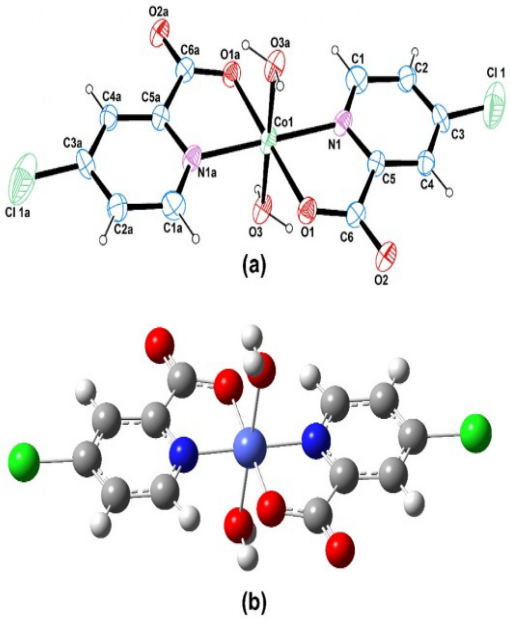

Fig. 2a). The crystal structure and b) the optimized molecular geometry (obtained by B3LYP/LanL2DZ) for $[Co(4Clpca)_2(H_2O)_2]$ complex.

(2), 6.9101 (18) Å, with α, β, and γ angles of 101.686 (8)°. The crystal is prism-shaped and orange in color, exhibiting a monoclinic system and a C2/c space group. The experimentally obtained crystal structure was optimized by using B3LYP/LanL2DZ and CAM-B3LYP/LanL2DZ levels. The Co(II) metal ion was located in the center of an octahedral coordination sphere. Two 4-chloropyridine-2-carboxylic acid molecules occupy the equatorial plane, while two H_2O molecules are located in the axial plane, causing a distorted octahedral coordination sphere around the central Co(II) ion. 4Clpca ligand forms chelate rings by coordinating to the central metal through the donor N and O atoms.

Table 2 displays the experimental and theoretical bond lengths and bond angles of the Co(II) complex structure. The Co1-O3 and Co1-O3a axial bond lengths were experimentally observed as 2.1067 (12) and 2.1067 (12) Å. On the other hand, the equatorial N1-Co1, N1a-Co1, O1a-Co1, and O1-Co1 bond lengths were obtained as 2.1216 (15), 2.1215 (15), 2.1071 (11) and 2.1071 (11) Å, respectively. The theoretical bond lengths between the central metal ion and donor N/O atoms were calculated at the range of 2.4289–1.9264 Å and 2.2459–1.9284 Å for B3LYP and CAM-B3LYP levels, respectively. The theoretical and experimental values of the Co(II) complex were found to be in good agreement with the results reported for similar structures [12,21]. The small shifts observed between experimental and theoretical results are attributed to the phase difference between XRD (solid-state) and DFT (gas phase) [22,48].

The experimentally determined bond lengths for C6-O1, C6-O2, C6a-O1a, and C6a-O2a are 1.2734 (18), 1.2425 (18), 1.2734 (18) and 1.2425 (18) Å, respectively. Theoretical calculations reproduce these bond lengths as 1.2985, 1.2186, 1.2986, and 1.2184 Å for B3LYP, and 1.3238, 1.2454, 1.3238, and 1.2454 Å for CAM-B3LYP level, respectively. These results indicate that the C6-O1 and C6a-O1a bonds are in the single bond character, demonstrating that 4-chloro-pyridine-2-carboxylate ligand coordinates to Co(II) ion through the O1 and O1a atoms [21,28,49]. The bond lengths of C3-Cl1 and C3-Cl1a experimentally obtained as 1.7420 (18) Å were calculated as 1.7461 and 1.7462 Å for B3LYP, 1.7917 and 1.7918 Å for CAM-B3LYP, as would be expected [13,15,50].

As shown in Table 2, the bond lengths and angles between the central Co(II) ion and N/O donor atoms are different due to the electronegativity properties of donor atoms and the resonance effects of substituents. Therefore, the Co(II) complex under consideration is defined with a distorted octahedral structure. This proves to us that our crystal geometry has a distorted octahedral structure while showing that it is in line with the findings from other studies [12,25,51]. Table 3 presents the parameters of hydrogen bonding geometry for the Co(II) complex. The

Table 3
Experimentally determined hydrogen bond geometry of the [Co $(4Clpca)_2(H_2O)_2$] molecule (values in Å and °).

D—H···A	D—H	H···A	D···A	D—H···A	Symmetry codes
C1—H1···O3^{i}	0.93	2.59	3.517 (2)	173	−x+1/2, y+1/2, −z+1/2
C4—H4···Cl1^{ii}	0.93	2.83	3.7378 (18)	164	−x+1, −y+1, −z+1
O3—H3B···O2^{i}	0.81 (2)	1.93 (2)	2.7262 (17)	168 (2)	−x+1/2, y+1/2, −z+1/2
O3—H3A···O2^{iii}	0.80 (2)	2.00 (2)	2.7893 (16)	170 (2)	x, −y+1, z−1/2

Table 2
The selected theoretical and experimental bond lengths (Å) and bond angles (°) for $[Co(4Clpca)_2(H_2O)_2]$ complex obtained using B3LYP/LanL2DZ and CAM-B3LYP/LanL2DZ levels.

$[Co(4Clpca)_2(H_2O)_2]$							
Bond L	XRD	B3LYP	CAM-B3LYP	Bond A.	XRD	B3LYP	CAM-B3LYP
O3-Co1	2.1067 (12)	2.4289	2.2459	C1a N1a Co1	128.44 (11)	127.87	126.32
O3a-Co1	2.1067 (12)	2.4173	2.2458	C1-N1-Co1	128.44 (11)	127.88	126.32
N1-Co1	2.1216 (15)	1.9457	1.9284	H3aA-O3a-Co1	123.3 (15)	122.71	131.81
N1a-Co1	2.1215 (15)	1.9452	1.9284	H3A-O3-Co1	120.6 (14)	121.59	131.80
O1a-Co1	2.1071 (11)	1.9268	1.9375	O3-Co1-O3a	180.00 (7)	180.00	180.00
O1-Co1	2.1071 (11)	1.9264	1.9375	C6a-O1a- Co1	116.02 (9)	116.12	115.20
C3-Cl1	1.7420 (18)	1.7461	1.7917	C6-O1-Co1	116.02 (9)	116.12	115.20
C3a-Cl1a	1.7420 (18)	1.7462	1.7918	C5a-N1a-Co1	112.89 (10)	112.30	112.85
C5-N1	1.3425 (19)	1.3466	1.3458	N1-Co1-O1a	101.56 (4)	96.066	95.668
C5a-N1a	1.3425 (19)	1.3400	1.3529	N1a-Co1-O1	78.43 (4)	96.011	95.666
C1a-N1a	1.340 (2)	1.3466	1.3458	O1-Co1-O3a	86.90 (4)	95.730	81.471
C1-N1	1.340 (2)	1.3398	1.3458	O1-Co1-O3	86.90 (4)	95.603	81.477
C6 O1	1.2734 (18)	1.2985	1.3238	N1 Co1 O3a	87.87 (5)	94.610	86.450
C6a O1a	1.2734 (18)	1.2986	1.3238	N1a Co1 O3	87.87 (5)	94.471	86.453
C6 O2	1.2425 (18)	1.2186	1.2454	N1a-Co1-O3a	92.13 (5)	85.528	93.548
C6a O2a	1.2425 (18)	1.2184	1.2454	N1 Co1 O3	92.13 (5)	85.389	93.548
O3a-H3aB	0.809 (15)	0.9648	0.9724	O1-Co1-O3a	93.11 (4)	84.396	98.529
O3 H3B	0.809 (15)	0.9648	0.9764	O3 Co1 O1a	93.10 (4)	84.269	98.522
O3a-H3aA	0.809 (15)	0.9632	0.9764	N1-Co1-O1	78.43 (4)	83.979	84.332
O3-H3A	0.809 (15)	0.9631	0.9724	N1a-Co1-O1a	78.2 (2)	83.9428	84.332

crystal deconstructs the molecules into a three-dimensional network through O—H···O, C—H···O and C—H···Cl intermolecular H bonds. All interactions responsible for the stacking of the complex appear to be strong hydrogen bonds, and therefore it can be concluded that the thermal stability of the complex is high. The H-bonding interaction of O3—H3B···O2^{i} is the strongest one in Co(II) crystal with the symmetry code of −x+1/2, y+1/2, −z+1/2 [H···A = 1.93(2) Å, D···A = 2.7262 (17) Å].

3.2. Hirschfield surface analysis

Hirshfeld surface analysis is a powerful method for visualizing and understanding intermolecular interactions in crystal structures. This analysis accurately quantifies interactions by highlighting close contacts between molecules through a detailed and informative surface map. As a result, it is widely recognized as an essential research tool in the field of crystallography. Hirshfeld surface analysis offers a unique opportunity to study the interactions of each atom with its environment in the crystal structure. This analysis provides crucial information for deciphering hydrogen bonds between molecules, van der Waals interactions, and other non-covalent interactions [52].

The intermolecular interactions and interaction distance in [Co(4Clpca)$_2$(H$_2$O)$_2$] complex were calculated using the Crystal Explorer program [47]. The 3D Hirshfeld surfaces (d_{norm}, shape-index, and curvedness) of the Co(II) complex are illustrated in Fig. 3. The d_{norm} illustration uses a color scheme where red color represents interactions shorter than van der Waals radii, the blue color represents interactions longer than van der Waals radii, and white represents interactions of approximately the same length as van der Waals radii. The intense red spots on the oxygen atoms of the H$_2$O ligand and the carboxylate group clearly indicate a strong H-bonding interaction [53,54]. The shape index of the Hirshfeld surface presented in Fig. 3(b) is used to visualize the π–π stacking interactions by the presence of adjacent red and blue triangles [55]. Fig. 3(b) demonstrates that Co(II) complex has red triangles on the pyridine rings, suggesting that the π–π stacking interactions are available in the crystal. Fig. 3(c) also demonstrates that pyridine rings and chelate rings are defined as regions of low surface curvature, while the regions around the aqua ligands, Cl atoms and non-coordinated carboxylate O atoms are defined as regions of very sharp surface curvature [54,56].

Quantitative data on the properties and diversity of intermolecular interactions for the [Co(4Clpca)$_2$(H$_2$O)$_2$] complex is obtained by creating 2D fingerprint plots for each interatomic contact. Fig. 4 provides a comprehensive illustration of overall interactions, including interactions beyond elemental interactions. The reciprocal outside (external) and inside (internal) interactions have been considered for Co(II) complex. d_e and d_i represent the distances from a point on the Hirshfeld surface to the nearest atoms outside (external) and inside (internal) the surface, respectively. The data show that the main interactions are mostly between H-H, H-O and H-Cl atoms, and these interactions contribute 25.2 %, 22.7 % and 17.6 % to the total interaction, respectively. As a result, it can be said that van der Waals interactions and hydrogen bond interactions are the main factors in the formation of the Co(II) crystal structure which is under consideration. In addition, due to these interactions, the thermal stability of the Co(II) complex is expected to be high, which is an important requirement in nonlinear optical applications.

3.3. Vibrational analysis

Vibrational analysis accurately determines the potential energy surface of a molecule and its vibrational modes. This analysis is crucial in various applications, including strengthening molecular bonds, determining geometric structures, and identifying new molecular systems. The FT-IR spectrum of the [Co(4Clpca)$_2$(H$_2$O)$_2$] complex was recorded in the range of 4000-400 cm^{-1}. The vibrational wavenumbers

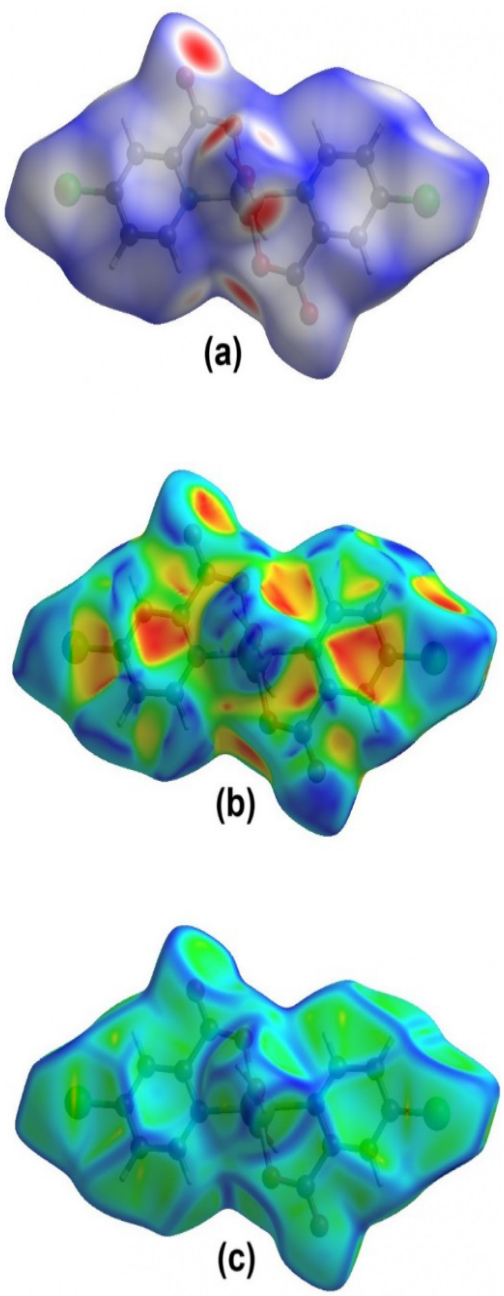

Fig. 3. Hirshfeld surface (HS) plotted over (a) d_{norm}, (b) shape-index, and (c) curvedness for [Co(4Clpca)$_2$(H$_2$O)$_2$] complex.

were also calculated using the Gaussian 16 software with the B3LYP and CAM-B3LYP levels in conjunction with LanL2DZ basis set. The DFT levels are known to produce results at larger wavenumbers than experimental corresponding data due to the anharmonicity, electron correlation, and basis set deficiency. The theoretical wavenumbers were multiplied by a scale factor of 0.96 to align them with the experimental data. Fig. 5 and Table 4 present the experimental and theoretical vibrational spectra and the characteristic vibrational modes for [Co(4Clpca)$_2$(H$_2$O)$_2$] complex.

The OH stretching vibrations originated from the H$_2$O ligand for the coordination complexes were reported at the range of 3235–3700 cm^{-1} [18,33]. In the newly synthesized [Co(4Clpca)$_2$(H$_2$O)$_2$] complex discussed in this study, the vibration band for OH stretching was

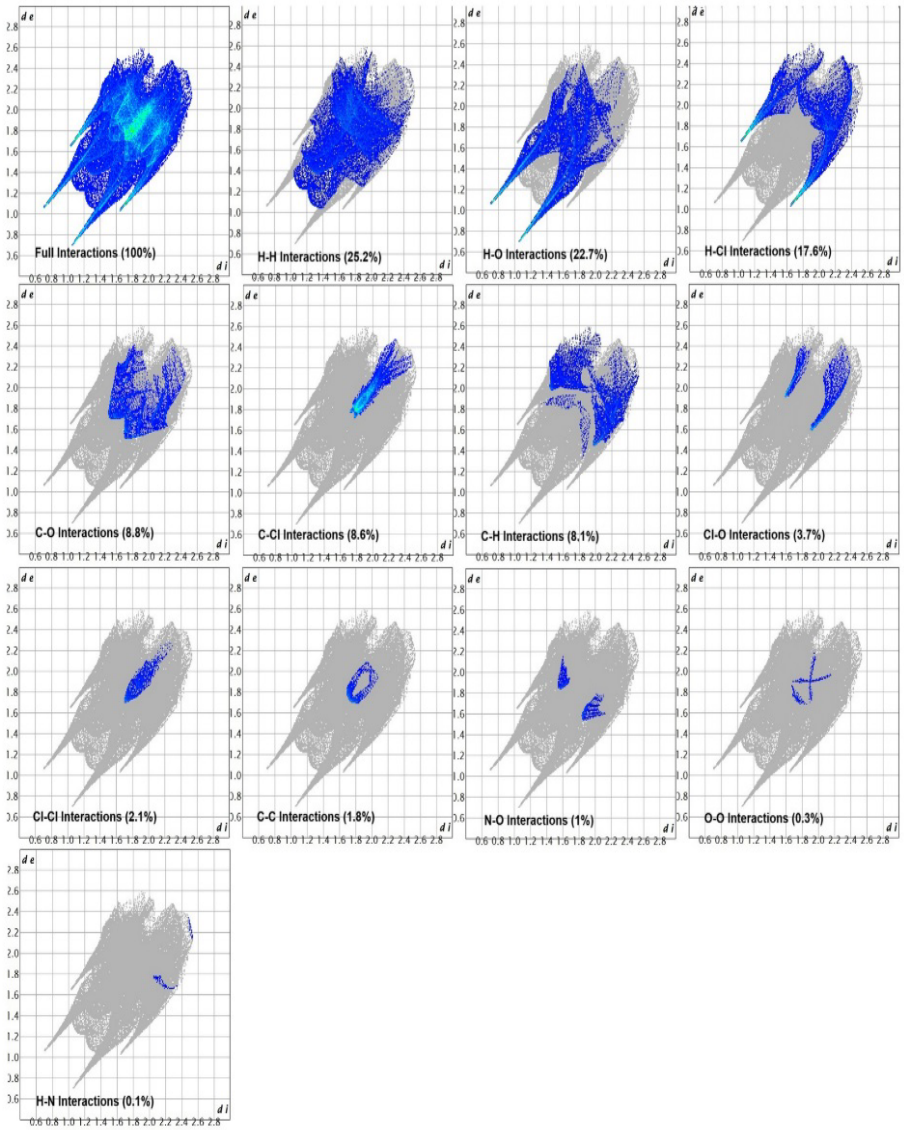

Fig. 4. 2D fingerprint plots for $[Co(4Clpca)_2(H_2O)_2]$ complex for the overall and individual interactions.

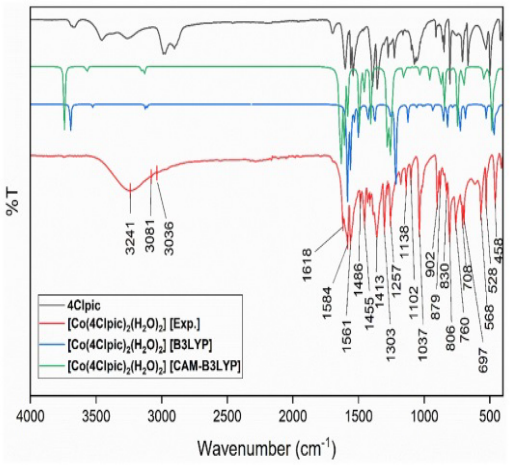

Fig. 5. Experimental and theoretical IR spectrum for 4Clpca and $[Co(4Clpca)_2(H_2O)_2]$ complex.

experimentally measured at 3245 cm^{-1}, providing accurate and reliable data. The corresponding theoretical data for this vibration band has been calculated as 3693 and 3741 cm^{-1} for B3LYP and CAM-B3LYP levels. The overestimation, especially in OH stretching vibrations, is high since the experimental spectra were recorded in the solid phase in which the intermolecular interactions are dominant, while the theoretical spectrum is calculated in the isolated gas phase in which the intermolecular interactions are quite weak. Siwiderski et al. reported that the aromatic ring CH stretching vibrations (ν CH) were observed at the range of 3090-2934 cm^{-1} for the alkali metal complexes containing pyrazine2-carboxylic acid and pyrazine 2,3-dicarboxylic acid [57]. In the present study, the CH stretching vibrations for the Co(II) complex were observed at 3078 and 3035 cm^{-1}, as would be expected. B3LYP and CAM-B3LYP levels have also predicted the CH stretching vibration at the range of 3149-3108 cm^{-1}, as consistent with the experimental data.

In the vibrational spectra of the carboxylic acid complexes, the characteristic vibrational bands of the carboxylate anion are observed. These include asymmetric and symmetric stretching vibration bands for the carboxylate anion (COO^-). It was reported that the asymmetric COO^- stretching vibrations (ν CO) appear at the range of 1631–1613

Table 4
The experimental and theoretical vibrational wavenumbers (cm^{-1}) for[Co $(4Clpca)_2(H_2O)_2$] complex.

Assignments	Exp.(cm^{-1})	CAM B3LYP (cm^{-1})	B3LYP (cm^{-1})
ν OH	3245	3741	3693
ν CH	3078	3149	3125
ν CH	3035	3132	3108
ν CO	1619	1636	1584
ν CC	1586	1609	1560
ν CN	1561	1582	1533
β HOH	1486	1492	1499
β HCC	1454	1457	1425
β HCC	1411	1406	1377
ν CN	1301	1269	1270
ν CO	1256	1254	1217
β HCC	1135	1153	1123
β HCC	1102	1148	1135
Ring bre.	1036	1035	1011
γ HCCC	902	955	932
γ HCCC	877	876	854
τ CCCC	830	844	823
τ CCCC	806	801	779
ν CCl	759	744	726
ν OCo	707	731	712
τ CCCC	696	698	684
γ HCCC	568	541	527
τ CCCC	526	530	517
ν NCo	458	471	455

cm^{-1}, while the symmetric ones appear 1385–1369 cm^{-1} for the metal-carboxylate coordination complexes [57]. In the present study, the asymmetric ν CO stretching vibration was observed at 1619 cm^{-1} and calculated at 1584/1636 cm^{-1} by using B3LYP/CAM-B3LYP level. The symmetric ν CO stretching vibration band was also observed at 1256 cm^{-1}. The asymmetric and symmetric ν CO bands for a single 4-Chloro--pyridine-2-carboxylic acid ligand were observed at 1698 and 1226 cm^{-1}, and the difference between them is 472 cm^{-1}. The difference in wavenumber between symmetric and asymmetric ν CO bands for Co(II) has been found as 363 cm^{-1}, demonstrating that 4-Chloro-pyridine-2--carboxylic acid ligand coordinates to Co(II) ion through the carboxylate group O atom. Avcı et al. also reported the crystal structure and vibrational spectrum for a novel Cu(II) complex containing a 6-Bromo-pyridine-2-carboxylic acid ligand. The CC and CN stretching vibrations for the 6-Bromopyridine-2-carboxylic acid ligand were reported at the regions of 1545-1049 cm^{-1} and 1489-1340 cm^{-1}, respectively [58]. In the present study, ν CC and ν CN vibrations were observed at 1586, 1560 and 1301 cm^{-1}. B3LYP level also calculated these band at 1560, 1533 and 1270 cm^{-1}. According to the IR spectrum of 6-Bromopyridine-2-carboxylic acid ligand presented in Fig. 5, the pyridine ring breathing vibration band was observed experimentally at 998 cm^{-1}. The same band for Co(II) complex was observed at 1036 cm^{-1}, and calculated at 1011 and 1035 cm^{-1} by using B3LYP and CAM-B3LYP levels, respectively. The shif in the ring breathing vibrations band also demonstrates that the ligand coordinates to the Co(II) ion through the piridin N atom. The other important vibrational bands observed and calculated for Co(II) complexes were presented in Table 4, and these vibrational wavenumbers are consistent with the literature [12,21,22,28,30,50, 59–63].

3.4. UV–Vis spectrum and FMO energies

UV–Vis spectroscopy is a highly effective analytical technique that offers valuable insights into a molecule's electronic structure and energy levels. The theoretical UV–Vis spectrum for the [$Co(4Clpca)_2(H_2O)_2$] complex was calculated using the TD-B3LYP/LanL2DZ and TD-CAM-B3LYP/LanL2DZ levels, and the solvent effect was taken into account by using the CPCM method [44,45]. The experimental and theoretical electronic absorption spectra for the [$Co(4Clpca)_2(H_2O)_2$] complex were designated in Fig. 6. Since there is no electronic absorption band in the

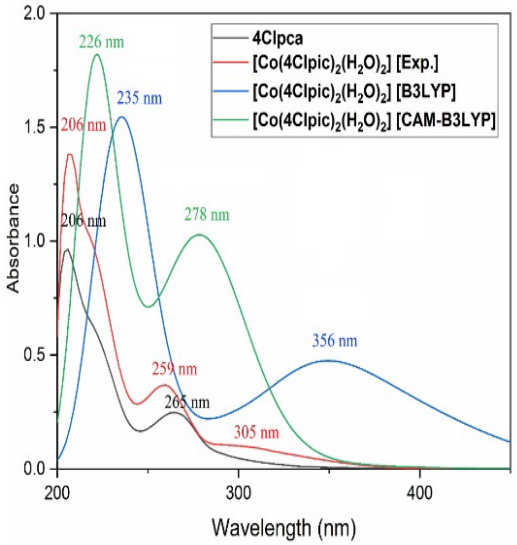

Fig. 6. Experimental and theoretical UV–Vis spectra for 4Clpca and [Co $(4Clpca)_2(H_2O)_2$] complex.

range of 450–900 nm, this region was removed from the experimental and theoretical spectra.

In the experimental UV–Vis spectrum of [Co(4Clpca)2(H2O)2] complex, the bands observed at 206 and 259 nm were assigned as $\pi \rightarrow \pi^*$ and $n \rightarrow \pi^*$ electronic transitions. The corresponding data in the theoretical spectrum was calculated at 226 and 278 nm by using CAM-B3LYP level, respectively. B3LYP level also reproduces these electronic absorption bands at 235 and 274 nm, respectively. The highest experimental absorption band observed at 305 nm was calculated as 294 and 295 nm by using B3LYP and CAM-B3LYP levels. According to Table 5, the main electronic charge transfer at 294 nm is HOMO-2α→LUMO α (22 %). Fig. 7 also demonstrates that HOMO-2α→LUMO α is a transition from the Co(II) ion to the pic ligands known as metal-ligand charge transfer (MLCT). The calculated spectra has also an electronic absorption band at 356 nm, which is assigned as MLCT band and defined by the transition of HOMOα→LUMO+2α. Therefore, it can be clearly concluded from Fig. 7 that the electronic charge transfer at 356 nm occurs from Co(II) to the 4Clpca ligand.

[$Co(4Clpca)_2(H_2O)_2$] complex has an unrestricted open-shell spin state. So, both α- and β-spin molecular orbitals are available for the [Co $(4Clpca)_2(H_2O)_2$] complex. When Table 5 is examined carefully, the dominant contributions to the electronic absorption bands are from the α-spin FMOs. Therefore, only α-spin FMOs and their energies are presented in Fig. 7.

Understanding the electronic structure of metal-organic coordination complexes is fundamental for elucidating their electronic properties and reactivity. Therefore, the highest occupied molecular orbital (HOMO) and lowest unoccupied molecular orbital (LUMO) energies for Co(II) complex were calculated by using B3LYP/LanL2DZ and CAM-B3LYP/LanL2DZ levels. According to B3LYP level results, the HOMO and LUMO energies were calculated as −6.4494 and −2.4672 eV, respectively. These energies provide crucial insights into the electronic properties and reactivity of the Co(II) complex. The energy gap between the HOMO and LUMO (ΔE = −6.4494 eV - (−2.4672 eV) = 3.9823 eV) reflects the complex's electronic charge transfer ability. A smaller ΔE suggests a more facile electron transfer, which may be pertinent in redox reactions involving the Co(II) complex. The relatively small ΔE in this case indicates that electronic transitions involving the transfer of electrons are likely to occur readily. The electronic structure, as elucidated by HOMO and LUMO energies, dictates the reactivity of the Co(II) complex. Lower-energy HOMO orbitals can participate in bonding

Table 5
The experimental and theoretical electronic absorption wavelengths, oscillator strengths, and significant contributions for the $[Co(4Clpca)_2(H_2O)_2]$ complex.

	Exp.	CAM-B3YLP		B3YLP/LanL2DZ		
	λ (nm)	λ (nm)	Oscillator str.	λ (nm)	Oscillator str.	Important contributions
Co (II) Complex	206	226	0.0159	235	0.0615	HOMO-12α→LUMO α (49 %)
	259	278	0.0517	274	0.0121	HOMO-3α→LUMO+2α (23 %)
	305	295	0.0543	294	0.0327	HOMO-2α→LUMO α (22 %)
	–	335	0.0022	356	0.1217	HOMOα→LUMO+2α (54 %)

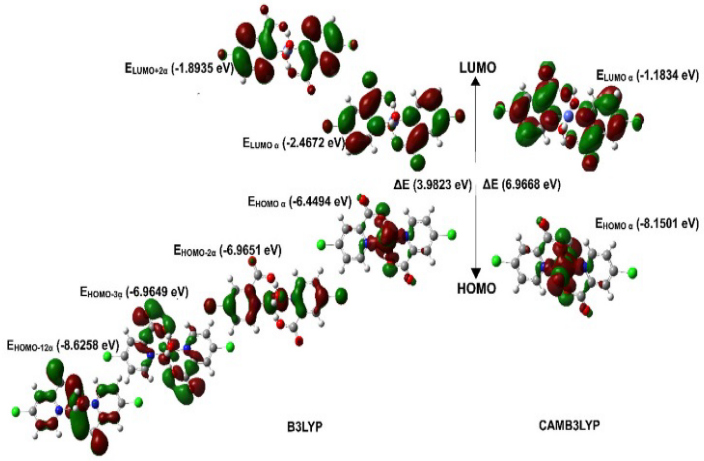

Fig. 7. Frontier molecular orbitals (FMOs) and their energies for $[Co(4Clpca)_2(H_2O)_2]$ complex.

interactions, while higher-energy LUMO orbitals can accept electrons during catalytic cycles. The HOMO energy reflects the stability of the complex's highest occupied electron. A lower HOMO energy indicates stronger ligand field effects, implying a greater degree of electron delocalization onto the ligands.

The important quantum chemical parameters calculated using the HOMO and LUMO energies are presented in Table 6. These parameters include chemical hardness (η), which measures the resistance of a molecule to change electronic re-configuration; electronegativity (χ), which indicates the tendency of an atom to attract electrons; electrophilicity index (w), which quantifies the electrophilic nature of a molecule; and chemical softness (S), which represents the inverse of chemical hardness. These values calculated by equations (1)–(4) are crucial in explaining the optical and chemical properties of the complex, providing insights into its reactivity and electronic behavior. Chemical hardness and softness are crucial factors in determining the kinetic stability of a molecule. Molecules with small energy gaps are considered soft, while those with large energy gaps are considered hard and, therefore, more stable molecules [64]. The η and S parameters have been calculated as 1.9911 eV and 0.2473 eV^{-1}, respectively.

Table 6
The chemical hardness (η), electronegativity (χ), electrophilicity index (W), chemical softness (S) and FMO energies for $[Co(4Clpca)_2(H_2O)_2]$ complex and 4Clpca ligand obtained by B3LYP/LanL2DZ and CAM-B3LYP/LanL2DZ levels.

Parameter	4Clpca		$[Co(4Clpca)_2(H_2O)_2]$	
	B3LYP	CAM-B3LYP	B3LYP	CAM-B3LYP
E_{HOMO} (eV)	−7.5118	−9.2407	−6.4494	−8.1501
E_{LUMO} (eV)	−2.5518	−1.2264	−2.4672	−1.1834
ΔE (eV)	4.9999	8.0144	3.9823	6.9668
χ (eV)	5.0518	5.2336	4.4583	4.6668
η (eV)	2.4999	4.0072	1.9911	3.4834
W(eV)	5.1042	3.4176	4.9913	3.1261
S(eV^{-1})	0.2000	0.1248	0.2473	0.1435

$$\eta = \frac{(E_{LUMO} - E_{HOMO})}{2} \quad (1)$$

$$\chi = -\frac{(E_{LUMO} + E_{HOMO})}{2} \quad (2)$$

$$W = \frac{\chi^2}{2\eta} \quad (3)$$

$$S = \frac{1}{\eta} \quad (4)$$

The electrophilicity index [64] evaluates the energy decrease resulting from maximum electron flow between HOMO and LUMO orbitals. It is well known that compounds with a high electrophilicity index or small nucleophilic index exhibit high biological activity. The electrophilicity index for $[Co(4Clpca)_2(H_2O)_2]$ complex was calculated as 4.9913 and 3.1261 eV by using B3LYP and CAM-B3LYP levels. Furthermore, increasing the chemical softness (S) value of the complexes corresponds to increased biological activities. In order to provide a deep understanding of the effect of complexation, the HOMO and LUMO energies of the 4Clpca ligand were also calculated, and the obtained results were presented in Table 6. According to Table 6, the 4Clpca ligand is more stable than the $[Co(4Clpca)_2(H_2O)_2]$ complex with the HOMO energy of −7.5118 eV (B3LYP) and −9.2407 eV (CAM-B3LYP). Additionally, the $[Co(4Clpca)_2(H_2O)_2]$ complex is a more chemically soft system than the 4Clpca ligand, and It is understood that there is a greater tendency to enter into chemical reactions through new interactions. So, the $[Co(4Clpca)_2(H_2O)_2]$ complex under investigation is a relatively soft metal-organic coordination complex, susceptible to new reactions due to the uncoordinated carboxylate oxygen via covalent bonds or H-bonding interactions. Additionally, the relatively small HOMO-LUMO energy gap is also an indicator of higher dipole moment and, therefore, higher nonlinear optical properties [21].

3.5. Natural bond orbital analysis

The Natural Bond Orbital (NBO) method allows researchers to identify donor-acceptor interactions and assess the extent of electron delocalization in molecules. This is achieved by analyzing the electron density distribution in terms of natural atomic orbitals. The NBO method is particularly useful for studying hyperconjugative interactions between molecular orbitals, where electrons typically shift from occupied orbitals (donors) to empty orbitals (acceptors) [65]. These interactions play a fundamental role in influencing the overall electronic structure and properties of molecules. The participation of a greater number of electrons in hyperconjugation leads to increased conjugation and higher stabilization energy for the system [66]. The NBO analysis for Co(II) was conducted using the B3LYP and CAM-B3LYP levels in conjunction with the LanL2DZ basis set. The high energy hyperconjugative interactions in the Co(II) complex are presented in Table 7. The natural charge of the Co (II) ion in the complex, which is +2 in the free state, was calculated to be +0.76409. The NBO analysis also predicted the electronic configuration of the Co(II) ion as [core]$4S^{(0.23)}3d^{(7.60)}4p^{(0.39)}4d^{(0.01)}5p^{(0.01)}$ with 17.99256 core electrons, 8.22905 valence electrons, 0.01429 Rydberg electrons, and 26.23591 total electrons. When it comes to CAM-B3LYP results, the electronic configuration of Co(II) ion is [core] $4S^{(0.11)}3d^{(3.33)}5p^{(0.21)}$ with 17.99227 core electrons, 8.24683 valence electrons, 0.01484 Rydberg electrons, 26.25393 total electrons. CAM-B3LYP level also predicts the natural charge of Co(II) ion is 0.74607. The calculated natural charges of the metal ions in the complex are smaller than those of the free ions, indicating that ligand-to-metal charge transfers are more dominant than those in the opposite direction [67,68]. The high-energy interactions of LP O/N → LP* Co are also presented in Table 7. These intense interactions are strongly indicative of a six-coordinated Co(II) center, with the donor N and O atoms playing a pivotal role. Higher interaction energies imply more intense interactions, which means that bond lengths between interacting atoms are shorter than those of atoms with lower interaction energies. For instance, the hyperconjugative interaction energies of LP (2) O1→LP* (5) Co1, LP (2) O3→LP*(8) Co1 and LP (1) N1→LP*(4) Co1 were calculated as 20.58, 15.53 and 23.81 kcal/mol by using B3LYP level, respectively. A high $E^{(2)}$ value indicates the presence of strong interactions between the electron-donor and electron-acceptor groups, as well as a higher degree of conjugation within the entire system. According to Table 7, the lowest interaction energy between LP N/O and LP* Co was determined as LP (2) O3/O3a → LP (8) Co1 with the hyperconjugative interaction energy of 15.53 kcal/mol(B3LYP) and 18.67 kcal/mol (CAM-B3LYP). The optimized molecular structures also demonstrated that the longest Co(II)-N/O bond lengths are the Co(II)-O3 and Co(II)-O3a, as would be expected. Moreover, the Jahn-Teller effect for Co(II) complex can be detected by using NBO analysis. The other important interactions with high interaction energies presented in Table 7 are important indicators of electronic charge transfers in the Co (II) complex.

3.6. Molecular electrostatic potential (MEP)

A molecular electrostatic potential is an invaluable tool in chemistry that enables the visualization of electrophilic or nucleophilic reactive sites within molecular systems [69]. To investigate the electronic charge distribution of the $[Co(4Clpca)_2(H_2O)_2]$ complex, the MEP surface was theoretically implemented to find the electrophilic and nucleophilic sites using the B3LYP and CAM-B3LYP levels in conjunction with LanL2DZ level [70]. The 3D representation of the MEP surfaces is shown in Fig. 8. The different colors used in the MEP surface represent different values of the electrostatic potential: green represents the zero potential region, red represents the most negative region, and blue represents the most positive electrostatic potential region. The sequence of potential increases in the MEP map is as follows: red < orange < yellow < green < blue. The color code of the MEP for $[Co(4Clpca)_2(H_2O)_2]$ complex ranges from $-6.521\ e^{-2}$ to $+6.521\ e^{-2}$ for B3LYP and $-8.857\ e^{-2}$ to $+8.857\ e^{-2}$ for CAM-B3LYP. In this range, blue indicates the strongest attraction, while red indicates repulsion. Positive potential regions are primarily located around hydrogen atoms attached to O3 and O3a atoms. For this reason, the $[Co(4Clpca)_2(H_2O)_2]$ complex can interact with other chemical ligands or complexes through the H-bonding interactions. On the other hand, negative potential sites are found around the electronegative oxygen atoms O2 and O2a, as would be expected [71]. So, the $[Co(4Clpca)_2(H_2O)_2]$ complex can participate in new reactions through covalent bonds or H-bonding interactions through the uncoordinated carboxylate O atom. The remaining species in the complex are surrounded by yellow and green regions. Due to its high chemical activity, this complex is suitable for both electrophilic and nucleophilic reactions [72].

3.7. Static nonlinear optical properties

To investigate the optical properties of the $[Co(4Clpca)_2(H_2O)_2]$ complex, mean polarizability (α), first-order hyperpolarizability (β), and second-order hyperpolarizability (γ) parameters are calculated, and the obtained results are presented in Table 8. The mean polarizability provides information about the linear optical properties of a chemical

Table 7
High-energy hyper conjugative interactions obtained by the B3LYP and CamB3LYP methods for the $[Co(4Clpic)_2(H_2O)_2]$ complex.

				B3LYP			CAM B3LYP		
Type	Bonding	Type	Antibonding	E^2 (kcal/mol)	$E(j) - E(i)^b$ (a.u.)	$F(i,j)$ (a.u)	E^2 (kcal/mol)	$E(j) - E(i)$ (a.u.)	$F(i,j)$ (a.u)
LP (2)	O1	LP*(5)	Co1	20.58	0.68	0.134	23.96	0.81	0.176
LP (2)	O1a	LP*(5)	Co1	20.57	0.68	0.134	23.96	0.81	0.176
LP (2)	O3	LP*(8)	Co1	15.53	0.72	0.150	18.67	0.83	0.157
LP (2)	O3a	LP*(8)	Co1	15.53	0.72	0.150	18.67	0.83	0.157
LP (1)	N1a	LP*(4)	Co1	23.81	0.29	0.114	31.02	0.38	0.146
LP (1)	N1	LP*(4)	Co1	23.81	0.29	0.114	31.02	0.38	0.146
LP (3)	O1	π*	C6-C5	32.98	0.27	0.120	5.27	0.98	0.091
LP (2)	O2	σ*	C6-C5	12.53	0.64	0.115	10.85	0.72	0.113
LP (2)	O2	σ*	C6-O1	12.53	0.64	0.115	14.77	0.78	0.137
LP (2)	O2a	σ*	C6a-O1a	9.16	0.60	0.094	10.85	0.72	0.113
LP (3)	O1a	π*	C6a C5a	32.98	0.27	0.120	40.78	0.38	0.157
LP (2)	O2a	σ*	C6a C5a	12.53	0.64	0.115	10.88	0.72	0.113
π	C5a-N1a	π*	C1a-C2a	11.86	0.34	0.080	16.74	0.43	0.108
π	C3a 4a	π*	C5a N1a	14.86	0.26	0.080	22.37	0.33	0.112
π	C3a-4a	π*	C1a-C2a	9.38	0.29	0.068	13.17	0.38	0.092
π	N1 C5	π*	C1 C2	11.86	0.34	0.080	16.74	0.43	0.108
π	C1-C2	π*	C3-C4	11.67	0.28	0.072	17.65	0.36	0.101
π	C3-C4	π*	C5-N1	14.86	0.26	0.080	22.37	0.33	0.112

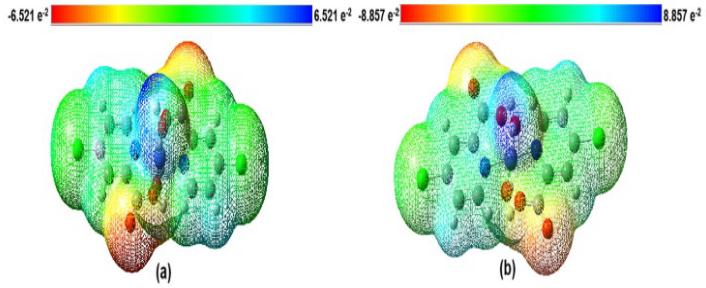

Fig. 8. 3D Molecular electrostatic potential a) B3LYP/LanL2DZ level, b) CAM-B3LYP/LanL2DZ level for $[Co(4Clpca)_2(H_2O)_2]$ complex.

Table 8
The dipole moment (Debye), static polarizability ($\times 10^{-23}$ esu), anisotropy of polarizability ($\times 10^{-23}$ esu), first-order hyperpolarizability ($\times 10^{-30}$ esu), and second-order hyperpolarizability ($\times 10^{-36}$ esu) for the 4Clpca ligand and $[Co(4Clpca)_2(H_2O)_2]$ complex calculated by B3LYP/LanL2DZ and CAM-B3LYP/LanL2DZ levels.

Parameter	4Clpca		$[Co(4Clpca)_2(H_2O)_2]$	
	B3LYP	CAM-B3LYP	B3LYP	CAM-B3LYP
μ (Debye)	1.1892	1.7826	0.0121	0.0014
α (0;0)	1.1133	1.1447	3.1260	2.9040
Δα (0;0)	3.6131	1.0445	3.1996	2.7887
β (0;0,0)	4.1969	3.0532	0.0018	0.0007
γ (0;0,0,0)	1.1892	3.2938	60.891	30.805

system. According to B3LYP results, the dipole moment values of the 4Clpca and Co(II) complex are 1.1892 and 0.0121 Debye. The 4Clpca ligand coordinated to the Co(II) ion forms a centrosymmetric crystal structure. Therefore, there is a decrease in the magnitude of dipole moment vectors. The static polarizability and anisotropy values of the Co(II) complex were calculated as 3.1260×10^{-23} and 3.1996×10^{-23} esu by using B3LYP level. The first-order static hyperpolarizability value of the Co(II) complex is 0.0018×10^{-30} esu, while the second-order static hyperpolarizability value is 60.891×10^{-36} esu. Due to the centrosymmetric crystal structure of $[Co(4Clpca)_2(H_2O)_2]$ complex, the dipole moments almost vanish, and therefore, the first-order hyperpolarizability parameter of the complex is obtained as negligible.

In a recent study, the β (0; 0,0) parameter was calculated as 4.51×10^{-30} and 4.21×10^{-30} esu for Mn(II) and Zn(II) complexes containing 6-bromopyridine-2-carboxylic acid [73]. In the same study, γ (0; 0,0,0) parameter was calculated as 208.45×10^{-30} and 8.91×10^{-30} esu, respectively. So, the γ (0; 0,0,0) parameter for Co(II) complex is comparable with the previously reported data [73], while the β (0; 0,0) parameter for Co(II) complex is obtained less than the similar structure [73] due to the high symmetry of Co(II) complex. When comparing the μ and β (0; 0,0) parameters obtained for the 4Clpca and Co(II) complex, after the 4Clpca ligand binds to the Co(II) ion, the μ and β (0; 0,0) parameters are decreased due to the formation of centrosymmetric structure. In another study, the β (0; 0,0) and γ (0; 0,0,0) parameters for Cu (II) complex incorporating chalcone and 2,2′-bipyridine mixed ligands were reported. The β (0; 0,0) and γ (0; 0,0,0) parameters for Cu(II) complex were reported as 20.36×10^{-30} esu and 2775.176×10^{-36} esu, respectively [74]. So, it was also concluded that the presence of secondary ligands in metal complexes dramatically induces both first- and second-order hyperpolarizability parameters.

3.8. Frequency-dependent nonlinear optical properties

For the investigation of frequency-dependent first-order hyperpolarizability, the electro-optic Pockel's effect (EOPE) β(ω; ω,0) and electric field-induced second harmonic generation (ESHG) β(-2ω; ω,ω) were considered, while for the second hyperpolarizability, dc-Kerr effect γ(-ω; ω,0,0) and second harmonic generationγ(-2ω; ω,ω,0) were calculated. Calculations of α, β, and γ at the frequencies of ω = 0.0856252 a.u (λ = 532 nm) and ω = 0.0428126 au. (λ = 1064 nm) for 4Clpca and Co (II) complex have been carried out using B3LYP/LanL2DZ and CAM-B3LYP/LanL2DZ levels, and the obtained results are given in Table 9. The significant increases were detected in the parameters of frequency-dependent α (-ω; 0), β(-ω; ω,0), and γ (-ω; ω,0,0) with complex formation. In addition, Table 9 clearly shows that the increase in the frequency value of the applied external field is accompanied by a decrease in the frequency-dependent parameters α (-ω; 0), Δα (-ω; 0) and γ (-ω; ω,0,0).

B3LYP level predicted the dc-Kerr coefficient values for 4Clpca and Co(II) complex as 6.0267×10^{-36} esu and 329.59×10^{-36} esu at 0.0856252 au., respectively. The SHG γ(-2ω; ω,ω,0) parameters for 4Clpca and Co(II) complex were obtained as 163.70×10^{-36} esu and 433.93×10^{-36} esu at 0.0856252 au., while the same parameter was calculated as 9.8944×10^{-36} esu and 174.40×10^{-36} esu at 0.0428126 au. Consequently, Co(II) complex has higher frequency-dependent second-order hyperpolarizability (γ (-ω; ω,0,0) and γ (-2ω; ω,ω,0)) than the 4Clpca ligand at 0.0856252 au. When the results are compared again, it is seen that the Co(II) metal-organic complex shows a more active NLO property than the single ligand [5,21,26,48,50,51,75–87]. So, it can be said that $[Co(4Clpca)_2(H_2O)_2]$ complex under investigation can be considered as a potential candidate especially for second-order hyperpolarizability applications.

4. Conclusion

A novel $[Co(4Clpca)_2(H_2O)_2]$ complex of 4-Chloro-pyridine-2-carboxylic acid ligand has been prepared and structurally characterized using single-crystal X-ray diffraction.The spectroscopic properties of the Co(II) complex have been evaluated by FT-IR and UV–Vis spectra. Both XRD and FT-IR results demonstrated that the Co(II) ion is located at the center of the distorted octahedral coordination sphere. In order to provide a detailed investigation, density functional theory calculations on structural, spectroscopic, and optical properties were carried out via the B3LYP/LanL2DZ and CAM-B3LYP levels. B3LYP and CAM-B3LYP results demonstrated that there is a strong electronic absorption band at 356 nm, assigned as LMCT interaction. FMO analysis also demonstrated that the coordination of the 4Clpca ligand to the Co(II) metal ion decreases HOMO energy, resulting in a more chemically stable complex. After pca ligand coordinates to the Co(II) ion, a novel complex with a centrosymmetric structure is formed, then the dipole moment vectors in the complex vanish each other, and therefore, there is a decrease in the dipole moment value. Therefore, a decrease in the static first-order hyperpolarizability parameter was detected. However, a significant increase in the static second-order hyperpolarizability parameter, which is independent of crystal symmetry, accompanied by complex formation. When it comes to frequency-dependent NLO properties, the γ (-w; w,0,0) and γ (-2w; w,w,0) increase after the 4Clpca ligand binds to Co(II) ion. It was concluded that the Co(II) complex under investigation especially at

Table 9
The dynamic polarizability ($\times 10^{-23}$ esu), anisotropy of polarizability ($\times 10^{-23}$ esu), first-order hyperpolarizability ($\times 10^{-30}$ esu), second-order dynamic hyperpolarizability ($\times 10^{-36}$ esu) for 4Clpca ligand and $[Co(4Clpca)_2(H_2O)_2]$ complex obtained by B3LYP/LanL2DZ levels.

Parameter	4Clpca				$[Co(4Clpca)_2(H_2O)_2]$			
	ω = 0.0856252 au		ω = 0.0428126 au		ω = 0.0856252 au		ω = 0.0428126 au	
	B3LYP	CAM-B3LYP	B3LYP	CAM	B3LYP	CAM-B3LYP	B3LYP	CAM-B3LYP
α (-ω;0)	1.2631	4.6548	1.2060	1.1593	3.5215	3.1200	3.1984	2.9517
Δα (-ω;0)	1.2176	1.1169	1.1369	1.0643	3.9752	3.1470	3.3325	2.8657
β(-ω;ω,0)	5.1102	4.0480	0.4559	3.2597	0.0118	0,0126	0.0250	0.0007
β(-2ω;ω,ω)	14.982	8.8334	5.4037	3.7084	0.0950	0.7861	0.0600	0.0011
γ (-ω;ω,0,0)	6.0267	4.4217	7.9765	3.5237	329.59	10.043	71.148	35.008
γ (-2ω;ω,ω,0)	163.70	11.557	9.8944	4.0814	433.93	−1198	174.40	49.156

ω = 0.0428126 au. frequency is a potential candidate for third-order NLO applications.

CRediT authorship contribution statement

Merve Şimşek: Writing – original draft, Visualization, Validation, Investigation. **Ömer Tamer:** Writing – review & editing, Writing – original draft, Visualization, Supervision, Methodology, Investigation, Conceptualization. **Necmi Dege:** Visualization, Validation, Formal analysis, Data curation. **Davut Avcı:** Writing – review & editing, Supervision, Software. **Yusuf Atalay:** Visualization, Supervision, Software, Methodology.

Funding

This work was supported by the Scientific Research Projects Unit of Sakarya University (Project number: 2023-19-44-48)

Declaration of competing interest

The authors declare that they have no known competing financial interests or personal relationships that could have appeared to influence the work reported in this paper.

Acknowledgements

The authors thank to Scientific and Technological Researches Center, Sinop University, Türkiye, for the use of the Bruker D8-QUEST diffractometer.

Appendix A. Supplementary data

Supplementary data to this article can be found online at https://doi.org/10.1016/j.mssp.2024.109179.

Data availability

Data will be made available on request.

References

[1] D.R. Kanis, M.A. Ratner, T.J. Marks, Design and construction of molecular assemblies with large second-order optical nonlinearities. Quantum chemical aspects, Chem. Rev. 94 (2002) 195–242.
[2] F. Meyers, S.R. Marder, B.M. Pierce, J.L. Brédas, No Title, Chem. Phys. Lett. 228 (1994) 171.
[3] M. Nakano, H. Fukui, T. Minami, K. Yoneda, Y. Shigeta, R. Kishi, B. Champagne, E. Botek, T. Kubo, K. Ohta, K. Kamada, Erratum to: (Hyper)polarizability density analysis for open-shell molecular systems based on natural orbitals and occupation numbers, Theor. Chem. Acc. 130 (2011) 725–726.
[4] B.C. Bernard Kirtman, David M. Bishop, Electric field simulation of substituents in Donor–Acceptor polyenes: a comparison with ab initio predictions for dipole moments, polarizabilities, and hyperpolarizabilities, Am. Chem. Soc. 122 (33) (2000) 8007–8012.
[5] S. Di Bella, Second-order nonlinear optical properties of transition metal complexes, Chem. Soc. Rev. 30 (2001) 355–366.
[6] V. Guerchais, H. Le Bozec, in: H. Bozec, V. Guerchais (Eds.), Metal Complexes Featuring Photochromic Ligands BT - Molecular Organometallic Materials for Optics, Springer Berlin Heidelberg, Berlin, Heidelberg, 2010, pp. 171–225.
[7] B.J. Coe, Switchable nonlinear optical metallochromophores with pyridinium electron acceptor groups, Accounts of chemical research 39 (2006) 383–393.
[8] Y. L. Chen, Y. G. Wang, Q. Yu, Recent advances in photomechanical crystals made from metal–organic and organometallic complexes, Organometallics 42 (2023) 2159–2170.
[9] N.S. Khalid Muhammad, Tahir Suleman, Shafiq Iqra, Munawar Khurram Shahzad, Morais Sara, Braga Ataualpa, A theoretical approach towards designing of banana shaped non fullerene chromophores using efficient acceptors moieties: exploration of their NLO response properties, Opt. Quant. Electron. 55 (2023).
[10] J.K. Abbott, B. Smith, T. Cook, Z.-L. Xue, Synthesis of organometallic compounds, Modern Inorganic Synthetic Chemistry (2017) 247–277. Elsevier.
[11] Ö. Tamer, H. Mahmoody, K.F. Feyzioğlu, O. Kılınç, D. Avci, O. Orun, N. Dege, Y. Atalay, Synthesis of the first mixed ligand Mn (II) and Cd (II) complexes of 4-methoxy-pyridine-2-carboxylic acid, molecular docking studies and investigation of their anti-tumor effects in vitro, Appl. Organomet. Chem. 34 (2020) e5416.
[12] Ö. Tamer, S.A. Tamer, Ö. İdil, D. Avcı, H. Vural, Y. Atalay, Antimicrobial activities, DNA interactions, spectroscopic (FT-IR and UV-Vis) characterizations, and DFT calculations for pyridine-2-carboxylic acid and its derivates, J. Mol. Struct. 1152 (2018) 399–408.
[13] Ö. Tamer, A unique manganese (II) complex of 4-methoxy-pyridine-2-carboxylate: synthesis, crystal structure, FT-IR and UV–Vis spectra and DFT calculations, J. Mol. Struct. 1144 (2017) 370–378.
[14] Ö. Tamer, H. Mahmoody, K. Feyzioğlu, O. Kılınç, D. Avci, O. Orun, N. Dege, Y. Atalay, Synthesis of the first mixed ligand Mn (II) and Cd (II) complexes of 4 methoxy-pyridine-2-carboxylic acid, molecular docking studies and investigation of their anti-tumor effects in vitro: first mixed ligand complexes of 4-methoxy-pyridine-2-carboxylic ac, Appl. Organomet. Chem. 34 (2019) e5416.
[15] N.E.A. El-Gamel, G.G. Mohamed, Synthesis, spectral and thermal characterization of 6 hydroxymethyl pyridine 2 carboxylic acid methyl ester and its complexes, Journal of Thermal Analysis and Calorimetry 81 (2005) 111–118.
[16] K.S. Małecki J. G, A. Maroń, M. Penkala, Synthesis, molecular, spectroscopic and catalytic characterization of ruthenium(II) complexes with pyridine-2-carboxylic acid derivatives ligands, Polyhedron 48 (1) (2012) 21–30.
[17] H. Vural, M. Orbay, Synthesis, crystal structure, spectroscopic investigations and DFT calculations of the copper(II) complex of 4-(Trifluoromethyl)pyridine-2-carboxylic acid, J. Mol. Struct. 1146 (2017).
[18] Z.X. Yu, W.H. Fang, Y.Q. Feng, Z.R. Sha, S.J. Feng, Eight new coordination polymers containing rigid 4-(4-carboxy-phenyl)-pyridine-2-carboxylic acid: synthesis, structural diversity, fluorescence and magnetic properties, Inorg. Chim. Acta. 507 (2020) 119600.
[19] B.Y. Turan-Zitouni G, K. Güven, Synthesis and antimicrobial activity of some imidazo-[1,2-a]pyridine-2- carboxylic acid arylidenehydrazide derivatives, Boll. Chim. Farm. 140 (2001) 397–400.
[20] Y.K. Márquez-Flores, M.E. Campos-Aldrete, H. Salgado-Zamora, J. Correa-Basurto, M.E. Meléndez-Camargo, Acute and chronic anti-inflammatory evaluation of imidazo[1,2-a]pyridine carboxylic acid derivatives and docking analysis, Med. Chem. Res. 21 (2012) 3491–3498.
[21] M. Şimşek, Ö. Tamer, N. Dege, D. Avcı, H. Mahmoody, Y. Atalay, A new mixed ligand zinc(II) complex of 3-hydroxy and 4-chloro substituted pyridine-2-carboxylic acid: synthesis, characterization, NLO properties and DFT calculation, Mater. Today Commun. 38 (2024) 108021.
[22] B. Li, J. Wang, H. Song, H. Wu, X. Chen, X. Ma, Synthesis, crystal structure, and BSA interaction with a new Co(II) complex based on 5 (trifluoromethyl)pyridine 2 carboxylic acid, J. Coord. Chem. 72 (2019) 2562–2573.
[23] D. Avcı, S. Altürk, F. Sönmez, Ö. Tamer, A. Başoğlu, Y. Atalay, B.Z. Kurt, N. Dege, Synthesis, spectral properties, in vitro α-glucosidase inhibitory activity and quantum chemical calculations of novel mixed-ligand M(II) complexes containing 1,10 phenanthroline, Appl. Organomet. Chem. 34 (2020) e5412.
[24] D. Avcı, Altürk Sümeyye, Sönmez Fatih, Tamer Ömer, Başoğlu Adil, Atalay Yusuf, Kurt Belma Zengin, Dege Necmi, Synthesis, spectral properties, α-glucosidase inhibition, second-order and third-order NLO parameters and DFT calculations of Cr(III) and V(IV) complexes of 3-methylpicolinic acid, J. Mol. Struct. 1220 (2020).
[25] D.A. Sümeyye Altürk, Ömer Tamer, Yusuf Atalay, Onur Şahin A cobalt (II) complex with 6-methylpicolinate: synthesis, characterization, second- and third-order

nonlinear optical properties, and DFT calculations, J. Phys. Chem. Solid. 98 (2016) 71–80.
[26] S. Altürk, D. Avcı, A. Başoğlu, Ö. Tamer, Y. Atalay, N. Dege, Copper(II) complex with 6-methylpyridine-2-carboxyclic acid: experimental and computational study on the XRD, FT-IR and UV–Vis spectra, refractive index, band gap and NLO parameters, Spectrochim. Acta Mol. Biomol. Spectrosc. 190 (2018) 220–230.
[27] D. Avcı, S. Altürk, F. Sönmez, Ö. Tamer, A. Başoğlu, Y. Atalay, B.Z. Kurt, N. Dege, Three novel Cu(II), Cd(II) and Cr(III) complexes of 6–Methylpyridine–2–carboxylic acid with thiocyanate: synthesis, crystal structures, DFT calculations, molecular docking and α-Glucosidase inhibition studies, Tetrahedron 74 (2018) 7198–7208.
[28] D. Avcı, S. Altürk, F. Sönmez, Ö. Tamer, A. Başoğlu, Y. Atalay, B.Z. Kurt, N. Dege, Novel Cu(II), Co(II) and Zn(II) metal complexes with mixed ligand: synthesis, crystal structure, α-glucosidase inhibition, DFT calculations, and molecular docking, J. Mol. Struct. 1197 (2019) 645–655.
[29] D. Avcı, S. Altürk, F. Sönmez, Ö. Tamer, A. Başoğlu, Y. Atalay, B. Zengin Kurt, N. Dege, Novel metal complexes containing 6-methylpyridine-2-carboxylic acid as potent α glucosidase inhibitor: synthesis, crystal structures, DFT calculations, and molecular docking, Mol. Divers. 25 (2021) 171–189.
[30] N. Dege, Ö. Tamer, M. Şimşek, D. Avcı, M. Yaman, A. Başoğlu, Y. Atalay, Experimental and theoretical approaches on structural, spectroscopic (FT IR and UV-Vis), nonlinear optical, and molecular docking analyses for Zn (II) and Cu (II) complexes of 6-chloropyridine-2 carboxylic acid, Appl. Organomet. Chem. 36 (2022) e6678.
[31] N. Dege, Ö. Özge, D. Avcı, A. Başoğlu, F. Sönmez, M. Yaman, Ö. Tamer, Y. Atalay, B. Zengin Kurt, Concentration effects on optical properties, DFT, crystal characterization and α glucosidase activity studies: novel Zn(II) complex, Spectrochim. Acta Mol. Biomol. Spectrosc. 262 (2021) 120072.
[32] N. Dege, Ö. Tamer, M. Yaman, A. Başoğlu, D. Avcı, Y. Atalay, Crystallographic, spectroscopic, thermal, optical investigations and density functional theory calculations for novel Co(II) and Mn(II) complexes, Appl. Phys. A 127 (2021) 132.
[33] D. Avcı, Y. Saeedi, A. Başoğlu, N. Dege, S. Altürk, Ö. Tamer, Y. Atalay, Novel Mn(II) and Zn(II) complexes of 6-bromopicolinic acid as a potential optical material: synthesis, spectral characterizations, linear, and nonlinear optical properties and density functional theory calculations, Appl. Organomet. Chem. 35 (2021) e6125.
[34] G.M. Sheldrick, A short history of SHELX, Acta Crystallogr., Sect. A: Found. Crystallogr. 64 (1) (2008) 112–122.
[35] G.M. Sheldrick, SHELXT–Integrated space-group and crystal-structure determination, Acta Crystallogr. A: Foundations and Advances 71 (1) (2015) 3–8.
[36] B.A.I.M.W.U. APEX2.
[37] C.F. Macrae, I.J. Bruno, J.A. Chisholm, P.R. Edgington, P. McCabe, E. Pidcock, L. Rodriguez Monge, R. Taylor, J. Streek, P.A. Wood, Mercury CSD 2.0–new features for the visualization and investigation of crystal structures, J. Appl. Crystallogr. 41 (2) (2008) 466–470.
[38] L.J. Farrugia, WinGX and ORTEP for windows: an update, J. Appl. Crystallogr. 45 (4) (2012) 849–854.
[39] n. Gaussian, B. Revision, M.J. Frisch, G.W. Trucks, H.B. Schlegel, P.M.W. Gill, B. G. Johnson, M.A. Robb, J.R. Cheeseman, T. Keith, G.A. Petersson, J. A. Montgomery, K. Rhagavachari, M.A. Al-Laham, V.G. Zakrzewski, J.V. Ortiz, J. B. Foresman, J. Cioslowski, B.B. Stefanov, A. Nanayakkara, M. Challacombe, C. Y. Peng, P.Y. Ayala, W. Chen, M.W. Wong, J.L. Andres, E.S. Replogle, R. Gomperts, R.L. Martin, D.J. Fox, J.S. Binkley, D.J. Defrees, J. Baker, J.P. Stewart, M. Head Gordon, C. Gonzalez, J.A. Pople, Gaussian, 1995.
[40] W.Y.C. Lee, R.G. Parr, Development of the Colle-Salvetti correlation-energy formula into a functional of the electron density, Phys. Rev. B 37 (1988) 785–789.
[41] T. Yanai, D.P. Tew, N.C. Handy, A new hybrid exchange–correlation functional using the Coulomb-attenuating method (CAM-B3LYP), Chem. Phys. Lett. 393 (1–3) (2004) 51–57.
[42] T.H. Dunning Jr., P.J. Hay, Modern Theoretical Chemistry, 1976.
[43] P.J. Hay, W.R. Wadt, Ab initio effective core potentials for molecular calculations. Potentials for the transition metal atoms Sc to Hg, J. Chem. Phys. 82 (1) (1985) 270–283.
[44] V. Barone, M. Cossi, Quantum calculation of molecular energies and energy gradients in solution by a conductor solvent model, J. Phys. Chem. 102 (11) (1998) 1995–2001.
[45] M. Cossi, N. Rega, G. Scalmani, V. Barone, Energies, structures, and electronic properties of molecules in solution with the C-PCM solvation model, J. Comput. Chem. 24 (6) (2003) 669–681.
[46] S. Gorelsky, SWizard Program, 2010.
[47] P.R. Spackman, M.J. Turner, J.J. McKinnon, S.K. Wolff, D.J. Grimwood, D. Jayatilaka, M.A. Spackman, CrystalExplorer: a program for Hirshfeld surface analysis, visualization and quantitative analysis of molecular crystals, J. Appl. Crystallogr. 54 (3) (2021) 1006–1011.
[48] K. Aswaniya, M.B.J. Raj, S. Gowri, G. Vinitha, Promising computational, structural, vibrational and optical properties of piperazinium bis(2-carboxypyridine) monohydrate (PBCPM) crystal for NLO device applications, Optik 246 (2021) 167836.
[49] D. Avcı, S. Altürk, F. Sönmez, Ö. Tamer, A. Başoğlu, Y. Atalay, B.Z. Kurt, N. Dege, Correction to: novel metal complexes containing 6-methylpyridine-2-carboxylic acid as potent α-glucosidase inhibitor: synthesis, crystal structures, DFT calculations, and molecular docking (Molecular Diversity 25 (1) (2021) 171–189, https://doi.org/10.1007/s11030-020.
[50] S. Altürk, D. Avcı, B.Z. Kurt, Ö. Tamer, A. Başoğlu, F. Sönmez, Y. Atalay, N. Dege, Two New Co(II) Complexes of Picolinate: Synthesis, Crystal Structure, Spectral Characterization, α-Glucosidase Inhibition and TD/DFT Study, Journal of Inorganic and Organometallic Polymers and Materials 29 (2019) 1265–1279.
[51] K. Anitha, V. Balachandran, Assessment of long-range corrected and conventional DFT functional for the prediction of second – order NLO properties and other molecular properties of N-(2-cyanoethyl)-N-butylaniline – a vibrational spectroscopy study, Spectrochim. Acta Mol. Biomol. Spectrosc. 146 (2015) 66–79.
[52] D. Jayatilaka, S. Wolff, D. Grimwood, J. McKinnon, M. Spackman, CrystalExplorer: a tool for displaying Hirshfeld surfaces and visualising intermolecular interactions in molecular crystals, Acta Crystallographica Section A - ACTA CRYSTALLOGR A 62 (2006).
[53] Ö. Tamer, N. Dege, D. Avcı, Y. Atalay, The static and frequency-dependent second- and third-order nonlinear optical properties of Zn(II) and Ni(II) complexes of 4-methoxypyridine 2 carboxylic acid: a detailed experimental and theoretical study, Appl. Organomet. Chem. n/a e7206.
[54] A. Kumar, V. Hüch, V.J. Ram, Partially reduced thiochromene based oxathiahelicenes: crystallographic, computational and Hirschfeld surface analyses, CrystEngComm 15 (35) (2013) 7019–7030.
[55] N.Q. Shikhaliyev, S.T. Çelikesir, M. Akkurt, K.N. Bagirova, G.T. Suleymanova, F. A. Toze, Crystal structure and Hirshfeld surface analysis of (E)-1-(4-chlorophenyl)-2 [2, 2-dichloro-1 (4 fluorophenyl) ethenyl] diazene, Acta Crystallogr. E: Crystallographic Communications 75 (4) (2019) 465–469.
[56] R. Yadav, M. Trivedi, G. Kociok-Köhn, R. Prasad, A. Kumar, New Ni (II) 1, 2-bis (diphenylphosphino) ethane dithiolates: crystallographic, computational and Hirshfeld surface analyses, CrystEngComm 17 (47) (2015) 9175–9184.
[57] G. Świderski, H. Lewandowska, R. Świslocka, S. Wojtulewski, L. Siergiejczyk, A. Wilczewska, Thermal, spectroscopic (IR, Raman, NMR) and theoretical (DFT) studies of alkali metal complexes with pyrazinecarboxylate and 2, 3-pyrazinedi-carboxylate ligands, J. Therm. Anal. Calorim. 126 (2016) 205–224.
[58] D. Avcı, H.E. Cömert, F. Sönmez, N. Dege, Ö. Tamer, Y. Atalay, Comparative assessment of structure–property relationships of new Cu (II) complex in selected density functionals, Spectrochim. Acta Mol. Biomol. Spectrosc. 305 (2024) 123489.
[59] C. Ipek, H. Gümüs, M. Simsek, M. Tosun, DFT and molecular docking study of 1-(2'-Thiophen)-2-propen-1-one-3-(2,3,5-trichlorophenyl) (TTCP) molecule as antiviral to covid 19 main protease, Arabian J. Sci. Eng. 48 (1) (2023) 1031–1040.
[60] Ö. Tamer, M. Şimşek, D. Avcı, Y. Atalay, First and second order hyperpolarizabilities of flavonol derivatives: a density functional theory study, Spectrochim. Acta Mol. Biomol. Spectrosc. 283 (2022) 121728.
[61] Ö. Tamer, M. Şimşek, D. Avcı, Y. Atalay, Static/dynamic first and second order hyperpolarizabilities, optimized structures, IR, UV–Vis, 1H and 13C NMR spectra for effective charge transfer compounds: a DFT study, Spectrochim. Acta Mol. Biomol. Spectrosc. 286 (2023) 122005.
[62] N. Büyükkidan, A short review on structural concepts of metal complexes of proton transfer salts of pyridine-2-carboxylic acid, Journal of the Turkish Chemical Society Section A: Chemistry 10 (2023) 11–20.
[63] M. Nakai, F. Sekiguchi, M. Obata, C. Ohtsuki, Y. Adachi, H. Sakurai, C. Orvig, D. Rehder, S. Yano, Synthesis and insulin-mimetic activities of metal complexes with 3-hydroxypyridine-2-carboxylic acid, J. Inorg. Biochem. 99 (2005) 1275–1282.
[64] H.P. Gümüş, Ö. Tamer, D. Avcı, Y. Atalay, Effects of donor–acceptor groups on the structural and electronic properties of 4-(methoxymethyl)-6-methyl-5-nitro-2-oxo-1,2-dihydropyridine-3-carbonitrile, Spectrochim. Acta Mol. Biomol. Spectrosc. 132 (2014) 183–190.
[65] E. Paenurk, R. Gershoni-Poranne, P. Chen, Trends in metallophilic bonding in Pd–Zn and Pd–Cu complexes, Organometallics 36 (24) (2017) 4854–4863.
[66] G.H. Ipek Cengiz, Şimşek Merve, DFT and molecular docking study of 1-(2'-Thiophen)-2-propen-1-one-3-(2,3,5-trichlorophenyl) (TTCP) molecule as antiviral to covid-19 main protease, Arabian J. Sci. Eng. 48 (2023/01/01) 1040.
[67] N. Dege, Ö. Tamer, M. Yaman, A. Başoğlu, D. Avcı, Y. Atalay, Crystallographic, spectroscopic, thermal, optical investigations and density functional theory calculations for novel Co (II) and Mn (II) complexes, Appl. Phys. A 127 (2021) 1–17.
[68] M. Usman, R.A. Khan, A. Alsalme, W. Alharbi, K.H. Alharbi, M.H. Jaafar, M. Abu Khanjer, S. Tabassum, Structural, spectroscopic, and chemical bonding analysis of Zn (II) complex [Zn (sal)](H2O): combined experimental and theoretical (NBO, QTAIM, and ELF) investigation, Crystals 10 (4) (2020) 259.
[69] E. Scrocco, J. Tomasi, Electronic molecular structure, reactivity and intermolecular forces: an euristic interpretation by means of electrostatic molecular potentials, Adv. Quant. Chem. (1978) 115–193. Elsevier.
[70] G. Ramesh, B.V. Reddy, Barrier potential, structure (monomer and dimer), inter- and intra molecular interactions, vibrational analysis, Fukui functions, MESP, NBO, UV and NMR analysis of pyridine-3-carboxylic acid using spectroscopic and DFT approach, Polycycl. Aromat. Comp. 43 (3) (2023) 2488–2505.
[71] F.E.Ö. Özbek, G. Uğurlu, E. Kalay, H. Necefoğlu, Synthesis, characterization and computational studies of 4-[(Pyridine-3-carbonyl)-hydrazonomethyl]-benzoic acid, J. Mol. Struct. 1215 (2020) 128247.
[72] M. Şimşek, Ö. Tamer, N. Dege, D. Avcı, H. Mahmoody, Y. Atalay, A new mixed-ligand zinc (II) complex of 3-hydroxy and 4-chloro substituted pyridine-2-carboxylic acid: synthesis, characterization, NLO properties and DFT calculation, Mater. Today Commun. 38 (2024) 108021.
[73] D. Avcı, Y. Saeedi, A. Başoğlu, N. Dege, S. Altürk, Ö. Tamer, Y. Atalay, Novel Mn (II) and Zn (II) complexes of 6-bromopicolinic acid as a potential optical material: synthesis, spectral characterizations, linear, and nonlinear optical properties and density functional theory calculations, Appl. Organomet. Chem. 35 (3) (2021) e6125.
[74] R. Gaur, P. Kallem, Structural and theoretical study of copper (II) complex incorporating chalcone and 2, 2'-bipyridine mixed ligands: a probable candidate for optical material, New J. Chem. 46 (42) (2022) 20366–20376.

[75] J. Sun, G. Wang, C. Liu, Y. Shi, M. Zhao, Synthesis of four pyrene-containing chalcone derivatives: achieving excellent third-order nonlinear optical properties by optimizing halopyridines, Opt Laser. Technol. 109 (2019) 600–607.
[76] M.R.S.A. Janjua, M. Amin, M. Ali, B. Bashir, M.U. Khan, M.A. Iqbal, W. Guan, L. Yan, Z.M. Su, A DFT study on the two-dimensional second-order nonlinear optical (NLO) response of terpyridine substituted hexamolybdates: physical insight on 2D inorganic–organic hybrid functional materials, Eur. J. Inorg. Chem. 2012 (2012) 705.
[77] Y.S. Mary, H.T. Varghese, C.Y. Panicker, T. Thiemann, A.A. Al-Saadi, S.A. Popoola, C. Van Alsenoy, Y. Al Jasem, Molecular conformational analysis, vibrational spectra, NBO, NLO, HOMO LUMO and molecular docking studies of ethyl 3 (E) (anthracen-9-yl)prop-2-enoate based on density functional theory calculations, Spectrochimica Acta – Part A: Molecular and Biomolecular Spectroscopy 150 (2015) 533–542.
[78] Y. Zhang, C.-Y. Zhao, W.-H. Fang, X.-Z. You, A molecular design view on the first hyperpolarizability of salicylideneaniline derivatives, Theor. Chem. Acc. 96 (1997) 129–134.
[79] O. Maury, H. Le Bozec, Molecular engineering of octupolar NLO molecules and materials based on bipyridyl metal complexes, Acc. Chem. Res. 38 (2005) 691.
[80] E.D. D'Silva, G.K. Podagatlapalli, S.V. Rao, D.N. Rao, S.M. Dharmaprakash, New, high efficiency nonlinear optical chalcone Co crystal and structure property relationship, Cryst. Growth Des. 11 (2011) 5362–5369.
[81] T. Chandra Shekhara Shetty, C.S. Chidan Kumar, K.N. Gagan Patel, T.S. Chia, S. M. Dharmaprakash, P. Ramasami, Y. Umar, S. Chandraju, C.K. Quah, Optical nonlinearity of D-A-π-D and D-A-π-A type of new chalcones for potential applications in optical limiting and density functional theory studies, J. Mol. Struct. 1143 (2017) 306–317.
[82] N.J. Long, Organometallic compounds for nonlinear optics—the search for en light-enment, Angew Chem. Int. Ed. Engl. 34 (1995) 21–38.
[83] H.S. Nalwa, Organometallic materials for nonlinear optics, Appl. Organomet. Chem. 5 (1991) 349–377.
[84] J. Binoy, M.K. Marchewka, V.S. Jayakumar, The 'partial resonance' of the ring in the NLO crystal melaminium formate: study using vibrational spectra, DFT, HOMO–LUMO and MESP mapping, Spectrochim. Acta Mol. Biomol. Spectrosc. 104 (2013) 97–109.
[85] J. Jayabharathi, V. Thanikachalam, M.V. Perumal, Physicochemical and solvatochromic analysis of an imidazole derivative as NLO material, Spectrochim. Acta Mol. Biomol. Spectrosc. 85 (2012) 31–37.
[86] Ö. Tamer, D. Avcı, Y. Atalay, Synthesis, X-Ray crystal structure, photophysical characterization and nonlinear optical properties of the unique manganese complex with picolinate and 1,10 phenantroline: toward the designing of new high NLO response crystal, J. Phys. Chem. Solid. 99 (2016) 124–133.
[87] G. Hennrich, I. Asselberghs, K. Clays, A. Persoons, Tuning octopolar NLO chromophores: synthesis and spectroscopic characterization of persubstituted 1,3,5-Tris(ethynylphenyl)benzenes, J. Org. Chem. 69 (2004) 5077.

Journal of Molecular Structure 1342 (2025) 142707

Contents lists available at ScienceDirect

Journal of Molecular Structure

journal homepage: www.elsevier.com/locate/molstr

Exploring the structural, vibrational, thermal, and nonlinear optical properties of a novel Cu(II) complex of 6-fluoro-pyridine-2-carboxylic acid

Ömer Tamer [a,*], Merve Şimşek [a], Davut Avcı [a], Adil Başoğlu [a], Mohamed Bensebaa [b], Mebarek Boukelkoul [b], Necmi Dege [c], Yusuf Atalay [a]

[a] Sakarya University, Physics Department, Faculty of Science, 54187, Sakarya, , Türkiye
[b] Ferhat ABBAS Setif1 University,Laboratoire de Physique Quantique et Systemes Dynamiques, Department of Physics, Faculty of Sciences, Setif, Algeria
[c] Ondokuz Mayıs University, Physics Department, Faculty of Science, 55139 Samsun, Türkiye

ARTICLE INFO

Keywords:
6 fluoro pyridine 2 carboxylic acid
Copper complex
Frequency-dependent hyperpolarizability
FT-IR and UV–Vis, DFT

ABSTRACT

This study reports the synthesis, crystal structure, spectroscopic, electronic, thermal and nonlinear optical properties of a novel Cu(II) complex of 6-fluoro-pyridine-2-carboxylic acid (6Fpca) ligand. The [Cu (6Fpca)$_2$•(H$_2$O)] complex was crystallized in the orthorhombic *Pbca* space group with a distorted tetragonal pyramidal coordination sphere around the central Cu(II) ion. The coordination sphere around the central Cu(II) ion was also proved by FT-IR and theoretical IR spectra. UV–Vis spectra for the Cu(II) complex revealed that the π→π*, n→π* and ligand-metal charge transfer interactions occur in the Cu(II) complex. The first-order hyperpolarizability β(-ω;ω,0) value for the [Cu(6Fpca)$_2$•(H$_2$O)] complex was 22.265 × 10^{-30} esu at 0.0856252 au, exhibiting a decrease to 11.823 × 10^{-30} esu at 0.0428126 au. Similarly, the second-order hyperpolarizability γ (-w; w,0,0) value was 111.07 × 10^{-30} esu at 0.0856252 au and decreased to 38.352 × 10^{-30} esu at 0.0428126 au. These results showed that the Cu(II) complex demonstrated a high degree of nonlinear optical (NLO) activity at 0.0856252 au.

1. Introduction

Nonlinear optical (NLO) materials represent a fascinating and crucial domain in the field of optics and photonics for technological advancement [1,2]. These materials exhibit a nonlinear response to intense light, providing a foundation for applications ranging from signal processing and imaging to telecommunications. At its core, the field of nonlinear optics explores how the optical properties of materials deviate from linear behavior when subjected to high-intensity light [3]. This departure from linearity gives rise to a rich array of phenomena, including second harmonic generation (SHG), optical rectification, and frequency mixing [4,5]. Using these nonlinear effects is pivotal for the development of devices in order to promote modern communication systems, medical imaging technologies, and emerging areas such as quantum optics.

Organic nonlinear optical materials, with their conjugated structures and push-pull chromophores, have been at the forefront of research due to their versatility and tunable properties [6]. Inorganic crystals, characterized by specific crystal symmetries, and semiconductors exhibit large macroscopic nonlinearities, providing unique advantages for various applications [7]. Metal-organic coordination complexes, a relatively recent addition to the nonlinear optical materials toolkit, bridge the gap between organics and inorganics, offering a promising avenue for tailored and responsive materials [8]. Transition metal complexes are showcased as efficient nonlinear optical materials, capable of generating harmonics and exhibiting a range of nonlinear phenomena. By virtue of their versatile electronic structures and tunable properties, transition metal complexes stand as key contributors to the advancement of nonlinear optical materials and technologies [9]. The electronic interactions between the metal center and surrounding ligands grants these metal complexes a unique set of electronic states and energy levels, allowing precise control over their optical behavior. Typically, transition metal ions have partially filled d orbitals, and the coordination with organic ligands introduces additional energy levels and alters the distribution of electron density. The specific changes depend on factors such as the nature of the transition metal, the type of ligands involved, and the coordination geometry [10]. The binding of the organic ligand to the transition metal ion can result in the splitting of

* Corresponding author.
E-mail address: omertamer@sakarya.edu.tr (Ö. Tamer).

https://doi.org/10.1016/j.molstruc.2025.142707
Received 16 March 2025; Received in revised form 12 April 2025; Accepted 16 May 2025
Available online 17 May 2025
0022-2860/© 2025 Elsevier B.V. All rights are reserved, including those for text and data mining, AI training, and similar technologies.

the d orbitals, known as ligand field splitting. This phenomenon gives rise to different energy levels for the electrons in the d orbitals, leading to a modified electronic structure [11].

Up to now, a number of metal complexes including azo-based ligands [12], pyridine-carboxylates [13–17], porphyrins [18], dithiolanes [19], chalcones [20] have been reported to investigate structure-property relationships and present a promising candidate to nonlinear optical materials. Understanding the structure-property relationships in nonlinear optical materials is essential for optimizing material's performance. This involves the detailed evaluating the electronic and geometric properties that govern their nonlinear responses. The interaction between metal and its coordination environment, ligand types, and overall molecular architecture is explored in the context of optimizing nonlinear optical responses. This insight is crucial for the rational design of transition metal complexes with tailored properties for specific nonlinear optical applications. A detailed literature research exhibited that no studies have been conducted to synthesis and investigate the relationship between the structural and nonlinear optical properties of metal complexes containing 6-fluoropyridine-2-carboxylic acid. The main motivations of this study are that the 6-fluoropyridine-2-carboxylic acid structure is a good chelator for metal ions and contains electronegative F atom in its structure as well as Cu(II) ion having unpaired electron and ability to exhibit various metal-ligand charge transfer transitions. In the present study, Cu(II) metal complexes of 6-fluoropyridine-2-carboxylic acid have been reported to investigate the geometric structure, spectroscopic and electronic properties, static and frequency-dependent nonlinear optical properties.

2. Material and methods

2.1. Synthesis

The Cu(II) metal complex was synthesized using high-quality chemicals supplied from Merck. Accordingly, no additional purification process was employed for the chemicals utilized in this study. The synthesis of Cu(II) complex was conducted by synthesis scheme presented in Fig. 1. The initial step involved the solution of 0.2 mmol of 6-fluoropyridine-2-carboxylic acid (6Fpca) in a mixture of ethanol and water (30 mL, 1:1). Subsequently, 0.1 mmol of $[Cu(CH_3COO)_2{\bullet}H_2O]$ metal salt was added and stirred continuously for 1.5 h at 50 °C at 400 rpm. The resulting solution was then left to evaporate at room temperature for a period of two weeks. Blue-colored crystals suitable for X-ray diffractometer were obtained from the blue color solution.

2.2. Experimental methods

Crystallographic data were collected using a Stoe IPDS II diffractometer with Mo-Kα radiation (λ = 0.71073 Å) at 293 K. The crystal structure was determined and refined using SHELXT [21] and SHELXL [22], respectively. Mercury software [23] was used to convert the file from cif format to mol2 format used as input file by GaussView 6.0. Additional software tools, including PLATON [24], WinGX [25], and PublCIF [26], were utilized in the crystallographic analysis process. Crystallographic data and refinement parameters for the Cu(II) complex

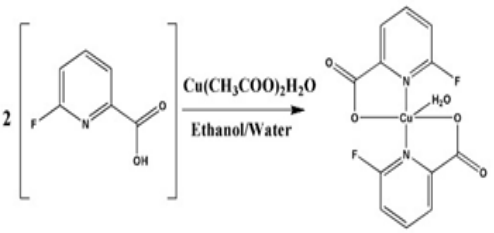

Fig. 1. General synthesis scheme for $[Cu(6Fpca)_2{\bullet}(H_2O)]$ complex.

are presented in Table 1. FT-IR spectra for the Cu(II) complex and 6Fpca ligand was recorded in the 4000 to 400 cm^{-1} range using a Perkin ELMER Spectrum-Two FT-IR spectrophotometer. UV–Vis spectrum of the Cu(II) complex and 6Fpca was obtained in the 800–200 nm range using a HITACHI U-2900 UV/Vis spectrophotometer in ethanol solvent. TG-DTA analysis of the Cu(II) metal complex was studied by NETZSCH STA 449F1 analyzer where the heating rate was suitably controlled at 10 °C min^{-1} under nitrogen atmosphere and the weight loss was measured from ambient temperature to 1000 °C.

2.3. Computational methods

The theoretical calculation of the Cu(II) complex was performed using the Gaussian 16 software [27]. This software enables a comprehensive analysis of the ground state geometry, vibrational spectrum, frontier molecular orbitals, molecular electrostatic potential surface, dipole moment (μ), polarizability (α), first and second-order static/dynamic hyperpolarizabilities (β and γ). The visualization of the theoretical results was also carried out using GaussView 6.0 [28]. DFT calculations were performed using the B3LYP [29,30] level with the LanL2DZ [31,32] basis set for the Cu(II) complex in a doublet spin state. To test the compatibility of the B3LYP method on the Cu(II) complex, geometric optimization calculations were also repeated with the B2PLYPD [33,34] and MP2 [35,36] methods. The UV–Vis spectrum of the Cu(II) complex was calculated with the same basis set, considering the solvent effect through the Continuous Solvent Potential Approach (CPCM) method [37,38], which allows for the consideration of the influence of the ethanol solvent. The identification of molecular orbitals in the electronic absorption bands observed in the UV–Vis spectra was conducted with the aid of the SWIZARD software [39], which facilitated a confident and accurate outcome. To eliminate the well-known overestimation of DFT levels, the vibrational wavenumbers were scaled by a factor of 0.96 [40]. The linear and nonlinear optical parameters, such as polarizability and first- and second-order hyperpolarizability parameters, were calculated using the same DFT level both in the absence and presence of additional radiation (ω=0.0856252 and 0.0428126 au)

Table 1
Structural refinement and crystal parameters for $[Cu(6Fpca)_2{\bullet}(H_2O)]$ complex.

Cu(II) Complex	
Crystal data	
CCDC	2390,148
Chemical formula	$2(C_{12}H_8CuF_2N_2O_5)$
M_r	723.49
Crystal system, space group	Orthorhombic, *Pbca*
Temperature (K)	293
a, *b*, *c* (Å)	12.9927 (7), 12.9521 (6), 14.9287 (7)
V (Å^3)	2512.2 (2)
Z	4
Radiation type	Mo *Kα*
μ (mm^{-1})	1.79
Data collection	
Diffractometer	STOE *IPDS* 2
Absorption correction	Integration (*X RED32*; Stoe & Cie, 2002)
T_{min}, T_{max}	0.514, 0.636
No. of measured, independent and observed [$I > 2\sigma(I)$] reflections	63,362, 4827, 3250
R_{int}	0.062
$(\sin\theta/\lambda)_{max}$ ($Å^{-1}$)	0.772
Refinement	
$R[F^2 > 2\sigma(F^2)]$, $wR(F^2)$, *S*	0.063, 0.193, 1.11
No. of reflections	4827
No. of parameters	203
No. of restraints	4
H-atom treatment	H-atom parameters constrained
$\Delta\rho_{max}$, $\Delta\rho_{min}$ (e Å^{-3})	1.06 - 0.66

3. Results and discussion

3.1. Analysis of geometric structures

The crystal structure of the [Cu(6Fpca)$_2$•(H_2O)] complex was determined and refined, providing comprehensive insight into its molecular architecture. The Cu(II) complex crystallizes in the orthorhombic space group *Pbca* with the following unit cell dimensions: a = 12.9927 (7) Å, b = 12.9521 (6) Å, and c = 14.9287 (7) Å. The unit cell angles are α = 90(5)°, β = 90(6)°, and γ = 90(5)°, resulting in a unit cell volume of 2512.2(2) Å^3. There are four formula units per unit cell (Z = 4), which is indicative of the complex packing within the crystal lattice (Table 1). As shown in Fig. 2a, the asymmetric unit of the Cu(II) complex consists of two 6-floropyridine-2-carboxylate ligands, occupying the equatorial plane, and a H_2O ligand located in the axial plane. Accordingly, the Cu (II) complex has a distorted square pyramidal coordination sphere around the central Cu(II) ion. The 6Fpca ligand coordinates the central Cu(II) ion through the N and O atoms of the donor, forming a five-membered chelate ring.

In a similar square pyramidal Cu(II) complex recently reported, Cu-O bond lengths were reported in the range of 1.919(1)–1.934(1) Å [41]. In our study, the equatorial bond lengths of Cu–N and Cu–O atoms in [Cu (6Fpca)$_2$•(H_2O)] were in the range of 1.932 (3)-2.054 (3) Å and the axial bond distance of Cu–O3 was observed as an extended bond at 2.336 (3) Å. The O3 occupies the apical pyramidal position at 2.336 (3) Å and a deviation of Cu(II) from the basal plane of 0.343 Å. This axial elongation is due to Jahn-Teller effect which is a characteristic of Cu(II) complexes [42]. The Cu–O bond lengths between the metal and H_2O ligand were also reported at 2.486 (4) Å [16], 2.661 (2) Å [43] and 2.0072 (17) Å [44] for the similar Cu(II) complexes. The Cu–O (carboxylate) bond lengths were also reported at 1.949 (2) Å [43], 1.9094 (15) Å and 2.0943 (16) Å [44] and 1.971 (3) Å [16], as consistent with our results. The carboxylate group C—O bond lengths of O1–C1 and O2–C1 were observed as 1.283 (3) and 1.237 (6) Å, demonstrating the single and double bond characters, respectively. In a previous study reported for similar crystal structures, the C–O bond lengths with single bond character were reported as 1.255 (2) and 1.250 (3) Å while those with double bond character were reported at 1.246 (2) and 1.241 (3) Å [45]. Solomon et al. [46] reported four different Cu(II) complexes containing the fluoro-pyridine moiety. The C–F bond lengths in Ni(II), Cu(II), and Co(II) complexes were also reported [47,48]. Politeo et al. also reported a Ni (II) complex of 6-fluoronicotinate, and the C–F bond distance was reported as Å 1.357(3) [49]. In our study, the C–F bond distance was observed as 1.3230 (3) Å and calculated as 1.3806 Å, as would be expected.

When it comes to the bond angles, N1–Cu–O1, O1–Cu–O3, and N1–Cu–O3 bond angles for the Cu(II) complex have been observed as 82.27 (10)°, 93.69 (10)° and 92.64 (1)° respectively. These bond angles demonstrated that the Cu(II) complex has a distorted square pyramidal coordination geometry around the central Cu(II) ion. The chelating angles of N1-Cu-O1 and N2–Cu–O4 were observed at 97.29 (9)° and 82.27 (9)°. The chelate coordination angles through the donor N and O atoms to the central metal ions have been reported to be approximately 74.8° [50]. The bond lengths and angles for Cu(II) complex were also calculated by using B3LYP/LanL2DZ level, and the obtained results were presented in Table 2 and **Table S1**, respectively, as compared with XRD results. The crystal packing interactions, along with the hydrogen bond patterns for Cu(II) complex, are presented in **Table S2**. In the case of Cu (II) complex, The O—H•••O, C—H•••F, C—H•••N and C—H•••O type H-bonding interactions occur between two neighboring complexes with different symmetry codes presented in **Table S2**. The strongest interactions were found as conventional H-bonding interactions of O3—H3A···O5^{v} and O3—H3B···O2^{viii}, with the H···A lengths of 2.01 (2) and 2.24 (4) Å, respectively.

3.2. Powder X-ray diffraction analysis

Powder X-ray diffraction analysis was performed to confirm the crystalline nature of the Cu(II) complex and to derive structural insights based on peak positions and full width at half maximum (FWHM) values. Fig. 3 demonstrates the experimental and theoretical powder XRD spectrum of the Cu(II) complex recorded at the 2θ = 5–50° range. The diffraction pattern exhibits well-defined peaks, indicating a high degree of crystallinity. The most intense diffraction peak was observed at 2θ = 16.56°, corresponding to a d-spacing of 5.37 Å, suggesting the presence of a layered structural arrangement within the unit cell. Additional characteristic peaks at higher angles further support the periodicity and ordered nature of the molecular packing. The presence of sharp peaks, along with low FWHM values, suggests that the crystallites are well-formed and possess limited strain-induced broadening. The average crystallite size (d_{XRD}) of the Cu(II) complex was obtained by using Scherrer's Equation [51]. The d_{XRD} value was found to be 37.98 nm, indicating that the Cu(II) complex's crystallite size is in the nanoscale

Table 2
Experimental and theoretical bond distances (Å) obtained by B3LYP, B2PLYPD and MP2 levels and LanL2DZ basis set for [Cu(6Fpca)$_2$•(H_2O)] complex.

Bond	Experimental	B3LYP	B2PLYPD	MP2
Cu1–O4	1.932 (3)	1.9350	1.9376	1.95006
Cu1–O1	1.943 (2)	1.9493	1.9403	1.94860
Cu1–N1	2.054 (3)	2.1025	2.0933	2.14093
Cu1–N2	2.054 (3)	2.2466	2.2481	2.26334
Cu1–O3	2.336 (3)	2.0404	2.0122	2.03039
C6–F1	1.3230 (3)	1.3806	1.3895	1.40966
O1–C1	1.283 (3)	1.3265	1.3335	1.34158
N1–C2	1.358 (4)	1.3699	1.3772	1.39357
N1–C6	1.327 (4)	1.3336	1.3371	1.34878
O2–C1	1.237 (4)	1.2516	1.2587	1.27080
C2–C3	1.386 (4)	1.3995	1.4041	1.41794
C2–C1	1.517 (4)	1.5247	1.5300	1.54409
C3–C4	1.398 (4)	1.4097	1.4154	1.42633
C6–C5	1.386 (4)	1.4006	1.4040	1.41481

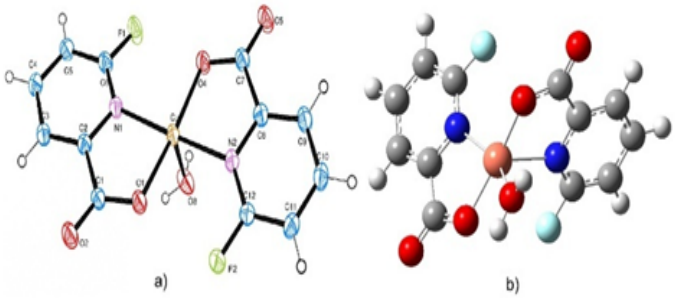

Fig. 2. a) ORTEP drawing (50 % probability ellipsoids) of molecular structure (the hydrogen atoms are placed in the calculated positions as spheres of arbitrary radius) and b) the optimized molecular geometry (obtained by B3LYP/LanL2DZ) for [Cu(6Fpca)$_2$•(H_2O)] complex.

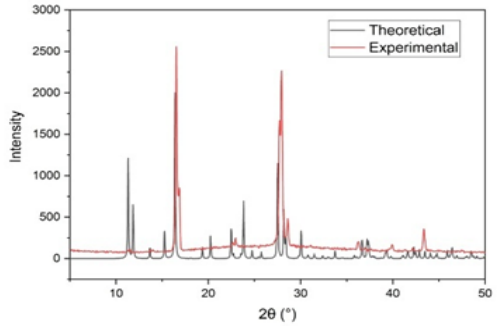

Fig. 3. Overlay of the experimentally collected powder diffractogram and the simulated powder diffractogram.

range [52]. The thermal stability of this geometry, as indicated by thermogravimetric analysis (TGA), suggests a well-defined coordination environment that remains intact up to 214 °C before ligand decomposition occurs.

3.3. Hirsfeld surface analysis

The intermolecular interactions and interaction distances in [Cu(6Fpca)$_2$•(H$_2$O)] complex were calculated using the Crystal Explorer 17.5 program [53,54]. The 3D Hirshfeld surfaces, namely, dnorm, shape-index, and curvedness for the newly synthesized Cu(II) complex, are presented in Fig. 4. The color scale for Hirshfeld surfaces is also provided in Table 3. According to Fig. 4(a), the intense red spots on the noncoordinated O atom of the carboxylate group, an oxygen atom of the H$_2$O group, F atoms as well as C6 atom of 6Fpca clearly indicate a strong H-bonding interaction through these atoms. The dnorm values for the Cu (II) complex range from −0.4543 (red) to 1.2510 (blue) au. The shape index of the Hirshfeld surface obtained for Cu(II) complex (see in Fig. 4 **(b)**) is used to reveal the π–π stacking interactions by the presence of adjacent triangles in blue and red colour. Fig. 4**(b)** displays that Cu(II) complex has red triangles on the pyridine rings, but has no blue triangle, indicating the absence of the π–π stacking interactions in the Cu(II) crystal under consideration. Fig. 4**(c)** also reveals that 6Fpca ligand and chelate rings are defined as regions of low surface curvature, while the regions around the H$_2$O ligand and the boundary parts of molecular geometry of the Cu(II) complex are defined as regions of very sharp surface bending [55].

The nature and strength of the interactions are analyzed in detail through 2D fingerprint plots [56,57]. Further insight into the nature of intermolecular interactions can be derived from the analysis of 2D fingerprint plots. **Figure S1** and Table 4 illustrate the primary interaction areas that contribute more strongly to crystal packing of Cu(II) complex. The most common interaction areas were calculated between the oxygen and hydrogen atom surfaces, which constitute 33.1 % of the total contacts, respectively. The subsequent important contribution (15.8 %) to the overall interaction are predicted between the fluorine and hydrogen atom surface areas. These high proportions emphasize the critical role of oxygen and fluorine atoms in the 6Fpca ligand in establishing hydrogen bonds with hydrogen atoms. Such interactions are particularly important for stabilizing the Cu(II) complex and are essential for crystal packing. The electron-withdrawing properties of oxygen and fluorine atoms increase the acidity of nearby hydrogen atoms, making them more likely to engage in hydrogen bonding, thereby enhancing the stability of the molecular framework. The surface area interactions between carbon and hydrogen atoms, which account for 13.4 % of the total interaction, are generally weaker than hydrogen bonds involving electronegative atoms like fluorine and oxygen. Fluorine-carbon and oxygen-carbon surface area interactions, which represent 5.3 % and 4.1 % of the total contacts, respectively, reflect the close association of fluorine and oxygen atoms with the carbon backbone of the 6Fpca ligand. These interactions impact the electronic characteristics of the Cu(II) complex by altering the electron density distribution throughout the 6Fpca ligand. These interactions also

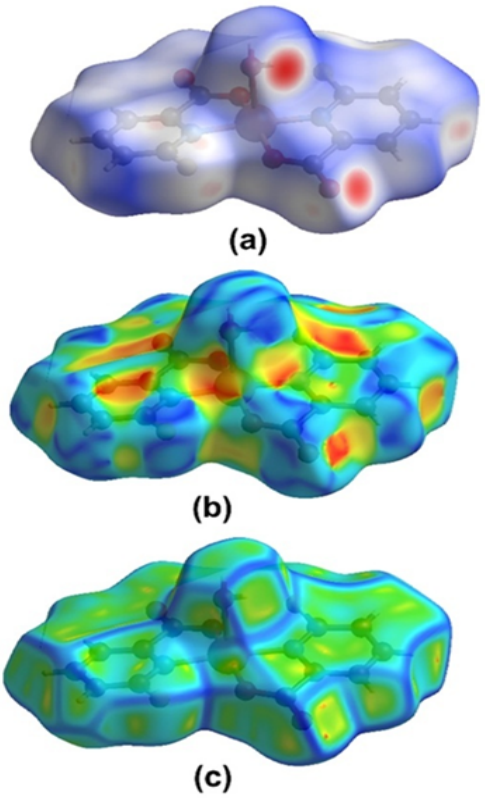

Fig. 4. Hirschfeld surface (HS) plotted over (a) dnorm, (b) shape-index, and (c) curvedness for [Cu(6Fpca)$_2$•(H$_2$O)].

Table 3
Surface property information (Å) for [Cu(6Fpca)$_2$•(H$_2$O)].

Mode	Minimum interaction	Mean interaction	Maximum interaction
d_{norm}	−0.4543	0.3484	1.2510
d_i	0.7792	1.6568	2.4563
d_e	0.7781	1.6703	2.4741
Shape Index	−0.9964	0.2522	0.9972
Curvedness	−3.4076	−0.9717	0.3001
Fragment Patches	0.0000	5.6163	13.000

Table 4
Fingerprint percentage of the total surface area for closed contact between atoms inside and outside the surface for [Cu(6Fpca)$_2$•(H$_2$O)].

Atom Surfaces %	O	N	H	C	F
O	1.9	1.2	33.1	4.1	–
H	33.1	3.8	12.5	13.4	15.8
C	4.1	0.1	13.4	5.2	5.3
F	–	–	15.8	5.3	1.5
Cu	2.1	–	–	–	–

influence the dipole moments and overall polarity of the Cu(II) complex, potentially affecting its reactivity and interactions with other molecules. The other surface area interactions contributing the Cu(II) crystal packing were determined to be as follows: 12.5 % for H···H, 5.2 % for C···C, and 3.8 % for N···H.

3.4. Vibrational analysis

The FT-IR and theoretical IR spectra for the 6Fpca ligand and Cu(II) complex are provided in **Table S3**. The FT-IR spectra for 6Fpca ligand and Cu(II) complex were recorded in the range of 4000–400 cm^{-1} and presented in Fig. 5. The theoretical IR spectra for ligand and Cu(II) complex calculated by B3LYP/LanL2DZ level were also presented in Fig. 5, as compared with the FT-IR spectra. The selected vibrational modes for the Cu(II) complex with their potential energy distribution are given in **Table S3**.

Ulahannan et al. reported the FT-IR and Raman spectra for the quinoline-7-carboxylic acid derivative, and the COOH group OH stretching vibration band was reported at 3544 cm^{-1} [58]. In a recent study performed for a carboxylic acid derivative, the ν OH stretching was reported at 3434 cm^{-1} [59]. In pyridine-2-carboxylic acid derivatives, the weak vibration band originating from the OH stretching of the carboxyl group (COOH) was probably combined with the CH stretching vibration and could not be clearly detected in the FT-IR spectrum [60]. The same vibration mode (ν OH) for the 6Fpca ligand could not be detected in the FT-IR spectrum. However, the ν OH stretching vibration for the COOH group of the 6Fpca ligand was calculated at 3390 cm^{-1} by using B3LYP level. This COOH stretching band obtained for the 6Fpca ligand disappeared in the new Cu(II) complex after the ligand interacted with Cu(II) metal. In the newly synthesized Cu(II) complex, the OH stretching bands appeared due to the H$_2$O ligand coordinated to the Cu(II) metal center [61]. For the Cu (II) complex, this OH stretching vibration originating from the H$_2$O ligand was observed at 3449 cm^{-1} and calculated at 3543 cm^{-1}. The differences between the FT-IR and theoretical IR spectra are derived from the phase difference between the experimental and theoretical methods. Theoretical calculations were performed in the gas phase for the isolated structure, where intermolecular interactions are very weak, while the FT-IR spectra were recorded in the solid state, where intermolecular interactions are dominant. The aromatic CH stretching vibrations for similar structures are reported at 3085 cm^{-1} and 3082 cm^{-1} [13]. In this study, the measured CH stretching vibrations for the Cu(II) complex were obtained at 3087 cm^{-1}, while the calculated theoretical results were found in the range of 3135 cm^{-1} to 3097 cm^{-1}.

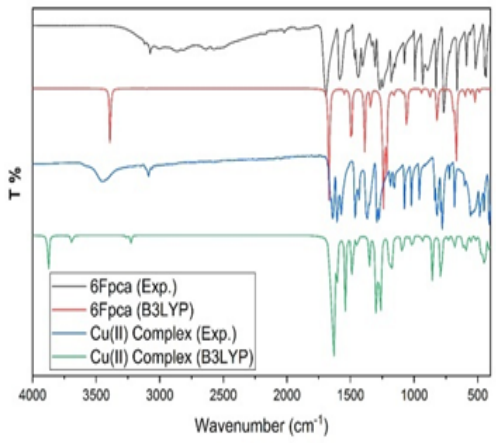

Fig. 5. FT-IR spectra of [Cu(6Fpca)$_2$•(H$_2$O)] complex and 6Fpca ligand.

The aromatic ring ν CC stretching vibration for similar metal-carboxylate complexes was reported at 1600 cm^{-1} [62] and 1489 cm^{-1} [63]. In the present study, the —ν CC stretching vibrations for the Cu(II) complex were observed at 1607–914 cm^{-1}, while the same bands were calculated in the range 1582–900 cm^{-1}. In the FT-IR spectrum for the 6Fpca ligand, the symmetric and asymmetric COO stretching vibrations were observed at 1248 and 1690 cm^{-1}, respectively. In the Cu(II) complex of 6-fluoropyridine-2-carboxylic acid, the characteristic bands assigned to the vibrations of carboxylate anion –COO$^-$ appear. The asymmetric COO$^-$ vibration was observed at 1639 cm^{-1}, while the symmetric one was found at 1274 cm^{-1} for the Cu(II) complexes. The corresponding vibration modes were also calculated at 1594 and 1248 cm^{-1}, respectively. It is well known that the difference between the wavenumbers of the asymmetric and symmetric stretching vibrations of the COO$^-$ group may be useful to estimate coordination geometry for the Cu(II) complex under investigation [64,65]. The wavenumber difference for symmetric and asymmetric COO$^-$ groups was observed as 419 cm^{-1}, indicating the monodentate coordination through the COO$^-$ group. The in-plane bending carboxylate group vibrations (β OCO) were also observed at 778 and 722 cm^{-1} for the Cu(II) complex [66–68].

It was reported that the ring breathing vibration band for 6-chloropyridine-2-carboxylic acid was observed at 989 cm^{-1}. The same band for the Zn(II) and Cu(II) complexes of 6-chloropyridine-2-carboxylic acid was also reported at 1008 cm^{-1} [44]. The ring breathing vibration mode (τ CCCN) for the Cu(II) complex under consideration was observed at 1020 cm^{-1} and calculated at 1007 cm^{-1}. This wavenumber shift is an indicator of coordination through pyridine N atom to central Cu(II) ion. The C-F bending vibrations observed at 1188 and 914 cm^{-1} was calculated at the range of 1220–894 cm^{-1}. Overall, the strong correlation between the experimental and theoretical FT-IR data confirms the accuracy of the DFT model employed and provides detailed insights into the vibrational characteristics of the Cu(II) complex.

3.5. Thermal analysis studies

The thermal character of the Cu(II) complex has been studied using Thermogravimetric-Differential Thermal Analysis (TG-DTA). To understand the thermal behavior of the Cu(II) complex; the decomposition stages, temperature ranges, mass reduction, and final products observed in each step of TG-DTA curves. The TG-DTA graph recorded for the Cu (II) complex presented in Fig. 6 shows a two-stage mass loss in the range of 125–253 C. In the first stage (125–214 C), mass loss of F atoms and H$_2$O ligand, which coordinate to the Cu(II) ion, was observed (experimental 14.6 %, calculated 15.4 %). In the second stage (214–253 C), the experimentally observed 35.08 % (calculated 34.8 %) mass loss was explained by the loss of pyridine rings other than the coordinating N atom. A slow mass loss was observed in the range of 253–332 C due to the removal of pyridine N atoms in the Cu(II) complex (experimental 7.8 %, calculated 7.7 %). In the range of 332–344 C, a rapid mass loss is observed, which is due to the removal of the non-coordinated O atoms from the metal center of the carboxyl group (experimental 8.0 %, calculated 8.8 %). At this stage, it was concluded that only the CuC_2O_2 structure remained from the Cu(II) complex. As a result of the continuous and slow mass loss in the range of 344–1000 C, it is understood that the last residue corresponds to the Cu(II) metal ion (experimental 17.6 %, calculated 17.5 %).

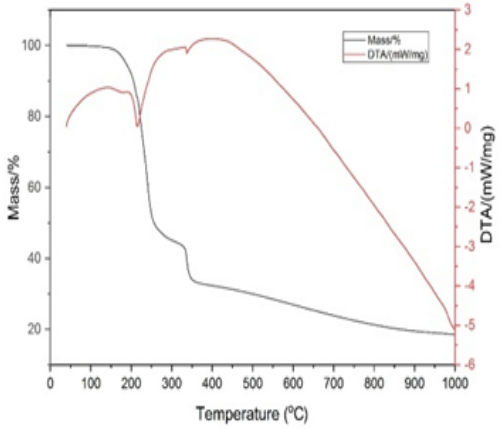

Fig. 6. TG-DTA thermogram with a heating rate of 10 °C.min^{-1} under N_2 for the Cu(II) complex.

3.6. UV–Vis spectral analysis

The absorption bands at 209 nm, 227 nm, and 244 nm calculated for Cu(II) complex typically indicate π-π* transitions or *n*-π* transitions within the 6-fluoropyridine-2-carboxylic acid ligand. The corresponding experimental electronic absorption bands were observed at 213 and 263 nm (Fig. 7). Table 5 demonstrates that the main electronic transitions occurred among the β-spin molecular orbitals. The absorption band calculated at 263 nm is originating the electronic transition from SOMO-4 to SUMO+2 with a main contribution of 40 %. In this spectral region, the transition metal ions often exhibit ligand-to-metal charge transfer (LMCT) or metal-to-ligand charge transfer (MLCT) transitions [69]. In the case of LMCT, an electron from a filled ligand orbital (usually a lone pair or a π orbital) is excited to an empty d orbital of the transition metal ion. Conversely, in MLCT, an electron from a d orbital of the metal ion is excited to an empty π* orbital of the ligand. The Cu(II) complex exhibited a LMCT absorption band observed 369 nm and calculated at 383 nm. This absorption band is originated by the transitions of SOMO-6→SUMO β (29 %) and SOMO-7→SUMO β (21 %).

3.7. Frontier molecular orbital (FMO) analysis

The analysis of SOMO (Singly Occupied Molecular Orbital) and SUMO (Singly Unoccupied Molecular Orbital) energies provides valuable insights into the electronic structures and reactivity of ligand and their metal complexes. In this study, the SOMO and SUMO energies of the 6Fpca ligand with its corresponding Cu(II) complex was calculated by using B3LYP/LanL2DZ level, and the obtained results were presented in Fig. 8 and Table 6 Since the β-spin molecular orbitals are dominant in UV–Vis electronic transitions of the 6Fpca and Cu(II) complexes, the SOMO and SUMO energy values were analyzed by considering β-spin results. The SOMO energies for the 6Fpca and Cu(II) complex was calculated as −8.1844 and -6.8244 eV, respectively, demonstrating that the SOMO energy increases upon coordination with Cu(II). This indicates that the ligand's highest occupied molecular orbital becomes less stable when coordinated to the Cu(II) metal ion. The SUMO energies were also calculated as −3.6446 and −3.5151 eV for the 6Fpca and Cu (II) complex, respectively.

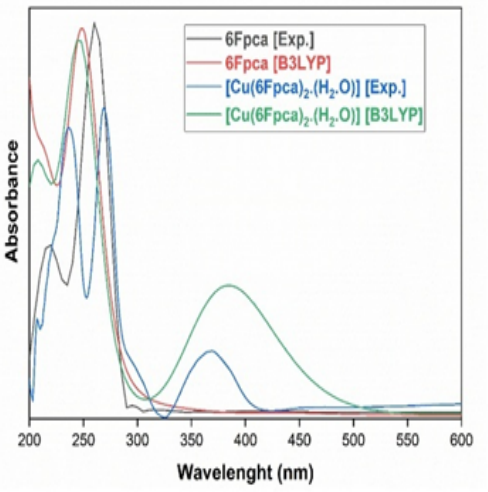

Fig. 7. The experimental and theoretical UV–Vis spectra for the 6Fpca ligand and [Cu(6Fpca)$_2$•(H$_2$O)] complex.

The energy gap between SOMO and SUMO is used as an important indicator of the chemical reactivity and stability of the investigated systems [57]. The SOMO-SUMO energy gaps were obtained as 4.5398 and 3.3094 eV for the 6Fpca, and Cu(II) complex, respectively. These energy gaps indicate that the 6Fpca ligand has higher stability and lower reactivity than its corresponding Cu(II) complex. The coordination of the 6Fpca ligand to the Cu(II) significantly alters its electronic structure. The chemical hardness (η) of the Cu(II) complex was calculated as 1.6547 eV, while the corresponding value for 6Fpca ligand was calculated as 2.2699 eV. The chemical softness (S) parameter indicates that the complex possesses some flexibility in its electronic structure, allowing for potential interactions with nucleophilic or electrophilic species [70]. The S parameter for the 6Fpca and Cu(II) complex was also obtained as 0.4405 and 0.3022 eV^{-1}, respectively. Electronegativity (χ) is a measure of the tendency of the complex to attract electrons, while the electrophilicity index (W) reflects the overall electrophilic character of the molecule [71]. The Cu(II) complex exhibited an electronegativity value of 5.1698 eV, indicative of its ability to attract electron density from surrounding species, particularly during coordination with the functional ligands. The electrophilicity index (W) of 8.0760 eV suggests that the Cu(II) complex is highly electrophilic, making it an excellent candidate for reactions with nucleophiles. When comparing these results to similar complexes reported in the literature, the electronic parameters, including the HOMO-LUMO gap and chemical hardness, are consistent with Cu(II) complexes containing pyridine derivatives [72, 73].

E_g (optical band gap energy) value is calculated using the Tauc and Menth equation of $[(\alpha h\nu)=C(h\nu-Eg)^{1/2}]$ [74]. In this eq., the absorption coefficient α is found by equation of $\alpha = 2.303A/d$ by taking into account d and *A* depicting the width of the cuvette (1 cm) and absorbance in the UV–Vis region. h and ν stands for Planck's constant and frequency of light. 'C' is a constant which is considered as 1 for the ideal case. By extrapolating the linear region of the plot $(\alpha h\nu)^2$ vs. hν (**Figure S2**) to α = 0 absorption, the values of direct optical band gap (E_g) of the complex has been evaluated as 3.1 eV.

3.8. Molecular electrostatic potential (MEP) analysis

The electrostatic potential values for 6Fpca and Cu(II) complex were calculated in the range of −7.9172 -7.917e^{-2} and −8.707 – 8.707e^{-2}, respectively. It is observed that the negative electrostatic potential value of the new complex obtained by the coordination of the 6Fpca ligand to the Cu(II) ion becomes even smaller. The MEP surface of the 6Fpca ligand presented in Fig. 9 shows the electron donor N and O atoms represented by red color are the negative electrostatic potential region. In the Cu(II) complex, the oxygen atoms of the carboxyl group have the highest electron density, as expected for an electron-withdrawing carboxylate anion. This suggests that these sites are highly probable candidates for acting as nucleophilic centers, participating in coordination with the Cu(II) ion. These sites are crucial for comprehending the manner in which the ligand binds to the metal center and how it may

Table 5
The experimental and theoretical wavelengths, oscillator intensities, and significant contributions for the Cu(II) complex.

Exp.	TD-B3LYP/LanL2DZ		
λ (nm)	λ (nm)	Oscillator str.	Important contributions
213	209	0.0121	SOMO-7→SUMO+3 β (50 %),SOMO-4→SUMO+3 β(21 %)
–	227	0.0705	SOMO 12→SUMOβ (38 %), SOMO 14→SUMO β(12 %)
263	244	0.1288	SOMO-4→SUMO+2 β (40 %), SOMO-5→SUMO+1 α (12 %)
369	383	0.0655	SOMO-6→SUMO β (29 %), SOMO-7→SUMO β (21 %)

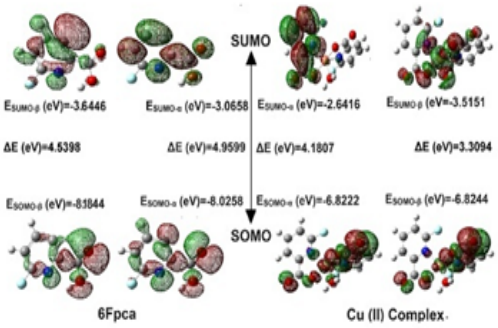

Fig. 8. Frontier molecular orbitals (FMOs) for 6Fpca ligand and [Cu $(6Fpca)_2•(H_2O)$] complex.

Table 6
The chemical hardness parameter(η), electronegativity parameters (χ), ektrofilic index (W), chemical softness (S) and FMO energys for 6Fpca ligand, [Cu $(6Fpca)_2•(H_2O)$ complex obtained by B3LYP/LanL2DZ levels.

Parameter	6Fpca		Cu(II) Complex	
	α-spin	β -spin	α-spin	β -spin
E_{SOMO} (eV)	−8.0258	−8.1844	−6.8222	−6.8244
E_{SUMO} (eV)	−3.0658	−3.6446	−2.6416	−3.5151
ΔE (eV)	4.9599	4.5398	4.1807	3.3094
χ (eV)	5.5458	5.9146	4.7319	5.1698
η (eV)	2.4799	2.2699	2.0903	1.6547
W(eV)	6.2008	3.9703	5.3559	8.0760
$S(eV^{-1})$	0.4032	0.4405	0.2392	0.3022

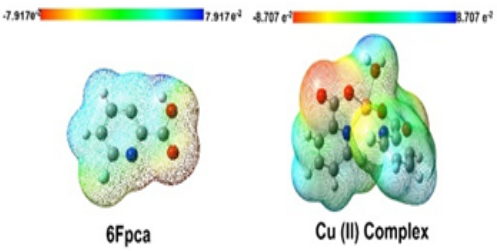

Fig. 9. The MEP surfaces [Cu$(6Fpca)_2•(H_2O)$] complex and 6Fpca ligand calculated by B3LYP/LanL2DZ level.

interact with other species in a catalytic or biological environment [75]. From these findings, it seems that the 6Fpca ligand forms the complex structure by binding with the electron acceptor Cu atom and N, O atoms. This distribution confirms the expected coordination chemistry of the Cu (II) ion in a tetragonal pyramidal coordination geometry with strong ligand-metal interactions. When it comes to the MEP surface calculated for Cu(II) complex, the highest negative potential is found around the non-coordinated carboxylate group O atoms [76]. Additionally, a relatively smaller negative potential is found over the F atoms. Fig. 9 shows that especially the H atoms of the H_2O group carry the highest positive potential on the Cu(II) complex.

3.9. NBO analysis

The coordination geometry and electronic structure of the [Cu $(6Fpca)_2•(H_2O)$] complex were also investigated using Natural Bond Orbital (NBO) analysis at the B3LYP/LanL2DZ level. Key donor-acceptor interactions and their corresponding stabilization energies ($E^{(2)}$) are summarized in Table 7, which highlights the most significant hyperconjugative interactions contributing to the electronic structure of the Cu(II) complex under consideration. Higher $E^{(2)}$ values suggest stronger interactions and greater stabilization of the molecular system [77]. The electronic configuration and calculated natural charge for the Cu(II) complex ion is [core] $4S^{(0.13)}$ $3d^{(4.32)}$ $5p^{(0.19)}$ and +0.85316. When the Cu(II) complex is formed, the natural charge of Cu(II) central ion is found to be smaller than that of the free ion (2+). This result indicates that the charge transfer from ligand to metal in the complex is higher than the charge transfer from metal to ligand [78].

The lone pairs (LP(3)) on the oxygen atoms (O1 and O4) of the 6-fluoropyridine-2-carboxylate ligands strongly interact with the unoccupied orbitals of the Cu(II) ion (LP*(5) and LP*(6)). The hyperconjugative interactions between LP(3) O1 → LP*(5) Cu1 have a stabilization energy of 24.02 kcal/mol, while LP(3) O4 → LP*(6) Cu1 displays a higher stabilization energy of 29.49 kcal/mol. These interactions suggest strong coordination between the oxygen atoms and the Cu(II) center, reinforcing the distorted tetragonal pyramidal geometry of the complex. The interaction LP(1) N1 → LP*(6) Cu1 has an $E^{(2)}$ value of 18.12 kcal/mol,

Table 7
High-energy donor and acceptor orbital interactions obtained by NBO analysis for the [Cu$(6Fpca)_2•(H_2O)$] complex calculated by B3LYP/LanL2DZ level.

Type	Donor	Type	Acceptor	E^2 (kcal/mol)	$E(j)-E(i)^b$ (a.u.)	$F(i,j)^0$ (a.u)
LP (3)	O1	LP* (5)	Cu1	24.02	0.21	0.100
LP (1)	N1	LP* (6)	Cu1	18.12	0.57	0.129
LP (3)	O4	LP* (6)	Cu1	29.48	0.18	0.02
LP (1)	N2	LP* (6)	Cu1	12.43	0.51	0.102
LP (2)	O3	LP* (8)	Cu1	21.50	0.79	0.165
LP (2)	O1	π*	O2–C1	35.21	0.27	0.123
LP (2)	O2	σ*	O1–C1	11.25	0.64	0.115
LP (1)	C3	π*	N1–C2	81.04	0.09	0.124
LP (2)	O4	π*	O5–C7	36.39	0.26	0.124
LP (2)	O5	σ*	O4–C7	12.43	0.64	0.115
LP (1)	C9	π*	N2–C8	73.57	0.09	0.122
π	N1–C2	π*	C6 C5	13.96	0.32	0.087
π	N1–C2	LP(1)	C3	11.39	0.21	0.077
π	C6–C5	LP* (1)	C4	26.57	0.16	0.097
π	N2–C8	LP(1)	C9	12.12	0.21	0.078
π	N2–C8	π*	C12–C11	14.16	0.32	0.087
π	C12–C11	LP* (1)	C10	26.42	0.16	0.096

while LP(1) N2 → LP*(6) Cu1 has a much larger stabilization energy of 12.43 kcal/mol. This disparity suggests a stronger coordination effect from N1 compared to N2, possibly due to a difference in bond distances or orbital overlap between the ligands and the Cu(II) ion, which further affects the overall geometry of the complex. The water molecule in the axial position of the distorted tetragonal pyramidal structure also plays an essential role in the stabilization of the complex. The lone pair (LP(2)) on the oxygen atom (O3) interacts with the unoccupied orbitals of the Cu (II) ion LP(2) O3 → LP*(8) Cu1, with an E(2) value of 21.50 kcal/mol. This interaction suggests that the water ligand contributes significantly to the axial coordination and helps maintain the overall geometry of the complex.

Additional hyperconjugative effects are observed between lone pairs on oxygen atoms and π* orbitals on the carboxylate and pyridine rings. For instance, the interaction LP(2) O1 → π* O2-C1 has an $E^{(2)}$ value of 35.21 kcal/mol, while LP(2) O4 → π*O4-C7 shows a smaller stabilization energy of 36.39 kcal/mol. The π-conjugation in the pyridine ring also facilitates important donor-acceptor interactions, such as π N1-C2 → π* C6-C5 with an $E^{(2)}$ value of 13.96 kcal/mol, and π C6-C5 → LP* (1) C4 at 26.57 kcal/mol. Interactions between the π orbitals of the pyridine rings are observed, including π N2-C7 → LP*(1) C8 with an $E^{(2)}$ value of 12.12 kcal/mol and π N2-C7 → π* C12-C11 with an energy of 14.16 kcal/mol. These hyperconjugative interactions help stabilize the overall structure of the complex by distributing electron density across the ligands and contributing to the rigidity of the coordination geometry. The hyperconjugative interactions highlighted in the NBO analysis strongly support the distorted tetragonal pyramidal geometry of the [Cu $(6Fpca)_2•(H_2O)$] complex. The significant stabilization energies, particularly from the lone pairs on the coordinating atoms (O1, O4, N1, N2, and O3), reinforce the strong coordination between the ligands and the Cu(II) ion. Interactions containing O4 give higher stabilization energy compared to the opposite interactions containing O1, while interactions containing N1 give higher stabilization energy compared to the opposite interactions containing N2. These results may be indicative of asymmetric coordination contributing to the distortion resulting from an ideal tetragonal pyramidal geometry.

3.10. Static NLO properties

The static NLO parameters, including the dipole moment (μ), static polarizability (α), static anisotropy of polarizability (Δα), and the first- and second-order static hyperpolarizability (β and γ, respectively), are presented in Table 8. These parameters offer insight into the overall molecular polarizability and the ability of the molecule to interact with external electric fields. The 6Fpca ligand exhibits a dipole moment of 6.2115 Debye, while the Cu(II) complex has a lower dipole moment of 4.4356 Debye. The reduction in dipole moment upon complexation indicates that the coordination of two 6Fpca ligands and one water molecule to the Cu(II) center leads to a more symmetrical charge distribution in the complex compared to the free 6Fpca ligand. The Cu(II) complex shows a significantly higher static polarizability (2.5943×10^{-30} esu) compared to the 6Fpca ligand (1.0373×10^{-23} esu). This increase is expected due to the larger size and coordination environment of the Cu(II) complex, which allows for greater electron cloud distortion.

Table 8
The dipole moment (Debye), static polarizability ($\times 10^{-23}$esu), static anisotropy of polarizability ($\times 10^{-23}$esu), first-order static hyperpolarizability ($\times 10^{-30}$esu), and second-order static hyperpolarizability ($\times 10^{-36}$ esu) of the 6Fpca ligand and Cu(II) complex analyzed using B3LYP/LanL2DZ level.

Parameter	6Fpca	Cu(II) Complex
μ	6.2115	4.4356
α(0;0)	1.0373	2.5943
Δα(0;0)	0.9208	1.1687
β(0;0,0)	1.6537	3.0188
γ(0;0,0,0)	3.5860	19.667

The Cu(II) complex shows a higher first-order hyperpolarizability (3.0188×10^{-30} esu) compared to the 6Fpca ligand (1.6537×10^{-30} esu). This increase in β is due to the complex's larger electronic framework and the coordination of multiple ligands to the metal center, which enhances charge transfer and electron delocalization [79]. The second-order static hyperpolarizability (γ), which corresponds to third-order NLO properties such as the Kerr effect, is also significantly larger for the Cu(II) complex (19.667×10^{-36} esu) compared to the 6Fpca ligand (3.586×10^{-36} esu). This substantial increase is attributable to the lower energy electronic transitions between the ligand and central metal ion, which enhances third-order NLO responses [76].

3.11. Frequency-dependent NLO properties

The frequency-dependent NLO parameters were calculated for two frequencies: ω = 0.0856252 au and ω = 0.0428126 au, and the results are presented in Table 9. At both frequencies, the Cu(II) complex demonstrates significantly higher polarizability than the 6Fpca ligand. For example, at ω = 0.0856252 au, the α parameter of the Cu(II) complex is 2.9862×10^{-23} esu, whereas that of the 6Fpca ligand is 1.5051×10^{-23} esu. Similarly, at ω = 0.0428126 au, the α parameters are 2.7249×10^{-23} esu and 1.0521×10^{-23} esu, respectively. The higher polarizability of the Cu(II) complex is consistent with its more extended electronic system, which responds more readily to external fields at different frequencies. The β is significantly enhanced for the Cu(II) complex compared to the 6Fpca ligand. At ω = 0.0856252 au, the Cu(II) complex exhibits β(-ω;ω,0) value of 22.265×10^{-30} esu, while the 6Fpca ligand has a much lower value of 2.6564×10^{-30} esu. At ω = 0.0428126 au, the β(-ω;ω,0) parameter for the Cu(II) complex and the 6Fpca ligand are 11.823×10^{-30} esu and 1.5006×10^{-30} esu, respectively. The electric field-induced second harmonic generation (ESHG) parameter β (−2ω;ω,ω) was also found to be larger for the Cu(II) complex. This significant enhancement in the Cu(II) complex is attributed to the increased charge transfer capability between the Cu(II) center and the coordinated ligands, which facilitates greater electron delocalization under an oscillating electric field.

The second-order dynamic hyperpolarizability (γ) follows similar trends, with the Cu(II) complex showing much higher values than the 6Fpca ligand. For example, at ω = 0.0856252 au, the dc-Kerr coefficient γ (-ω;ω,0,0) value for the Cu(II) complex is 111.07×10^{-36} esu, compared to 6.2421×10^{-36} esu for the 6Fpca ligand. At ω = 0.0428126 au, the γ (-2ω;ω,ω,0) parameter for the Cu(II) complex increases to 169.67×10^{-36} esu, while the same parameter for the 6Fpca ligand is 5.1435×10^{-36} esu. The increase in γ (-ω; ω,0,0) and γ (−2 ω;ω,ω,0) for the Cu(II) complex indicates a significant enhancement in its third-order NLO properties, which can be attributed to the complex's larger electronic system and coordination-induced electron delocalization. So, the asymmetry introduced by the distortion and the additional coordination of the water molecule enhances the electron delocalization and charge transfer within the complex, leading to higher polarizability and hyperpolarizability values compared to the free 6Fpca ligand. The

Table 9
The frequency-dependent polarizability ($\times 10^{-23}$esu), anisotropy of polarizability ($\times 10^{-23}$esu), first-order hyperpolarizability ($\times 10^{-30}$esu) and second-order hyperpolarizability ($\times 10^{-36}$ esu) for 6Fpca and Cu(II) complex obtained by B3LYP/LanL2DZ level.

Parameter	ω=0.0856252 au		ω=0.0428126 au	
	6Fpca	Cu(II) Complex	6Fpca	Cu(II) Complex
α(-ω;0)	1.5051	2.9862	1.0521	2.7249
Δα(-ω;0)	1.0034	1.7865	0.9399	1.4298
β(-ω;ω,0)	2.6564	22.265	1.5006	11.823
β(−2ω;ω,ω)	1.1328	14.206	2.4437	20.806
γ(-ω;ω,0,0)	6.2421	111.07	3.9497	38.352
γ(−2ω;ω,ω,0)	25.448	147.52	5.1435	169.670

strong donor-acceptor interactions between the metal center and the ligands play an important role in inducing the NLO response of the complex.

4. Conclusion

A novel Cu(II) complex of 6-fluoropyridine-2-carboxylic acid (6Fpca) ligand has been crystalized in this study. The crystal structure of the Cu (II) complex revealed a distorted tetragonal pyramidal geometry. The SOMO-SUMO energy gap analysis showed that the Cu(II) complex had a smaller energy gap (3.3094 eV) compared to the ligand (4.5398 eV), indicating higher reactivity and enhanced charge transfer capability within the complex, crucial for its NLO performance. E_g optical band gap energy value is also calculated using the Tauc and Menth equation at 3.1 eV, as comparable with the theoretically obtained band gap energy. The absorption band observed experimentally at 369 nm and theoretically at 383 nm in the UV–Vis spectrum of the Cu(II) complex is thought to be a metal-ligand charge transfer interaction. This new LMCT absorption band, which occurs due to the coordination of the 6Fpca ligand to the Cu (II) ion, is also thought to be the source of the developing NLO parameters of the Cu(II) complex. It is concluded that the static first and second order hyperpolarizability parameters (β and γ) calculated for the Cu(II) complex (3.0188×10^{-30} esu and 19.667×10^{-36} esu) are higher than the values calculated for the 6Fpca ligand (1.6537×10^{-30} esu and 3.586×10^{-36} esu). These increases observed in both static and frequency dependent NLO parameters are due to low energy electronic transitions between the Cu(II) ion and the donor atoms. Consequently, the static and frequency-dependent NLO parameters showed a remarkable increase in both second harmonic generation (SHG) and Kerr effect-related third-order NLO responses in the Cu(II) complex, making it a promising candidate for advanced optical and photonic applications.

Funding

This work was supported by the Scientific Research Projects Unit of Sakarya University (project numbers: 2023-19-44-48).

CRediT authorship contribution statement

Ömer Tamer: Writing – review & editing, Writing – original draft, Software, Methodology, Conceptualization. **Merve Şimşek:** Writing – original draft, Visualization, Software, Formal analysis. **Davut Avcı:** Writing – review & editing, Supervision, Software, Methodology. **Adil Başoğlu:** Visualization, Validation, Formal analysis. **Mohamed Bensebaa:** Visualization, Validation, Investigation. **Mebarek Boukelkoul:** Visualization, Validation, Investigation. **Necmi Dege:** Visualization, Validation, Resources. **Yusuf Atalay:** Supervision, Software, Resources, Methodology.

Declaration of competing interest

The authors declare that they have no known competing financial interests or personal relationships that could have appeared to influence the work reported in this paper.

Supplementary materials

Supplementary material associated with this article can be found, in the online version, at doi:10.1016/j.molstruc.2025.142707.

Data availability

Data will be made available on request.

References

[1] S.D. Bella, Second order nonlinear optical properties of transition metal complexes, Chem. Soc. Rev. 30 (6) (2001) 355–366.
[2] M. Nakano, K. Yamaguchi, A proposal of new organic third-order nonlinear optical compounds. Centrosymmetric systems with large negative third-order hyperpolarizabilities, Chem. Phys. Lett. 206 (1–4) (1993) 285–292.
[3] Y. x. Zhang, Y. h. Wang, Nonlinear optical properties of metal nanoparticles: a review, RSC. Adv. 7 (71) (2017) 45129–45144.
[4] A. Karakas, A. Migalska Zalas, Y. El Kouari, A. Gozutok, M. Karakaya, S. Touhtouh, Quantum chemical calculations and experimental studies of third-order nonlinear optical properties of conjugated TTF-quinones, Opt Mater 36 (1) (2013) 22–26.
[5] S. Muhammad, A.G. Al Sehemi, Z. Su, H. Xu, A. Irfan, A.R. Chaudhry, First principles study for the key electronic, optical and nonlinear optical properties of novel donor acceptor chalcones, Journal of Molecular Graphics and Modelling 72 (2017) 58–69.
[6] C. Bosshard, Organic Nonlinear Optical Materials, CRC press2020.
[7] S. Muhammad, Quantum chemical design of triple hybrid organic, inorganic and organometallic materials: an efficient two-dimensional second-order nonlinear optical material, Mater. Chem. Phys. 220 (2018) 286–292.
[8] M.S. Kodikara, R. Stranger, M.G. Humphrey, Computational studies of the nonlinear optical properties of organometallic complexes, Coord. Chem. Rev. 375 (2018) 389–409.
[9] P.G. Lacroix, I. Malfant, C. Lepetit, Second order nonlinear optics in coordination chemistry: an open door towards multi-functional materials and molecular switches, Coord. Chem. Rev. 308 (2016) 381–394.
[10] S. Di Bella, A. Colombo, C. Dragonetti, S. Righetto, D. Roberto, Zinc (II) as a versatile template for efficient dipolar and octupolar second-order nonlinear optical molecular materials §, Inorganics. (Basel) 6 (4) (2018) 133.
[11] Y. Zhang, B. Champagne, Understanding the second-order nonlinear optical properties of one-dimensional ruthenium (II) ammine complexes, The Journal of Physical Chemistry C 117 (4) (2013) 1833–1848.
[12] Q. Xie, Z. Shao, Y. Zhao, L. Yang, Q. Wu, W. Xu, K. Li, Y. Song, H. Hou, Novel photo controllable third order nonlinear optical (NLO) switches based on azobenzene derivatives, Dyes and Pigments 170 (2019) 107599.
[13] Ö. Tamer, N. Dege, D. Avcı, Y. Atalay, The static and frequency-dependent second- and third-order nonlinear optical properties of Zn (II) and Ni (II) complexes of 4-methoxypyridine-2-carboxylic acid: a detailed experimental and theoretical study, Appl. Organomet. Chem. 37 (9) (2023) e7206.
[14] H. Vural, M. Orbay, Synthesis, crystal structure, spectroscopic investigations and DFT calculations of the copper (II) complex of 4-(Trifluoromethyl) pyridine-2-carboxylic acid, J. Mol. Struct. 1146 (2017) 669–676.
[15] A. Ravichandran, R. Rathika, M. Kumaresavanji, Growth and Z-scan analysis of semi organic bis (picolinic acetate) zinc (II) single crystal for third order NLO applications, J. Mol. Struct. 1224 (2021) 129048.
[16] H. Vural, A novel copper (II) complex containing pyrimidine-4-carboxylic acid: synthesis, crystal structure, DFT studies, and molecular docking, J. Mol. Struct. 1265 (2022) 133390.
[17] N. Dege, Ö. Tamer, M. Yaman, A. Başoğlu, D. Avcı, Y. Atalay, Crystallographic, spectroscopic, thermal, optical investigations and density functional theory calculations for novel Co (II) and Mn (II) complexes, Applied Physics A 127 (2021) 1–17.
[18] N.S. Narendran, R. Soman, C. Arunkumar, K. Chandrasekharan, Third order nonlinear optical investigations of meso tetrakis (2, 3, 5, 6-tetrafluoro N, N-dimethyl-4-anilinyl) porphyrin and its metal complexes, Spectrochimica Acta Part A: Molecular and Biomolecular Spectroscopy 136 (2015) 838–844.
[19] P. Deplano, L. Pilia, D. Espa, M.L. Mercuri, A. Serpe, Square-planar d8 metal mixed-ligand dithiolene complexes as second order nonlinear optical chromophores: structure/property relationship, Coord. Chem. Rev. 254 (13–14) (2010) 1434–1447.
[20] F.K. Bine, N.S. Tasheh, J.N. Ghogomu, A quantum chemical screening of two imidazole-chalcone hybrid ligands and their Pd, Pt and Zn complexes for charge transport and nonlinear optical (NLO) properties: a DFT study, Computational Chemistry 9 (4) (2021) 215–237.
[21] G.M. Sheldrick, SHELXT–Integrated space group and crystal structure determination, Acta Crystallographica Section A: Foundations and Advances 71 (1) (2015) 3–8.
[22] G.M. Sheldrick, Crystal structure refinement with SHELXL, Acta Crystallographica Section C: Structural Chemistry 71 (1) (2015) 3–8.
[23] C.F. Macrae, I.J. Bruno, J.A. Chisholm, P.R. Edgington, P. McCabe, E. Pidcock, L. Rodriguez-Monge, R. Taylor, J. Streek, P.A. Wood, Mercury CSD 2.0–new features for the visualization and investigation of crystal structures, J. Appl. Crystallogr. 41 (2) (2008) 466–470.
[24] A. Spek, Single-crystal structure validation with the program PLATON, J. Appl. Crystallogr. 36 (1) (2003) 7–13.
[25] L.J. Farrugia, WinGX suite for small-molecule single-crystal crystallography, J. Appl. Crystallogr. 32 (4) (1999) 837–838.
[26] S.P. Westrip, publCIF: software for editing, validating and formatting crystallographic information files, J. Appl. Crystallogr. 43 (4) (2010) 920–925.
[27] M.J. Frisch, G.W. Trucks, H.B. Schlegel, G.E. Scuseria, M.A. Robb, J.R. Cheeseman, G. Scalmani, V. Barone, G.A. Petersson, H. Nakatsuji, X. Li, M. Caricato, A.V. Marenich, J. Bloino, B.G. Janesko, R. Gomperts, B. Mennucci, H.P. Hratchian, J.V. Ortiz, A.F. Izmaylov, J.L. Sonnenberg, D. Williams-Young, F. Ding, F. Lipparini, F. Egidi, J. Goings, B. Peng, A. Petrone, T. Henderson, D. Ranasinghe, V.G. Zakrzewski, J. Gao, N. Rega, G. Zheng, W. Liang, M. Hada, M. Ehara, K. Toyota, R. Fukuda, J. Hasegawa, M. Ishida, T. Nakajima, Y. Honda, O. Kitao, H. Nakai, T.

Vreven, K. Throssell, J.A. Montgomery, Jr., J.E. Peralta, F. Ogliaro, M.J. Bearpark, J.J. Heyd, E.N. Brothers, K.N. Kudin, V.N. Staroverov, T.A. Keith, R. Kobayashi, J. Normand, K. Raghavachari, A.P. Rendell, J.C. Burant, S.S. Iyengar, J. Tomasi, M. Cossi, J.M. Millam, M. Klene, C. Adamo, R. Cammi, J.W. Ochterski, R.L. Martin, K. Morokuma, O. Farkas, J.B. Foresman, D.J. Fox, Gaussian 16, Revision C.01, Gaussian, Inc., Wallingford CT, 2016.

[28] V. GaussView, Roy Dennington, Todd A. Keith, and John M. Millam, Semichem Inc., Shawnee Mission, KS, 2016.

[29] C. Lee, W. Yang, R.G. Parr, Development of the Colle-Salvetti correlation-energy formula into a functional of the electron density, Physical review B 37 (2) (1988) 785.

[30] A.D. Becke, Density-functional exchange-energy approximation with correct asymptotic behavior, Physical review A 38 (6) (1988) 3098.

[31] P.J. Hay, W.R. Wadt, Ab initio effective core potentials for molecular calculations. Potentials for the transition metal atoms Sc to Hg, J. Chem. Phys. 82 (1) (1985) 270–283.

[32] W.R. Wadt, P.J. Hay, Ab initio effective core potentials for molecular calculations. Potentials for main group elements Na to Bi, J. Chem. Phys. 82 (1) (1985) 284–298.

[33] S. Grimme, Semiempirical hybrid density functional with perturbative second-order correlation, J. Chem. Phys. 124 (3) (2006).

[34] T. Schwabe, S. Grimme, Double-hybrid density functionals with long-range dispersion corrections: higher accuracy and extended applicability, Physical Chemistry Chemical Physics 9 (26) (2007) 3397–3406.

[35] M. Head-Gordon, J.A. Pople, M.J. Frisch, MP2 energy evaluation by direct methods 153 (6) (1988) 503–506. Chemical physics letters.

[36] M.J. Frisch, M. Head-Gordon, J.A. Pople, A direct MP2 gradient method, Chem. Phys. Lett. 166 (3) (1990) 275–280.

[37] V. Barone, M. Cossi, Quantum calculation of molecular energies and energy gradients in solution by a conductor solvent model, The Journal of Physical Chemistry A 102 (11) (1998) 1995–2001.

[38] M. Cossi, N. Rega, G. Scalmani, V. Barone, Energies, structures, and electronic properties of molecules in solution with the C-PCM solvation model, J. Comput. Chem. 24 (6) (2003) 669–681.

[39] S. Gorelsky, SWizard Program, University of Ottawa, Ottawa, Canada, 2010.

[40] May N.S.R.D.N, NIST Computational Chemistry Comparison and Benchmark Database, in: D. Russell, I.I.I. Johnson (Eds.), Release, EditorRelease, 22, 2022. May, https://cccbdb.nist.gov/vibscalejust.asp.

[41] H.A. El-Ghamry, K. Yamauchi, K. Sakai, T.A. Farghaly, Unexpected structure of enaminone Pd (II) complex in comparison with Cu (II) complex: synthesis, characterization, DNA binding and antitumor activity, Inorganica Chim. Acta 516 (2021) 120117.

[42] J. Conradie, M. Conradie, K. Tawfiq, S. Coles, G. Tizzard, C. Wilson, J. Potgieter, Jahn–Teller distortion in 2-pyridyl-(1, 2, 3)-triazole-containing copper (ii) compounds, New Journal of Chemistry 42 (19) (2018) 16335–16345.

[43] S. Kansız, A.M. Qadir, N. Dege, S.H. Faizi, Two new copper (II) carboxylate complexes based on N, N, N′, N′-tetramethylethyleneamine: synthesis, crystal structures, spectral properties, dft studies and hirshfeld surface analysis, J. Mol. Struct. 1230 (2021) 129916.

[44] N. Dege, Ö. Tamer, M. Şimşek, D. Avcı, M. Yaman, A. Başoğlu, Y. Atalay, Experimental and theoretical approaches on structural, spectroscopic (FT-IR and UV–Vis), nonlinear optical, and molecular docking analyses for Zn (II) and Cu (II) complexes of 6-chloropyridine-2-carboxylic acid, Appl. Organomet. Chem. 36 (6) (2022) e6678.

[45] M. Bensbaa, M. Şimşek, E. Derin, Ö. Tamer, N. Dege, D. Avcı, M. Boukelkoul, Y. Atalay, Influence of Co (II) and Cd (II) metal ions on structural, electronic and nonlinear optical properties of 4-methoxypyridine-2-carboxylic acid complexes: an experimental and computational study, Mater. Today Commun. (2024) 109403.

[46] B.L. Solomon, C.P. Landee, M.M. Turnbull, J.L. Wikaira, Copper (II) complexes of 2-amino-5-chloro-3-fluoropyridine: syntheses and magnetic properties of (3, 5-FCAP) 2CuX2 and (3, 5-FCAPH) 2CuX4, J. Coord. Chem. 67 (23–24) (2014) 3953–3971.

[47] J. Allan, D. Brown, R. Nuttall, D. Sharp, The thermal decomposition of metal complexes—III: the decomposition of some pyridine and substituted-pyridine complexes of cobalt (II) halides, Journal of Inorganic and Nuclear Chemistry 26 (11) (1964) 1895–1902.

[48] J. Allan, D. Brown, R. Nuttall, D. Sharp, The thermal decomposition of metal complexes—IV: the preparation and thermal decomposition of some pyridine and substituted-pyridine complexes of nickel (II) halides, Journal of Inorganic and Nuclear Chemistry 27 (7) (1965) 1529–1536.

[49] N. Politeo, M. Pisačić, M. Đaković, V. Sokol, B.-M. Kukovec, The first coordination compound of 6-fluoronicotinate: the crystal structure of a one-dimensional nickel (II) coordination polymer containing the mixed ligands 6-fluoronicotinate and 4, 4′-bipyridine, Acta Crystallographica Section E: Crystallographic Communications 76 (4) (2020) 500–505.

[50] G. Świderski, R. Łyszczek, S. Wojtulewski, M. Kalinowska, R. Świsłocka, W. Lewandowski, Comparison of structural, spectroscopic, theoretical and thermal properties of metal complexes (Zn (II), Mn (II), Cu (II), Ni (II) and Co (II)) of pyridazine-3-carboxylic acid and pyridazine-4-carboxylic acids, Inorganica Chim. Acta 512 (2020) 119865.

[51] B. Warren, X-ray Diffraction, Dover, New York, 1990, p. 253.

[52] M. Şimşek, D. Avcı, F. Sönmez, A. Başoğlu, Ö. Tamer, Y. Atalay, Unveiling the NLO potential of new Zn (II) complex of 6-methylpyridine-2-carboxaldehyde: experimental/DFT study on spectral, static, and frequency-dependent linear/nonlinear optical parameters, Appl. Organomet. Chem. (2024) e7798.

[53] D. Jayatilaka, S. Wolff, D. Grimwood, J. McKinnon, M. Spackman, CrystalExplorer: a tool for displaying Hirshfeld surfaces and visualising intermolecular interactions in molecular crystals, Acta Crystallographica Section A - ACTA CRYSTALLOGR A 62 (2006).

[54] J.J. McKinnon, D. Jayatilaka, M.A. Spackman, Towards quantitative analysis of intermolecular interactions with Hirshfeld surfaces, Chemical Communications (37) (2007) 3814–3816.

[55] M.A. Spackman, D. Jayatilaka, Hirshfeld surface analysis, CrystEngComm. 11 (2009) 19–32.

[56] P.R. Spackman, M.J. Turner, J.J. McKinnon, S.K. Wolff, D.J. Grimwood, D. Jayatilaka, M.A. Spackman, {\it CrystalExplorer}: a program for Hirshfeld surface analysis, visualization and quantitative analysis of molecular crystals, J. Appl. Crystallogr. 54 (2021) 1006–1011.

[57] Ö. Tamer, M. Şimşek, N. Dege, D. Avcı, Y. Atalay, The effect of complex formation on the static and frequency-dependent nonlinear optical properties: a combined experimental and theoretical investigation, Spectrochimica Acta Part A: Molecular and Biomolecular Spectroscopy (2024) 125138.

[58] R.T. Ulahannan, C.Y. Panicker, H.T. Varghese, C. Van Alsenoy, R. Musiol, J. Jampilek, P. Anto, Spectroscopic (FT-IR, FT-Raman) investigations and quantum chemical calculations of 4-hydroxy-2-oxo-1, 2-dihydroquinoline-7-carboxylic acid, Spectrochimica Acta Part A: Molecular and Biomolecular Spectroscopy 121 (2014) 404–414.

[59] V.D. Vitnik, Ž.J. Vitnik, The spectroscopic (FT-IR, FT-Raman, l3C, 1H NMR and UV) and NBO analyses of 4-bromo-1-(ethoxycarbonyl) piperidine-4-carboxylic acid, Spectrochimica Acta Part A: Molecular and Biomolecular Spectroscopy 138 (2015) 1–12.

[60] Ö. Tamer, S.A. Tamer, Ö. İdil, D. Avcı, H. Vural, Y. Atalay, Antimicrobial activities, DNA interactions, spectroscopic (FT-IR and UV–Vis) characterizations, and DFT calculations for pyridine-2-carboxylic acid and its derivates, J. Mol. Struct. 1152 (2018) 399–408.

[61] Ö. Tamer, A unique manganese (II) complex of 4-methoxy-pyridine-2-carboxylate: synthesis, crystal structure, FT-IR and UV–Vis spectra and DFT calculations, J. Mol. Struct. 1144 (2017) 370–378.

[62] K. Yuan, X. Ye, W. Liu, K. Liu, D. Wu, W. Zhao, Z. Qian, S. Li, C. Huang, Z. Yu, Preparation, characterization and antibacterial activity of a novel Zn (II) coordination polymer derived from carboxylic acid, J. Mol. Struct. 1241 (2021) 130624.

[63] S.R. Boruah, R.D. Purkayastha, S. Chowdhury, P. Das, R.M. Gomila, A. Frontera, Synthesis, structural characterization, DNA binding ability and luminescent sensing of nitroaromatics by a mononuclear zinc (II) carboxylate complex, Inorganica Chim. Acta 572 (2024) 122247.

[64] T. Aycan, F. Öztürk, S. Demir, N. Özdemir, H. Paşaoğlu, Cobalt (III) complex of substituted nalidixic acid: synthesis, characterization (IR, UV, EPR), single crystal X-ray, antimicrobial activity, Hirshfeld surface analysis and molecular docking, J. Mol. Struct. 1225 (2021) 129043.

[65] H. Paşaoğlu, S. Güven, Z. Heren, O. Büyükgüngör, Synthesis, spectroscopic and structural investigation of ZnI2 (nicotinamide) 2, ZnI2 (isonicotinamide) 2 and [Zn (H2O) 2 (picolinamide) 2] I2, J. Mol. Struct. 794 (1–3) (2006) 270–276.

[66] S. Altürk, D. Avcı, A. Başoğlu, Ö. Tamer, Y. Atalay, N. Dege, Copper(II) complex with 6-methylpyridine-2-carboxyclic acid: experimental and computational study on the XRD, FT-IR and UV–Vis spectra, refractive index, band gap and NLO parameters, Spectrochimica Acta Part A: Molecular and Biomolecular Spectroscopy 190 (2018) 220–230.

[67] D. Avcı, S. Altürk, F. Sönmez, Ö. Tamer, A. Başoğlu, Y. Atalay, B.Z. Kurt, N. Dege, Novel Cu(II), Co(II) and Zn(II) metal complexes with mixed-ligand: synthesis, crystal structure, α-glucosidase inhibition, DFT calculations, and molecular docking, J. Mol. Struct. 1197 (2019) 645–655.

[68] D. Avcı, S. Altürk, F. Sönmez, Ö. Tamer, A. Başoğlu, Y. Atalay, B.Z. Kurt, N. Dege, Three novel Cu(II), Cd(II) and Cr(III) complexes of 6–methylpyridine–2–carboxylic acid with thiocyanate: synthesis, crystal structures, DFT calculations, molecular docking and α-glucosidase inhibition studies, Tetrahedron. 74 (2018) 7198–7208.

[69] O. Tamer, B. Sariboga, I. Ucar, O. Buyukgungor, Spectroscopic characterization, X-ray structure, antimicrobial activity and DFT calculations of novel dipicolinate copper(II) complex with 2,6-pyridinedimethanol, Spectrochim. Acta a Mol. Biomol. Spectrosc. 84 (1) (2011) 168–177.

[70] R.G. Pearson, Absolute electronegativity and hardness: application to inorganic chemistry, Inorg. Chem. 27 (4) (1988) 734–740.

[71] P.K. Chattaraj, D.R. Roy, Update 1 of: electrophilicity index, Chem. Rev. 107 (9) (2007) PR46–PR74.

[72] D. Avcı, H.E. Cömert, F. Sönmez, N. Dege, Ö. Tamer, Y. Atalay, Comparative assessment of structure–property relationships of new Cu (II) complex in selected density functionals, Spectrochimica Acta Part A: Molecular and Biomolecular Spectroscopy 305 (2024) 123489.

[73] H. Vural, Ö. İdil, Synthesis, spectroscopic investigation and biological activities of copper (II) complex of 2-(2, 4-difluorophenyl) pyridine: a combined theoretical and experimental study, J. Mol. Struct. 1177 (2019) 242–248.

[74] D. Avcı, Ö. Özge, A. Başoğlu, F. Sönmez, Ö. Tamer, N. Dege, Y. Atalay, Synthesis, crystal structures, and DFT calculations: novel Mn (II), Co (II) and Ni (II) complexes of N-(pyridin-2-ylmethylene) methanamine with isothiocyanate as promising optical materials, Opt. Quantum. Electron. 55 (5) (2023) 408.

[75] J.S. Murray, P. Politzer, The electrostatic potential: an overview, Wiley Interdisciplinary Reviews: Computational Molecular Science 1 (2) (2011) 153–163.

[76] M. Şimşek, Ö. Tamer, N. Dege, D. Avcı, H. Mahmoody, Y. Atalay, A new mixed-ligand zinc(II) complex of 3-hydroxy and 4-chloro substituted pyridine-2-

carboxylic acid: synthesis, characterization, NLO properties and DFT calculation, Mater. Today Commun. 38 (2024) 108021.
[77] F. WEINHOLD, C.R. LANDIS, A.E. Reed, F. WEINHOLD, Intermolecular interactions from a natural bond orbital, donor-acceptor viewpoint Intermolecular interactions from a natural bond orbital, donor-acceptor viewpoint, Chem. Educ. Res. Pract. 2 (2001) 91–104.
[78] Ö. Tamer, 2 Piridinkarboksilik Asit İçeren Bazı Geçiş Metal Komplekslerinin Sentezi, Yapılarının Analizi Ve Doğrusal Olmayan Optik Özelliklerinin İncelenmesi (2016) 224.
[79] M.S. Kodikara, R. Stranger, M.G. Humphrey, Computational studies of the nonlinear optical properties of organometallic complexes, Coord. Chem. Rev. (2018).

ÖZGEÇMİŞ

Ad-Soyad : Merve ŞİMŞEK

ÖĞRENİM DURUMU:

- **Lisans:** 2014, Giresun Üniversitesi, Fen-Edebiyat Fakültesi, Fizik
- **Yükseklisans:** 2019, Giresun Üniversitesi, Fen Bilimleri Enstitüsü, Fizik Bölümü
- **Doktora:** 2021-2025, Sakarya Üniversitesi, Fen Bilimleri Enstitüsü, Fizik Bölümü

ESERLER:

- Ipek, C., Gümüş, H., **Şimşek, M** (2021). Search potential antiviral candidate for treatment of Covid-19 based on molecular docking and DFT calculations. Turkish Physical Society 37th International Physcis Congress/Erzurum.
- N. Dege, Ö. Tamer, **M. Şimşek**, D. Avcı, M. Yaman, A. Başoğlu, Y. Atalay, (2022). Experimental and theoretical approaches on structural, spectroscopic (FT-IR and UV-Vis), nonlinear optical, and molecular docking analyses for Zn (II) and Cu (II) complexes of 6-chloropyridine-2-carboxylic acid, Applied Organometallic Chemistry. 36 e6678. https://doi.org/https://doi.org/10.1002/aoc.6678
- Ö. Tamer, **M. Şimşek**, D. Avcı, Y. Atalay, (2022). First and second order hyperpolarizabilities of flavonol derivatives: A density functional theory study, Spectrochimica Acta - Part A: Molecular and Biomolecular Spectroscopy. 283 https://doi.org/10.1016/j.saa.2022.121728.
- Ipek, C., Gümüş, H., **Şimşek, M**. *et al.* (2023). DFT and Molecular Docking Study of 1-(2′-Thiophen)-2-propen-1-one-3-(2,3,5-trichlorophenyl) (TTCP) Molecule as Antiviral to Covid-19 Main Protease. *Arab J Sci Eng* **48**, 1031–1040 https://doi.org/10.1007/s13369-022-07293-4
- Ö. Tamer, **M. Şimşek**, D. Avcı, Y. Atalay, (2023). Static/dynamic first and second order hyperpolarizabilities, optimized structures, IR, UV–Vis, 1H and 13C NMR spectra for effective charge transfer compounds: A DFT study, Spectrochimica Acta Part A: Molecular and Biomolecular Spectroscopy. 286 122005. https://doi.org/https://doi.org/10.1016/j.saa.2022.122005.
- **M. Şimşek**, Ö. Tamer, N. Dege, D. Avcı, H. Mahmoody, Y. Atalay, (2024). A new mixed-ligand zinc(II) complex of 3-hydroxy and 4-chloro substituted pyridine-2-carboxylic acid: Synthesis, characterization, NLO properties and DFT calculation, Materials Today Communications 38 108021. https://doi.org/10.1016/j.mtcomm.2024.108021.

- M. Bensbaa, **M.Şimşek,** E. Derin, Ö. Tamer, N. Dege, D. Avcı, M. Boukelkoul, Y. Atalay, (2024). Influence of Co(II) and Cd(II) metal ions on structural, electronic and nonlinear optical properties of 4-methoxypyridine-2-carboxylic acid complexes: An experimental and computational study, Materials Today Communications 40, 109403. https://doi.org/10.1016/j.mtcomm.2024.109403.
- Ö. Tamer, **M. Şimşek**, N. Dege, D. Avcı, Y. Atalay, (2025). The effect of complex formation on the static and frequency-dependent nonlinear optical properties: A combined experimental and theoretical investigation, Spectrochimica Acta Part A: Molecular and Biomolecular Spectroscopy, 325, 125138. https://doi.org/10.1016/j.saa.2024.125138.
- **M. Şimşek**, Ö. Tamer, N. Dege, D. Avcı, Y. Atalay, (2025). Investigation on the effect of complex formation on prominent high static/dynamic first and second hyperpolarizability of Co(II) complex including 4-chloro-Pyridine-2-Carboxylic acid, Materials Science in Semiconductor Processing, 188, 109179. https://doi.org/10.1016/j.mssp.2024.109179.
- Ö. Tamer, **M. Şimşek**, D. Avcı, A. Başoğlu, M. Bensebaa, M. Boukelkoul, N. Dege, Y. Atalay, (2025). Exploring the structural, vibrational, thermal, and nonlinear optical properties of a novel Cu (II) complex of 6-fluoro-pyridine-2-carboxylic acid, Journal of Molecular Structure, 142707. https://doi.org/10.1016/j.molstruc.2025.142707.
- Ö. Tamer, O. Kurt, **M. Şimşek**, D. Avcı, N. Dege, Y. Atalay, (2025). Design and Characterization of Mixed Ligand Mn (II) Complex With 4-Iodo-Pyridine-2-Carboxylic Acid for Enhanced Nonlinear Optical Applications: A Theoretical and Experimental Approach, Applied Organometallic Chemistry 39 (7), e70247, Journal of Molecular Structure, 142707. https://doi.org/10.1002/aoc.70247
- Ö. Tamer, H. Vural, D. Avcı, **M. Şimşek**, A. Gebeş, Y. Atalay, (2025). An experimental and theoretical investigation on the structural, spectroscopic (IR and UV–Vis) and static/frequency-dependent nonlinear optical properties for a novel high-spin Mn(II) complex of 3,5-difluoropyridine-2-carboxylic acid, Applied Organometallic Chemistry 39 (7), e70247, Journal of Molecular Structure 1337, 142191.https://doi.org/10.1016/j.molstruc.2025.142191